T2R2 東京科学大学 リサーチリポジトリ
Science Tokyo Research Repository

論文 / 著書情報
Article / Book Information

題目(和文)	
Title(English)	Identification and functional analysis of a Protruding Acidic Patch, PAP, a novel motif of Schizosaccharomyces pombe Rad51
著者(和文)	AfsharNegar
Author(English)	Negar Afshar
出典(和文)	学位:博士(理学), 学位授与機関:東京工業大学, 報告番号:甲第12049号, 授与年月日:2021年9月24日, 学位の種別:課程博士, 審査員:岩﨑 博史,田口 英樹,林 宣宏,村上 聡,加納 ふみ,中戸川 仁
Citation(English)	Degree:Doctor (Science), Conferring organization: Tokyo Institute of Technology, Report number:甲第12049号, Conferred date:2021/9/24, Degree Type:Course doctor, Examiner:,,,,,
学位種別(和文)	博士論文
Type(English)	Doctoral Thesis
Note	List of publications Title A novel motif of Rad51 serves as an interaction hub for recombination auxiliary factors, Authors Negar Afshar, Bilge Argunhan, Maierdan Palihati, Goki Taniguchi, Hideo Tsubouchi, Hiroshi Iwasaki, Citation eLife 2021, 10, e64131,https://doi.org/10.7554/eLife.64131, Pub. date 25 January 2021

Powered by T2R2 (Science Tokyo Research Repository)



東京工業大学
Tokyo Institute of Technology

Identification and functional analysis of a Protruding Acidic Patch, PAP, a novel motif of *Schizosaccharomyces pombe* Rad51

Negar Afshar

A thesis submitted in partial fulfilment of the requirements for the degree of Doctor of Philosophy

Department of Life Science
Graduate School of Bioscience and Biotechnology
Tokyo Institute of Technology

2021

Acknowledgments

I would like to extend my gratitude to Professor Hiroshi Iwasaki for his immense support during my professional and personal life in Japan. Having never experienced living in a different country to my family, Prof. Iwasaki's caring and encouraging presence certainly filled my family's absence for me. I felt welcomed and included immediately upon joining the lab and this feeling of joy and comfort quickly allayed my fears and yearning for home. I have learnt so much from Prof. Iwasaki through direct and indirect interactions. I have benefited substantially from his scientific insight, intuition, and guidance, and for that, I thank him wholeheartedly.

I also thank Dr Hideo Tsubouchi who has been a great mentor of mine for many years. Dr Tsubouchi's teachings has had an active role in shaping my professional outlook and persona.

I am especially thankful to Dr Bilge Argunhan, who is my favourite colleague, best friend and husband. I greatly appreciate his boundless moral and professional support over the years, especially during the last five years, which has been extremely important to me.

Last but not least, I am grateful to my family in Iran and in the UK for their constant support and trust in me. It goes without saying that I owe it all to my amazing father, mother, and sister who have been my first leaders and cheerleaders in life. Their immeasurable love, optimism, and belief have always been my driving force to achieve higher.

List of publications arising from this thesis

Afshar N, Argunhan B*, Palihati M, Taniguchi G, Tsubouchi H, Iwasaki H* (2021). A novel motif of Rad51 serves as an interaction hub for recombination auxiliary factors. *eLife* 10: e64131. DOI: 10.7554/eLife.64131

*co-corresponding authors

Table of Contents

ACKNOWLEDGMENTS **0**

LIST OF PUBLICATIONS ARISING FROM THIS THESIS **2**

ABSTRACT **7**

LIST OF ABBREVIATIONS AND TERMS **8**

LIST OF FIGURES AND TABLES **11**

CHAPTER 1: INTRODUCTION **13**

1.1 Homologous Recombination 14

1.2 Role of RecA-family recombinase Rad51 in HR 19

1.3 Recombination auxiliary factors 25

1.4 Research purpose 36

CHAPTER 2: METHODS AND MATERIALS **37**

2.1 General yeast techniques 37

2.1.1 Storage and growth of yeast strains *37*

2.1.2 Genetic crosses *37*

2.1.3 Genetic manipulation of yeast *38*

2.1.4 Preparation of genomic DNA *38*

2.2 General molecular biology techniques 39

2.2.1 Polymerase chain reaction (PCR) *39*

2.2.2 Homology-based cloning *40*

2.2.3 Transformation of Escherichia coli *41*

2.2.4 Plasmid extraction from E. coli *41*

2.2.5 Escherichia coli competent cell preparation *41*

2.3 DNA damage sensitivity 42

2.3.1 Spot test *42*

2.3.2 Clonogenic survival assay *42*

2.3.3 Immunofluorescence microscopy *43*

2.4 PROTEIN ANALYSIS 44

2.4.1 TCA preparation of yeast proteins *44*

2.4.2 SDS-PAGE and Western blotting of yeast proteins *45*

2.4.3 In vivo immunoprecipitation (IP) *45*

2.5 PROTEIN PURIFICATION 47

2.5.1 Rad51, Rad51-E206A and Rad51-EED *47*

2.5.2 RPA *48*

2.5.3 Swi5-Sfr1 *49*

2.5.4 Rad52 *50*

2.5.5 Rad54 *50*

2.6 IN VITRO ANALYSIS 52

2.6.1 Electrophoretic mobility shift assay (EMSA) *52*

2.6.2 ATPase assay *52*

2.6.3 Three-strand exchange assay *53*

2.6.4 In vitro IP *55*

2.7 SEQUENCE ALIGNMENTS AND STRUCTURAL MODELS 56

CHAPTER 3: IDENTIFICATION OF THE PAP (PROTRUDING ACIDIC PATCH) IN SCHIZOSACCHAROMYCES POMBE RAD51 **58**

3.1 RESEARCH OBJECTIVES 58

3.2 RESULTS 58

3.2.1 The PAP is situated on the opposite face of the SpRad51 ATPase core domain *58*

3.2.2 The PAP is comprised of E205, E206, and D209 residues *62*

3.2.3 The PAP is on the exterior of the Rad51 presynaptic filament *65*

3.2.4 Evolutionary conservation of the PAP *68*

CHAPTER 4: IN VIVO AND IN VITRO ANALYSIS OF RAD51-E206A **72**

4.1 RESEARCH OBJECTIVES 72

4.2 RESULTS 72

4.2.1 rad51-E206A is defective for DNA repair that is promoted by Rad55-Rad57 *72*

4.2.2 rad51-E206A is specifically defective for interaction with Rad55-Rad57 *76*

4.2.3 Rad51-E206A forms a less stable complex with Rad55-Rad57 in vivo *80*

4.2.4 Rad51-E206A retains normal recombinase activity and can be stimulated by Swi5-Sfr1 *83*

CHAPTER 5: THE PAP IS ESSENTIAL FOR RAD51-DEPENDENT DNA REPAIR **87**

5.1 RESEARCH OBJECTIVES 87

5.2 RESULTS 87

5.2.1 PAP is required for Rad51-mediated DNA repair *87*

5.2.2 PAP is important for DNA repair promoted by Rad55-Rad57 *91*

5.2.3 PAP is important for Rad55-Rad57–independent DNA repair *94*

5.2.4 Negative character of the PAP may be important for Rad51-mediated DNA repair *97*

5.2.5 The PAP is crucial for the recruitment of Rad51 to DNA damage sites *100*

CHAPTER 6: IN VITRO ANALYSIS OF RAD51-EED **103**

6.1 RESEARCH OBJECTIVES 103

6.2 RESULTS 103

6.2.1 Rad51-EED is not intrinsically defective *103*

6.2.2 Rad51-EED can be stimulated by Swi5-Sfr1 *107*

CHAPTER 7: THE PAP IS IMPORTANT FOR THE INTERACTION OF RAD51 WITH BOTH RAD52 AND RAD54 **110**

7.1 RESEARCH OBJECTIVES 110

7.2 RESULTS 110

7.2.1 PAP is essential for the Rad51-Rad52 interaction *110*

7.2.2 PAP is important for Rad51-Rad54 interaction *114*

CHAPTER 8: DISCUSSION **117**

8.1 RESULTS SUMMARY 117

8.2 THE PAP FACILITATES INTERACTION OF RAD51 WITH MULTIPLE AUXILIARY FACTORS 119

8.3 THE PAP IS AN EVOLUTIONARY CONSERVED MOTIF THAT IS INTEGRAL TO RECOMBINATIONAL DNA REPAIR 130

8.4 INTERPLAY BETWEEN RAD55-RAD57 AND SWI5-SFR1 132

BIBLIOGRAPHY **135**

Abstract

The most severe form of DNA damage is a double-strand break (DSB). A single DSB divides a normal chromosome into two pathological chromosomes and can lead to genome instability, which is a potent driver of cell death and tumorigenesis. Homologous recombination (HR) is the mechanism responsible for accurately repairing DSBs. The RecA-family recombinase Rad51 forms a right-handed helical filament on single-stranded DNA that possesses the enzymatic activities central to HR. Although Rad51 is the key protein in HR, multiple auxiliary factors — including Rad52, Rad54, Rad55-Rad57, and Swi5-Sfr1 — interact with Rad51 to promote its recruitment to DNA damage sites and potentiate its activity. Despite the many studies on auxiliary factors, it is still unclear how they interact with Rad51. Here, I characterised an acidic patch of *Schizosaccharomyces pombe* Rad51 that is comprised of three residues (E205, E206, and D209) and protrudes out of the exterior of the Rad51 nucleoprotein filament on the opposite face to the catalytic domain. I refer to this acidic patch as the PAP (Protruding Acidic Patch). An *S. pombe* strain harbouring mutations in all three residues of the PAP (*rad51-EED*) phenocopies *rad51Δ,* indicating that the PAP is essential for Rad51-dependent DNA repair. The DNA repair defect of *rad51-EED* is due to impairments in the mechanisms promoting recruitment of Rad51 to DNA damage sites. Pertinently, mutation of the PAP abolished the physical interaction with Rad52 and impaired complex formation with Rad55-Rad57. Furthermore, biochemical reconstitutions demonstrated that mutation of the PAP also impaired the interaction with Rad54, indicating that a single motif is important for the interactions with multiple auxiliary factors. I propose that the PAP is a fundamental, evolutionarily conserved motif of Rad51 that facilitates interactions with auxiliary factors and is therefore essential for recombinational DNA repair.

List of abbreviations and terms

%	Percentage
Å	Angstrom
ADP	Adenosine diphosphate
Ala	Alanine
Asp	Asparagine
ATP	Adenosine triphosphate
Bleo	Bleomycin
°C	Degrees
C_α	Alpha Carbon
CPT	Camptothecin
Css	Circular single strand
DA	D209A
D-loop	Displacement loop
DSB	Double strand break
dsDNA	Double stranded DNA
EA	E206A
E.coli	Escherichia coli
EE	E205A-E206A
EED	E205A-E206A-D209A
EK	E206K
EMSA	Electrophoretic mobility shift assay
Fig	Figure
FRET	Fluorescence Resonance Energy Transfer

Glu	Glutamic acid
HR	Homologous recombination
H. sapiens	Homo sapiens
HU	Hydroxyurea
IgG	Immunoglobulin G
In	Input
IP	Immunoprecipitation
IR	Ionizing radiation
JM	Joint molecule
Lds	Linear double strand
Lss	Linear single strand
Lys	Lysin
mM	Millimole
mL	Millilitre
Min	Minute
NC	Nicked Circular
NTP	Nucleoside Triphosphate
PAP	Protruding Acidic Patch
PD	Partial Duplex
Phe	Phenylalanine
S5S1	Swi5-Sfr1
S. cerevisiae	Saccharomyces cerevisiae
SDSA	Synthesis Dependent Strand Annealing
SDS-PAGE	Sodium Dodecyl Sulphate-Polyacrylamide Gel Electrophoresis
S. pombe	Schizosaccharomyces pombe

ssDNA	Single Stranded DNA
SUB	Substrate
TCA	Trichloroacetic acid
UV	Ultraviolet light
WT	Wild Type
Y2H	Yeast Two Hybrid
µg	Microgram
µl	Microliter
µm	Micrometer
µM	Micromolar
µM nt	Micromolar nucleotide

List of Figures and Tables

Figure 1.1.	Molecular model of Homologous Recombination (HR)	17
Figure 3.2.1.	Depiction of the PAP location on an *Sp*Rad51 monomer	60
Figure 3.2.2.	PAP is comprised of three acidic residues	63
Figure 3.2.3.	PAP is conserved in *H. sapiens* and *S. cerevisiae*	66
Figure 3.2.4.	PAP is conserved in eukaryotic Dmc1 and archaeal RadA	69
Figure 4.2.1.	*rad51-E206A* exhibits sensitivity to DNA damage only in the *sfr1Δ* background	74
Figure 4.2.2.	Rad55-Rad57–dependent DNA repair is impaired in *rad51-E206A* mutant background	78
Figure 4.2.3.	E206A mutation rendered a reduction in Rad51 and Rad55-Rad57 in vivo complex formation	81
Figure 4.2.4.	Rad51-E206A is not intrinsically defective	85
Figure 5.2.1.	Mutation of the PAP impairs Rad51-mediated DNA repair and reduces in vivo complex formation with Rad55-Rad57	89
Figure 5.2.2.	Individual and collective mutations of PAP residues render Rad55-Rad57 dependent DNA repair defective	92
Figure 5.2.3.	PAP is also involved in Rad55-Rad57 independent DNA repair	95
Figure 5.2.4.	*rad51-E206K* phenocopies the DNA damage sensitivity of *rad51-EED*	98

Figure 5.2.5.	*rad51-EED* is defective in mechanisms promoting recruitment of Rad51 to sites of DNA damage	101
Figure 6.2.1.	The EED mutation does not impair the intrinsic activity of Rad51	105
Figure 6.2.2.	Rad51-EED is responsive to Swi5-Sfr1 stimulation	108
Figure 7.2.1.	The PAP is essential for Rad51-Rad52 interaction	112
Figure 7.2.2.	PAP is also important for the Rad51-Rad54 interaction	115
Figure 8.2.	Homology model of the *Sp*Rad51 presynaptic filament showing the polymerisation motif (F108), PAP residues, and Y2H interaction mutants	123
Table 1.3.	Percentage of sequence similarity among HR factors in eukaryotes	30

Chapter 1: Introduction

Protecting the integrity of genomic sequence information is integral to the existence of any living organism. While mutagenesis can generate genetic diversity and confer an evolutionary advantage, it can also contribute to development of cancer and accelerate the process of ageing. Double-stranded DNA (dsDNA) is the molecule of inheritance that encodes our genomic information and is composed of four nucleotides: adenine, guanine, cytosine and thymine. Each DNA strand backbone consists of interchanging sugar (deoxyribose) and phosphate groups. One of the four bases is attached to each sugar molecule and the DNA double helix is formed through hydrogen bonding between complementary nucleotides: adenine pairing with thymine and cytosine with guanine (Travers & Muskhelishvili, 2015). The DNA double helix is invariably prone to modification and damage through exposure to endogenous and exogenous agents. Endogenous DNA damage can arise from the DNA molecule's interaction with its immediate surroundings, which can include the reactive byproducts of cellular metabolism, or during regular DNA transactions such as DNA replication (Mehta & Haber, 2014). Exogenous factors such as ionizing radiation (IR), ultraviolet (UV) radiation, and other genotoxic chemicals can also cause DNA damage (Hakem, 2008).

Various types of DNA damage exist. A DNA double-strand break (DSB) involves a scission in both strands of the double helix and results in the separation of a normal chromosome into two pathological chromosomes. A single DSB is capable of causing cell death, thus establishing DSBs as the most severe form of DNA damage. During the S and G2 phases of the cell cycle, where sister chromatids are available, homologous recombination (HR) is the major mechanism responsible for accurately repairing DSBs. Additionally, cell cycle dependent activation of HR

coincides with DNA replication, where HR also plays critical roles (Ait Saada et al., 2018). Accordingly, defects in HR results in genome instability, which is a potent driver of cell death and diseases such as cancer (Prakash et al., 2015). Thus, understanding the molecular mechanisms of HR may be of therapeutic benefit to humans.

1.1 Homologous Recombination

In order to repair a DSB, the DNA ends that are exposed at the DSB site are resected to form single-stranded DNA (ssDNA) with 3' termini. These 3' overhangs are produced first through short range resection by the MRN-Ctp1 complex (Jensen & Russell, 2016) followed by further long range resection by factors such as Exo1, Rqh1 and Dna2 (Daley et al., 2020). In order to prevent degradation and to remove secondary structures on the DNA, the ssDNA overhangs are immediately coated with the ssDNA-binding protein Replication Protein A (RPA) (Caldwell & Spies, 2020). Subsequently, RPA is displaced to allow polymerisation of the RecA-family recombinase Rad51, which is the key factor in HR. The right-handed helical nucleoprotein filament formed by Rad51 on the 3' overhang is called the presynaptic filament (Sun et al., 2020). The presynaptic filament is able to carry out homology search in order to locate a segment of dsDNA with substantial sequence similarity to the ssDNA (Greene, 2016). When a homologous dsDNA template is identified, the Rad51 filament invades into the intact dsDNA, forming base pairs with the strand that is complementary to the filamentous ssDNA and displacing the non-complementary strand. Following formation of this recombination intermediate, which is called a displacement loop (D-loop), lost genetic information can be recovered by extension of the 3'-end of the invading strand using the complementary strand as a template for DNA synthesis (McVey et al., 2016). Having been extended, the invading strand is

able to base pair with the ssDNA overhang on the opposite side of the DSB. Following further gap filling by DNA synthesis and ligation of resultant nicks, DSB repair is complete. This mode of HR is known as synthesis-dependent strand annealing (SDSA). In addition to extension by DNA synthesis at the 3'-end, the D-loop can be expanded at the 5'-end by Rad51-driven DNA strand exchange, which increases the extent of base pairing between the two DNA molecules and stabilises the D-loop intermediate. Through subsequent incorporation of the second DNA end of the DSB into the D-loop structure, a double Holliday junction can form. Holliday junctions can be processed through resolution or dissolution. Structure-specific endonucleases known as resolvases can cleave the Holliday junction intermediate and depending on which strands are cut, the repair outcome can be either crossover or non-crossover (Mehta & Haber, 2014). Dissolution entails branch migration of the two Holliday junctions towards each other until a hemicatenated intermediate is formed. This intermediate can be decatenated by a topoisomerase-helicase complex consisting of Topoisomerase III, the RecQ helicase Rqh1, and their accessory factor Rmi1. Decatenation results in non-crossover outcomes (Bizard & Hickson, 2014). Contrary to the prevalence of double Holliday junctions in the budding yeast *Saccharomyces cerevisiae,* where these processes are most extensively studied, single Holliday junctions are the predominant recombination intermediates in the fission yeast *Schizosaccharomyces pombe* (Cromie et al., 2006). Although the reason for this disparity is not well understood, the cleavage of D-loop structures before double Holliday junctions formation in *S. pombe* has been proposed to be at least partly responsible (Doe et al., 2004).

Predominantly, the observed outcome of SDSA were gene conversions with infrequent crossover association. Therefore, the consensus was that SDSA is a type of HR mechanism that results in non-crossovers. Alternatively, a D-loop intermediate can be created by the invading strand annealing to the end of the 3' overhang from the other side of the DSB, resulting in single Holliday junction formation. And depending on the resolution of the single Holliday junction, SDSA can also result in crossovers (Paques & Haber, 1999). Rad51-dependent HR consistently results in gene conversions as well, but whether it will be accompanied by a crossover or a non-crossover outcome depends on the downstream events. Crossover and non-crossover outcomes are distinguished based on whether flanking genetic information is reciprocally exchanged during HR. In a practical sense, this is typically identified by examining the distribution of auxotrophic or drug-resistance markers in meiotic progeny. The formation and resolution of a single Holliday junction, which is more relevant to this thesis, is shown in **Figure 1.1.**

All of these HR events solve the immediate threat to genome stability by repairing the DSB. However, superfluous or dysregulated HR can drive gross chromosomal rearrangements, which destabilize the genome, and cause loss of heterozygosity, which can result in the phenotype of mutant recessive alleles being expressed. Thus, HR can be thought of as a double-edged sword. Indeed, numerous DNA translocases and helicases, which are collectively referred to as anti-recombinases, function to restrict the genome destabilizing effects of HR by disassembling the Rad51 presynaptic filament and/or dissociating recombination intermediates (Huselid & Bunting, 2020). Thus, Rad51 is tightly regulated by multiple functionally distinct auxiliary factors and anti-recombinases to ensure sufficient and appropriate HR proficiency.

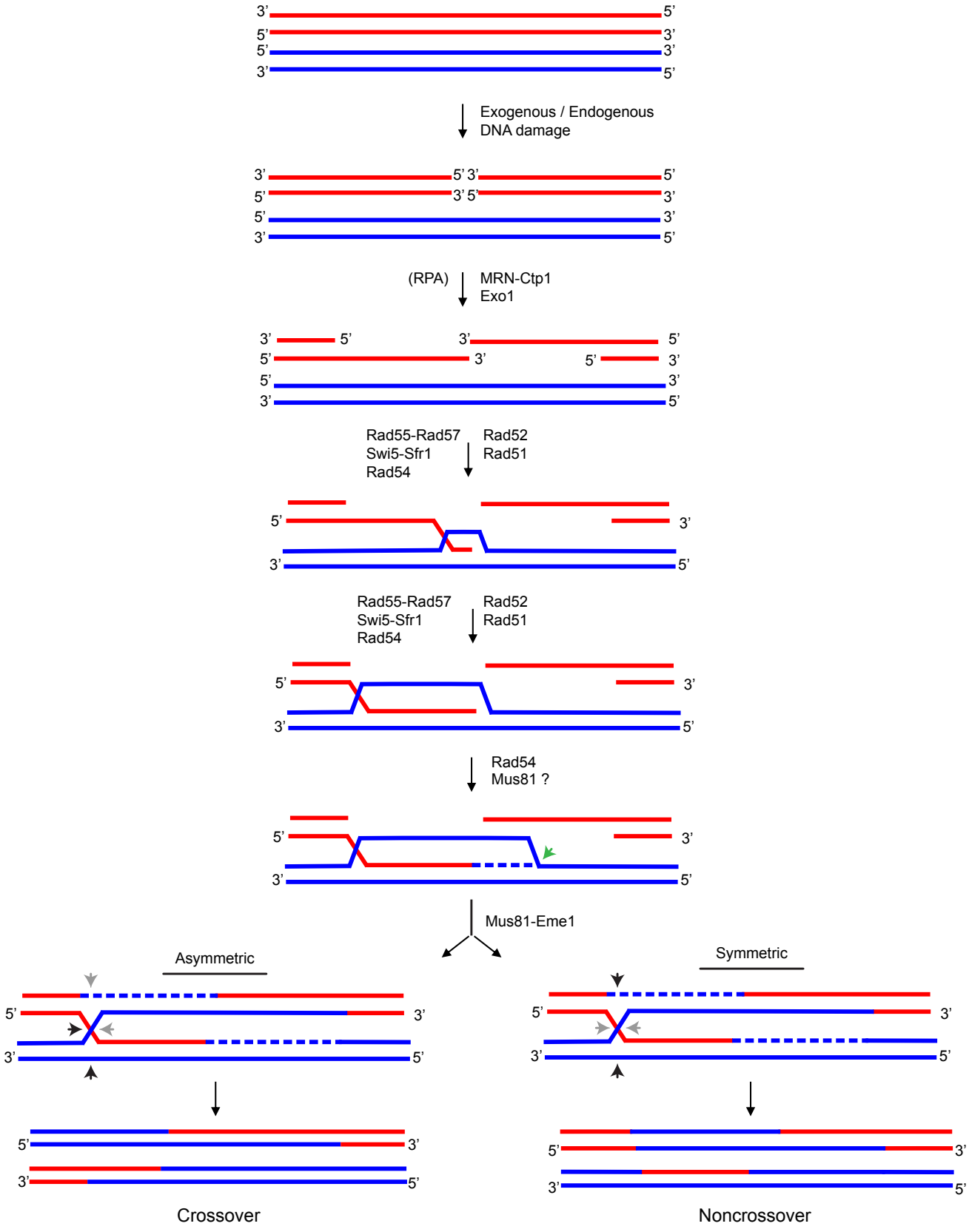

3'
5'
Exogenous / Endogenous
DNA damage
(RPA)
MRN-Ctp1
Exo1
Rad55-Rad57
Swi5-Sfr1
Rad54
Rad52
Rad51
Rad54
Mus81 ?
Mus81-Eme1
Asymmetric
Symmetric
Crossover
Noncrossover

Figure 1.1. Molecular model of Homologous Recombination (HR)

Depiction of series of events taking place after occurrence of a double-strand break (DSB) on the red chromosome (recipient molecule) and the use of intact blue chromosome (donor molecule) for repair. The DSB is processed by several nucleases in order to produce 3' overhang ssDNA, which is coated by RPA. Subsequently, the RecA-famliy recombinase Rad51 forms a helical filament on this ssDNA with the help of multiple auxiliary factors, which also promote the ability of the Rad51 filament to invade into the template chromosome. This results in the formation of a recombination intermediate called a D-loop. D-loop cleavage (green arrow) results in single Holliday junction formation, which can be resolved in several different ways. If strands indicated by the same-coloured arrows are cut, the outcome is non-crossover. And if strands indicated by different coloured arrows are cut, the outcome will be crossover.

1.2 Role of RecA-family recombinase Rad51 in HR

The tubulins, the actins, and the RecA-family of recombinases are the most well known protein families that form filaments and hydrolyse nucleoside triphosphate (NTP). The outstanding feature of RecA-family recombinases is that they form nucleoprotein filaments with ssDNA or dsDNA, within which the monomers are able to carry out steady-state hydrolysis of ATP (Cox et al., 2005). Nucleoprotein filaments formed on ssDNA are capable of identifying homologous dsDNA then driving the DNA strand exchange reaction, which lies at the heart of HR.

The underlying biochemistry of HR was first extensively studied with RecA from the bacterium *Escherichia coli* (Kowalczykowski et al. 1994; Prentiss et al. 2015), which is considered to be the prototypical homologous recombinase, hence why this group of proteins are more commonly referred to as RecA-family recombinases. RecA-family recombinases have been identified in all three domains of life and even in some viruses including the T4 bacteriophage, where the corresponding protein is known as UvsX (Beernink & Morrical, 1999). Importantly, the fundamental mechanisms underlying RecA-family recombinase-driven DNA strand exchange are highly conserved (Liu et al., 2011a). Thus, the mechanism of HR is universally dependent on an ssDNA nucleoprotein filament (Galkin et al., 2006). A nucleotide binding core domain comprised of Walker A and B motifs required for ATP binding and hydrolysis (Saraste et al., 1990) are highly conserved in all RecA-family proteins. In addition, the main DNA binding sites (site I and site II) are also conserved features among RecA-family recombinases (Liu et al. 2011a). There are, however, some differences between bacterial RecA and its orthologs. RecA contains a DNA binding domain at the C-terminus (Prentiss et al., 2015) that is absent in its eukaryotic and archaeal orthologs, which are known as Rad51 and RadA, respectively. Instead,

Rad51 and RadA have an additional DNA binding domain at the N-terminus that is absent in RecA (Aihara et al., 1999; Shin et al., 2003). These additional DNA binding sites located in the N-terminal half of Rad51/RadA are separated from the ATPase core domain by a flexible linker (Pellegrini et al., 2002; Shin et al., 2003). Whether this difference is of functional significance is not clear. However, it has been suggested that the C-terminal lobe of RecA facilitates the transition between “inactive” and “active” states of the presynaptic filament (Yu et al., 2001), which may be related to differences in the rate of ATP hydrolysis and filament dynamics that makes RecA distinct from its orthologs (VanLoock et al., 2003).

The focus of this study is on eukaryotic Rad51, which was first identified in *S. cerevisiae* and shown to be critical for recombinational DNA repair (Shinohara et al. 1992). *S. cerevisiae* Rad51 (*Sc*Rad51, and equivalent notation hereafter) was shown to exhibit homologous DNA pairing and ATP-dependent strand exchange activity, firmly establishing Rad51 as the eukaryotic ortholog of RecA (Sung, 1994). The *S. pombe* ortholog of Rad51 was discovered soon after and also shown to be critical for recombinational DNA repair (Muris et al., 1993). *Sp*Rad51 is a 39.9-kDa protein (365 amino acids), and like all RecA-family recombinases, it exists as an oligomer in solution and forms right-handed helical filaments on both ssDNA and dsDNA (Sauvageau et al., 2005). Oligomerization of Rad51 is achieved through the polymerisation motifs that are defined as the BRC-peptide interaction domain. Characteristic feature of this interaction is the presence of the FxxA consensus sequence. The conserved elbow linker residue Phe, positions itself into a hydrophobic pocket of an adjacent Rad51 subunit and stabilises Rad51 monomer-monomer interaction. Following this ball-socket-type interaction, another contact point is established on the loop region containing the FxxA consensus sequence that results

in extension of the central β-sheet of the adjacent monomer (Shin et al., 2003; Cole et al., 2011). During DSB repair, Rad51 is functional when it can polymerise and form a nucleoprotein filament on the invading ssDNA. Rad51 forms a right-handed nucleoprotein filament and results in extension of the DNA 1.5 times more than the original B-form configuration (Prentiss et al., 2015). The DNA binding regions of Rad51 lie within two binding sites: primary site I and secondary site II. Site I include L1 and L2 loops and it largely consists of positively charged residues that highly favour interactions with the phosphate backbone. Presynaptic filament is formed through interaction of site I with ssDNA. The L1 and L2 loops are naturally disordered regions of Rad51 that only gain order in the presence of ssDNA. Site II is suggested to be facilitating the homology search and capturing of donor dsDNA in addition to functioning as an “entry gate” to deliver not just dsDNA but also ssDNA to site I (Ito et al., 2020). Site I and site II are part of a bigger catalytic core domain of Rad51 that also contains the Walker A and Walker B motifs, which are known to be required for ATP binding and hydrolysis (Zhang & Wigley, 2008). These motifs are highly conserved in RecA family of recombinases and they are also present in other enzymes such as F_0/F_1-ATPase/synthases that utilise nucleotide binding and hydrolysis to carry out their biological functions. F_1-ATPase displays two modes of ATP hydrolysis: low ATP and high ATP mode. RecA-promoted ATP hydrolysis seems to resemble the high ATP mode of the hexametric F_1-ATPase, during which cooperativity is ATP-induced, there is efficient release of the ADP hydrolysis product and there is no reversibility in the reaction. On the other hand, *Hs*Rad51 mimics the low ATP mode of the F_1-ATPase. Possibly in order to achieve a high ATP mode where there is a timely sequence of ATP hydrolysis that will drive efficient strand exchange, eukaryotic Rad51s require additional help from auxiliary factors to enhance protomer

cooperativity (Tombline et al., 2002). Perhaps, the RecA family of recombinases utilise ATP to control the directionality of the strand exchange reaction and ATP ensures the correct assembly/oligomerization of a Rad51 presynaptic filament (Zhang & Wigley, 2008). Therefore, ATP binding is required during filament formation, but hydrolysis is suppressed until the whole system, in this case the presynaptic filament, is fully competent (Ito et al., 2020). In the context of the Rad51 presynaptic filament, ATP is situated at the interface between two monomers (Story & Steitz, 1992). Studies suggests that there are many interface conformations along the Rad51 filament with similar interaction energies (VanLoock et al., 2003) and this observation is consistent with the idea that waves of hydrolysis result in rotations of the RecA presynaptic filament and possibly the Rad51-ssDNA filament (Cox et al., 2005). It is suggested that conformational changes in the L1 loop may be important for ATP hydrolysis by the Rad51 filament and if hydrolysis is propagating through the filament in waves, such changes should be coordinated by the consecutive monomers (Cox, 2007). Additionally, structural analysis show that L1 loop contributes to the stability of the monomer-monomer interactions in the presynaptic filament (Prentiss et al., 2015). Befitting of its importance, presynaptic filament formation/stability is the most highly regulated step in HR and numerous recombination auxiliary factors are known to be involved in this step (described in detail below).

The Rad51 presynaptic filament must interrogate the genome for homologous sequences in a biologically relevant timescale through a process known as the homology search. The mechanism of homology search by the presynaptic filament has been a focal point of research in the field of HR. Analysis of the repair of an inducible site-specific DSB in *S. cerevisiae* suggested that it takes 30-60 min for Rad51 filament formation and a further 30-60 min to identify a homologous donor

sequence (White & Haber, 1990; Sugawara et al., 2003). Although this may seem slow on the biological timescale, it is important to note that the *S. cerevisiae* genome is approximately 12 Mb long, thus it is astonishing that a region homologous to several hundred nucleotides of ssDNA can even be located at all.

Based on the notion that the presynaptic filament is a single DNA binding entity searching for its target sequence, several distinct mechanisms have been proposed for the homology search (Greene, 2016): hopping, which involves sequential binding, dissociation, and re-binding events; sliding, which involves one-dimensional diffusion of the filament along dsDNA without dissociation; and intersegmental transfer, whereby the filament moves a substantial distance along the dsDNA molecule by skipping a segment (e.g., through a DNA loop). However, single-molecule analyses have demonstrated that the primary mechanisms through which RecA (and presumably Rad51) locates homology involves short-range sliding and intersegmental transfer (Forget & Kowalczykowski, 2012; Ragunathan et al., 2012). Furthermore, it was recently shown that RecA, *Sc*Rad51, and *Hs*Rad51 rapidly sample dsDNA and reject sequences that do not have at least 8 nucleotides of homology (Lee et al., 2015; Qi et al., 2015), highlighting the importance of microhomology sampling in the homology search. It was also suggested that a single presynaptic filament can contact multiple points along a dsDNA molecule, thus increasing the speed with which at least 8 nucleotides of homology is encountered (Forget & Kowalczykowski, 2012). Finally, biochemical reconstitutions with *S. cerevisiae* proteins indicated that the recombination auxiliary factor Rad54 can facilitate the homology search (Crickard et al., 2020). This also raises the possibility that other auxiliary factors may be involved in enhancing the homology search. The different mechanisms promoting the homology search likely have synergistic effects, perhaps explaining how the Rad51

presynaptic filament is able to locate relatively short stretches of homology among the significantly more abundant non-homologous sequences.

Relatively little is known about the DNA strand exchange reaction itself, which constitutes the molecular transactions that occur after homology is encountered. It had been proposed that RecA-driven DNA strand exchange involves two distinct three-stranded intermediates (Bianchi et al., 1983): a paranemic joint, in which the the invading strand is in complex with the dsDNA but does not form base pairs with the complementary strand; and a plectonemic joint, in which the invading strand has paired with the complementary strand and displaced the non-complementary strand. However, there was no direct evidence for this, and it was not known whether the mechanisms of DNA strand exchange would be the same for Rad51. This is at least partly because the DNA strand exchange reaction involves labile intermediate structures that are sensitive to experimental manipulation. Recently, the application of fluorescence resonance energy transfer (FRET)-based real-time analysis with *Sp*Rad51 provided direct evidence in support of a model involving two distinct recombination intermediates (Ito et al., 2018; Ito et al., 2020). The intermediates were referred to as C1 (paranemic) and C2 (plectonemic). The Swi5-Sfr1 recombination auxiliary factor complex was shown to promote transitioning of C1 into C2 and the subsequent release of the non-complementary strand that signifies the completion of DNA strand exchange. Furthermore, early analysis combining conventional strand exchange assays with restriction enzyme digestion as an indirect readout of heteroduplex formation suggested that *Sc*Rad54 accelerates the rate of strand exchange approximately threefold (Solinger & Heyer, 2001a).

1.3 Recombination auxiliary factors

The section above clearly established that Rad51 possesses the activities that lie at the heart of HR: the identification of homologous dsDNA and DNA strand exchange. However, it also revealed that recombination auxiliary factors are involved in every step of HR, including presynaptic filament formation, homology search, and finally DNA strand exchange. Multiple distinct auxiliary factors have been identified in *S. pombe* including Rad52, Rad54, the Rad51 paralogs Rad55-Rad57, Swi5-Sfr1, and the lesser studied Shu complex (Ostermann et al., 1993; Muris et al., 1996; Khasanov et al., 1999; Tsutsui et al., 2000; Akamatsu et al., 2003; Khasanov et al., 2004; Martín et al., 2006). While direct analysis of some factors in *S. pombe* is limited (Rad52, Rad54, and Rad55-Rad57), these factors are mostly conserved in *S. cerevisiae* and humans. Thus, the content for these auxiliary factors is mainly from other model systems, but given the evolutionary conservation of HR mechanisms, similar results are expected in *S. pombe*. Indeed, some homologous proteins, as well as analogous proteins, have even been identified in prokaryotes, demonstrating that the requirement for modulation of RecA-family recombinases is also widely conserved (Liu et al., 2011a). However, the discussion of these is beyond the scope of this introductory text, which will focus on eukaryotic systems.

Rad52

The recruitment of Rad51 to DSBs is strongly dependent on Rad52 (Gasior et al., 1998; Sugawara et al., 2003; Wolner et al., 2003; Lisby et al., 2004; Miyazaki et al., 2004). Rad52 is the main mediator protein in both *S. cerevisiae* and *S. pombe*, meaning that it is primarily responsible for promoting Rad51 filament formation on RPA-coated ssDNA (Sung, 1997a; New et al., 1998; Shinohara & Ogawa, 1998;

Kurokawa et al., 2008). This is thought to be due to the ability of Rad52 to simultaneously interact with both Rad51 and RPA, and thus target Rad51 to RPA-ssDNA complexes at resected DSBs (Song et al., 2000; Krejci et al., 2002; Kurokawa et al., 2008). Consistently, *rad52*Δ strains of both *S. cerevisiae* and *S. pombe* show a marked reduction in the formation of DNA damage induced Rad51 foci (Gasior et al., 2001; Lorenz et al., 2009), which are cytological entities that represent Rad51 nucleoprotein filaments at sites of ongoing DNA repair.

Rad52 also possesses ssDNA annealing activity, which is thought to be important late in HR (Mortensen et al., 1996; Sugiyama et al., 1998; Sugiyama et al., 2006) and for a subset of HR events that require Rad52 but not Rad51; this also explains why the DNA damage sensitivity of the *rad52*Δ mutant exceeds that of *rad51*Δ (and all other HR mutants) (Symington, 2002; McEachern & Haber, 2006). By contrast, the absence of Rad52 does not confer any obvious sensitivity to DNA damage in mammalian cells (Rijkers et al., 1998). This is because the tumour suppressor protein BRCA2 functions as the main mediator in mammals, with Rad52 relegated to a supporting role (Jensen et al., 2010; Feng et al., 2011; Liu & Heyer, 2011b).

Rad54

Rad54 belongs to the Swi2/Snf2-family of proteins, which utilize the energy derived from ATP hydrolysis to translocate on dsDNA (Pazin & Kadonaga, 1997; Amitani et al., 2006). Rad54 is unique among recombination auxiliary factors in that its absence does not obviously impair the recruitment of Rad51 to DSBs (Sugawara et al., 2003; Miyazaki et al., 2004). Nevertheless, it is notable that Rad54 shows the highest degree of conservation among auxiliary factors (**Table 1.3**), highlighting its importance for HR (Mazin et al., 2010). This astonishing level of functional conservation is evident from

the fact that *Hs*Rad54 can partially complement the DNA damage sensitivity of the *S. cerevisiae rad54*Δ mutant (Kanaar et al., 1996). It is perhaps because Rad54 possesses a clear enzymatic activity and is so highly conserved that it is among the most extensively characterized auxiliary factors.

In both *S. cerevisiae* and *S. pombe*, *rad54*Δ strains are as sensitive to DNA damage as *rad51*Δ, indicating that, much like Rad52, Rad54 is essential for Rad51 activity in vivo (Jiang et al., 1996; Muris et al., 1997). Biochemical reconstitutions have demonstrated that *Sc*Rad54 and *Hs*Rad54 physically bind their cognate Rad51 and stimulate both its ability to form D-loops and drive DNA strand exchange activity (Petukhova et al., 1998; Solinger et al., 2001b; Sigurdsson et al., 2002). The fact that maximal stimulation is observed when *Sc*Rad54 is added to reactions after Rad51 presynaptic filament formation indicates that Rad54 functions primarily in the synaptic/postsynaptic phases of DNA strand exchange (Mazin et al., 2000; Solinger & Heyer, 2001a; Solinger et al., 2001b), consistent with in vivo observations indicating that Rad51 recruitment to DSBs is normal in *rad54*Δ (Sugawara et al., 2003; Miyazaki et al., 2004). Although recent single molecule analysis with *S. cerevisiae* proteins has revealed a role for Rad54 in enhancing the homology search (Crickard et al., 2020) and some have suggested that Rad54 may function even earlier to stabilize the Rad51 presynaptic filament (Mazin et al., 2003; Wolner et al., 2003), the most established role of Rad54 in HR is in promoting Rad51-driven D-loop formation and strand exchange (Mazin et al., 2010; Ceballos & Heyer, 2011). How this is achieved at the molecular level is not exactly known, but it has been proposed that strand invasion by the Rad51 presynaptic filament is facilitated by the fact that Rad54 translocation on dsDNA leads to some local DNA unwinding (Petukhova et al., 1999; Mazin et al., 2000; Komen et al., 2000; Ristic et al., 2001). Furthermore, the ability of Rad54 to drive

branch migration is thought to be essential for its ability to stimulate Rad51-driven DNA strand exchange (Bugreev et al., 2006).

Another interesting role of Rad54 is in promoting the dissociation of Rad51-dsDNA complexes. Because these complexes resemble the products of completed DNA strand exchange, their dissociation is thought to allow recycling of Rad51 (Solinger et al., 2002). Furthermore, the ATPase cycle of RecA-famliy recombinases is linked to their DNA binding, with the hydrolysis of ATP thought to be responsible for dissociation from DNA (Prentiss et al., 2015; Sun et al., 2020). Because RecA has an ATPase rate ~100-fold greater than Rad51, it has an intrinsic ability to dissociate from dsDNA, whereas Rad51 requires the help of Rad54 (and possibly other translocases) to dissociate unproductive “dead-end” complexes with dsDNA (Shah et al., 2010; Mason et al., 2015). Consistent with this notion, the dissociation of Rad51 from dsDNA by Rad54 requires the ATPase activity of both proteins (Li et al., 2007). The dissociation of Rad51 from D-loop recombination intermediates is also critically important to allow polymerases to access the 3’-end of the invading strand and utilize it as a primer for synthesis-dependent extension (Li & Heyer, 2009). Paradoxically, biochemical reconstitutions demonstrated that the D-loops formed by Rad51 can be disassembled by Rad54 (Sigurdsson et al., 2002; Komen et al., 2002; Bugreev et al., 2007). The ability of Rad54 to promote both the formation of D-loops by Rad51 and their disassembly was recently shown to depend on the exact DNA substrates used; D-loops formed with ssDNA substrates that better mimic the in vivo situation — by being substantially longer than the typical oligonucleotide ssDNA used in D-loop assays or containing a 5’ dsDNA tail — are more resistant to Rad54-mediated disruption (Wright & Heyer, 2014).

Rad51 paralogs

Rad55 and Rad57 are both paralogs of Rad51 that share significant sequence similarity in their ATPase core domain (Bonilla et al., 2020). Early genetic analyses in *S. cerevisiae* first suggested that Rad55 and Rad57 are required for HR (Game & Mortimer, 1974; Lovett & Mortimer, 1987), with subsequent analysis suggesting that they promote Rad51-dependent DNA repair (Hays et al., 1995; Johnson & Symington, 1995). In *S. pombe*, Rad55 was identified based on homology to its *S. cerevisiae* counterpart and Rad57 was isolated through genetic screening (Khasanov et al., 1999; Tsutsui et al., 2000). Unlike *rad52*Δ, which is more sensitive to DNA damage than *rad51*Δ, and *rad54*Δ, which is as sensitive as *rad51*Δ, *rad55*Δ*/rad57*Δ mutants in both *S. cerevisiae* and *S. pombe* show relatively mild sensitivity to DNA damage (Johnson & Symington, 1995; Khasanov et al., 1999; Tsutsui et al., 2000). Yeast two-hybrid analysis suggested that Rad55, but not Rad57, interacts with Rad51 in *S. cerevisiae*, whereas the opposite was seen in *S. pombe* (Hays et al., 1995; Johnson & Symington, 1995; Tsutsui et al., 2001). Biochemical analysis with *S. cerevisiae* proteins suggested that Rad55 and Rad57 exist as an obligate heterodimer that promotes Rad51 filament formation on RPA-coated ssDNA (Sung, 1997b). Consistent with the notion that Rad55-Rad57 function by promoting the association of Rad51 with DNA, the *rad51-I345T* allele, which encodes a mutant protein with increased affinity for DNA, was isolated based on its ability to partially bypass the requirement for Rad55-Rad57 (Fortin & Symington, 2002; Malik & Symington, 2008). Moreover, biochemical reconstitutions demonstrated that Rad55-Rad57 can

	Percentage (%) of sequence homology				
	Rad51	**Rad52**	**Rad54**	**Rad55**	**Rad57**
	S. pombe				
S. cerevisiae	68.3	33.2	56.4	20.8	36.3
H. sapiens	74	32.8	36.7	—	—
	S. cerevisiae				
H. sapiens	66.4	31.6	38.1		

Table 1.3. Percentage of sequence similarity among HR factors in eukaryotes

Percentage of protein sequence homology of HR factors among *S. pombe*, *S. cerevisiae* and *H. sapiens*. Alignments were made by Clustal Omega using UniProt protein sequences with the following identifiers: *S. pombe* Rad51 (P36601) Rad52 (P36592) Rad54 (P41410) Rad55 (O14129) Rad57 (Q9UUL2), *S. cerevisiae* Rad51 (P25454) Rad52 (P06778) Rad54 (P32863) Rad55 (P38953) Rad57 (P25301), *H. sapiens* Rad51 (Q06609) Rad52 (P43351) Rad54 (Q9Y620). Comparison between *S. pombe* and *H. sapiens* Rad55-Rad57 is not mentioned as their direct homologs are still to be identified.

stabilize the Rad51 presynpatic filament against disruption by the Srs2 anti recombinase (Liu et al., 2011d). These in vitro results are supported by cytological analysis in both *S. cerevisae* and *S. pombe* demonstrating that Rad51 foci are reduced in the absence of Rad55/Rad57 (Gasior et al., 1998; Gasior et al., 2001; Akamatsu et al., 2007).

Rad51 paralogs also exist in higher eukaryotes. However, the situation is complicated by the existence of a greater number of paralogs, with six identified in humans (Bonilla et al., 2020): RAD51B, RAD51C, RAD51D, XRCC2, XRCC3, and SWSAP1. The absence of any Rad51 paralog in human cells results in sensitivity to DNA damaging agents and a reduction in Rad51 foci, although the effects are not identical (Liu et al., 2011c; Garcin et al., 2019). Notably, the RAD51B-RAD51C complex has been shown to stabilize Rad51 presynaptic filaments and stimulate Rad51-driven DNA strand exchange (Sigurdsson et al., 2001; Amunugama et al., 2013), essentially mirroring results obtained with *Sc*Rad55-Rad57. However, combined with existence of a greater number of Rad51 paralogs, the evolutionary divergence of this protein family has made it difficult to state with certainty which (if any) of the vertebrate paralogs correspond to yeast Rad55-Rad57 (Lin et al., 2006). Based on the fact that RAD51C and XRCC3 arose before the other paralogs (Lin et al., 2006), and the observation that they form a distinct heterodimeric complex (although RAD51C also exists in complex with RAD51B, RAD51D, and XRCC2) (Masson et al., 2001), it is tempting to speculate that they most closely resemble yeast Rad55-Rad57. Indeed, phylogenetic analysis of *Sp*Rad57 suggested that it is most closely related to XRCC3 (Tsutsui et al., 2000). Regardless of this point, the bulk of the available evidence suggests that Rad51 paralogs have an evolutionarily conserved role in modulating the Rad51 presynaptic filament. However, elucidation of

the molecular mechanisms involved have been hampered by the low cellular expression and tendency to form insoluble aggregates in overexpression systems (Bonilla et al., 2020).

Swi5-Sfr1

Sfr1 was first identified in *S. pombe* as an interacting partner of Rad51 that forms a complex with Swi5 to promote Rad51-dependent DNA repair (Akamatsu et al., 2003). Biochemical reconstitutions demonstrated that Swi5-Sfr1 stimulates Rad51-driven DNA strand exchange by potentiating Rad51's ATPase activity and stabilising the Rad51 presynaptic filament (Haruta et al., 2006; Kurokawa et al., 2008). Homologs of Swi5-Sfr1 have been identified in several organisms including *S. cerevisiae*, mice, and humans (Tsubouchi & Roeder, 2004; Hayase et al., 2004; Akamatsu et al., 2010; Yuan & Chen, 2011), firmly establishing Swi5-Sfr1 as an evolutionarily conserved auxiliary factor (Argunhan et al., 2017a). While Swi5-Sfr1 promotes Rad51-dependent DNA repair in *S. pombe*, mice, and humans, Sae3-Mei5 (Swi5-Sfr1 in *S. cerevisiae*) is completely dispensable for DNA repair in mitotic (i.e., somatic) cells of *S. cerevisiae*. This is because Sae3-Mei5 is expressed only in meiotic (i.e., germline) cells, where it promotes meiotic HR by stimulating the meiosis-specific RecA-family recombinase Dmc1 (Tsubouchi & Roeder, 2004; Hayase et al., 2004). While Swi5-Sfr1 has been shown to stimulate both Rad51 and Dmc1 in *S. pombe* (Haruta et al., 2006), it seems to only stimulate Rad51 in mice (Su et al., 2014). However, the fact that SWI5-SFR1 is upregulated in mouse testes points towards an involvement in meiotic HR (Akamatsu et al., 2010). Whereas Sae3-Mei5 physically interacts with both Rad51 and Dmc1 but only stimulates the latter (Ferrari et al., 2009; Say et al., 2011), Swi5-Sfr1 physically and functionally interacts with both Rad51 and Dmc1 in *S. pombe* (Haruta

et al., 2006). By contrast, Swi5-Sfr1 does not show any obvious interaction, physical or functional, with Dmc1 in mice (Su et al., 2014). Thus, it is possible that *S. pombe* represents an intermediary species with respect to Swi5-Sfr1 function.

Alternatively, the lack of functional interaction between Rad51 and Sae3-Mei5 may be related to the absence of an Fbh1 (F-box DNA helicase 1) homolog in *S. cerevisiae*. Fbh1 has been shown to act as an anti-recombinase in *S. pombe* and mammals, where it disrupts Rad51 presynaptic filaments (Osman et al., 2005; Morishita et al., 2005; Lorenz et al., 2009; Fugger et al., 2009; Simandlova et al., 2013; Tsutsui et al., 2014). Importantly, *Sp*Swi5-Sfr1 has been shown to stabilize Rad51 filaments against disruption by Fbh1 (Tsutsui et al., 2014). Thus, it is tempting to speculate that the functional interaction between Rad51 and Swi5-Sfr1 is required only in species possessing an Fbh1 homolog. Whatever the reason for these differences, there is clear biochemical evidence to conclude that Swi5-Sfr1 in *S. pombe* and mice, and Sae3-Mei5 in *S. cerevisiae*, stimulate RecA-family recombinases through highly similar mechanisms, namely ATPase potentiation and stabilisation of presynaptic filaments (Haruta et al., 2006; Kurokawa et al., 2008; Ferrari et al., 2009; Tsai et al., 2012; Murayama et al., 2013; Su et al., 2014; Lu et al., 2018).

In *S. pombe*, the *rad57*Δ and *sfr1*Δ mutants show relatively mild sensitivity to DNA damage, while the *rad57*Δ *sfr1*Δ double mutant is as sensitive as the *rad51*Δ single mutant. Based on this additivity, it was proposed that Rad55-Rad57 and Swi5-Sfr1 function independently of each other to promote Rad51-dependent DNA repair (Akamatsu et al., 2003; Akamatsu et al., 2007). However, it was recently shown that Rad55-Rad57 can suppress defects in the physical interaction between Swi5-Sfr1 and Rad51 (Argunhan et al., 2020). Moreover, partially purified Rad55-Rad57 was shown to interact with purified Swi5-Sfr1, suggesting that, while capable of functioning

independently of each other, the two auxiliary factors collaboratively promote HR in *S. pombe* (Argunhan et al., 2020).

The Shu complex

The Shu complex is the least studied recombination auxiliary factor. Typically, the complex consists of a SWIM-domain containing protein thought to be involved in Zn binding (Makarova et al., 2002) and a highly diverged Rad51 paralog(s) (Martino & Bernstein, 2016). In *S. cerevisiae*, the Shu complex consists of Shu1, Shu2, Csm2, and Psy3 (Shor et al., 2005). Shu2 contains a SWIM domain, while Csm2 and Psy3 are both highly diverged Rad51 paralogs. By contrast, the Shu complex only contains three subunits in *S. pombe*: Sws1 contains a SWIM domain, whereas Rlp1 and Rdl1 are both highly diverged Rad51 paralogs (Khasanov et al., 2004; Martin et al., 2006). The absence of any Shu complex subunit confers only mild DNA damage sensitivity in both *S. cerevisiae* and *S. pombe* (Khasanov et al., 2004; Shor et al., 2005; Martin et al., 2006). Biochemical reconstitutions with *S. cerevisiae* proteins have shown that the Shu complex can stimulate Rad51 activity in a manner that is dependent on Rad55-Rad57, which is thought to function as a molecular bridge to facilitate Rad51 potentiation by the Shu complex (Gaines et al., 2015). This is likely necessitated by the fact that the Shu complex itself seems incapable of binding Rad51, as physical interactions could not be detected by conventional methods including as yeast two-hybrid and co-immunoprecipitation (Khasanov et al., 2004; Martin et al., 2006; Gaines et al., 2015). The Shu complex is also conserved in humans, where it consists of SWS1 and SWSAP1, which are the SWIM-domain and Rad51 paralog subunits, respectively (Liu et al., 2011c).

1.4 Research purpose

It is abundantly clear that Rad51 is regulated by a plethora of auxiliary factors across multiple evolutionarily diverged species such as *S. cerevisiae*, *S. pombe*, and humans. Other than the Shu complex, all other auxiliary factors directly interact with Rad51, which is thought to be critical for Rad51 potentiation and thus regulation of HR. Despite this, the region(s) of Rad51 responsible for interacting with its auxiliary factors remains unknown. Previous attempts to identify auxiliary factor binding sites have typically relied on the yeast two-hybrid approach and truncation of Rad51 (Tsutsui et al., 2001; Krejci et al., 2001). Given that the active form of RecA-family recombinases is a nucleoprotein filament, interactions observed with truncated proteins may not be representative of the physiological situation. Moreover, RecA-family recombinases are notoriously recalcitrant to epitope tagging and protein fusions, which make them poorly suited for yeast two-hybrid analysis. This raises the possibility that a different approach would be more favourable for identifying Rad51 motifs involved in binding auxiliary factors. In the following chapters, I will describe the identification and functional analysis of a novel motif of *Sp*Rad51 that is important for binding to multiple auxiliary factors. Utilizing a combination of in vivo and in vitro approaches, I show that the protruding acidic patch (PAP) motif is essential for Rad52 binding and important for both Rad55-Rad57 and Rad54 binding. Mutation of the PAP eliminates Rad51-dependent DNA repair without impairing the intrinsic activity of Rad51, indicating that the PAP is essential for HR.

Chapter 2: Methods and Materials

2.1 General yeast techniques

2.1.1 Storage and growth of yeast strains

All equipment and media were sterilised by autoclaving and procedures were performed under aseptic conditions. Yeast strains were stored in 20% glycerol at -80℃. Growth of yeast on plates (solid medium) and sporulation on plates was always conducted at 30℃. Growth of yeast in culture (liquid medium) and sporulation in culture was always conducted at 30℃, 200 RPM.

2.1.2 Genetic crosses

Approximately equal amounts of cells from two strains were mixed in 50 µL of dH_2O. 10 µL of the cell mixture were spotted on sporulation media [Glucose, Potassium dihydrogen phosphate, Leucine, Uracil, Arginine, Histidine, Agar and 1000x vitamin stock (Nicotinic acid, Inositol, Biotin and Sodium pantothenate)] (SPA5S) and left for 3 days at 26℃. Mating was confirmed by monitoring cells using a Nikon ECLIPSE 50i light microscope and identifying those with a characteristic zygote morphology. A quarter of the sporulated cells were taken and resuspended in 100 µL of dH_2O and 10 µL of the cell solution was plated on rich media (Glucose, Yeast Extract, Uracil, Adenine, Leucine, Histidine, Arginine and Agar) (YE5S) and left at 30℃ for 1 hour. Putative zygotes were picked with a tetrad dissection microscope (Singer SporePlay SPO-002) and allowed to form single colonies. After 3 to 4 days of incubation at 30℃, colonies with the desired markers were identified by replica plating onto selective plates.

2.1.3 Genetic manipulation of yeast

Yeast were transformed according to the lithium acetate/single-stranded carrier DNA/polyethylene glycol method (Hagan et al., 2016). Briefly, for four transformations, three single colonies were inoculated in 50 mL YE5S and incubated at 30℃ for roughly 13 hours until cells reached log phase (~1 x 10^7 cells/mL). After washing with dH_2O, cells were pelletized and resuspended in premixed 800 µL 50% PEG, 100 µL 1 M lithium acetate, 5 µL single-stranded salmon sperm DNA (10 mg/mL) and DNA of interest. After heat-shock treatment at 42℃ for 15 minutes, cells were briefly pelletized again, before being resuspended in 100 µL 1M sorbitol and spread on YE5S plate. After incubation at 30℃ for 2-3 days, correct transformants were isolated after replica plating the YE5S plate onto desired selective media. All genetic manipulations were confirmed by sanger sequencing.

2.1.4 Preparation of genomic DNA

A small amount of yeast cells was resuspended in 100 µL of sorbitol solution (0.9 M sorbitol, 0.1 M Tris (pH 8), 0.1 M EDTA (pH 8)) and treated with 0.2 µL beta-mercaptoethanol and 0.4 µL of zymolyase at 30℃ for 30 minutes. Cells were gently centrifuged (3000 RPM, 3 minutes) and resuspended in 100 µL 50:20 TE (50 mM Tris-20 mM EDTA), before mixing with 10 µL of 10% SDS
and storing at 65℃ for 20 minutes. Cell suspensions were then supplemented with 40 µL of 5 M potassium acetate and stored on ice for at least 30 minutes. Once firmly pelletized (150000 RPM, 5 minutes), DNA was purified by ethanol precipitation.

2.2 General molecular biology techniques

2.2.1 Polymerase chain reaction (PCR)

All PCR reagents were stored at -20℃. PCR was performed using either DreamTaq (Thermo Fisher Scientific) or Primestar GXL (Takara) polymerases with a Takara PCR Thermal Cycler Dice. A stock containing 2.5 mM of each dNTP was prepared from 100 mM stocks of each individual dNTP (Roche). Listed below are the conditions for each polymerase. Primers were used from a stock concentration of 4 μM. (mins - minutes, secs - seconds).

DreamTaq

Total volume	10 μL	Cycling condition
dH_2O	5.95 μL	95℃ 2 min
Buffer	1 μL	95℃ 10 sec
dNTPs	1 μL	58℃ 10 sec
Primer F	0.5 μL	72℃ 1 min
Primer R	0.5 μL	72℃ 3 min
DNA polymerase	0.05 μL	
DNA template	1 μL	

Primestar GXL

Total volume	30 μL	Cycling condition
dH_2O	17 μL	98℃ 2 min
Buffer	6 μL	98℃ 10 sec

dNTPs	2.4 µL	58℃ 10 sec
Primer F	1.5 µL	68℃ 2 min
Primer R	1.5 µL	68℃ 5 min
DNA polymerase	0.6 µL	
DNA template	1 µL	

When required, PCR products were purified and concentrated using silica spin columns (MonoFas Purification Kit, GL Sciences Inc.).

2.2.2 Homology-based cloning

Desired PCR fragment containing homology to the vector is subjected to DpnI digest for 2 hours at 37℃. DNA fragment is then purified using the MonoFas purification kit and stored in 10:0.1 TE (10 mM Tris-0.1 mM EDTA). Next, the vector which in this case is pET11b is cut with NdeI and BamHI restriction enzymes (NEB). In order to prevent self-ligation, the linearised vector is then subjected to rAPid Alkaline Phosphotase treatment (Roche) for 2 hours at 37℃ and afterwards it is purified using the MonoFas purification kit and stored in 10:0.1 TE (10 mM Tris-0.1 mM EDTA). Using the In-Fusion HD cloning kit (Takara), 50-100 ng of linearised vector is mixed with 3x as many of the PCR fragment, the In-Fusion mix and dH_2O. Following 15 minutes of incubation at 50℃ and then on ice, the cloned pET11b vector is ready for *E. coli* transformation. All cloning was verified by sanger sequencing.

2.2.3 Transformation of *Escherichia coli*

To amplify plasmid DNA, a 100 µL aliquot of DH5α competent cells was thawed on ice and mixed with DNA. After a further 3 minutes on ice, this mixture was transferred to 42℃ for 50 seconds. Upon addition of 0.5 mL lysogeny broth (LB), this mixture was incubated at 37℃ for 50 minutes, before finally spreading on a LB plates supplemented with desired antibiotics.

2.2.4 Plasmid extraction from *E. coli*

Colonies growing on selective plates were resuspended in 2 mL of LB supplemented with desired antibiotics and left to grow overnight at 37℃, 200 RPM. Plasmid DNA was extracted from cells using a FastGene Plasmid Mini kit (Nippon Genetics).

2.2.5 *Escherichia coli* competent cell preparation

In order to make *E. coli* strains for purification of desired proteins, competent cells of BL21-CodonPlus (DE3)-RIPL strain were prepared fresh before each transformation. The strain is first inoculated in 2 mL of LB supplemented with antibiotics and incubated at 37℃, 200 RPM overnight. 100 µL was then seeded into 10 mL of fresh LB supplemented with antibiotics and incubated at 37℃, 200 RPM until OD_{600} = ~0.35 is achieved. The cells were pelletized and resuspended in 3 mL of cold transformation buffer (10 mM (piperazine-N,N`-bis(2-ethanesufonic acid)) PIPES, 15 mM $CaCl_2$-$2H_2O$, 0.25 mM KCl). The cell mixture was centrifuged and resuspended in 1 mL of cold transformation buffer and incubated on ice for 15 minutes. Cells were then centrifuged for 5 minutes at 150000 RPM and resuspended in 500 µL of cold transformation buffer. For each transformation, 100 µL of competent cells were used

alongside 3 µL of desired plasmid expressing the protein of interest. Transformation was done as described in **Transformation of *E. coli*** section.

2.3 DNA damage sensitivity

2.3.1 Spot test

Single colonies were streaked from -80℃ stock on YE5S plate and left to grow for 2 to 3 days at 30℃. One single colony was inoculated in 2 mL of liquid YE5S agitating overnight at 30℃. The next day, 0.25 to 0.5 x 10^6 cells/mL were seeded into 2 mL of fresh YE5S and left to reach log phase (~1 x 10^7 cells/mL). For each strain, 0.5 x 10^7 cells were collected and pelletized. The pellets were resuspended in 250 µL dH_2O and 150 µL of it were transferred onto column 1 of a sterile 96-well plate. In order to prepare five serial dilutions, 135 µL dH_2O was added into columns 2 to 5. The serial dilutions were prepared by transferring 15 µL of thoroughly resuspended column 1 through to column 5. For each dilution, 5 µL of thoroughly resuspended cell mixtures were spotted on no treatment YE5S plate, genotoxic treated YE5S plates and YE5S plate acutely exposed to Ultraviolate-C (UV) using a standard UV chamber.

2.3.2 Clonogenic survival assay

For clonogenic survival assays, cells were prepared as described in section **2.3.1 Spot test**. 100 µL of each strain was spread onto YE5S plates and left to dry in the clean bench area. One at a time, plates were exposed to specified doses of acute UV irradiation. Colonies were counted after 3 to 4 days of incubation at 30°C and survival percentage was expressed relative to the number of colonies on the untreated plate.

Statistical analysis was by unpaired two-tailed t-test using GraphPad Prism (version 8).

2.3.3 Immunofluorescence microscopy

70 mL of log phase YE5S culture originating from a single colony was harvested and pelletized. Cell pellets were resuspended in 35 mL dH_2O and divided into two equal aliquots. Aliquot 1 is mock treated without any exposure to UV, aliquot 2 is placed at the centre of a petri dish and acutely exposed to 200 J/m^2 UV-A irradiation. Both aliquots are centrifuged at 2300 *g* 2 minutes and the pellets are resuspended in 1 mL YE5S and transferred into 34 mL YE5S in designated flasks. The cultures were then incubated at 30°C shaking at 200 RPM for 3 hours. 6 mL of -UV cells and 9 mL of +UV cells were harvested, pelletized and washed with 0.95 mL 1M sorbitol. Pellets were subsequently resuspended in 1 mL 1M sorbitol before gently mixing with 10 µL DTT, 20 µL zymolyase and 60 µL lysing enzyme (Sigma). Cells were incubated at 30℃ with gentle agitation for

30 minutes, before centrifuging (200 *g*, 3 minutes) and resuspending in 0.95 mL 1 M sorbitol-1x MES. Following further centrifugation (200 *g*, 2 minutes), pellets were resuspended with premixed PFA-1x MES (350 µL 3.3% PFA with 100 µL 1x MES) and spread onto microscopy slides (Superior Marienfeld). After semi-drying, these slides were washed twice with 0.4% Photoflo (Kodak) and allowed to fully dry. Slides were then stored in -20℃ until required. To immunostain, slides were incubated with 5% BSA-PBS for 30 minutes in a moist environment, before incubating overnight at 4℃ with 5% BSA-PBS supplemented with primary antibody. Slides were then washed by submerging in PBS-filled coplin jars, before incubating for 3 hours at room temperature with 5% BSA-PBS supplemented with secondary antibody. Slides were washed as

before and allowed to dry. 30 µL of mounting media supplemented with DAPI was added to each slide and spread with a cover slip before sealing. All slides were viewed and images captured using using a wide field fluorescent microscope (Nikon Eclipse 80i) with a 100x objective fitted with an sCMOS camera (C13440 Hamamatsu). The number of foci for each spread nucleus was quantified using FIJI (Schindelin et al. 2012) according to the following procedure. Following the application of a Gaussian blur (sigma = 2) to the Rad51 (green) channel, the DAPI (blue) and Rad51 channels were subjected to Auto Thresholding (MaxEntropy) and Auto Local Thresholding (Bernsen, radius = 13), respectively. The Rad51 channel was then subjected to the Watershed and Ultimate Points processes, followed by the Find Maxima function. The DAPI channel was subjected to the Analyze Particles process (≥200 pixels^2) to add the areas of nuclei to the Region-Of-Interest (ROI) Manager. These ROIs were then overlayed onto the Rad51 channel and the measure function of the ROI Manager was employed. The resulting RawIntDen value for each nucleus was then divided by 255 to yield the number of foci. A graph portraying the results was prepared using GraphPad Prism (version 8), which was also used for statistical analysis (Wilcoxon ranked sum test).

2.4 Protein analysis

2.4.1 TCA preparation of yeast proteins

All of the following was performed on ice. Cell pellets were resuspended with 1 mL of ice-cold dH_2O and mixed with 150 µL 1.85 M NaOH-7.5% beta-mercaptoethanol before leaving on ice for 15 minutes. 150 µL of 55% TCA was added and thoroughly mixed, followed by a further 10 minutes incubation on ice. Samples were centrifuged

(20000 *g*, 10 minutes) and supernatants were discarded. Samples were centrifuged again to remove residual supernatant and the pellets were solubilised in 100 µL HU buffer (800 µL urea buffer, 100 µL 1M DTT and 100 µL 2M Tris) and incubated with constant mixing at 65℃ 13000 RPM for 10 minutes, before storing at -20℃ until use.

2.4.2 SDS-PAGE and Western blotting of yeast proteins

Proteins were separated on 10% or 12% polyacrylamide gels with an acrylamide-to-bisacrylamide ratio of 29:1. Following separation, proteins were transferred to methanol-activated PVDF membranes overnight at 4℃. Membranes were then stained with Ponceau S (Sigma-Aldrich), imaged, and incubated in 0.1% Tween 20-PBS supplemented with 5% milk powder for 1 hour; all incubations were performed with gentle agitation. The milk solution was replaced with fresh milk solution containing the primary antibody of interest, and membranes were incubated for 1 hour. The primary antibody solution was removed, membranes were washed three times for 5 minutes with 0.1% Tween 20-PBS, and fresh milk solution containing the secondary antibody was added to membranes for 2 to 3 hours. The secondary antibody solution was removed and membranes were washed as before. Following short incubation in ImmunoStar Zeta chemiluminescence solution (FujiFilm Wako), membranes were imaged using FujiFilm LAS 4000 mini.

2.4.3 In vivo immunoprecipitation (IP)

A single colony was resuspended in 15 mL YE5S and grown 1 to 2 days at 30℃. This patch was then resuspended in 10 mL YE5S and grown with shaking at 30℃ for 24 hours. 0.2 to 0.4 x 10^6 cells/mL were seeded into 1 L of fresh YE5S in 5 L baffled flasks

and grown with shaking at 30℃ 200 RPM until they reached log phase. Cultures were then supplemented with 0.5 mM PMSF and harvested by centrifugation (6000 *g,* 15 min, 2℃) and pelleted cells were washed with 20 mL of yeast wash solution (50 mM HEPES [pH 7.5], 70 mM KOAc, 1 mM PMSF). Aliquots of 2 x 10^9 cells were pelleted, frozen in liquid nitrogen, and stored at -80℃ until use. A single cell pellet was resuspended in 400 µL of KA50 buffer (50 mM HEPES-KOH [pH 7.5], 50 mM KOAc, 5 mM MgOAc, 0.05% Igepal CA-630, 10% glycerol, 0.25 mM TCEP, 0.5 mM PMSF, 2x cOmplete protease inhibitor cocktail (Roche), 10 mM β-glycerophosphate, 10 mM NaF, 1 mM sodium orthovanadate) and mixed with an equal volume of glass beads (500 micron) on ice. Cells were then broken using a Yasui Kikai Multi-beads Shocker (2700 RPM, 30 sec on/off, 12 cycles, 2℃). The lysate was recovered, and the glass beads were washed with 200 µL of KA70 buffer and combined with the lysate. The lysate was then treated with 250 units of TurboNuclease (Accelagen) for 30 min at 4℃ with mixing. The lysate was then sequentially cleared (20000 g, 10 min, 2℃; then 20000 g, 5 min, 2℃), a sample was taken for immunoblotting (input sample) and mixed with an equal volume of 2x SDS loading buffer (120 mM Tris-HCl [pH 6.8], 4% SDS, 20% glycerol, 0.02% BPB, 200 mM DTT), and the remaining soluble cell extract was divided into three equal aliquots in protein Lo-Bind tubes (Eppendorf). Anti-V5 (mouse; MCA1360 Bio-Rad), anti-Rad51 (rabbit; Haruta et al., 2006), or ChromPure Human IgG (mock antibody; 009-000-003 Jackson Immunoresearch Laboratories) antibodies were premixed with Dynabeads Protein A (Thermo Fisher Scientific) and incubated with each aliquot of soluble cell extract with gentle mixing (3 hours, 4℃). Aqueous fractions were separated using a magnetic stand and the beads were

briefly washed with buffer KA70 (300 µL, x3). The beads were then resuspended in 75 µL of 1x SDS loading buffer and proteins were eluted using a thermomixer (IP

sample; 65℃ 10 min 1300 RPM). Samples were separated by SDS-PAGE, transferred to PVDF membranes and detected with the following antibodies: anti-V5, mouse (1:10,000; Bio-Rad); anti-Rad51, rat (1:10,000; Argunhan et al., 2020); anti-Rad52, rabbit (1:5,000; Kurokawa et al., 2008); and anti-Tubulin, mouse (1:10,000, T5168 Sigma-Aldrich). HRP-conjugated secondary antibodies were purchased from GE Healthcare (mouse, 1:5,000, NA931; rabbit, 1:5,000, NA934) or Jackson Immunoresearch Labs (rat, 1:10000, 712-035-153).

2.5 Protein purification

2.5.1 Rad51, Rad51-E206A and Rad51-EED

ORF of Rad51 wildtype/E206A/EED was cloned at the NdeI and BamHI site of pET11b to yield the following plasmids: pYK12, pNA42 and pBA161 respectively. BL21-CodonPlus (DE3)-RIPL competent cells transformed with respective plasmids was induced with 1 mM IPTG agitating for 15 hours at 18℃. Following protein induction, cells were sonicated in R buffer (10% Glycerol, 20 mM Tris-Cl (pH8), 1 mM EDTA,1 mM DTT) containing 300 mM NaCl. The lysate was cleared at 70,000 *g* for 1 hour. Protein in the lysate was extracted using Ammonium sulphate precipitation at 35% saturation. Protein containing pellet is resuspended in 150 mL P buffer (10% Glycerol, 20 mM Potassium dihydrogen phosphate, 20 mM Dipotassium hydrogenphosphate and 0.5 mM EDTA) and applied to 50 mL SP Sepharose column following flowthrough fraction collection. Next, 20 mL Q Sepharose chromatography was used with a linear gradient (200 mL 0.1-0.8 M KCl) and peak fractions were pooled and diluted to 100 mM KCl and loaded to 5 mL HiTrap Heparin HP column with a linear gradient (100 mL 0.1-0.7 M KCl). Partially purified protein fractions were collected, mixed and diluted to

100 mM KCl before further purification using 6 mL Resource Q chromatography with a liner gradient (50 mL 0.1-0.6 M KCl). Eluted peak sample was transferred to 3-12 mL capacity 10,000 MWCO Slide-A-Lyzer dialysis cassette (Thermo Fisher Scientific) and dialysed against 200 mM KCl overnight. The next day, dialysed sample is concentrated in an Amicon Ultra-4 Centrifugal Filters 10,000 MWCO (Merck Millipore), flash frozen and stored at -80℃. The concentration was estimated by measuring the A280 and using a molar extinction coefficient of 1.83 x 10^4 M^{-1} cm^{-1}.

2.5.2 RPA

According to Haruta et al. (2006), the heterotrimeric RPA complex was expressed from pET11b-RPA and pACYC184-11b-RPA1. BL21 (DE3) competent cells carrying the respective plasmids were induced with 1 mM IPTG agitating for 18 hours at 18℃. Harvested cells were pelletized and resuspended in R buffer. Cells were sonicated and lysate was cleared by centrifugation at 40,000 *g*
for 30 minutes. In order to precipitate DNA, 0.05% Polyethyleneimine (PEI) was added to the lysate and mixed for 30 minutes in cold room. Mixture was then centrifuged at 27000 *g* for 15 minutes and the supernatant fraction was transferred into a new beaker. Protein in the lysate was extracted using Ammonium sulphate precipitation at 45% saturation. Protein containing pellet was resuspended in R buffer, transferred to a dialysis cassette and dialysed against R buffer containing 100 mM NaCl. The dialysed sample was loaded on SP-Sepharose column and proteins were eluted using a linear gradient (0.1 M-1 M NaCl). The peak fractions were diluted three-fold and using a HiTrap Heparin column, sample was further purified with a linear gradient (0.3 M-1 M NaCl). Using a Superdex 200 pg gel filtration column, the peak fractions were developed in R buffer containing 1.5 M NaCl. Sample was concentrated in an Amicon

Ultra-4 Centrifugal Filters 30,000 MWCO (Merck Millipore), flash frozen and stored at -80℃. The concentration was estimated by measuring the A280 and using a molar extinction coefficient of 9.89 x 10^4 M^{-1} cm^{-1}.

2.5.3 Swi5-Sfr1

According to Haruta et al. (2006), Swi5-Sfr1 complex is co-expressed from pET21a plasmid transformed into BL21-CodonPlus(DE3) *E. coli* strain. Cell cultures were induced with 1 M IPTG and incubated at 18℃ for 16.5 hours. Cells were then centrifuged, and cells pellets were resuspended in 200 mM NaCl R buffer before lysis. After centrifuging at 40,000 g for 30 min, the soluble fraction was collected and incubated with 0.05% of Polyethyleneimine. Sample was centrifuged at 27000 g for 20 min and ammonium sulphate, at a final saturation concentration of 35% was added to the supernatant. Mixture was centrifuged again at 27000 g for 30 min and this time the pellet fraction is collected and washed in R buffer containing ammonium sulphate at a final saturation concentration of 50%. The pellet was then resuspended in R buffer containing 100 mM NaCl and dialysed against R buffer containing no salt. Dialysed sample was loaded onto a Q-Sepharose column and proteins eluted with a linear gradient (0 M-1 M NaCl). Peak fractions eluted at 200 mM NaCl were diluted with four-fold R buffer and applied to a HiTrap Heparin column. The peak fractions were pooled together and applied to a Superdex 200 pg gel filtration column containing 1.5 M NaCl R buffer. Sample was concentrated in an Amicon Ultra-4 Centrifugal Filters 10,000 MWCO (Merck Millipore), flash frozen and stored at -80℃. The concentration was estimated by measuring the A280 and using a molar extinction coefficient of 1.44 x 10^4 M^{-1} cm^{-1}.

2.5.4 Rad52

According to Kurokawa et al. (2008), BL21-CodonPlus(DE3)-RIPL *E. coli* strain was used to express Rad52 from pET11b plasmid. Rad52 expression was induced using 0.2 mM IPTG at 30℃ for 3 hours. Cell were harvested and in order to be lysed, the pellets were resuspended in 500 mM NaCl R buffer. The cleared lysate was then mixed with ammonium sulphate (30% saturation) in order to precipitate the protein. The mixture was then centrifuged, and the pellet fraction was collected and resuspended in 200 mM NaCl R buffer and loaded onto a Q-Sepharose column. Peak fractions eluted at 600 mM NaCl in R buffer were pooled together and diluted 3-fold and applied to HiTrap Heparin column. Peak fractions eluted at 500 mM NaCl were collected and diluted five-fold and applied to HiTrap SP column. Peak fractions eluted at 300 mM NaCl were collected and applied to a Superdex 16/60 200 pg column in 1 M NaCl. Eluted Rad52 sample was dialysed against R buffer containing 100 mM NaCl and afterwards applied to a Resource Q column, where peak fractions eluted at around 250 mM NaCl. Sample was concentrated in an Amicon Ultra-4 Centrifugal Filters 10,000 MWCO (Merck Millipore), flash frozen and stored at -80℃. The concentration was estimated by measuring the A280 and using a molar extinction coefficient of 2.93 x 10^4 M^{-1} cm^{-1}.

2.5.5 Rad54

Rad54 fused to an N-terminal tag—containing a hexahistidine tag, the Fh8 fusion partner (Costa et al., 2013), and a FLAG epitope, with a PreScission protease recognition site between the Fh8 and FLAG components (pBA110; *pET15b-6xHis-Fh8-PreScission-1xFLAG-rad54*$^+$)—was expressed in 20 L of *E. coli* strain BL21

(DE3) Star at an OD of ~0.45 with 1 mM IPTG at 18℃ for ~14h. Cells were harvested by centrifugation, washed with *E. coli* wash solution (50 mM Tris-Cl [pH 7.5], 150 mM NaCl, 1 mM PMSF). Cell pellets were then resuspended in 250 mL of R buffer containing 500 mM NaCl, 5 mM MgOAc, 0.5 mM ATP, 2 mM imidazole, 1 mM DTT, 0.5 mM PMSF, and 0.01% igepal CA-630. Cells were then disrupted by sonication and the lysate was cleared by ultracentrifugation (70,000 g 1h 2℃). The clarified lysate was incubated with 10 mL of cOmplete His-Tag Purification Resin (Roche) with gentle mixing (1 h 4℃). The resin was poured into a glass column (Bio-Rad Econo-column, 2.5 cm x 10 cm) and washed sequentially with the same buffer used for lysis and R buffer containing 500mM NaCl, 5 mM imidazole, 1 mM DTT, and 0.5 mM PMSF. Proteins were then eluted in R buffer containing 300 mM NaCl, 300 mM imidazole, and 0.5 mM TCEP. Eluates were combined, supplemented with PreScission protease (GE Healthcare), and dialyzed against 1 L of the same buffer without imidazole (overnight 4℃). The protein sample was diluted in 2x volumes of R buffer containing 0.5 mM TCEP and applied to a 1 mL HiTrap Q column equilibrated with R buffer containing 100mM NaCl and 0.5 mM TCEP. Rad54, which was found in the flow-through, was then applied to a 1 mL HiTrap Heparin column equilibrated with R buffer containing 100 mM NaCl and 0.5 mM TCEP. Proteins were then eluted with a linear gradient (20 mL 0.1-0.6 M NaCl). Peak fractions containing Rad54 were combined, diluted with 9x volumes of R buffer containing 0.5 mM TCEP, then applied to a 1 mL Resource S column equilibrated with R buffer containing 50 mM NaCl and 0.5 mM TCEP. Proteins were eluted with a linear gradient (20 mL 0.05-0.7M NaCl), then peak fractions were pooled and developed in a 16/60 Superdex 200 PG gel filtration column in R buffer containing 300 mM NaCl and 0.5 mM TCEP. Peak fractions were pooled, diluted with 2x volumes of R buffer containing 0.5 mM TCEP, and applied to a 1 mL

Resource S column. Proteins were eluted with a linear gradient (40 mL 0.1-0.5 M NaCl). Rad54 eluted at ~220 mM NaCl and was subsequently concentrated using a Vivaspin 6 centrifugal concentrator (30,000 MWCO), followed by a flash freeze and storage at -80℃. The concentration was estimated by measuring the A280 and using a molar extinction coefficient of 7.25 x 10^4 M^{-1} cm^{-1}.

2.6 In vitro analysis

2.6.1 Electrophoretic mobility shift assay (EMSA)

Rad51 (wild type, Rad51-E206A, or Rad51-EED) was incubated with 30 μMnt of PhiX174 virion DNA or 20 μMnt of ApaLI-linearized PhiX RFI DNA in EMSA buffer (30mM HEPES-KOH [pH 7.5], 150 mM KCl, 3 mM $MgCl_2$, 2 mM ATP, 1 mM DTT, 5% glycerol). The 10 μL reaction was incubated at 37℃ for 15 min and afterwards, 1.1μl of 2% glutaraldehyde was then added and incubation was continued for a further 5 min at 37℃. 2.5 μL of loading dye was added to the reaction and 3 μL of it was loaded onto a 0.8% agarose gel in TAE buffer and run for 120 min at 50 V. The gel was then stained with SYBR Gold (Thermo Fisher Scientific) and imaged using a LAS4000 mini (GE Healthcare). All DNA concentrations are in micromolar nucleotide (μM nt).

2.6.2 ATPase assay

According to Argunhan *et al* 2020, 5 μM of Rad51 or Rad51-E206A was mixed with 10 μMnt of PhiX174 virion DNA on ice in ATPase buffer (30 mM Tris-Cl [pH 7.5], 100 mM KCl, 3.5 mM $MgCl_2$, 1 mM DTT, 5% glycerol), and either 0.5 μM Swi5-Sfr1 or the equivalent volume of protein storage buffer was added. Reactions were then initiated through the addition of 0.5 mM ATP and 10 μL aliquots were withdrawn at the indicated

timepoints, immediately mixed with 2 µL of 120 mM EDTA and stored at room temperature. The concentration of inorganic phosphate was then measured with a commercial malachite green phosphate detection kit (BioAssay Systems) according to the manufacturer's instructions.

2.6.3 Three-strand exchange assay

Intrinsic

15 µM of Rad51 (wild type, Rad51-E206A, or Rad51-EED) was incubated with 30 µMnt PhiX174 virion DNA (NEB) for 5 min at 37℃ in strand exchange buffer (30 mM Tris-HCl [pH7.5], 1 mM DTT, 150 mM KCl, 3.5 mM $MgCl_2$, 2 mM ATP, 8 mM phosphocreatine, 8 units/mL creatine phosphokinase and 2.5% glycerol). Next, 1 µM of RPA was added to the reaction and after a 5 min incubation, the reaction was initiated with 20 µMnt of PhiX RFI DNA (NEB) linearized with ApaLI.

In the case of the shortened lds (linear double stranded) DNA substrate, a 1.6kb dsDNA fragment was employed instead, and this was prepared by digesting PhiX RFI DNA with both MfeI and XhoI. For timepoint 0, 10 µL was collected immediately after the addition of dsDNA and the remaining reaction was then incubated at 37℃. 10 µL aliquots were subsequently withdrawn at the indicated timepoints (15 min, 30 min, 60 min and 120 min). At each timepoint, samples were supplemented with 1 µL of psoralen (200 µg/mL) and subjected to psoralen-UV crosslinking to capture labile DNA structures. Reactions were then deproteinized through addition of 1.8 µL of stop solution (6.6 mg/mL proteinase K and 2.65% SDS) and incubation at 37℃ for 30 min. 2.5µl of loading dye (15% w/v Ficoll, 0.25% Bromophenol blue, 0.25% Xylene cyanol and 20mM Tris [pH 7.5]) was added to the reactions, and following mixing, 4 µL of the

reaction was loaded and resolved in a 0.8% agarose gel in TAE buffer (50 V 120 min). The gel was then stained with SYBR Gold (Thermo Fisher Scientific) and imaged using a LAS4000 mini (GE Healthcare).

Swi5-Sfr1

In strand exchange assays containing Swi5-Sfr1, 5 μM of Rad51 (wild type, Rad51-E206A, or Rad51-EED) was incubated with 10 μMnt PhiX174 virion DNA (NEB) for 5 min at 37℃ in strand exchange buffer containing 100 mM KCl instead. Next, 0.5 μM of Swi5-Sfr1 (or the indicated concentration) was added and following a 5 min incubation at 37℃, 1 μM of RPA was included. After a further 5 min at 37℃, the reaction was initiated with 10 μMnt of PhiX RFI DNA (NEB) linearized with ApaLI and incubated for 120 min at 37℃. Subsequent procedures were carried out as described above.

Rad54

In strand exchange assays containing Rad54, 7 μM of Rad51 (wild type, Rad51-E206A, or Rad51-EED) was incubated with 7 μMnt PhiX174 virion DNA (NEB) for 8 min at 37℃ in strand exchange buffer with 100 mM KCl instead. Next, 0.7 μM RPA was added and incubation was continued at 37℃ for 8 min. The reaction was then initiated with 14 μMnt of the shortened lds (described above) and immediately supplemented with the indicated concentration of Rad54. Incubation was continued for 120 min at 37℃ and subsequent procedures were carried out as described above.

Quantification was performed based on Haruta et al. (2006) except that FIJI software was employed (Schindelin et al., 2012). Briefly, background was subtracted using the rolling ball method, the signal corresponding to lds, NC/PD, and (JM/1.5) in a given lane was summed and set equal to 100%, and the signal for NC/PD and/or JM was expressed as a percentage of this.

2.6.4 In vitro IP

Purified proteins (250 nM each) were mixed together on ice in IP buffer (30 mM Tris-Cl [pH 7.5], 150 mM NaCl, 3.5 mM $MgCl_2$, 0.1% igepal CA-630, 0.25 mM TCEP, 1 mM ATP, 5% glycerol), input sample is taken and the rest of the reaction is incubated at 30℃ for 15 min. Reactions were then incubated on ice for 5 min and supplemented with either anti-FLAG M2 affinity agarose gel (Sigma-Aldrich) for IP of Rad54 or Dynabeads Protein A (ThermoFisher Scientific) preincubated with anti-Sfr1, anti-Rad51, or anti-Rad52 antibodies (Haruta et al., 2006; Kurokawa et al., 2008). Following mixing at 4℃ for 1.5 h, the beads were washed once with IP buffer and eluted in 1x SDS loading buffer (IP sample). Proteins were then separated by SDS-PAGE and detected by immunoblotting with anti-Rad51 (rat 1:10,000; Argunhan et al., 2020), anti-Sfr1 (mouse 1:200; Argunhan et al., 2020), anti-FLAG (mouse 1:10,000; Sigma-Aldrich F3165), or anti-Rad52 (rabbit 1:10,000; Kurokawa et al., 2008) antibodies. FIJI software (Schindelin et al., 2012) was used for quantification of in vitro IPs. Briefly, background subtraction was performed by the rolling ball method and the signal for IP'd and co-IP'd protein was quantified. The co-IP'd signal was then divided by the IP'd signal and expressed relative to wild type. Graphs were prepared using GraphPad Prism (version 8).

2.7 Sequence alignments and structural models

Sequence alignments were prepared using Clustal Omega (UniProt identifiers are: *S. pombe*, P36601; *S. cerevisiae*, P25454; *U. maydis*, Q99133; *C. elegans*, G5EGG8; *D. melanogaster*, Q27297; *G. gallus*, P37383; *M. musculus*, Q08297; *H. sapiens*, Q06609). All structural depictions were prepared using UCSF Chimera (Pettersen et al., 2004). The Coulombic Surface Coloring feature in UCSF Chimera was employed to depict surface charge. Monomer model of an *Sp*Rad51 was generated using Phyre2 software (intensive mode; Kelley et al., 2015) based on two known structures of *Sc*Rad51 (Conway et al., 2004; Chen et al., 2010), with Protein databank (PDB) identifiers 1SZP and 3LDA; and one known structure of *Hs*Rad51 (Short et al., 2016) with PDB identifier 5JZC. 46 residues (1-41 and 361-365) of the *Sp*Rad51 monomer with low homology to *Sc*Rad51 and *Hs*RAD51 were modelled ab initio and therefore, these low confidence regions were omitted from the model. The *Sp*Rad51-ssDNA filament model consisting of three monomers is a homology model that was described previously by Ito et al. (2020). This structure was previously deposited in the Biological Structure Model Archive (identification code BSM00017). The structure of Rad51-EED was analyzed by substituting E205, E206, and D209 to Ala through the Rotamer feature.

The *Hs*Rad51-ssDNA filament shown is the structure resolved by cryo-electron microscopy (Xu et al., 2017; PDB 5H1B), whereas the *Sc*Rad51-ssDNA filament shown is the structure solved by X-ray crystallography (Conway et al., 2004; PDB 1SZP, chains E and F). Note that ssDNA density is missing from the structure of the *Sc*Rad51-ssDNA filament model, despite the formation of crystals in the presence of ssDNA (Conway et al., 2004). The structure of the *Pyrococcus furiosus* RadA polymer was solved by X-ray crystallography (Shin et al., 2003; PDB 1PZN, chains G, A, and

B). The RecA monomer (Story et al., 1992; PDB 2REB) and ssDNA filament (Chen et al., 2008; 3CMU) structures were solved by X-ray crystallography.

Chapter 3: Identification of the PAP (Protruding Acidic Patch) in Schizosaccharomyces pombe Rad51

3.1 Research objectives

It is known that each auxiliary factor has a non-overlapping, distinct role, and they can all physically interact with Rad51. However, it is not known how this interaction takes place. To learn more about the relationship between Rad51 and its auxiliary factors, I sought to identify regions of Rad51 that are important for interactions with auxiliary factors.

3.2 Results

3.2.1 The PAP is situated on the opposite face of the *Sp*Rad51 ATPase core domain

Several motifs important for the enzymatic activity of Rad51 are located in the highly conserved ATPase core domain, which is characterized by a β-sheet consisting of mixed parallel and antiparallel β-strands (Story et al., 1992; Pellegrini et al., 2002; Shin et al., 2003; Conway et al., 2004). These include the Walker A and B motifs, which are important for ATP binding and hydrolysis (Saraste et al., 1990; Story & Steitz, 1992), and two DNA binding sites: Site 1, which is comprised of Loop 1 and Loop 2, and Site 2 (Howard-Flanders et al., 1984; Story et al., 1992). Initial examination of a homology (computational) model of *S. pombe* Rad51 (*Sp*Rad51, and equivalent notation hereafter) revealed that the surface of these regions is enriched in positive charge, consistent with their roles in ATP and DNA binding (**Figure 3.2.1A**, left). By contrast, on the opposite face of *Sp*Rad51, mostly negatively charged regions were found.

Additionally, I noticed a protruding acidic patch (PAP) with the most negative charge density (**Figure 3.2.1A**, right).

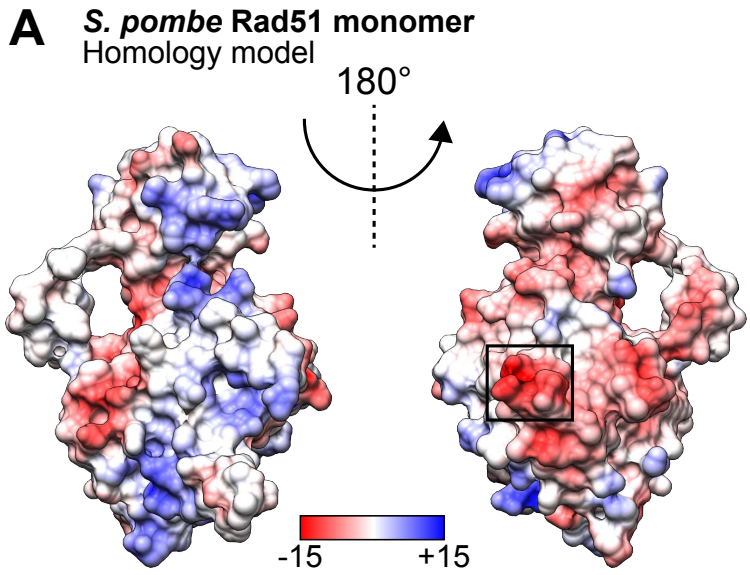

A
S. pombe Rad51 monomer
Homology model
180°
-15
+15

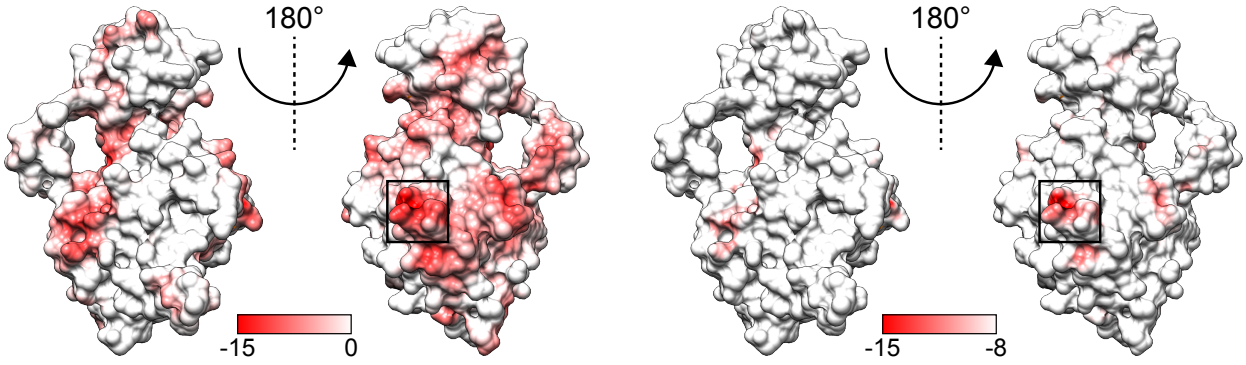
Figure 3.2.1. Depiction of the PAP location on an *Sp*Rad51 monomer

Homology model of an *Sp*Rad51 monomer (residues 42-360). Surface representation coloured according to Coulombic surface charge. The molecule on the left is rotated 180° to visualise the PAP on the right, with the region of interest squared. Numbers on the legend are in units of kcal/(mol•*e*).

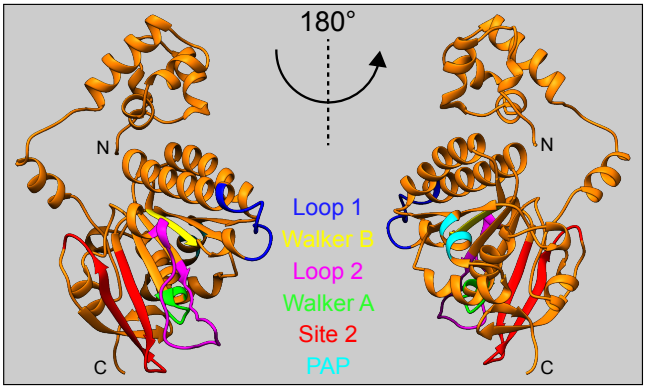
3.2.2 The PAP is comprised of E205, E206, and D209 residues

The PAP seems to be among the most negatively charged regions on the surface of *Sp*Rad51 (**Figure 3.2.2A** left panel). By changing the parameters of colouring even further, it became apparent that the PAP is likely the most negatively charged region (**Figure 3.2.2A** right panel). The PAP is situated on a short α-helix preceding the outermost β-strand of the central β-sheet (**Figure 3.2.2B**). Closer analysis of the homology model shows three acidic residues projecting out from this α-helix (**Figure 3.2.2C**), which were identified as E205, E206, and D209. Furthermore, sequence alignment revealed that the corresponding region in *Sc*Rad51 and *Hs*Rad51 shows some conservation (**Figure 3.2.2D**).

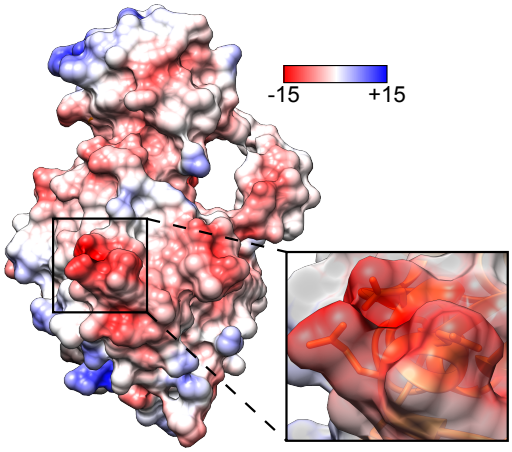
A ***S. pombe*** **Rad51 monomer**
Homology model



B ***S. pombe*** **Rad51 monomer**
Homology model



C ***S. pombe*** **Rad51 monomer**
Homology model



D ***S. pombe*** **Rad51 monomer**
Homology model

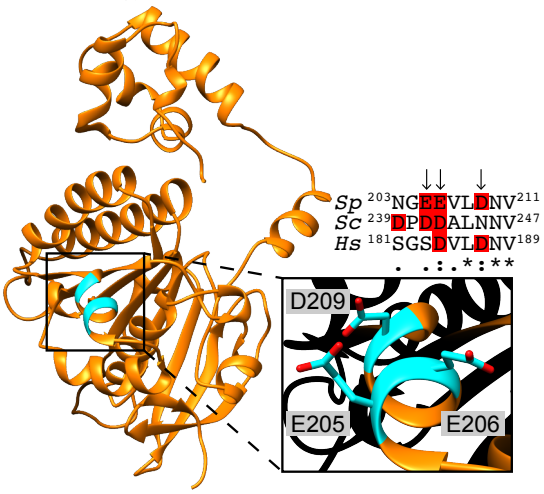


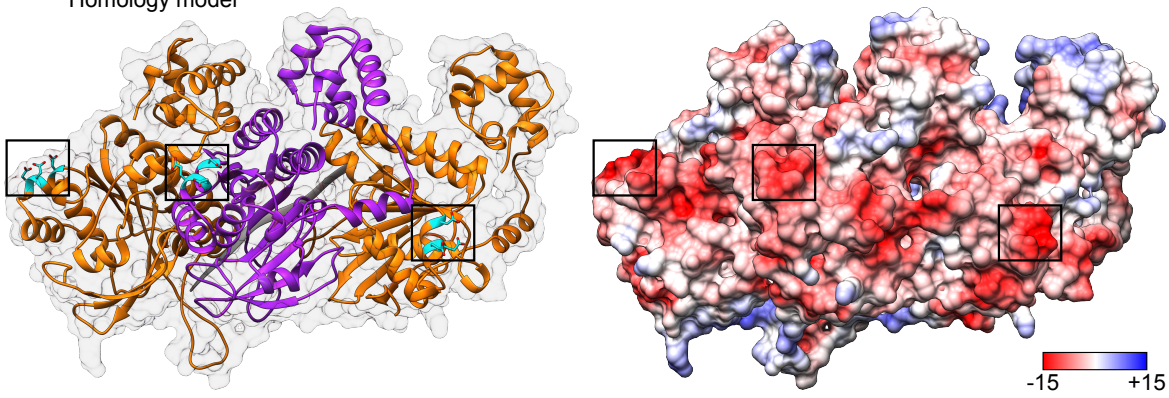
Figure 3.2.2. PAP is comprised of three acidic residues

(A) Surface representation of an *Sp*Rad51 monomer coloured according to Coulombic surface charge. The squared region forms a protruding acidic patch (PAP) that is among the most negatively charged regions on the surface of *Sp*Rad51. **(B)** Ribbon depiction of an *Sp*Rad51 monomer with relevant motifs highlighted. The molecules are oriented as in **Fig 3.2.1A**. **(C)** Surface representation coloured according to Coulombic surface charge. The PAP is enlarged with a semi-transparent surface revealing residues E205, E206, and D209, which have their side-chains shown. **(D)** Ribbon depiction of *Sp*Rad51 with the α-helix containing the PAP enlarged to illustrate the respective positions of each residue (coloured in cyan) with their side-chains revealed (O atoms in red). Sequence alignment shows the corresponding region in *S. pombe*, *S. cerevisiae* and *H. sapiens* (*Sp*, *Sc*, and *Hs*, respectively), with arrows indicating PAP residues in *S. pombe* and acidic residues highlighted in red. Numbers in legends of **(A, C)** are in units of kcal/(mol•*e*).

3.2.3 The PAP is on the exterior of the Rad51 presynaptic filament

E205, E206 and D209 were also examined in the context of a previously published homology model of the *Sp*Rad51 presynaptic filament (Ito et al., 2020) and found to form acidic patches constituting dense negatively charged regions on the exterior of the filament (**Figure 3.2.3A**). The equivalent α-helix in the *Hs*Rad51 presynaptic filament — the structure of which was determined by cryo-electron microscopy (Xu et al., 2017) — also had a negative surface charge (**Figure 3.2.3B**), as did the corresponding α-helix in the *Sc*Rad51 presynaptic filament (**Figure 3.2.3C**) — the structure of which was determined by X-ray crystallography (Conway et al., 2004). While E205 was replaced with a conservative Asp residue in *Sc*Rad51 and D209 was conserved in *Hs*Rad51, E206 is the only PAP residue that showed conservation in both *Sc*Rad51 and *Hs*Rad51 (**Figure 3.2.2D**). Thus, I initially focused on E206 for functional analysis, which will be described in the next chapter.

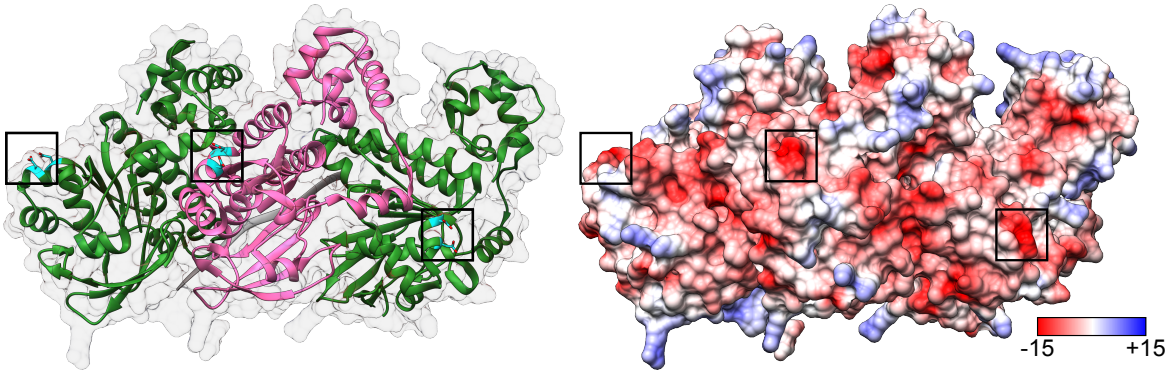
A ***S. pombe*** **Rad51-ssDNA filament**
Homology model



B

```
SpRad51 201GLNGEEVLDNVAY213
ScRad51 237GLDPDDALNNVAY249
HsRad51 179GLSGSDVLDNVAY191
          **. .:.*:****
```

H. sapiens **Rad51-ssDNA filament**
Cryo-electron microscopy structure (PDB 5H1B)



C

```
SpRad51 201GLNGEEVLDNVAY213
ScRad51 237GLDPDDALNNVAY249
HsRad51 179GLSGSDVLDNVAY191
          **. .:.*:****
```

S. cerevisiae **Rad51-ssDNA filament**
X-ray crystallography structure (PDB 1SZP)

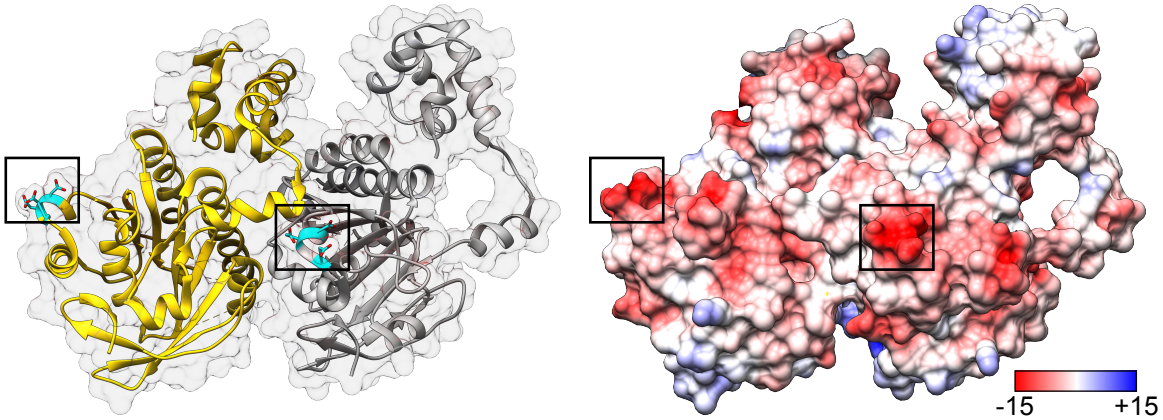


Figure 3.2.3. PAP is conserved in *H. sapiens* and *S. cerevisiae*

(A) Ribbon depiction of three *Sp*Rad51 monomers (alternating orange and purple) bound to ssDNA (9-mer poly-dT in grey) with a near-transparent surface for visualization (left). The side-chains of E205, E206, and D209 are revealed in cyan (O atoms in red) and their positions are squared. The surface is made opaque and coloured according to Coulombic surface charge to demonstrate that the PAP constitutes dense, negatively charged regions on the exterior of the presynaptic filament (right). **(B)** Ribbon depiction of three *Hs*Rad51 monomers (alternating green and pink) bound to ssDNA (9-mer poly-dT in grey) with a near-transparent surface (left). The side-chains of residues indicated in the sequence alignment are revealed in cyan (O atoms in red) and their positions are highlighted by squares. The surface is made opaque and coloured according to Coulombic surface charge to demonstrate that these residues constitute negatively charged patches on the exterior of the presynpatic filament (right). In the sequence alignment, arrows indicate PAP residues in *S. pombe* and acidic residues are highlighted in red. **(C)** Ribbon depiction of two *Sc*Rad51 monomers (yellow and grey) with a near-transparent surface (left) bound to ssDNA (not shown). The side-chains of residues indicated in the sequence alignment are revealed in cyan (O atoms in red) and their positions are highlighted by squares. The surface is made opaque and coloured according to Coulombic surface charge to demonstrate that these residues constitute negatively charged patches on the exterior of the presynaptic filament (right). In the sequence alignment, arrows indicate PAP residues in *S. pombe* and acidic residues are highlighted in red. Numbers in the legends of **(A-C)** are in units of kcal/(mol•*e*).

3.2.4 Evolutionary conservation of the PAP

Because negatively charged regions were seen in the equivalent α-helices of both *Sc*Rad51 and *Hs*Rad51 (**Figure 3.2.3B, C**), I sought to further examine the evolutionary conservation of the PAP. Sequence alignments suggest that the PAP is widely conserved among eukaryotes, with residues E206 and D209 each showing conservation in seven-out-of-eight eukaryotic Rad51 orthologs (**Figure 3.2.4A**). Interestingly, examination of a structural model revealed conservation of the PAP in Dmc1, the meiosis-specific RecA-family recombinase (**Figure 3.2.4B**). The archaeal RadA polymer also exhibited substantial structural conservation of the PAP (**Figure 3.2.4C**). By contrast, this region showed poor sequence conservation in bacterial RecA, and although a short α-helix at the equivalent position appeared to exist in the RecA monomer (**Figure 3.2.4D**), a loop was seen instead in the RecA presynaptic filament structure (**Figure 3.2.4E**). Furthermore, the negative charge of this region was partially due to the close proximity of residues E32 and D33 from the adjacent RecA monomer. I interpret these analyses to mean that the PAP is conserved in eukaryotic Rad51/Dmc1 and archaeal RadA, but not in bacterial RecA.

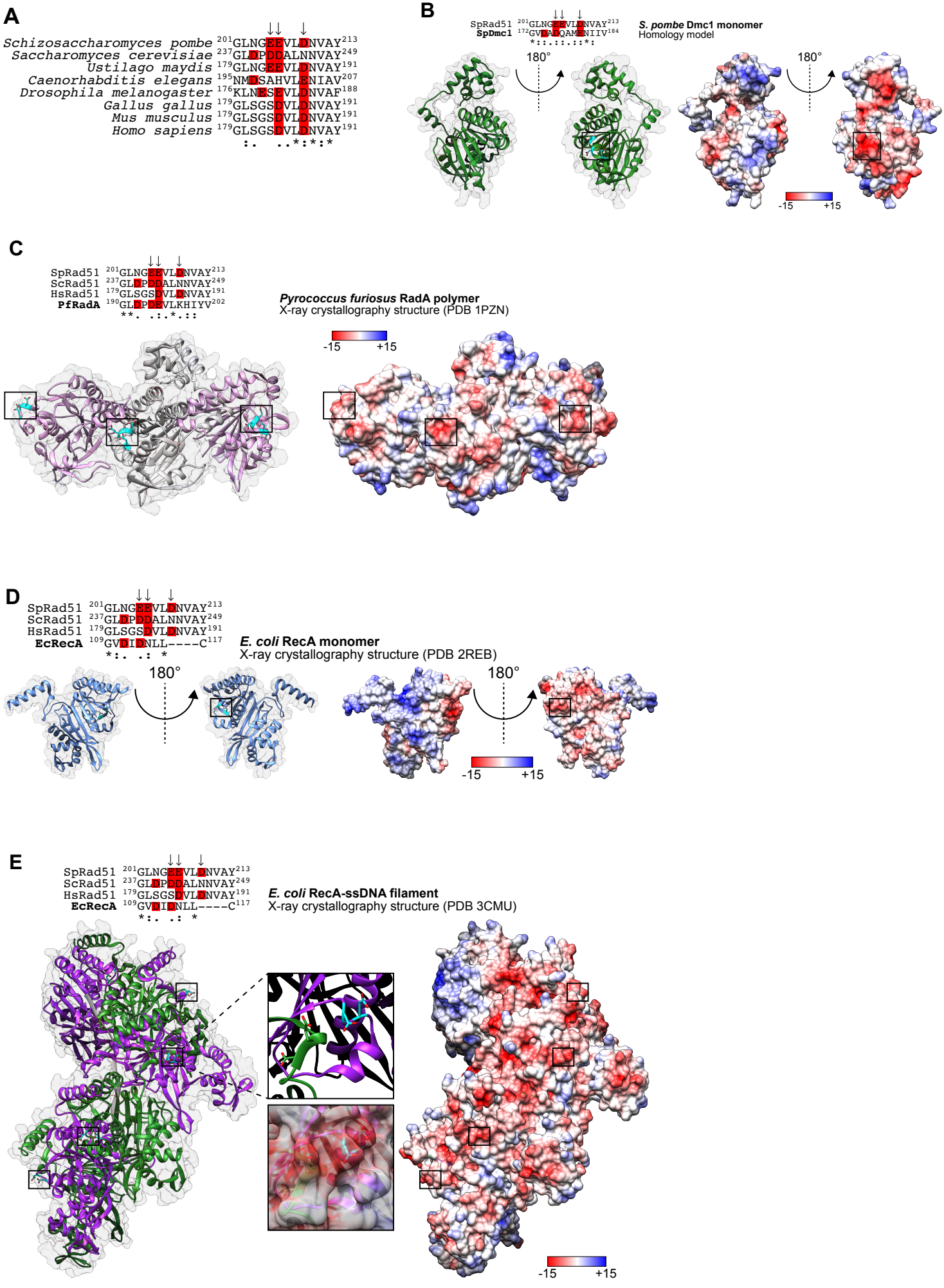

A
Schizosaccharomyces pombe 201GLNGEEVLDNVAY213
Saccharomyces cerevisiae 237GLDPDDALNNVAY249
Ustilago maydis 179GLNGEEVLDNVAY191
Caenorhabditis elegans 195NMDSAHVLENIAV207
Drosophila melanogaster 176KLNDSEVLDNVAF188
Gallus gallus 179GLSGSDVLDNVAY191
Mus musculus 179GLSGSDVLDNVAY191
Homo sapiens 179GLSGSDVLDNVAY191
B
SpRad51 201GLNGEEVLDNVAY213
SpDmc1 172GVDADQAMENIIV184
S. pombe Dmc1 monomer
Homology model
180°
180°
-15
+15
C
SpRad51 201GLNGEEVLDNVAY213
ScRad51 237GLDPDDALNNVAY249
HsRad51 179GLSGSDVLDNVAY191
PfRadA 190GLDPDEVLKHIYV202
Pyrococcus furiosus RadA polymer
X-ray crystallography structure (PDB 1PZN)
-15
+15
D
SpRad51 201GLNGEEVLDNVAY213
ScRad51 237GLDPDDALNNVAY249
HsRad51 179GLSGSDVLDNVAY191
EcRecA 109GVDIDNLL----C117
E. coli RecA monomer
X-ray crystallography structure (PDB 2REB)
180°
180°
-15
+15
E
SpRad51 201GLNGEEVLDNVAY213
ScRad51 237GLDPDDALNNVAY249
HsRad51 179GLSGSDVLDNVAY191
EcRecA 109GVDIDNLL----C117
E. coli RecA-ssDNA filament
X-ray crystallography structure (PDB 3CMU)
-15
+15

Figure 3.2.4. PAP is conserved in eukaryotic Dmc1 and archaeal RadA

(A) Sequence alignment of Rad51 from the indicated eukaryotic species. Arrows indicate PAP residues in *S. pombe* and acidic residues are highlighted in red. **(B)** Homology model of an *Sp*Dmc1 monomer (residues 15-332). Ribbon depictions (left) are in the same orientation as the surface representation coloured according to Coulombic surface charge (right). In each case, the molecule on the left is rotated 180° to visualise the protruding acidic patch (PAP) on the right, with the region of interest squared. The side-chains of residues indicated in the sequence alignment are revealed in cyan (O atoms in red) and their positions are highlighted by squares. In the sequence alignment, arrows indicate PAP residues in *S. pombe* and acidic residues are highlighted in red. **(C)** Ribbon depiction of three *Pyrococcus fusiosus* RadA monomers (alternating pink and grey) with a near-transparent surface (left). The side-chains of residues indicated in the sequence alignment are revealed in cyan (O atoms in red) and their positions are highlighted in squares. The surface is made opaque and coloured according to Coulombic surface charge to demonstrate that these residues constitute negatively charged patches (right). In the sequence alignment, arrows indicate PAP residues in *S. pombe* and acidic residues are highlighted in red. **(D)** Ribbon depictions of the *E. coli* RecA monomer (left) are in the same orientation as the surface representation coloured according to Coulombic surface charge (right). In each case, the molecule on the left is rotated 180° to visualise the equivalent of the protruding acidic patch (PAP) on the right, with the region of interest squared. The side-chains of residues indicated in the sequence alignment are revealed in cyan (O atoms in red) and their positions are highlighted by squares. In the sequence alignment, arrows indicate PAP residues in *S. pombe* and acidic residues are highlighted in red. **(E)** Ribbon depiction of six *E. coli* RecA monomers

(alternating purple and green) with a near-transparent surface (left) bound to ssDNA (15-mer poly-dT in grey). The side-chains of residues indicated in the sequence alignment are revealed in cyan (O atoms in red) and their positions in four monomers are highlighted in squares. One such region is enlarged to demonstrate that the indicated residues form a loop rather than the short α-helix observed in the monomer structure in **(D)**. The surface is made opaque and coloured according to Coulombic surface charge to demonstrate that these residues nevertheless constitute negatively charged patches on the exterior of the ssDNA filament (right), although closer examination reveals that this is partly due to two acidic residues in the adjacent monomer (shown enlarged). In the sequence alignment, arrows indicate PAP residues in *S. pombe* and acidic residues are highlighted in red. Numbers in the legends of **(B-E)** are in units of kcal/(mol•*e*).

Chapter 4: In vivo and In vitro analysis of Rad51-E206A

4.1 Research objectives

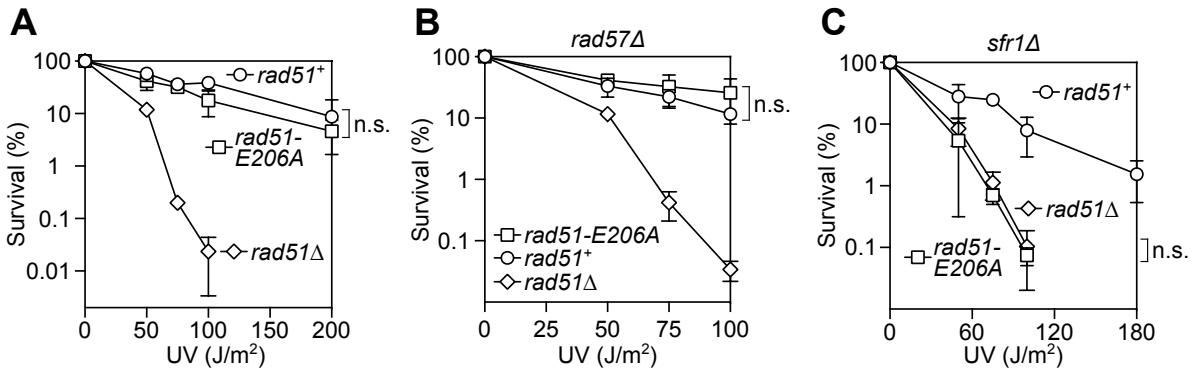
Because E206 is the only residue of the PAP that is conserved in both *Sc*Rad51 and *Hs*Rad51, I first focused my attention on this residue. To assess the importance of this residue, it was mutated to Ala (Rad51-E206A) and both in vivo and in vitro analyses were conducted. These analyses are described here.

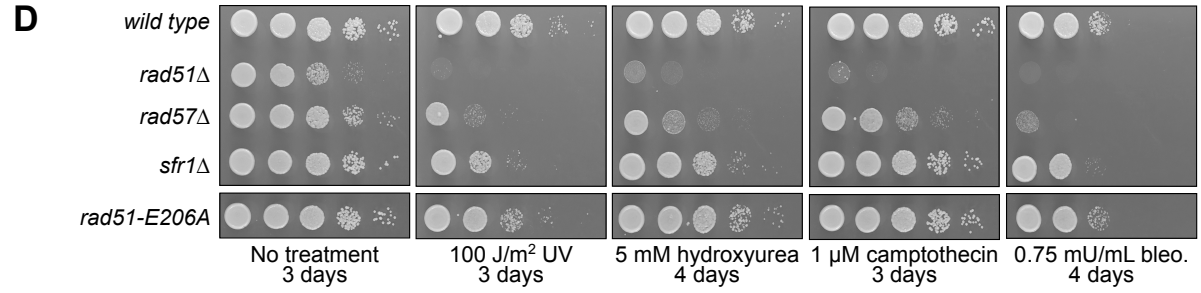
4.2 Results

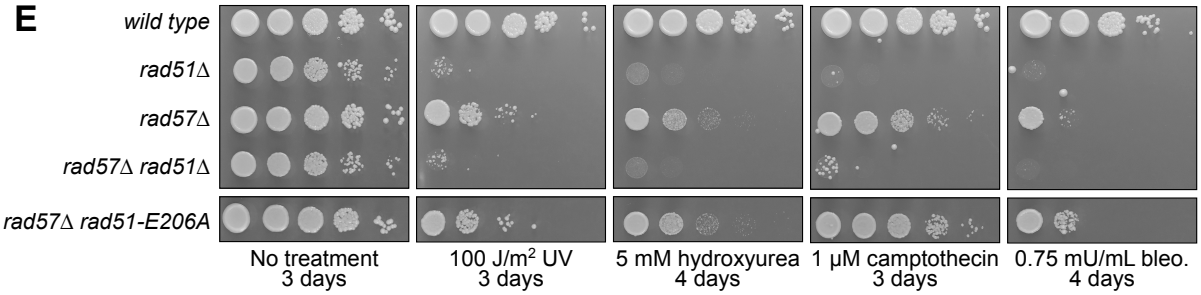
4.2.1 *rad51-E206A* is defective for DNA repair that is promoted by Rad55-Rad57

HR plays a particularly important role in the repair of ultraviolet light (UV)-induced DNA damage in *S. pombe* due to the existence of a UV damage endonuclease pathway (Yasui, 2013). An *S. pombe* strain containing the *rad51-E206A* mutation at the native locus was constructed to test if this mutation affects DNA repair. *rad51-E206A* showed the same resistance to UV-induced DNA damage as wild type in a clonogenic survival assay (**Figure 4.2.1A**), suggesting that this mutation does not affect the intrinsic ability of Rad51 to repair DNA. In the *rad57*Δ*/rad55*Δ background, Rad51-mediated HR is reduced but not abolished, and this remaining recombinational DNA repair is dependent on Swi5-Sfr1. There is a similar reduction in recombinational DNA repair in the *sfr1*Δ*/swi5*Δ background, where the remaining Rad51-mediated HR is dependent on Rad55-Rad57. However, the *rad57*Δ *sfr1*Δ double mutant displays a complete loss of Rad51-mediated DNA repair, phenocopying *rad51*Δ. Thus, employing the *rad57*Δ and *sfr1*Δ backgrounds allow for the evaluation of DNA repair promoted by Swi5-Sfr1 and Rad55-Rad57, respectively (Akamatsu et al., 2003). The

*rad51-E206A rad57*Δ strain was no more sensitive to UV than *rad57*Δ (**Figure 4.2.1B**), suggesting that Rad51-E206A is as proficient as wild-type Rad51 in Swi5-Sfr1–dependent DNA repair. By contrast, *rad51-E206A* was as sensitive as *rad51*Δ in the absence of Sfr1 (**Figure 4.2.1C**), indicating that the recombinational DNA repair promoted solely by Rad55-Rad57 is ablated by the Rad51-E206A mutation. The generality of these findings was confirmed by performing spot tests with several different genotoxins that induce replication fork stalling and a variety of DNA lesions. As it can be seen in **Figure 4.2.1D**, *rad51-E206A* exhibits the same resistance as wild type in response to other types of DNA damaging agents. Consistent with results from the clonogenic survival assay (**Figure 4.2.1B**), *rad51-E206A rad57*Δ shows comparable sensitivity to *rad57*Δ (**Figure 4.2.1E**). Moreover, in the absence of Sfr1, *rad51-E206A* was as sensitive as *rad51*Δ in response to all DNA damaging agents (**Figure 4.2.1F**), providing further evidence that Rad51-E206A is defective for the interaction with Rad55-Rad57.


A
B
C
rad57Δ
sfr1Δ
rad51+
rad51-E206A
rad51Δ
n.s.
Survival (%)
UV (J/m2)


D
wild type
rad51Δ
rad57Δ
sfr1Δ
rad51-E206A
No treatment 3 days
100 J/m2 UV 3 days
5 mM hydroxyurea 4 days
1 μM camptothecin 3 days
0.75 mU/mL bleo. 4 days


E
wild type
rad51Δ
rad57Δ
rad57Δ rad51Δ
rad57Δ rad51-E206A
No treatment 3 days
100 J/m2 UV 3 days
5 mM hydroxyurea 4 days
1 μM camptothecin 3 days
0.75 mU/mL bleo. 4 days

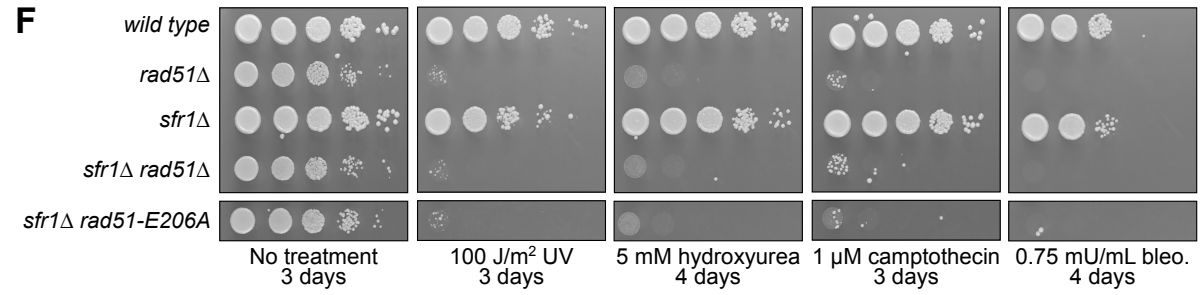

F
wild type
rad51Δ
sfr1Δ
sfr1Δ rad51Δ
sfr1Δ rad51-E206A
No treatment 3 days
100 J/m2 UV 3 days
5 mM hydroxyurea 4 days
1 μM camptothecin 3 days
0.75 mU/mL bleo. 4 days

Figure 4.2.1. *rad51-E206A* exhibits sensitivity to DNA damage only in the *sfr1Δ* background

(A-C) Following acute UV irradiation, a clonogenic assay was employed to test the survival of *rad51*$^{+}$, *rad51-E206A,* and *rad51*Δ in the wild-type background **(A)**, the *rad57*Δ background **(B)**, and the *sfr1*Δ background **(C)**. Statistical significance at the highest dose of UV was assessed by unpaired two-tailed t-test. n.s., not significant (**A**, $p = 0.506$; **B**, $p = 0.242$; **C**, $p = 0.593$). **(D-F)** 10-fold serial dilutions of each strain were spotted onto standard media containing DNA damaging agents, or onto standard media with or without acute UV exposure, as indicated. Following growth at 30°C for the indicated time, plates were imaged. Although cropped separately from other strains, the respective *rad51-E206A* strains were spotted onto the same plate in each case. Bleo., bleomycin.

Data in **(A-C)** are means of three independent experiments and error bars depict standard deviation.

4.2.2 *rad51-E206A* is specifically defective for interaction with Rad55-Rad57

The DNA damage sensitivity of *sfr1*Δ *rad51-E206A* is comparable in severity to *rad51*Δ, which itself shows similar sensitivity to *rad57*Δ *sfr1*Δ and *rad54*Δ (Muris et al., 1997; Akamatsu et al., 2003). The *rad52*Δ mutant is even more sensitive to DNA damage, although this added sensitivity stems from Rad51-independent roles of Rad52 (Doe et al., 2004); a mutation that abolishes the interaction between Rad51 and Rad52 would be expected to phenocopy *rad51*Δ, not *rad52*Δ. Thus, it is possible that the DNA damage sensitivity associated with *rad51-E206A*, which manifests in the *sfr1*Δ background, reflects a defect in the interaction of Rad51 with Rad52 or Rad54, rather than with Rad55-Rad57. I sought to distinguish between these possibilities genetically. Rqh1 is a RecQ-family helicase (homologous to Sgs1 in *S. cerevisiae* and the BLM and WRN helicases in humans) that functions in S phase to prevent the accumulation of toxic recombination intermediates that arise during DNA replication (Murray et al., 1997; Stewart et al., 1997). Accordingly, *rqh1*Δ cells are sensitive to the ribonucleotide reductase inhibitor hydroxyurea (HU). It was previously shown that *rad57*Δ and *sfr1*Δ robustly suppress the HU sensitivity of *rqh1*Δ whereas *rad52*Δ and *rad54*Δ do not, presumably because the former mutations reduce HR while the latter mutations eliminate it completely (Hope et al., 2005). If Rad51-E206A is defective in the interaction with Rad55-Rad57 rather than Rad52/Rad54, then the *rqh1*Δ *rad51-E206A* strain should phenocopy *rqh1*Δ *rad57*Δ rather than *rqh1*Δ *rad52*Δ*/rad54*Δ. Consistently, *rad51-E206A* suppressed the HU sensitivity of *rqh1*Δ to almost the same degree as *rad57*Δ (**Figure 4.2.2A**). Furthermore, the suppression conferred by *sfr1*Δ, which is dependent on Rad55-Rad57 (Hope et al., 2005), was ablated by *rad51-E206A*. By contrast, the suppression imparted by *rad57*Δ was epistatic to *rad51-E206A*, suggesting that they involve the same mechanism. At 5 mM HU, *rad57*Δ *sfr1*Δ

could partially suppress *rqh1*Δ sensitivity, whereas *rad51*Δ and *rad54*Δ could not. Importantly, the *sfr1*Δ *rad51-E206A* strain was still similar to *rad57*Δ *sfr1*Δ, strongly suggesting that the defect associated with *rad51-E206A* is related to Rad55-Rad57.

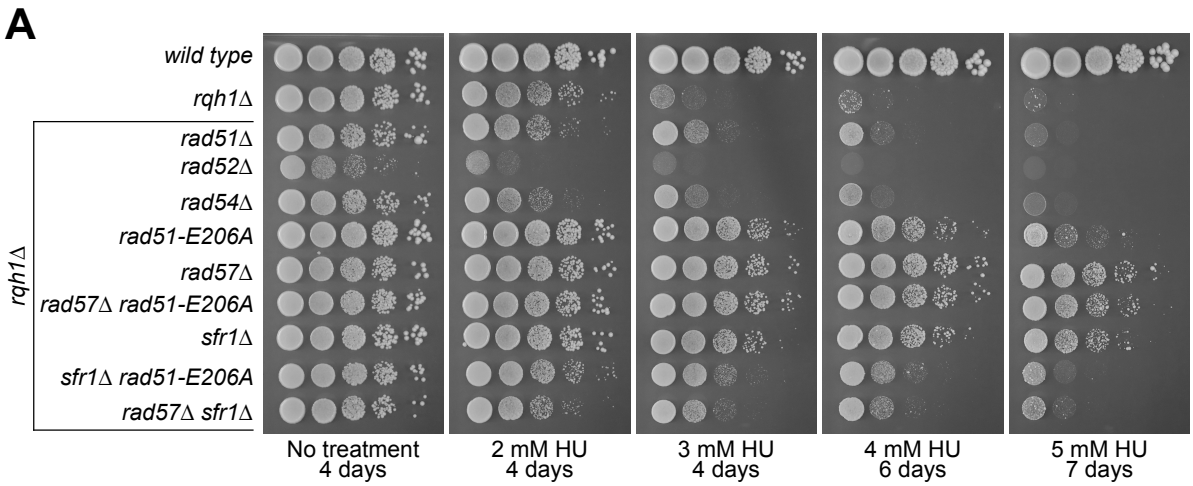
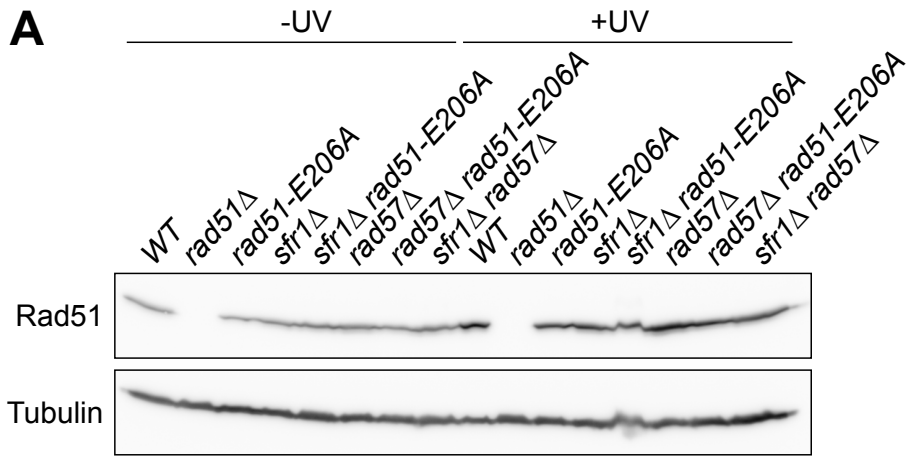

A
wild type
rqh1Δ
rad51Δ
rad52Δ
rad54Δ
rad51-E206A
rad57Δ
rad57Δ rad51-E206A
sfr1Δ
sfr1Δ rad51-E206A
rad57Δ sfr1Δ
rqh1Δ
No treatment
4 days
2 mM HU
4 days
3 mM HU
4 days
4 mM HU
6 days
5 mM HU
7 days

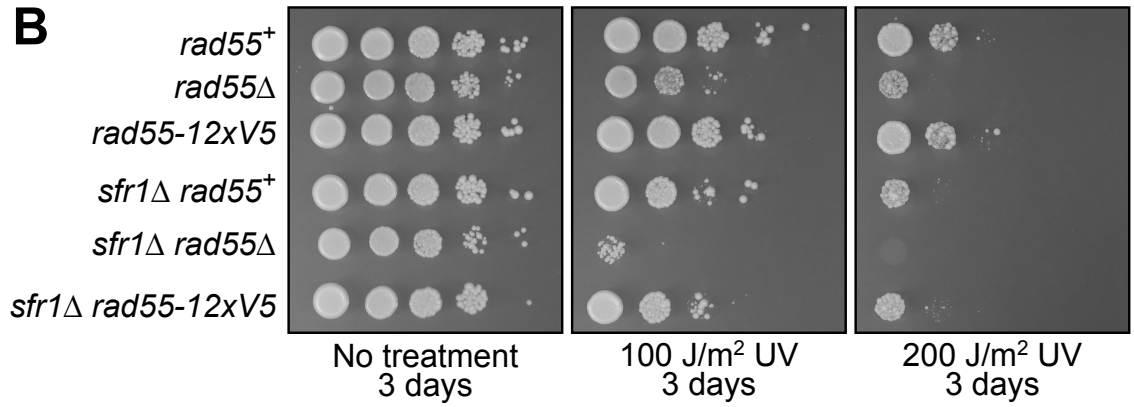
Figure 4.2.2. Rad55-Rad57–dependent DNA repair is impaired in *rad51-E206A* mutant background

(A) 10-fold serial dilutions of the indicated strains were spotted onto standard media without treatment or containing hydroxyurea (HU). Following growth for the indicated time at 30°C, plates were imaged.

4.2.3 Rad51-E206A forms a less stable complex with Rad55-Rad57 in vivo

The expression of Rad51-E206A from the native locus was assessed and found to be similar to wild type (**Figure 4.2.3A**), suggesting that the DNA repair defect of *rad51-E206A* is not caused by reduced protein stability. Previous studies involving yeast two-hybrid (Y2H) analysis has suggested that Rad51 can physically interact with Rad55-Rad57 (Tsutsui et al., 2001). Therefore, a feasible explanation for DNA damage sensitivity of *rad51-E206A* is that the E206A mutation disrupts the physical interaction between Rad51 and Rad55-Rad57. In order to conduct an *in vivo* co-immunoprecipitation (co-IP) experiment, a sequence encoding 12 copies of the V5 epitope was fused to *rad55*$^{+}$ at its native locus, yielding the *rad55-12xV5* strain. This strain was as resistant to DNA damage as the untagged wild type (*rad55*$^{+}$; **Figure 4.2.3B**), indicating that the tag does not interfere with the function of Rad55-Rad57 in DNA repair. Subsequently, co-IP experiments were performed in both *sfr1*$^{+}$ and *sfr1*Δ backgrounds. While robust signal was observed for wild-type Rad51, substantially less Rad51-E206A was seen to co-IP with Rad55 (**Figure 4.2.3C**), indicating that the E206A mutation impairs Rad51–Rad55-Rad57 complex formation. The presence of Sfr1 did not have an effect on complex formation, irrespective of the E206A mutation. These results suggest that the DNA repair defect associated with *rad51-E206A* is related to impaired Rad51–Rad55-Rad57 complex formation and that the suppression of this DNA damage sensitivity by Swi5-Sfr1 is not through enhancing physical binding.


A
-UV
+UV
WT
rad51Δ
rad51-E206A
sfr1Δ
sfr1Δ rad51-E206A
rad57Δ
rad57Δ rad51-E206A
sfr1Δ rad57Δ
WT
rad51Δ
rad51-E206A
sfr1Δ
sfr1Δ rad51-E206A
rad57Δ
rad57Δ rad51-E206A
sfr1Δ rad57Δ
Rad51
Tubulin


B
rad55+
rad55Δ
rad55-12xV5
sfr1Δ rad55+
sfr1Δ rad55Δ
sfr1Δ rad55-12xV5
No treatment
3 days
100 J/m2 UV
3 days
200 J/m2 UV
3 days

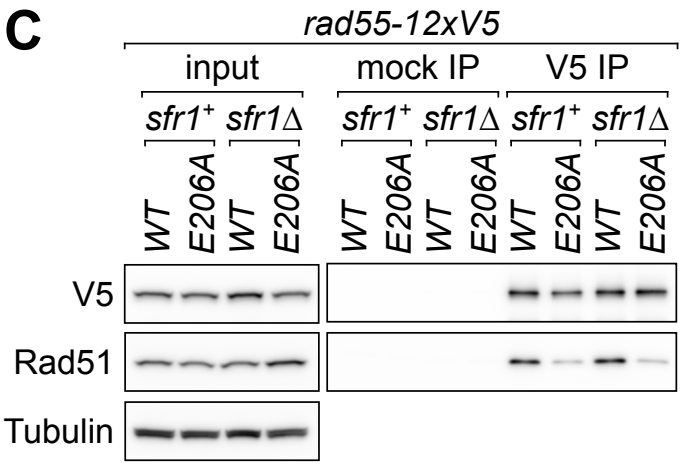

C
rad55-12xV5
input
mock IP
V5 IP
sfr1+
sfr1Δ
WT
E206A
V5
Rad51
Tubulin

Figure 4.2.3. E206A mutation rendered a reduction in Rad51 and Rad55-Rad57 in vivo complex formation

(A) The indicated strains were grown to log-phase, at which point cultures were split into two. One sub-culture was left untreated, and the other was UV-irradiated (200 J/m^2). Following recovery for 3 hours at 30°C, cellular levels of Rad51 were examined by immunoblotting. Tubulin serves as a loading control. **(B)** 10-fold serial dilutions of each strain were spotted onto standard media with or without acute UV exposure, as indicated. Following growth at 30°C for the indicated time, plates were imaged. **(C)** Soluble cell extracts treated with a benzonase-like nuclease were prepared from each strain under native conditions (input). Immunoprecipitation (IP) was then performed with mock (human IgG from non-immunized animal) or anti-V5 antibodies. Tubulin serves as a loading control.

4.2.4 Rad51-E206A retains normal recombinase activity and can be stimulated by Swi5-Sfr1

Although E206 does not belong to a canonical motif involved in ATP hydrolysis or DNA binding, it remained formally possible that the E206A mutation impaired the enzymatic activity of Rad51. Rad51-E206A was therefore purified to homogeneity from *E. coli* to investigate its biochemical properties (**Figure 4.2.4A**). First, the DNA binding abilities of Rad51-E206A was measured through the electrophoretic mobility shift assay (EMSA). Rad51-E206A shifted both ssDNA and dsDNA to a similar extent as wild-type Rad51 in both EMSAs (**Figure 4.2.4B, C**), suggesting that the E206A mutation does not affect the ability of Rad51 to bind DNA. In addition to DNA binding, ATP hydrolysis by Rad51 is important for the DNA strand exchange reaction (Ito et al., 2018). Furthermore, Swi5-Sfr1 stimulates the ATPase activity of Rad51 (Haruta et al., 2006). I therefore examined whether Rad51-E206A is proficient for ATP hydrolysis, both with and without Swi5-Sfr1. In the absence of Swi5-Sfr1, the ATP turnover number *(k_{cat})* of both Rad51 and Rad51-E206A was ~0.2 min^{-1} (**Figure 4.2.4D**). The inclusion of Swi5-Sfr1 elicited an approximately two-fold increase in ATP hydrolysis by both proteins, demonstrating that Rad51-E206A can hydrolyse ATP like wild type and is proficient for the ATPase stimulation imparted by Swi5-Sfr1.

Next, an assay with plasmid-sized DNA substrates was employed to examine the strand exchange activity of Rad51-E206A (**Figure 4.2.4E**). Rad51 drives the pairing of circular ssDNA (css) with homologous linear dsDNA (lds) to yield joint molecule intermediates (JMs). Following strand transfer over the length of the dsDNA substrate, JMs are converted into nicked-circular dsDNA molecules (NCs), which are the products in this assay. The different DNA species can be separated by agarose gel electrophoresis and visualized. Under my standard reaction conditions, wild-type

Rad51 cannot promote JM or NC formation in the absence of auxiliary factors (Haruta et al., 2006; Kurokawa et al., 2008). However, when reaction conditions were modified by increasing the concentrations of Rad51 and DNA substrates, both Rad51 and Rad51-E206A were seen to drive the efficient pairing of css and lds to produce JMs in the absence of auxiliary factors (**Figure 4.2.4F**). This allowed us to evaluate whether the E206A mutation impaired the intrinsic strand exchange activity of Rad51. Although neither protein was able to drive the robust accumulation of NC, I nevertheless quantified the total yield (JM + NC) at each time point and found them to be comparable for both Rad51 and Rad51-E206A. Genetic analysis suggested that Rad51-E206A is proficient for the DNA repair promoted by Swi5-Sfr1. To corroborate these findings, strand exchange reactions were supplemented with Swi5-Sfr1. Note that under these standard assay conditions, which differ from those employed above, Rad51 alone cannot promote JM or NC formation, thus allowing me to better examine the effect of Swi5-Sfr1 (Haruta et al., 2006; Kurokawa et al., 2008). The inclusion of Swi5-Sfr1 efficiently stimulated both Rad51 and Rad51-E206A, with a similar accumulation of JMs and NC observed in both cases (**Figure 4.2.4G**). Taken together, these results indicate that Rad51-E206A retains intrinsic recombinase activity and a functional interaction with Swi5-Sfr1.

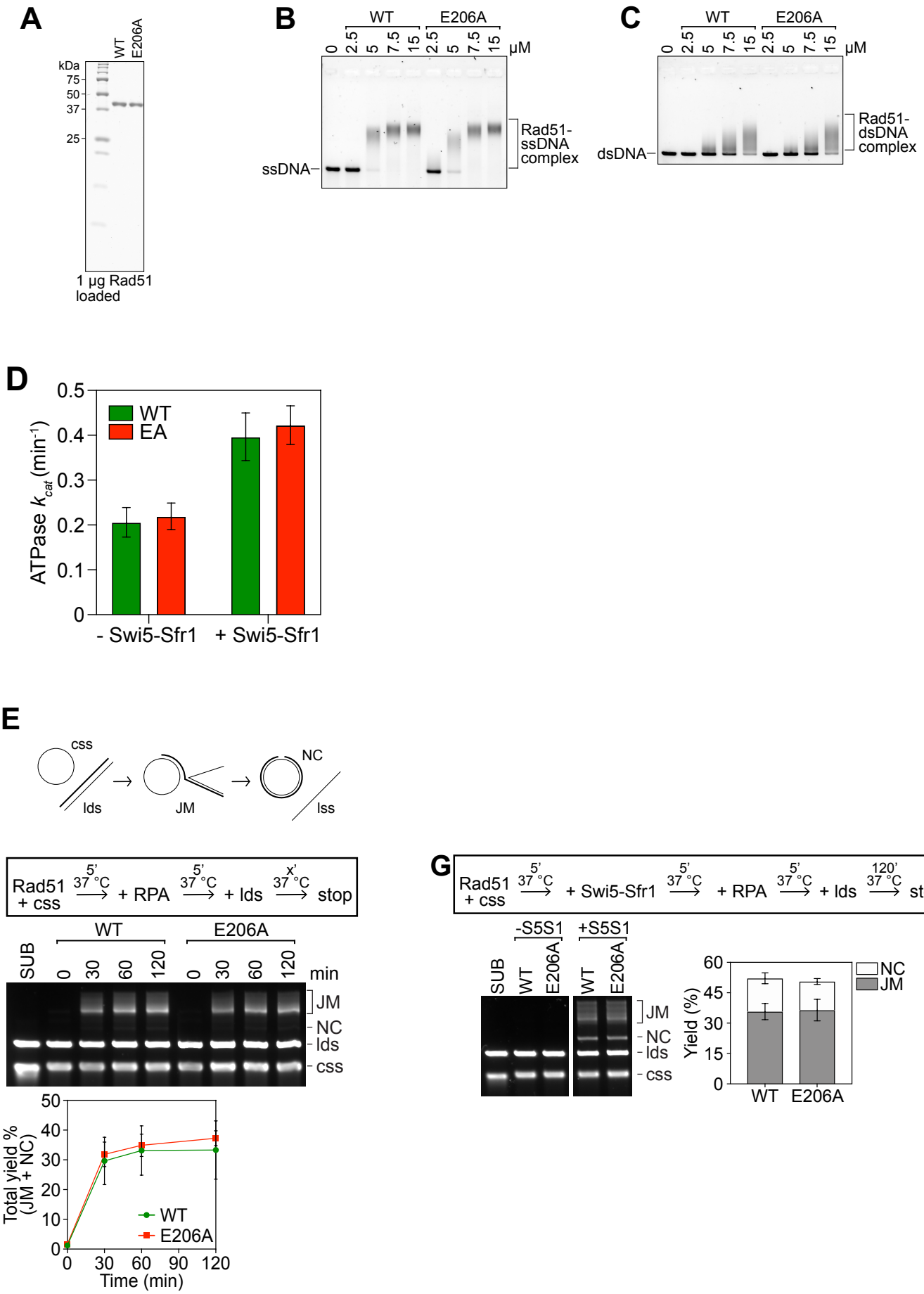

A
WT
E206A
kDa
75
50
37
25
1 µg Rad51 loaded
B
WT
E206A
0
2.5
5
7.5
15
2.5
5
7.5
15
µM
ssDNA
Rad51-ssDNA complex
C
WT
E206A
0
2.5
5
7.5
15
2.5
5
7.5
15
µM
dsDNA
Rad51-dsDNA complex
D
ATPase k_{cat} (min^{-1})
0.5
0.4
0.3
0.2
0.1
0
WT
EA
- Swi5-Sfr1
+ Swi5-Sfr1
E
css
lds
JM
NC
lss
F
Rad51 + css
5' 37 °C
+ RPA
5' 37 °C
+ lds
x' 37 °C
stop
WT
E206A
SUB
0
30
60
120
0
30
60
120
min
JM
NC
lds
css
Total yield % (JM + NC)
50
40
30
20
10
0
WT
E206A
0
30
60
90
120
Time (min)
G
Rad51 + css
5' 37 °C
+ Swi5-Sfr1
5' 37 °C
+ RPA
5' 37 °C
+ lds
120' 37 °C
stop
-S5S1
+S5S1
SUB
WT
E206A
WT
E206A
JM
NC
lds
css
Yield (%)
60
45
30
15
0
NC
JM
WT
E206A

Figure 4.2.4. Rad51-E206A is not intrinsically defective

(A) Purified Rad51 (WT) and Rad51-E206A (E206A) were examined by SDS-PAGE and coomassie staining. **(B,C)** The indicated concentrations of Rad51 (WT) or Rad51-E206A (E206A) were incubated with 30 μM nt PhiX174 virion DNA (ssDNA; **B**) or 20 μM nt of linearized PhiX174 RF I DNA (dsDNA; **C**), protein-DNA complexes were crosslinked with glutaraldehyde and then resolved by agarose gel electrophoresis. **(D)** The ATPase activity of 5 μM Rad51 (WT) and Rad51-E206A (EA) was measured in the presence of ssDNA (10 μM nt), with or without Swi5-Sfr1 (0.5 μM), and k_{cat} was calculated. **(E)** Schematic of the strand exchange assay with full-length DNA substrates (PhiX174 virion ssDNA and ApaLI-linearized PhiX174 RF I dsDNA). **(F)** Strand exchange reactions were conducted according to the scheme outlined above the gel. Rad51 (WT or E206A), 15 μM. RPA, 1 μM. cssDNA, 30 μM nt. ldsDNA, 20 μM nt. **(G)** Strand exchange reactions were conducted according to the scheme outlined above the gel. Rad51 (WT or E206A), 5 μM. Swi5-Sfr1 (S5S1), 0.5 μM. RPA, 1 μM. cssDNA, 10 μM nt. ldsDNA, 10 μM nt. Data in **(D, F, G)** are means of three independent experiments and error bars depict standard deviation.

Chapter 5: The PAP is essential for Rad51-dependent DNA repair

5.1 Research objectives

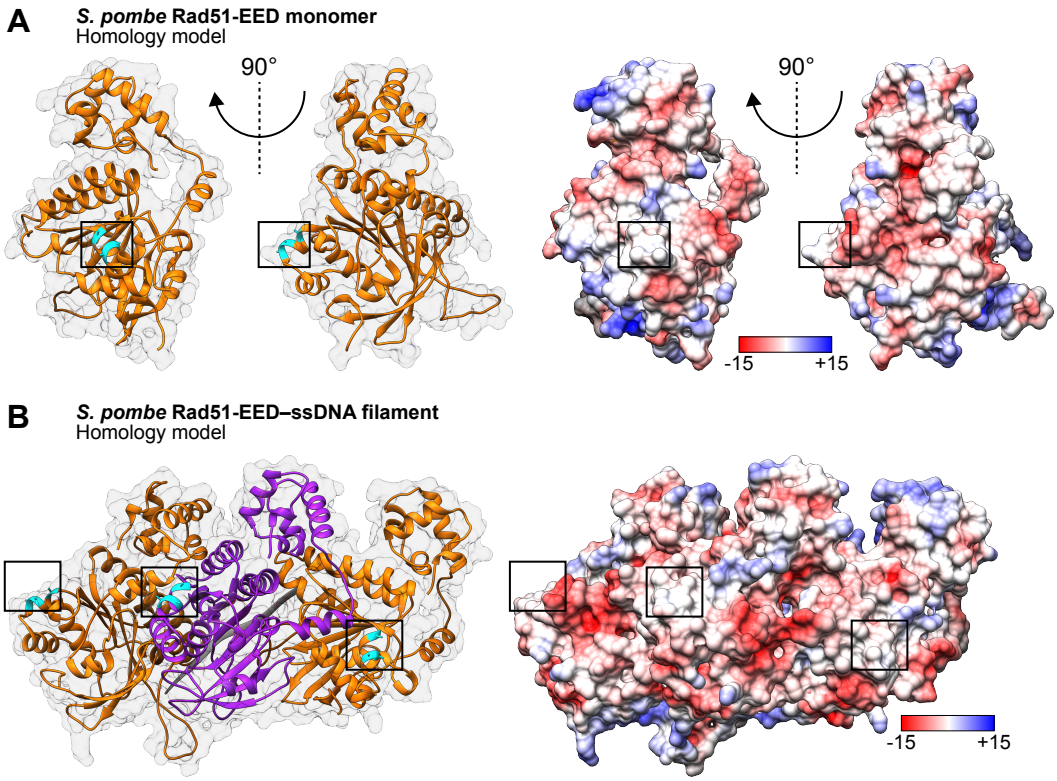
Results with Rad51-E206A suggested that the PAP is required specifically for the interaction with Rad55-Rad57. I sought to test the effects of other mutations in the PAP on DNA repair. Strains were constructed in which the *rad51*$^{+}$ gene at its native locus was replaced with *rad51-E205A*, *rad51-D209A*, *rad51-EE* (E205A, E206A), or *rad51-EED* (E205A, E206A, D209A).

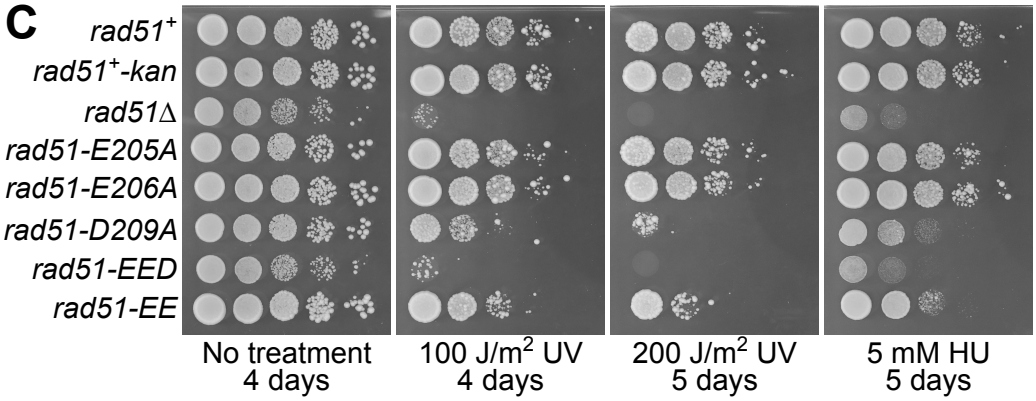
5.2 Results

5.2.1 PAP is required for Rad51-mediated DNA repair

Structural models revealed that the negative surface charge of the PAP is completely neutralized by the EED mutation without affecting its protruding nature (**Figure 5.2.1A, B**). Thus, I proceeded to examine the DNA damage sensitivity of the aforementioned mutant strains by spot-test. Like *rad51-E206A*, the *rad51-E205A* strain did not show any DNA damage sensitivity in the presence of both Rad55-Rad57 and Swi5-Sfr1 (**Figure 5.2.1C**). By contrast, *rad51-D209A* showed marked sensitivity to DNA damage, although it was still significantly more resistant than *rad51*Δ. Strikingly, the *rad51-EED* mutant was as sensitive to DNA damage as *rad51*Δ. Since the E205A and E206A mutations alone did not sensitize cells to DNA damage, but combining them with the partially functional D209A completely incapacitated Rad51, I also examined the *rad51-EE* strain, in which both Glu residues are mutated to Ala. Unlike *rad51-E205A* and *rad51-E206A*, *rad51-EE* showed moderate sensitivity to DNA damage,

although this was milder than the sensitivity of *rad51-D209A*. These results indicate that mutation of the PAP completely abolishes Rad51-dependent DNA repair, and while all three residues are important, D209 plays a more prominent role than E205 and E206. Because my data suggested that the E206A mutation impairs the interaction of Rad51 with Rad55-Rad57, in vivo co-IP experiments were performed to examine how other mutations in the PAP affect complex formation with Rad55-Rad57. A reduction in the amount of Rad51 that co-IPs with Rad55-12xV5 was observed in the *rad51-EE*, *rad51-D209A* and *rad51-EED* strains (**Figure 5.2.1D**), and the trend of this reduction roughly correlated with the DNA damage sensitivity of the corresponding mutants. This result suggests that the DNA damage sensitivity of PAP mutants is partly due to reduced complex formation with Rad55-Rad57. However, given that some complex formation was still observed in the *rad51-EED* strain, I infer that the PAP is important but not essential for complex formation with Rad55-Rad57.


A
S. pombe Rad51-EED monomer
Homology model
90°
90°
-15
+15
B
S. pombe Rad51-EED–ssDNA filament
Homology model
-15
+15


C
rad51+
rad51+-kan
rad51Δ
rad51-E205A
rad51-E206A
rad51-D209A
rad51-EED
rad51-EE
No treatment
4 days
100 J/m2 UV
4 days
200 J/m2 UV
5 days
5 mM HU
5 days

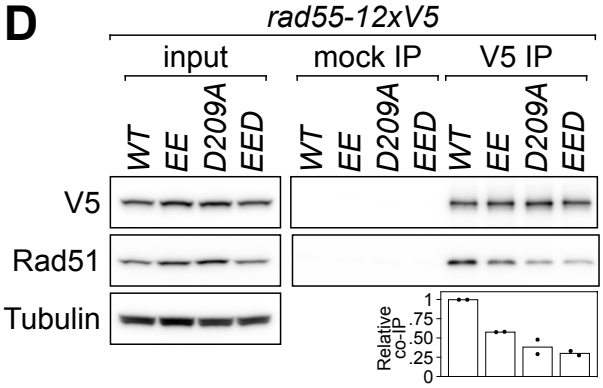

D
rad55-12xV5
input
mock IP
V5 IP
WT
EE
D209A
EED
V5
Rad51
Tubulin
Relative co-IP
1
.75
.50
.25
0

Figure 5.2.1. Mutation of the PAP impairs Rad51-mediated DNA repair and reduces in vivo complex formation with Rad55-Rad57

(A) Ribbon depiction of an *Sp*Rad51-EED monomer or **(B)** three *Sp*Rad51-EED monomers (alternating orange and purple) bound to ssDNA (9-mer poly-dT in grey), both with a near-transparent surface (left) with the side-chains of residues EED (E205A, E206A, D209A) revealed in cyan. The surface is made opaque and coloured according to Coulombic surface charge (right) to demonstrate that the EED mutation neutralizes the negative charge of the PAP. **(C)** 10-fold serial dilutions of the indicated strains were spotted onto standard media with or without acute UV irradiation, or standard media containing 5 mM hydroxyurea (HU). Following growth at 30°C for the indicated time, plates were imaged. **(D)** Soluble cell extracts treated with a benzonase-like nuclease were prepared from each strain under native conditions (input). Immunoprecipitation (IP) was then performed with mock (human IgG from non-immunized animal) or anti-V5 antibodies. Tubulin serves as a loading control. For quantification, Rad51 signal was normalized to V5 signal and expressed relative to wild type.

Data in **(D)** are the means of two independent biological replicates with individual values shown. Numbers in the legends of **(A)** and **(B)** are in units of kcal/(mol•*e*).

5.2.2 PAP is important for DNA repair promoted by Rad55-Rad57

In contrast to what was observed in the presence of Sfr1, *rad51-E205A* showed mild DNA damage sensitivity in the *sfr1*Δ background (**Figure 5.2.2A**) and this modest difference became more obvious at higher doses of UV irradiation (**Figure 5.2.2B**). Both the *rad51-EED* and *rad51-EE* mutants showed comparable sensitivity to *rad51*Δ in this background, as was expected from the phenotype of *rad51-E206A*. Notably, and in contrast to what was observed in the wild-type background, the *rad51-D209A* strain was as sensitive to DNA damage as *rad51*Δ in the absence of Sfr1. These results are consistent with the notion that the PAP is important for DNA repair promoted by Rad55-Rad57.

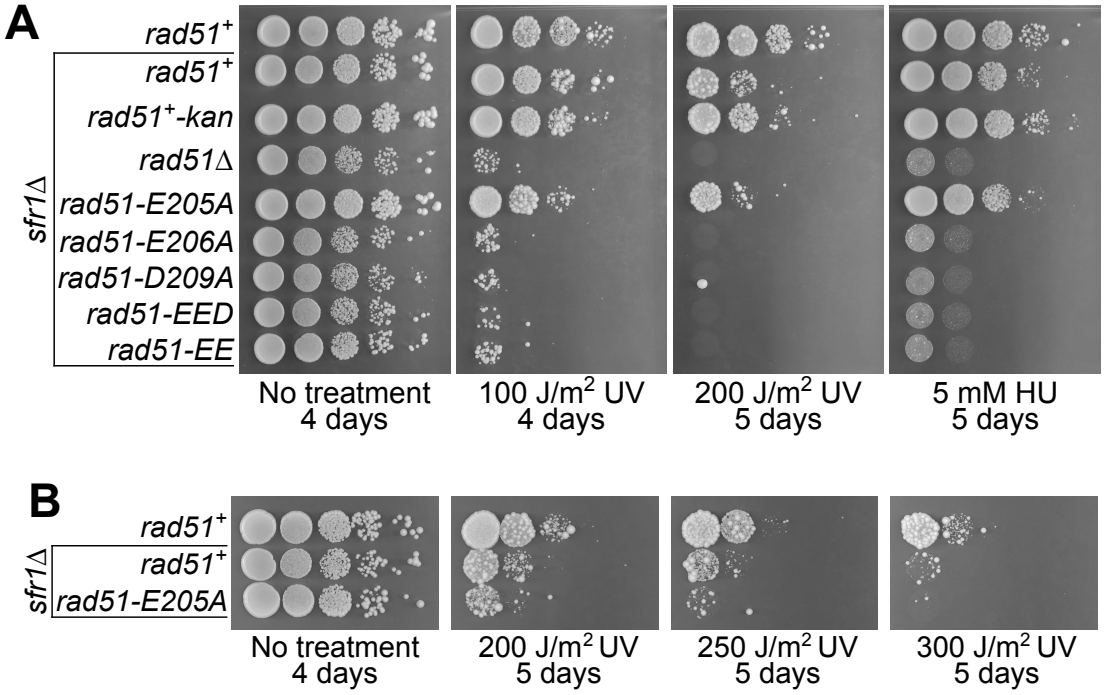

A
rad51+
rad51+
rad51+-kan
rad51Δ
rad51-E205A
rad51-E206A
rad51-D209A
rad51-EED
rad51-EE
sfr1Δ
No treatment
4 days
100 J/m2 UV
4 days
200 J/m2 UV
5 days
5 mM HU
5 days
B
rad51+
rad51+
rad51-E205A
sfr1Δ
No treatment
4 days
200 J/m2 UV
5 days
250 J/m2 UV
5 days
300 J/m2 UV
5 days

Figure 5.2.2. Individual and collective mutations of PAP residues render Rad55-Rad57 dependent DNA repair defective

(A) 10-fold serial dilutions of the indicated strains were spotted onto standard media with or without acute UV irradiation, or standard media containing 5 mM hydroxyurea (HU). Following growth at 30°C for the indicated time, plates were imaged. **(B)** 10-fold serial dilutions of the indicated strains were spotted onto standard media with or without acute UV irradiation. Following growth at 30°C for the indicated time, plates were imaged.

5.2.3 PAP is important for Rad55-Rad57–independent DNA repair

Because the DNA damage sensitivity of *rad51-EED* is similar to that of *rad51*Δ (**Figure 5.2.1C**), which clearly exceeds the sensitivity of *rad57*Δ, it seemed plausible that the PAP is also involved in Rad55-Rad57–independent DNA repair. To directly test this, PAP mutants were introduced into the *rad57*Δ background. The *rad51-E205A* mutant was as resistant to DNA damage as *rad51*$^{+}$ in the absence of Rad57, suggesting that Rad55-Rad57–independent DNA repair mechanisms are not impaired in this mutant (**Figure 5.2.3A**). By contrast, *rad51-EE* showed a modest increase in sensitivity compared to *rad51*$^{+}$. *rad51-D209A* was even more sensitive than *rad51-EE*, although this sensitivity was still not as severe as *rad51-EED* and *rad51*Δ. Consistently, *rad51-EED* and *rad51*Δ were the only strains among this set that showed a clear slow-growth phenotype (note the small colony size on the “No treatment” plate in **Figure 5.2.3A**). The fact that the D209A and EE mutations further sensitized *rad57*Δ cells to DNA damage, combined with the severe sensitivity of *rad51-EED*, suggests that Rad55-Rad57–independent DNA repair is also impaired in these mutants. These results imply that the PAP is also relevant to the function of auxiliary factors other than Rad55-Rad57.

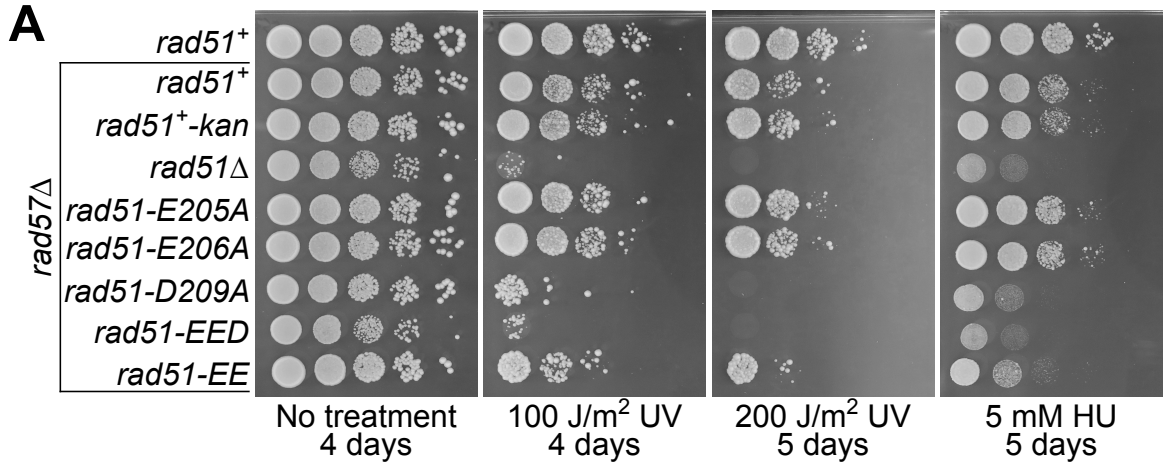

A
rad51+
rad51+
rad51+-kan
rad51Δ
rad51-E205A
rad51-E206A
rad51-D209A
rad51-EED
rad51-EE
rad57Δ
No treatment
4 days
100 J/m2 UV
4 days
200 J/m2 UV
5 days
5 mM HU
5 days

Figure 5.2.3. PAP is also involved in Rad55-Rad57 independent DNA repair

(A) 10-fold serial dilutions of the indicated strains were spotted onto standard media with or without acute UV irradiation, or standard media containing 5 mM hydroxyurea (HU). Following growth at 30°C for the indicated time, plates were imaged.

5.2.4 Negative character of the PAP may be important for Rad51-mediated DNA repair

The observation that combining E205A, E206A, and D209A mutations results in a more severe phenotype than individual mutations raised the possibility that the overall negative character of the PAP is important for Rad51-mediated DNA repair. If so, I reasoned that a charge reversal mutation would be more disruptive than the Asp/Glu-to-Ala mutations employed thus far. The E205A and E206A mutations did not sensitise cells to DNA damage in the presence of both Rad55-Rad57 and Swi5-Sfr1 (**Figure 5.2.1C**). However, because E206 shows a higher degree of conservation than E205, it was mutated to Lys, yielding the *rad51-E206K* strain. In stark contrast to the *rad51-E206A* strain, *rad51-E206K* showed a clear slow-growth phenotype and was as sensitive to DNA damage as *rad51*Δ in the presence of both Rad55-Rad57 and Swi5-Sfr1 (**Figure 5.2.4A**), just like *rad51-EED*. Taken together, these results suggest that the negative character of the PAP is required for recombinational DNA repair.

A

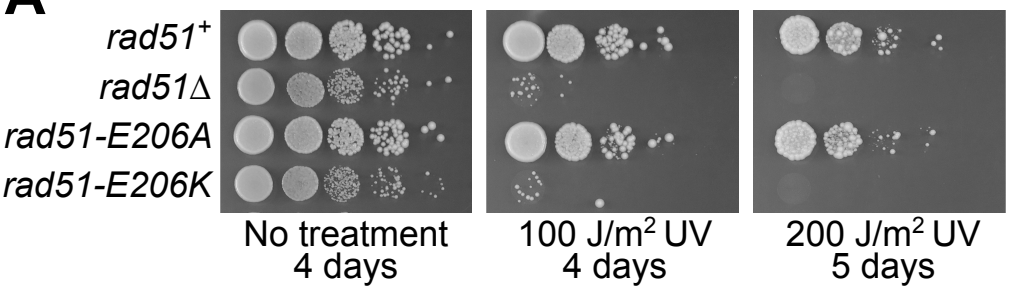

rad51+
rad51Δ
rad51-E206A
rad51-E206K
No treatment
4 days
100 J/m2 UV
4 days
200 J/m2 UV
5 days

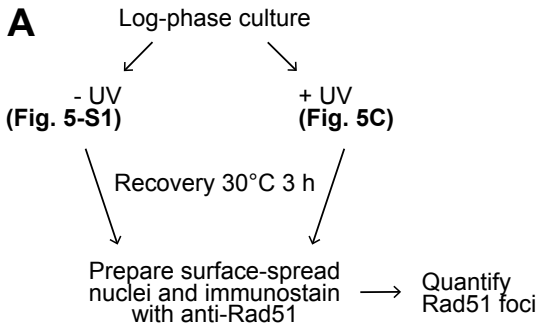
Figure 5.2.4. *rad51-E206K* phenocopies the DNA damage sensitivity of *rad51-EED*

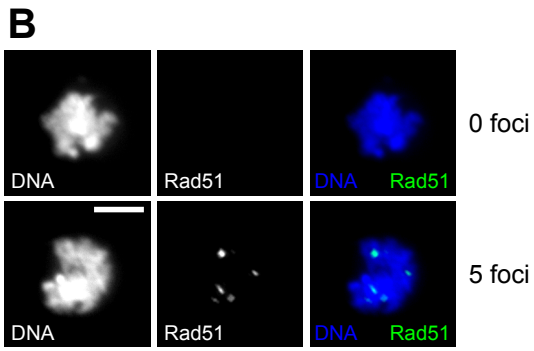
(A) 10-fold serial dilutions of the indicated strains were spotted onto standard media with or without acute UV irradiation. Following growth at 30°C for the indicated time, plates were imaged.

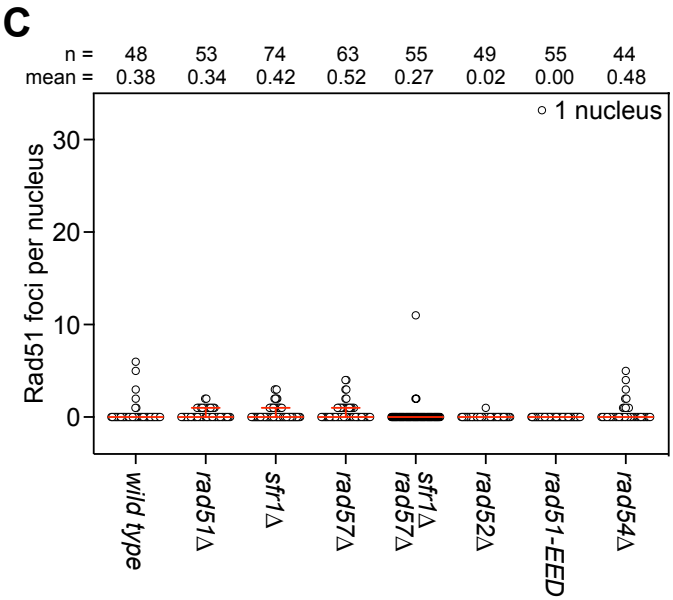
5.2.5 The PAP is crucial for the recruitment of Rad51 to DNA damage sites

To elucidate the mechanistic defects in DNA repair associated with neutralization of the PAP, previous immunostaining protocols for the visualization of Rad51 foci were adopted (Loidl & Lorenz, 2009; Argunhan et al., 2017b). Surface-spread nuclei were prepared from log-phase cultures, with or without prior UV irradiation, and immunostained with a polyclonal anti-Rad51 antibody (**Figure 5.2.5A**). Nuclei were then picked manually, and foci were quantified by an automated approach using FIJI software (Schindelin et al., 2012). Examples of nuclei scored by this method are shown in Figure 5.2.5B.

In the absence of UV irradiation, the vast majority of nuclei in all strains lacked Rad51 foci (**Figure 5.2.5C**). By contrast, UV-irradiated nuclei contained substantially more Rad51 foci, and this was not seen in the *rad51*Δ strain, confirming the DNA damage-dependence and specificity of these cytological entities (**Figure 5.2.5D**). Nuclei from wild-type and *rad52*Δ strains formed an average of 8.6 and 1.7 foci, respectively, in close agreement with a previous report (Lorenz et al., 2009). As expected, both *sfr1*Δ and *rad57*Δ strains formed fewer foci than wild type, and *rad57*Δ *sfr1*Δ formed even fewer foci still (Akamatsu et al., 2007). Strikingly, nuclei from *rad51-EED* showed a drastic reduction in the number of foci, much like the *rad57*Δ *sfr1*Δ double mutant and the *rad52*Δ single mutant. These results indicate that the severe DNA damage sensitivity of *rad51-EED* stems from defects in the mechanisms promoting the recruitment of Rad51 to sites of DNA damage.


A
Log-phase culture
- UV
(Fig. 5-S1)
+ UV
(Fig. 5C)
Recovery 30°C 3 h
Prepare surface-spread nuclei and immunostain with anti-Rad51
Quantify Rad51 foci


B
DNA
Rad51
DNA Rad51
0 foci
5 foci


C
n = 48 53 74 63 55 49 55 44
mean = 0.38 0.34 0.42 0.52 0.27 0.02 0.00 0.48
1 nucleus
Rad51 foci per nucleus
wild type
rad51Δ
sfr1Δ
rad57Δ
sfr1Δ rad57Δ
rad52Δ
rad51-EED
rad54Δ

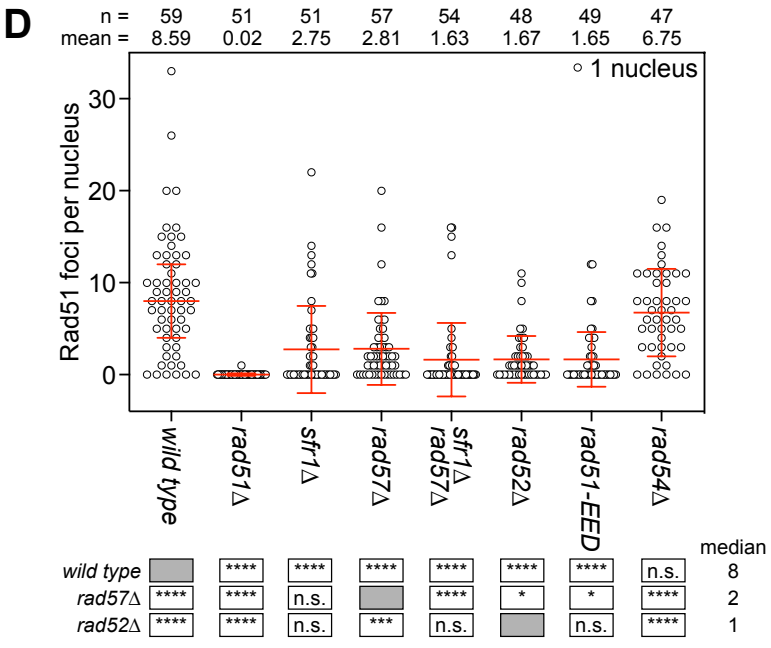

D
n = 59 51 51 57 54 48 49 47
mean = 8.59 0.02 2.75 2.81 1.63 1.67 1.65 6.75
1 nucleus
Rad51 foci per nucleus
wild type
rad51Δ
sfr1Δ
rad57Δ
sfr1Δ rad57Δ
rad52Δ
rad51-EED
rad54Δ
median
wild type 8
rad57Δ 2
rad52Δ 1

Figure 5.2.5. *rad51-EED* is defective in mechanisms promoting recruitment of Rad51 to sites of DNA damage

(A) Schematic of cytological analysis. **(B)** Representative images of UV-irradiated nuclear spreads containing 0 or 5 Rad51 foci. Scale bar, 5 μm. **(C,D)** The indicated strains were grown to log phase and cultures were split into two. One sub-culture was UV-irradiated (200 J/m^2; shown in **Figure 5.2.5D**) and the other was not (**Figure 5.2.5C**). Following 3 hours of recovery, nuclei were surface-spread and immunostained with a polyclonal PVDF-purified anti-Rad51 antibody. The indicated number of nuclei were manually picked, images in the DAPI and Rad51 channels were captured, and semi-automated quantification of foci was performed using FIJI software. Bars depict the median and interquartile range. Mean number of foci are shown for each strain. Statistical analysis was by Wilcoxon ranked sum test with the indicated median values. n.s., not significant ($p > 0.05$). *, $p < 0.05$. ***, $p < 0.001$. ****, $p < 0.0001$.

Chapter 6: In vitro analysis of Rad51-EED

6.1 Research objectives

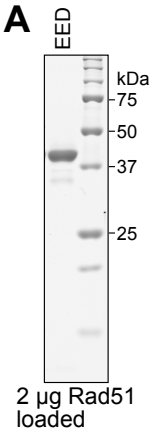
The DNA damage sensitivity of *rad51-EED* is clearly more severe than *rad57*Δ, pointing towards additional roles of the PAP beyond facilitating the interaction with Rad55-Rad57. This could reflect an impairment in the intrinsic activity of Rad51-EED. Alternatively, the EED mutation could impair the interaction with Swi5-Sfr1, since the phenotypes of *rad51-EED* are comparable to *rad57*Δ *sfr1*Δ. To test these two possibilities, I sought to analyse Rad51-EED biochemically.

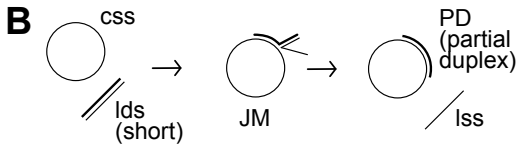
6.2 Results

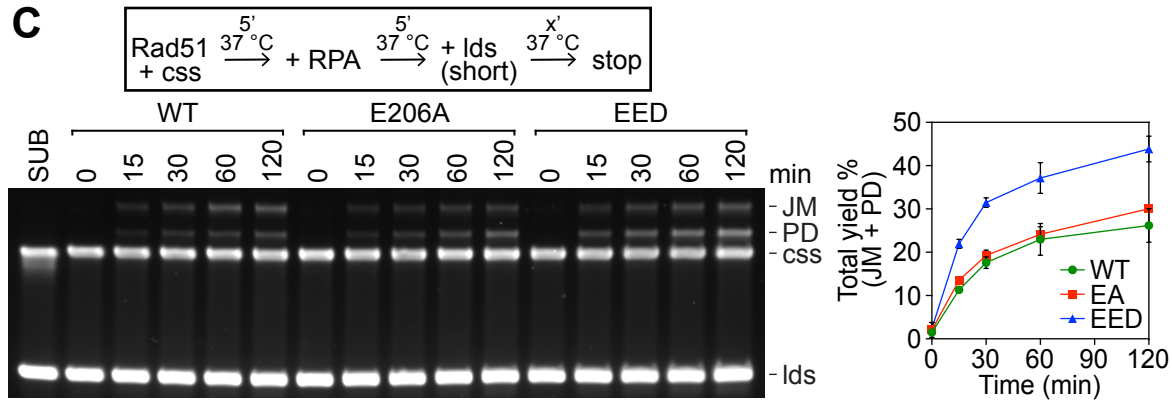
6.2.1 Rad51-EED is not intrinsically defective

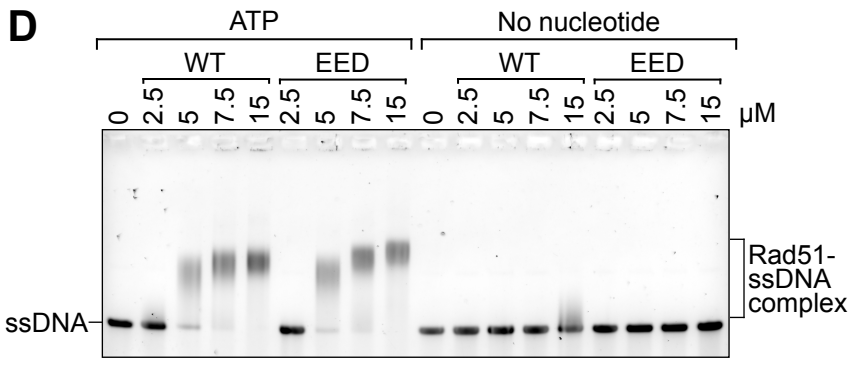
In order to measure the intrinsic activity of Rad51-EED, the protein was first purified to homogeneity from *E. coli* (**Figure 6.2.1A**). Because reaction products (NCs) were not observed in the assay that was previously employed to monitor the intrinsic strand exchange activity of Rad51 (**Figure 4.2.4E**), a shorter lds substrate was utilized with the reasoning that this might prove a less challenging substrate (**Figure 6.2.1B**). Both Rad51 and Rad51-E206A generated similar amounts of partial duplex molecules (PD), which are the reaction products in this assay (**Figure 6.2.1C**). Unexpectedly, Rad51-EED consistently displayed increased strand exchange activity. One reason for such an increased activity could be that Rad51-EED has an increased DNA binding affinity. However, Rad51-EED shifted ssDNA and dsDNA comparably to wild-type Rad51 in EMSAs (**Figure 6.2.1D, E**), suggesting that the EED mutation does not affect the ability of Rad51 to bind DNA. At the very least, these results indicate that mutation of

the PAP does not impair the intrinsic activity of Rad51, suggesting that the DNA damage sensitivity of *rad51-EED* is not due to an innate inability of the mutant protein to conduct HR.


A
EED
kDa
75
50
37
25
2 µg Rad51
loaded


B
css
lds
(short)
JM
PD
(partial
duplex)
lss


C
Rad51
+ css
5'
37 °C
+ RPA
5'
37 °C
+ lds
(short)
x'
37 °C
stop
WT
E206A
EED
SUB
0
15
30
60
120
min
JM
PD
css
lds
Total yield %
(JM + PD)
50
40
30
20
10
0
0
30
60
90
120
Time (min)
WT
EA
EED


D
ATP
No nucleotide
WT
EED
0
2.5
5
7.5
15
µM
ssDNA
Rad51-
ssDNA
complex

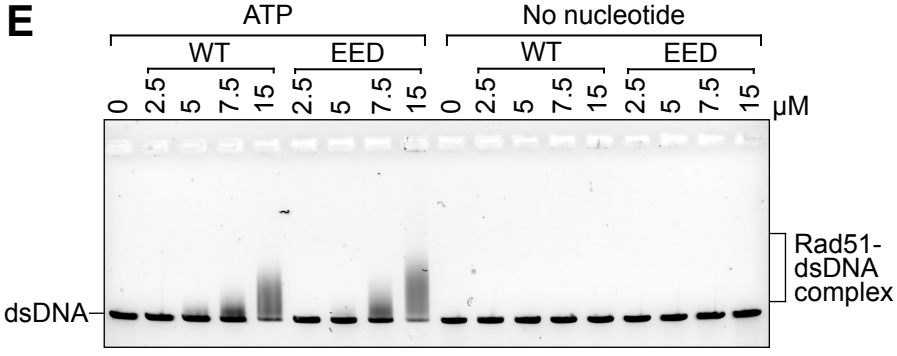
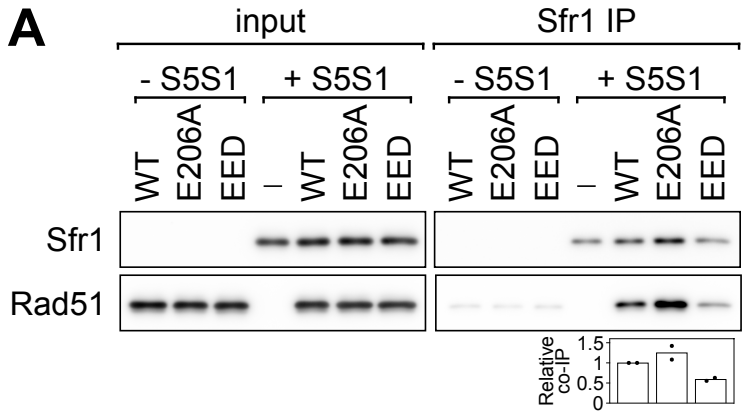

E
ATP
No nucleotide
WT
EED
0
2.5
5
7.5
15
µM
dsDNA
Rad51-
dsDNA
complex

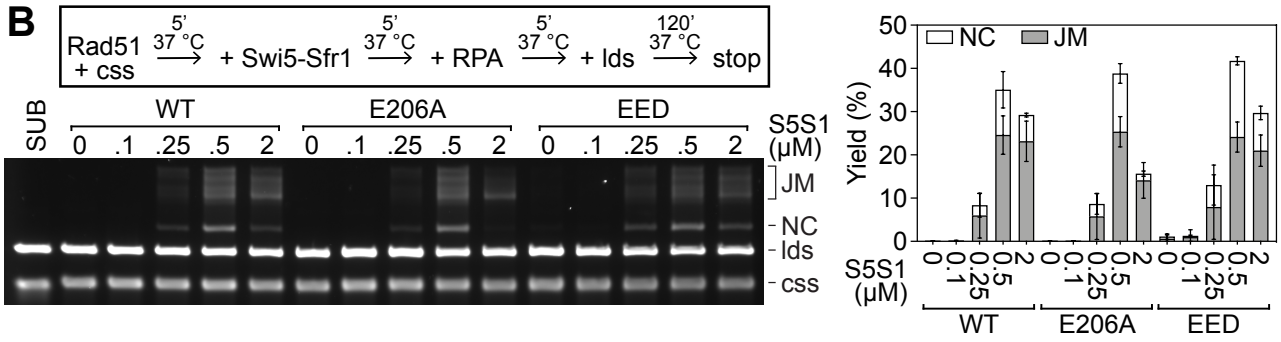
Figure 6.2.1. The EED mutation does not impair the intrinsic activity of Rad51

(A) Purified Rad51-EED was examined by SDS-PAGE and coomassie staining. **(B)** Schematic of the strand exchange assay with shortened DNA substrates (PhiX174 virion ssDNA and a 1.6kb fragment of PhiX RF I dsDNA). **(C)** Strand exchange reactions were conducted according to the scheme outlined above the gel. Rad51 (WT, E206A, or EED), 15 μM. RPA, 1 μM. cssDNA, 30 μM nt. ldsDNA, 20 μM nt. **(D, E)** The indicated concentrations of Rad51 (WT) or Rad51-EED (EED) were incubated with 30 μM nt PhiX174 virion DNA (ssDNA; **D**) or 20 μM nt of linearized PhiX174 RF I DNA (dsDNA; **E**) in the presence or absence of ATP. Protein-DNA complexes were then crosslinked with glutaraldehyde and resolved by agarose gel electrophoresis. Data in **(C)** are means of three independent experiments and error bars depict standard deviation.

6.2.2 Rad51-EED can be stimulated by Swi5-Sfr1

If the EED mutation impairs the interaction with Swi5-Sfr1, then the binding of Swi5-Sfr1 to Rad51-EED should be abrogated. Co-IP experiments with purified proteins revealed reproducible differences in the amount of Rad51-E206A and Rad51-EED that co-IP'd with Sfr1, but these differences were relatively subtle (**Figure 6.2.2A**). Moreover, using canonical strand exchange assay (**Figure 4.2.4E**), these differences in physical binding did not affect the stimulation of Rad51 by Swi5-Sfr1 (**Figure 6.2.2B**), suggesting that they are not of functional significance. I also examined the interaction of Swi5-Sfr1 with Rad51-E206K. Similar to Rad51-EED, I saw a reproducible reduction in the co-IP of Rad51-E206K with Sfr1, but this difference is relatively subtle (less than two-fold; **Figure 6.2.2C**). These results indicate that the mild impairment in the physical interaction of Swi5-Sfr1 with Rad51-EED is inconsequential, leading us to conclude that the severe DNA damage sensitivity of the *rad51-EED* strain is unlikely to be due to a defect in the interaction with Swi5-Sfr1.


A
input
Sfr1 IP
- S5S1
+ S5S1
WT
E206A
EED
–
Sfr1
Rad51
Relative co-IP
1.5
1
0.5
0


B
Rad51 + css
5' 37 °C
+ Swi5-Sfr1
+ RPA
+ lds
120' 37 °C
stop
SUB
WT
E206A
EED
0 .1 .25 .5 2
S5S1 (μM)
JM
NC
lds
css
Yield (%)
NC
JM
50
40
30
20
10
0

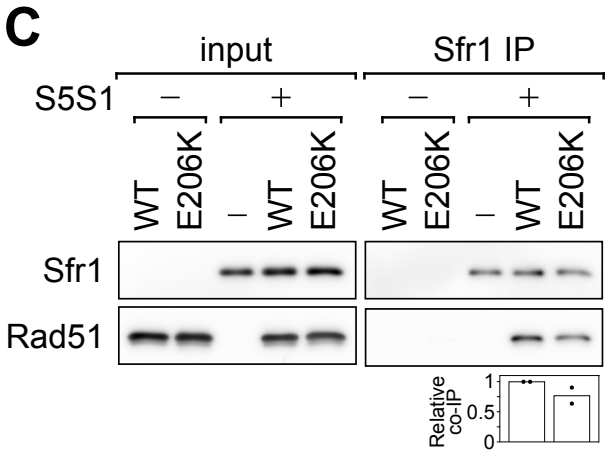

C
input
Sfr1 IP
S5S1
–
+
WT
E206K
Sfr1
Rad51
Relative co-IP
1
0.5
0

Figure 6.2.2. Rad51-EED is responsive to Swi5-Sfr1 stimulation

(A) Purified Rad51 (WT, E206A, or EED) was incubated with purified Swi5-Sfr1 (or the equivalent volume of protein storage buffer) and subjected to immunoprecipitation with an anti-Sfr1 antibody. For quantification, Rad51 signal was normalized to Sfr1 signal and expressed relative to wild type. **(B)** Strand exchange reactions were conducted according to the scheme outlined in Figure 6.2.2B. Rad51 (WT, E206A, or EED), 5 μM. Swi5-Sfr1 (S5S1), indicated. RPA, 1 μM. cssDNA, 10 μM nt. ldsDNA, 10 μM nt. **(C)** Purified Rad51 (WT or E206K) was incubated with purified Swi5-Sfr1 (or the equivalent volume of protein storage buffer) and subjected to immunoprecipitation with an anti-Sfr1 antibody. For quantification, Rad51 signal was normalized to Sfr1 signal and expressed relative to wild type.

Data in **(B)** are means of three independent experiments and error bars depict standard deviation. Data in **(A, C)** are the means of two independent experiments with individual values shown.

Chapter 7: The PAP is important for the interaction of Rad51 with both Rad52 and Rad54

7.1 Research objectives

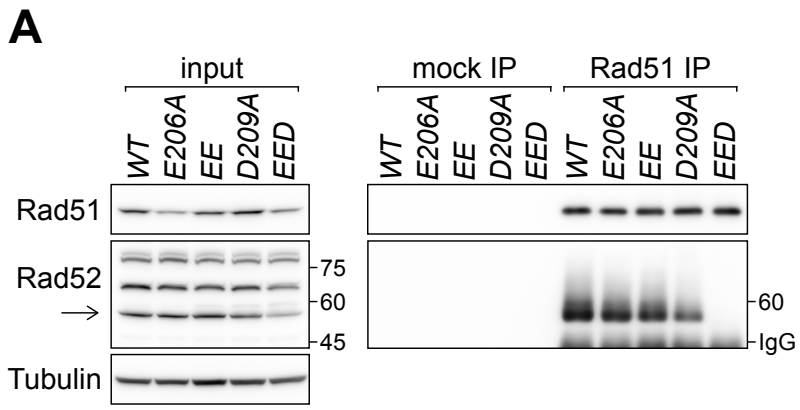
Based on biochemical analysis, Rad51-EED is not intrinsically defective. However, in vivo analysis clearly indicated that the DNA repair and Rad51 foci formation defects of *rad51-EED* are more severe than *rad57*Δ*.* Moreover, the *rad51-D209A* and *rad51-EE* mutants further sensitized *rad57*Δ to DNA damage, pointing towards defects in the promotion of Rad51 activity by other auxiliary factors (**Figure 5.2.3A**). Although the phenotype of *rad51-EED* is comparable to the *rad57*Δ *sfr1*Δ double mutant, biochemical analysis suggested that Rad51-EED retains a functional interaction with Swi5-Sfr1. This means that Rad52 and Rad54 are the two remaining auxiliary factors that might require PAP for their function in Rad51-mediated DNA repair. The interactions of Rad51-EED with Rad52 and Rad54 are explored in this chapter.

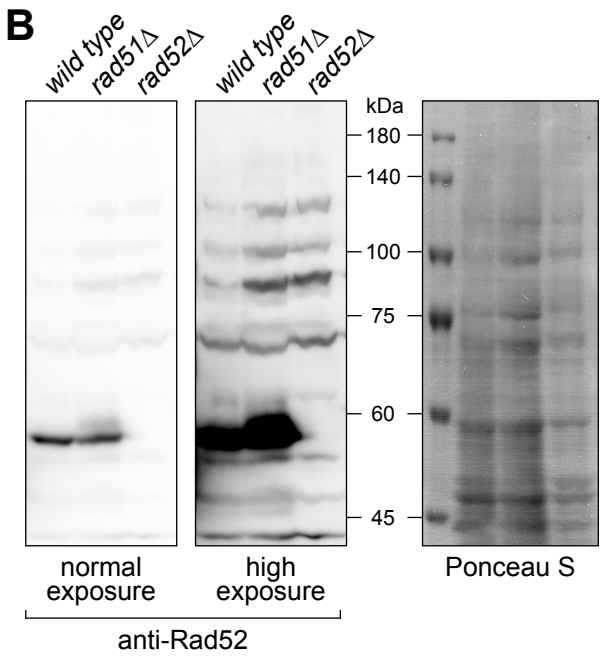
7.2 Results

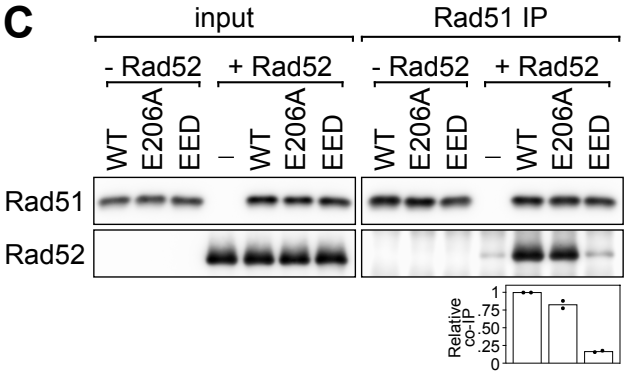
7.2.1 PAP is essential for the Rad51-Rad52 interaction

While a defect in the interaction with Rad54 could explain the severity of DNA damage sensitivity observed for *rad51-EED*, this is unlikely to be the cause of the sensitivity as *rad54*Δ is not defective in the recruitment of Rad51 to sites of DNA damage (**Figure 5.2.5D**). Thus, the remaining possibility that could account for the phenotypes of *rad51-EED* is that the EED mutation impairs the interaction of Rad51 with Rad52. To examine whether Rad51-Rad52 complex formation was affected by PAP mutations, in vivo co-IP experiments were performed. Comparable amounts of Rad52 were seen to co-IP with Rad51, Rad51-E206A, and Rad51-EE, whereas a clear reduction was

observed for Rad51-D209A (**Figure 7.2.1A**). Strikingly, Rad52 was completely undetectable in the Rad51-EED immunoprecipitate, indicating that the EED mutation ablates Rad51-Rad52 complex formation in vivo. These results suggest that the exquisite DNA damage sensitivity of *rad51-EED* is due to defects in the interactions with both Rad55-Rad57 and Rad52. The identity of the band indicated as Rad52 was verified by using a *rad52*Δ strain (**Figure 7.2.1B**). To directly test whether the EED mutation disrupts the binding of Rad51 to Rad52, a co-IP experiment was conducted with purified proteins. Comparable amounts of Rad52 co-IP'd with Rad51 and Rad51-E206A (**Figure 7.2.1C**). By stark contrast, only background levels of Rad52 were seen to co-IP with Rad51-EED. Similar results were obtained in the reciprocal co-IP experiment (**Figure 7.2.1D**). These results clearly indicate that the PAP is essential for the Rad51-Rad52 interaction.


A
input
mock IP
Rad51 IP
WT
E206A
EE
D209A
EED
Rad51
Rad52
Tubulin
75
60
45
60
IgG


B
wild type
rad51Δ
rad52Δ
kDa
180
140
100
75
60
45
normal exposure
high exposure
Ponceau S
anti-Rad52


C
input
Rad51 IP
- Rad52
+ Rad52
WT
E206A
EED
–
Rad51
Rad52
Relative co-IP
1
.75
.50
.25
0

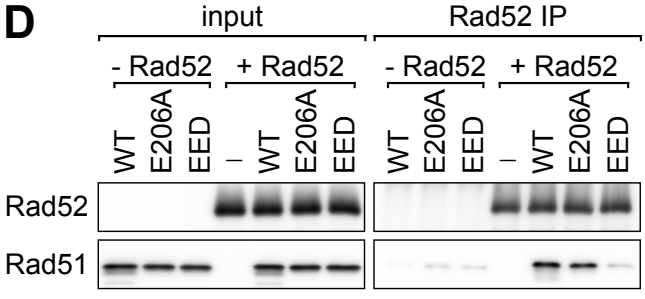

D
input
Rad52 IP
- Rad52
+ Rad52
WT
E206A
EED
–
Rad52
Rad51

Figure 7.2.1. The PAP is essential for Rad51-Rad52 interaction

(A) Soluble cell extracts treated with a benzonase-like nuclease were prepared from each strain under native conditions (input). Immunoprecipitation (IP) was then performed with mock (human IgG from non-immunized animal) or anti-Rad51 antibodies. Arrow denotes the Rad52 band (other bands were still observed in a *rad52*Δ strain, see **Figure 7.2.1B**) and numbers denote the position of the size markers in kDa. To ensure separation of Rad52 from the IgG heavy chain band, the IP samples were separated by 7% SDS-PAGE instead of the 12% SDS-PAGE employed for the input samples. As a result, the 45 kDa and 75 kDa bands of the size marker are not within the cropped area of the anti-Rad52 immunoblot for the IP sample. Tubulin serves as a loading control. **(B)** Cellular proteins were processed by the TCA method and subjected to immunoblotting with a polyclonal anti-Rad52 antibody to identify the Rad52 band. Ponceau S serves as a loading control. **(C)** Purified Rad51 (WT, E206A, or EED) was incubated with purified Rad52 (or the equivalent volume of protein storage buffer) and subjected to immunoprecipitation with anti-Rad51 antibody. For quantification, Rad52 signal was normalized to Rad51 signal and expressed relative to wild type. **(D)** Purified Rad51 (WT, E206A, or EED) was incubated with purified Rad52 (or the equivalent volume of protein storage buffer) and subjected to immunoprecipitation with anti-Rad52 antibody.

7.2.2 PAP is important for Rad51-Rad54 interaction

So far, my results demonstrated that the PAP is involved in the interaction of Rad51 with both Rad55-Rad57 and Rad52. I therefore considered the possibility that the PAP is commonly utilized by multiple auxiliary factors. To test this, I sought to examine the interaction of Rad51 with Rad54. Unlike Rad55-Rad57 and Rad52, Rad54 functions primarily in the later stages of HR (Sugawara et al., 2003; Lisby et al., 2004; Mazin et al., 2010). Defects in the recruitment of Rad51 to DNA damage sites — as seen in *rad51-EED* — would block downstream events, obscuring meaningful examination of the Rad51-Rad54 interaction by in vivo co-IP analysis. To circumvent this, Rad54 with an N-terminal FLAG tag was purified to near-homogeneity from *E. coli* (**Figure 7.2.2A**) and its physical interaction with Rad51-EED was examined in vitro. Similar amounts of Rad51 and Rad51-E206A were seen to co-IP with Rad54, whereas an approximately three-fold reduction in the co-IP of Rad51-EED was observed (**Figure 7.2.2B**). However, a two-fold reduction in the co-IP of Rad51-EED with Swi5-Sfr1 did not affect the functional interaction, as described earlier (**Figure 6.2.2A,B**). To examine whether the difference in physical binding between Rad51-EED and Rad54 is of functional significance, strand exchange reactions were conducted under conditions where wild-type Rad51 alone did not produce JM or PD molecules (Rad51-EED nevertheless showed increased intrinsic strand exchange activity [**Figure 7.2.2C**], as expected from previous experiments [**Figure 6.2.1C** and **6.2.2B**]). Remarkably, the EED mutation rendered Rad51 less sensitive to the stimulatory effect of Rad54, with approximately four-fold more Rad54 required to achieve maximal activity. These results indicate that, in addition to facilitating the interaction of Rad51 with Rad55-Rad57 and Rad52, the PAP is also important for the interaction with Rad54.

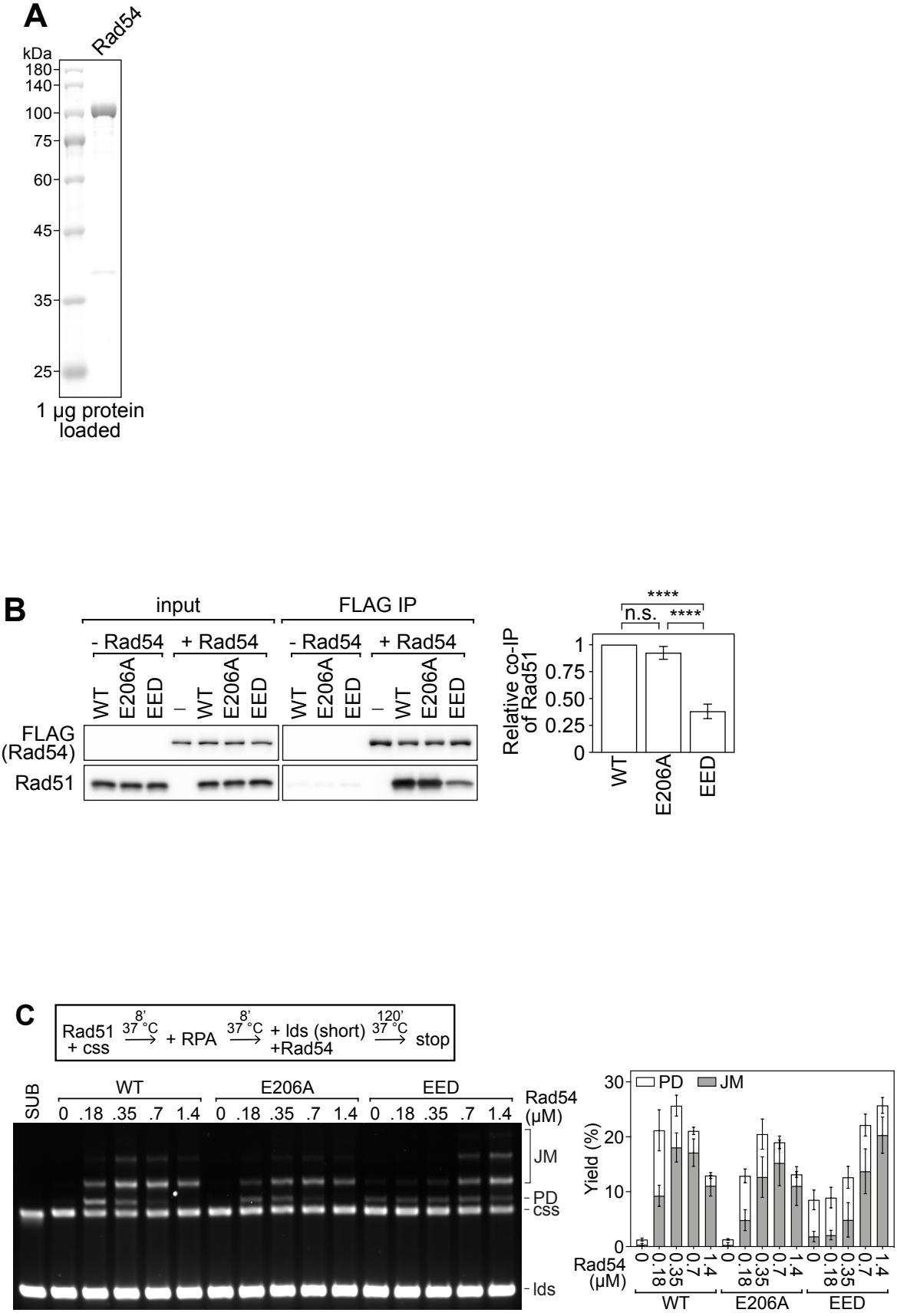

A
Rad54
kDa
180
140
100
75
60
45
35
25
1 µg protein loaded
B
input
FLAG IP
- Rad54
+ Rad54
WT
E206A
EED
FLAG (Rad54)
Rad51
****
n.s.
Relative co-IP of Rad51
C
Rad51 + css
8' 37 °C
+ RPA
+ lds (short) +Rad54
120' 37 °C
stop
SUB
Rad54 (µM)
JM
PD
css
lds
Yield (%)

Figure 7.2.2. PAP is also important for the Rad51-Rad54 interaction

(A) Purified FLAG-Rad54 was examined by SDS-PAGE and coomassie staining. **(B)** Purified Rad51 (WT, E206A, or EED) was incubated with purified FLAG-Rad54 (or the equivalent volume of protein storage buffer) and subjected to immunoprecipitation with FLAG-agarose resin. For quantification, Rad51 signal was normalized to FLAG-Rad54 signal and expressed relative to wild type. Statistical significance was assessed by one-way ANOVA with Tukey's multiple comparisons test. n.s., not significant (p = 0.2538). ****, $p < 0.0001$. **(C)** Strand exchange reactions were conducted according to the scheme outlined above the gel. Rad51 (WT, E206A, or EED), 7 μM. Rad54, indicated. RPA, 0.7 μM. cssDNA, 7 μM nt. ldsDNA, 14 μM nt. Data in **(B,C)** are means of three independent experiments and error bars depict standard deviation.

Chapter 8: Discussion

The results presented in this thesis uncover a novel and conserved motif of Rad51 called the protruding acidic patch (PAP). Data suggest that the PAP is integral to Rad51-mediated DNA repair and is the mutual binding site for three critical recombination auxiliary factors: Rad55-Rad57, Rad52 and Rad54. Here, I will briefly summarise the results presented in the preceding chapters then discuss the relevance of these findings with respect to the existing literature.

8.1 Results summary

The PAP is a novel motif of Rad51 which is located on the opposite side of the ATPase core domain and accounts for the most densely negative charged region (**Figure 3.2.1A**). The PAP is located on a short α-helix preceding the outermost β-strand of the central β-sheet (**Figure 3.2.2B**). Three acidic residues project out of this α-helix: E205, E206, and D209. Using a previously published homology model of the *Sp*Rad51 presynaptic filament (Ito et al., 2020), it is evident that PAP is situated on the exterior of the filament, distal to the catalytic core of Rad51 involved in ATP and DNA binding (**Figure 3.2.3A**). Based on the solved structures of the *Sc*Rad51(Conway et al., 2004) and *Hs*RAD51 (Xu et al., 2017) filaments, the PAP appears to be structurally conserved (**Figure 3.2.3B, C**), and sequence analysis revealed negatively charged residues at equivalent positions throughout numerous eukaryotic species (**Figure 3.2.4A**). Furthermore, based on a homology model, the PAP appears to be conserved in the meiosis-specific RecA-family recombinase Dmc1 (**Figure 3.2.4B**). Additionally, the PAP is structurally conserved in the archaeal RadA polymer (**Figure 3.2.4D**). Based on my analysis of the solved RecA monomer (Story et al., 1992; PDB 2REB)

and RecA filament (Chen et al., 2008; 3CMU) structures, the PAP does not seem to be conserved in bacterial RecA (**Figure 3.2.4D, E**).

E206 is the most conserved PAP residue among *Sp*Rad51, *Sc*Rad51, and *Hs*Rad51 (**Figure 3.2.2D**); I therefore initially focused on this residue to analyse PAP function. The *rad51-E206A* mutant strain did not exhibit any defect in DNA repair in the wild-type and *rad57*Δ backgrounds (**Figure 4.2.1A, B**), but was as sensitive as *rad51*Δ in the *sfr1*Δ background (**Figure 4.2.1C**). This is due to a specific defect in Rad55-Rad57 function (**Figure 4.2.2A**), which is related to a reduction in Rad51–Rad55-Rad57 complex formation (**Figure 4.2.3C**). I confirmed that the E206A mutation does not render Rad51 intrinsically defective (**Figure 4.2.4B, C, D and 6.2.1C**), arguing against the trivial possibility that this DNA damage sensitivity is due to the E206A mutation impairing the biochemical activity of Rad51. Furthermore, physical and functional interaction analysis suggested that Rad51-E206A retains a normal interaction with Rad52 (**Figure 7.2.1A, C, D**) and Rad54 (**Figure 7.2.2B,C**), which corroborate my genetic data suggesting that the E206A mutation specifically impairs the interaction of Rad51 with Rad55-Rad57. Taken together, these results clearly indicate that the PAP is important for the Rad51–Rad55-Rad57 interaction.

Mutation of all three PAP residues to Ala (*rad51-EED*) abrogated Rad51-mediated DNA repair, exhibiting a phenotype similar to *rad51*Δ (**Figure 5.2.1C**) and reduction of stable in vivo complex formation with Rad55-Rad57 (**Figure 5.2.1D**). Furthermore, the number of Rad51 foci is reduced in the *rad51-EED* strain to the same level as the *rad57*Δ *sfr1*Δ and *rad52*Δ mutant backgrounds, indicating that the EED mutation impairs the mechanisms promoting Rad51 recruitment to sites of DNA damage (**Figure 5.2.5D**). Interestingly, a charge reversal mutation whereby E206 is mutated to

Lys rather than Ala (*rad51-E206K*) phenocopied *rad51-EED*, displaying the same DNA damage sensitivity as the *rad51*Δ strain (**Figure 5.2.4A**).

Biochemical analysis revealed that Rad51-EED is not intrinsically defective (**Figure 6.2.1C**). Furthermore, despite a mild reduction in physical binding with Swi5-Sfr1, Rad51-EED did not exhibit any defect in potentiation by Swi5-Sfr1 (**Figure 6.2.2A, B**). By contrast, the EED mutation completely abolished Rad51-Rad52 complex formation in vivo and Rad51-Rad52 physical binding in vitro (**Figure 7.2.1A, C, D**). Additionally, the EED mutation caused an approximately three-fold reduction in Rad51-Rad54 physical binding (**Figure 7.2.2B**) and Rad51-EED was less sensitive to stimulation from Rad54 (**Figure 7.2.2C**), suggesting that this physical binding defect had functional consequences.

In conclusion, the PAP is a motif of Rad51 that is essential for Rad52 binding and important for the interactions with both Rad55-Rad57 and Rad54. Thus, the PAP is integral to recombinational DNA repair.

8.2 The PAP facilitates interaction of Rad51 with multiple auxiliary factors

The FxxA consensus sequence (^{108}FTTA^{111} in *Sp*Rad51) plays a key role in Rad51 oligomerization. The highly conserved Phe residue inserts into a hydrophobic pocket above the β-strand of the adjacent Rad51 monomer in order to promote oligomerization. It has been shown that some auxiliary factors such as BRCA2 also contain the FxxA motif and interact with Rad51 by mimicking the mechanism through which two Rad51 monomers bind each other; FxxA has therefore been proposed to function as a Rad51 interaction motif (Pellegrini et al., 2002; Shin et al., 2003). Neither Swi5 nor Sfr1 contain the FxxA consensus sequence and it was recently shown that

two non-FxxA sites in the intrinsically disordered N-terminal domain of Sfr1 are responsible for binding to Rad51 (Argunhan et al., 2020). However, other auxiliary factors in *S. pombe* do contain the FxxA consensus sequence, such as Rad57 (^{145}FELA^{148}), Rad52 (^{17}FNTA^{20} and ^{338}FISA^{341}) and Rad54 (^{804}FIRA^{807}). Interestingly, Rad55 does not contain the FxxA motif, which is consistent with Y2H analysis suggesting that Rad51 interacts with Rad57 but not Rad55 in *S. pombe* (Tsutsui et al., 2001). Furthermore, Y2H analysis by Kim et al. (2002) demonstrated that the minimum Rad51-interacting region of Rad52 lies within a C-terminal fragment (310-469) containing the ^{338}FISA^{341} sequence. Additionally, mutation of the Phe residue of the FxxA motif to Ala (F349A) in *Sc*Rad52 results in a complete loss of interaction with Rad51 (Kagawa et al., 2014). Collectively, these results suggest that Rad52, and possibly Rad57, utilise the FxxA motif to bind to Rad51.

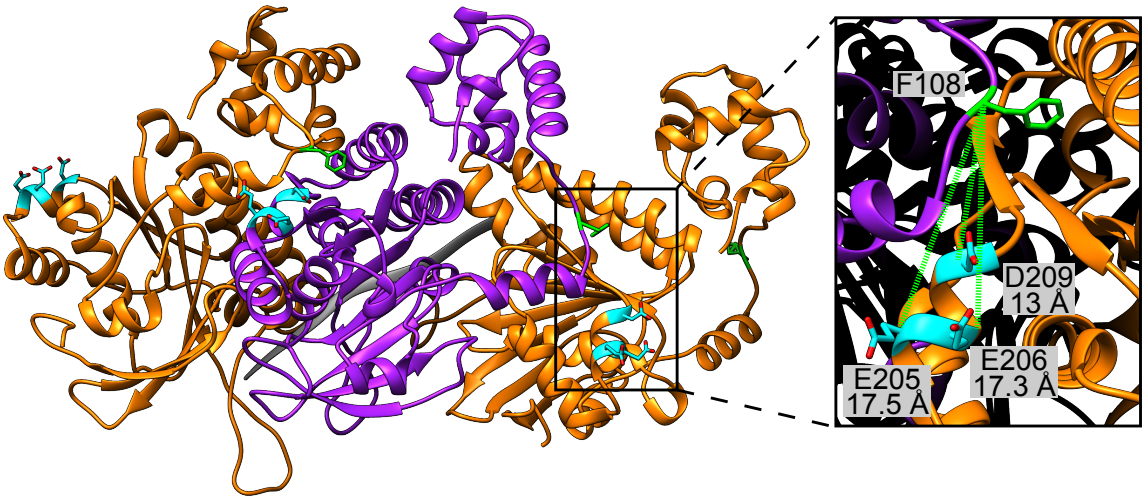
My data shows that mutating all three PAP residues renders Rad51 defective for interactions with Rad55-Rad57, Rad52 and Rad54 (**Figures 4.2.3C, 5.2.1D, 7.2.1** and **7.2.2**). By contrast, mutation of all three PAP residues resulted in only a mild defect in the physical interaction with Swi5-Sfr1, which did not translate to a functional defect (**Figures 6.2.2** and **4.2.4G**). While it is possible that the PAP has some role in facilitating the interaction between Rad51 and Swi5-Sfr1, results suggest it is not the primary binding site for Swi5-Sfr1. Rather, data suggest that the PAP is particularly important for auxiliary factors that employ Rad51 mimicry to bind to Rad51. Interestingly, in the context of the Rad51 presynaptic filament, the C_α-C_α distances between PAP residues and F108 of the adjacent monomer are 13.0 Å (D209), 17.3 Å (E206), and 17.5 Å (E205; **Figure 8.2A**). Here, I employ the presynaptic filament as a proxy to visualise the insertion of the Phe of FxxA into the hydrophobic pocket of Rad51. In reality, I postulate that the FxxA motif would belong to an auxiliary factor.

These distances are clearly too far for molecular interactions, making it very unlikely that the PAP directly interacts with the FxxA motif, consistent with the fact that the PAP is highly charged whereas FxxA is hydrophobic. I therefore predict that auxiliary factors may contain a basic region that is close in three-dimensional space to their FxxA motif; this negatively charged motif might be close enough to the PAP to participate in electrostatic interactions. Consistently, I infer that the overall negative character of the PAP is important for Rad51-mediated DNA repair since combining Asp/Glu-to-Ala mutations had a more drastic effect than individual mutations (**Figure 5.2.1C**), and unlike the E206A mutation, the E206K mutation completely abrogated Rad51-mediated DNA repair (**Figure 5.2.4A**). I propose that the PAP functions as an ancillary interaction site that augments FxxA interaction to stabilise inter-subunit contacts.

Kim et al. (2002) isolated several *Sp*Rad51 mutants through Y2H analysis that show loss of interaction with auxiliary factors. The G177S, C179F, G282D, and L274P mutations all result in disruption of the Rad51-Rad52 interaction. Interaction of Rad51 with Rad54 was also impaired as a result of the G177S and C179F mutations. Additionally, the C179F mutation abolished the interaction with Rad57. It is striking that both G177S and C179F mutations impair interactions with multiple auxiliary factors (G177S, Rad52 and Rad54; C179F, Rad52 and Rad57). Moreover, the fact that C179F also impairs the self-association of Rad51 is consistent with the notion that auxiliary factors interact with Rad51 via Rad51 mimicry. The C_{α}-C_{α} distances for the FxxA motif and these residues range from 11.5–20.4 Å, and at least some (G177 and C179) of these residues are reasonably close to the PAP (9–12 Å). It is therefore plausible that these mutations impair PAP function and/or F108 insertion, supporting the notion that multiple auxiliary factors employ Rad51 mimicry to interact with Rad51

via the PAP. I nevertheless acknowledge the limitations of Y2H analysis, which involves protein fusions that may affect protein function. Moreover, the mutation of a cysteine residues may affect tertiary structure through loss of a disulphide bridge, which could also explain the severe interaction defect of the C179F mutant (Kim et al., 2002).

A ***S. pombe*** **Rad51-ssDNA filament**
Homology model



B ***S. pombe*** **Rad51-ssDNA filament**
Homology model

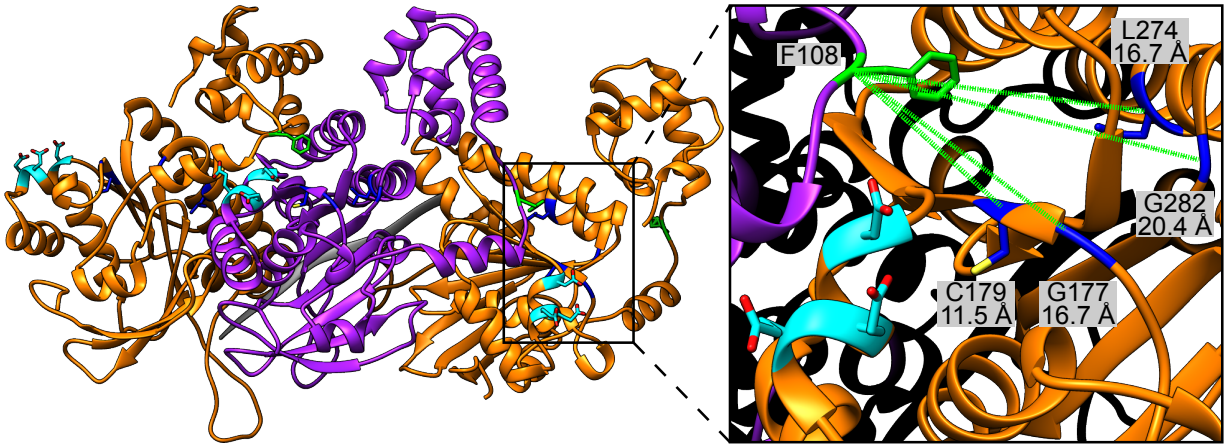


Figure 8.2. Homology model of the *Sp*Rad51 presynaptic filament showing the polymerisation motif (F108), PAP residues, and Y2H interaction mutants

(A,B) Ribbon depiction of three SpRad51 monomers (alternating orange and purple) bound to ssDNA (9-mer poly-dT in gray). Residues E205, E206, and D209 are colored in cyan with their side-chains shown (O atoms in red), and F108 is colored in green with its side-chain shown. The α-helix of the rightmost monomer containing E205, E206, and D209 is enlarged, along with the F108 residue of the central monomer, to illustrate the close proximity of these residues at the subunit interface. Dotted-green lines show the C_α-C_α distance between F108 and PAP residues **(A)** or residues (colored in blue with S atom in yellow) that were shown by Kim et al. (2002) to impair the interaction of Rad51 with its auxiliary factors in Y2H analysis **(B)**.

Mutating individual PAP residues resulted in reduced complex formation with Rad55-Rad57 in vivo, but even the collective mutation of PAP residues in the *rad51-EED* strain did not completely abolish in vivo complex formation (**Figures 4.2.3C** and **5.2.1D**). On the other hand, the D209A point mutation led to a marked reduction in Rad51-Rad52 complex, but this interaction was unaffected by the E206A mutation. However, the EED mutation completely abrogated this interaction (**Figure 7.2.1**). Similar results were obtained from the Rad54 interaction analysis in that the E206A mutation did not affect the physical or functional interaction with Rad54 whereas Rad51-EED showed clear defects (**Figure 7.2.2**). Unfortunately, biochemical analysis of the effect of PAP mutations on Rad51 stimulation by Rad55-Rad57 awaits the purification of this complex. Nevertheless, my in vivo data strongly suggest that the PAP is important for Rad55-Rad57 binding.

Results indicate that the PAP is important for Rad51-mediated DNA repair because it is essential for the Rad51-Rad52 interaction and important for the binding of Rad51 to both Rad55-Rad57 and Rad54. Rad52 is known to play a critical role in DNA repair because it promotes Rad51 filament formation on RPA-coated ssDNA and can anneal complementary ssDNA molecules. The ssDNA annealing domain is situated towards the N-terminal region and is highly conserved among eukaryotes. By contrast, the C-terminal half of Rad52 containing the Rad51 and RPA binding regions shows poor sequence conservation. This is likely because the C-terminal domain is intrinsically disordered (Singleton et al., 2002; Kagawa et al., 2002; Kagawa et al., 2014) and can tolerate random mutations more than structured regions (Daughdrill et al., 2007). Four point mutations in *Sp*Rad52 (S377F, S379L, P381S and P381L) were found to ablate the Y2H interaction with Rad51 (Kim et al., 2002); these residues are all in the C-

terminal half of *Sp*Rad52, which is consistent with the notion that this domain, which contains the FxxA motif (^{338}FISA^{341}), is involved in binding to Rad51.

Although the function of PAP is relevant to several auxiliary factors, this does not necessarily mean that they are competing to bind Rad51. As can be seen in Figure 3.2.3A, there are as many PAP motifs in the Rad51 presynaptic filament as there are Rad51 monomers, which increases the chances of non-competitive binding. Additionally, these auxiliary factors have non-overlapping roles, with Rad52 performing the most upstream function, followed by the requirement for Rad55-Rad57, and finally Rad54 (Sugawara et al., 2003; Lisby et al., 2004). Moreover, because the binding to Rad55-Rad57 and Rad54 is not completely lost in the PAP mutants, there may be other sites on Rad51 that facilitate binding independently of the PAP-FxxA axis. Raschle et al. (2004) showed that, at physiological ionic strength (150 mM KCl), a truncation mutant of *Sc*Rad54 lacking the 129 N-terminal amino acids cannot interact with *Sc*Rad51. However, under less stringent conditions (15 mM KCl), the same mutant maintains a specific interaction with *Sc*Rad51, pointing towards the existence of a second site within *Sc*Rad54 that can bind Rad51. The consensus FxxA motif could not be found within *Sc*Rad54, but YxxA (^{858}YGDA^{861}) and WxxA (^{754}WNPA^{757}) sequences in the C-terminal half of the protein were seen; these substitutions may be compatible with the ball-and-socket interaction mechanism given that WxxA did not abolish the interaction of BRC repeat peptides with Rad51 (Scott et al., 2016). It is likely that the N-terminal domain of Rad54, which is thought to be intrinsically disordered (Raschle et al., 2004; Thomä et al., 2005), interacts with Rad51 through an FxxA-independent mechanism, perhaps in a manner analogous to the intrinsically disordered N-terminal half of Sfr1 (Argunhan et al., 2020), whereas the C-terminal domain may interact via Rad51 mimicry involving (F/Y/W)xxA.

On the other hand, the auxiliary factors may have to compete with a Rad51 molecule attempting to interact with the terminal Rad51 monomer of the presynaptic filament through FxxA insertion. It is also possible that an auxiliary factor can interrupt the Rad51 filament by disrupting the FxxA insertion between two monomers and hence inserting itself into the filament (Pellegrini et al., 2002; Shin et al., 2003). If there is competition between Rad51 molecules and auxiliary factors for FxxA insertion, the PAP may stabilize the interaction between auxiliary factors and filamentous Rad51 molecules to allow them to better compete for FxxA insertion. Alternatively, electron microscopy experiments have shown that the Rad51 presynaptic filament forms from multiple nucleation events and is therefore not as continuous as the RecA filament (Ogawa et al., 1993); at least in the case of *Hs*RAD51, the terminal monomer of the filament is thought to serve as a binding site for the BRCA2 auxiliary factor (Shahid et al., 2014). Thus, it is also possible that any competition between auxiliary factors and Rad51 for FxxA insertion is alleviated in part by the relatively discontinuous nature of the Rad51 presynaptic filament.

Due to the severe DNA damage sensitivity of *rad51-EED*, I first sought to determine whether the EED mutation impairs the intrinsic activity of Rad51. The DNA binding activity of Rad51-EED was comparable to wild-type Rad51 (**Figure 6.2.1D,E**), and critically, the intrinsic strand exchange activity was not impaired (**Figure 6.2.1C**). However, unexpectedly, Rad51-EED displayed increased strand exchange activity compared to wild type. This was especially surprising given the severe phenotype of *rad51-EED*. Human RAD51 was shown to physically bind *Hs*RPA via RPA1 (the 70 kDa subunit of the heterotrimeric protein complex) by far-western analysis (Golub et al., 1998). Although similar experiments have not been conducted with *S. pombe* proteins, Y2H analysis pointed towards a weak interaction between *Sp*Rad51 and its

cognate Rpa1 (Tsutsui et al., 2001). It is therefore possible that any such interaction is enhanced by the EED mutation, leading to a higher local concentration of Rad51-EED in the vicinity of the ssDNA pre-occupied with RPA. Studies have shown that in vitro, there is a facilitated exchange between the free RPA present in solution and the ssDNA-bound RPA (Ma et al., 2017). Due to the increased local concentration of Rad51-EED, when a patch of free ssDNA becomes available during the facilitated exchange of RPA, Rad51-EED may take this opportunity to initiate filament nucleation. Moreover, because Rad51 filament assembly is cooperative, when nucleation has commenced under conditions of excess Rad51 (e.g., 15 μM Rad51 and 1 μM RPA in **Figure 6.2.1C**), Rad51 may be able to displace RPA and further facilitate filament formation (Ma et al., 2017; Gibb et al., 2014). The in vitro ability of Rad51 to displace RPA in the absence of auxiliary factors, which is the case in my intrinsic strand exchange reaction, is dependent on the presence of ATP (Gibb et al., 2014). Rad51-EED might also bind ATP stronger than wild type in vitro, and as a result, displace RPA and/or nucleate faster than wild-type Rad51. Additionally, ATP hydrolysis is important for the completion of DNA strand exchange and leads to the dissociation of Rad51-dsDNA (i.e., post-synaptic) complexes (Ito et al., 2018), so increased ATP hydrolysis and/or binding could enhance Rad51 activity through these two mechanisms. The PAP is not located anywhere close to the catalytic domain involved in ATP binding/hydrolysis. Nevertheless, it is plausible that mutation of three negatively charged residues in Rad51-EED could reduce the repulsion towards negatively charged ATP molecules, which could indirectly facilitate the catalytic binding of ATP.

Interestingly, individual PAP mutations impair Rad51-mediated DNA repair to varying degrees (**Figure 5.2.1C**). *rad51-D209A* showed the most severe phenotype,

whereas *rad51-E206A,* and to a lesser extent *rad51-E205A*, only display sensitivity in the *sfr1*Δ background, where HR is completely dependent on Rad55-Rad57 (**Figures 5.2.2A, 5.2.3A**). This observation is consistent with the idea that PAP is more pertinent for the function of Rad55-Rad57 than Swi5-Sfr1. In the *rad51-EE* strain, where both E205 and E206 residues are mutated to alanine, DNA damage sensitivity is observed even in the presence of Sfr1; this synergy implies that the function of E205 and E206 residues are related to each other (**Figure 5.2.1C**). Therefore, it is plausible that the ability of Sfr1 to suppress *rad51-E206A* is dependent on E205 (and D209), and therefore partial PAP function in mediating interactions with other auxiliary factors, which may compensate for the impaired interaction with Rad55-Rad57. More pertinently, although *rad51-D209A* showed clear sensitivity to DNA damage, it was still not as sensitive as *rad51*Δ, indicating that it retained some biological activity. This remaining activity was completely abrogated by additional mutation of E205 and E206 (*rad51-EED*) (**Figure 5.2.1C**). This additive effect seen when all three residues are mutated is consistent with the notion that the overall negativity of PAP is important for its function. This is supported by results showing that replacement of E206 with a positive lysine residue completely eliminates Rad51-dependent DNA repair, phenocopying *rad51-EED* and *rad51*Δ phenotype (**Figure 5.2.4A**). These results suggest that all three residues of the PAP are important for its function, although D209 seems to be more important than E206, which itself is more significant than E205. A notable observations from this trend is that possibly, the acidic residues closer to the site of FxxA play a more prominent role in facilitating this interaction

8.3 The PAP is an evolutionary conserved motif that is integral to recombinational DNA repair

Based on sequence alignments, the PAP is generally conserved among eukaryotes, with E206 and D209 residues each showing conservation in seven-out-of-eight Rad51 orthologs examined here (**Figure 3.2.4A**). The PAP of the meiosis-specific RecA-family recombinase Dmc1 is also conserved in *S. pombe* and *H. sapiens. Sp*Dmc1 PAP includes D174, D176, and E180, whereas the corresponding residues in *Hs*DMC1 are D180, D182, and D186. Although, the structure of *Sp*Dmc1 is yet to be determined, structural studies of *Hs*DMC1 have revealed an octameric ring structure with a similar polymerisation motif as Rad51 (Kinebuchi et al., 2004). In the case of *Hs*DMC1, it is the F85 from the FxxA consensus motif that establishes a ball-and-socket hydrophobic interaction with the adjacent monomer. Thus, given that the polymerization mechanism for Rad51 and Dmc1 is highly similar, it seems plausible that the PAP may also act as a landing pad for auxiliary factors that utilise DMC1 mimicry to interact with DMC1. The PAP motif of RadA consists of D192, D194 and E195 residues and oligomerization in archeal RadA involves the same kind of interactions, as these regions are highly conserved in RecA-family of recombinases. F97 is the phenylalanine residue of the FxxA consensus motif that inserts into a hydrophobic pocket formed by residues from the β_2, β_3 and α_{11} of the adjacent monomer (Shin et al., 2003).

By contrast to the eukaryotic RecA-family recombinases and *Pyrococcus furiosus* RadA, which I take as a representative example of archaeal RadA, bacterial RecA is the only ortholog lacking the PAP (**Figure 3.2.4D, E**). There are two striking features that clearly distinguish bacterial RecA from Rad51/Dmc1 and RadA: RecA filament formation does not involve the FxxA-dependent ball-and-socket mechanism,

and RecA is not regulated by an expanse of recombination auxiliary factors. The region of RecA that is conserved in Rad51/Dmc1 and RadA is the ATPase core, whereas the N- and C-termini are highly diverged (Story et al., 1992; Pellegrini et al., 2002; Shin et al., 2003). Importantly, whereas the N-terminal domain of RecA is known to play an important role in facilitating intersubunit interactions within the presynpatic filament (Prentiss et al., 2015), the N-terminal domain of Rad51 is involved in DNA binding, not intersubunit interactions (Aihara et al., 1999). Furthermore, Rad51 is regulated by Rad52, Rad54, Rad55-Rad57, and Swi5-Sfr1. While RecFOR fulfils an analogous function as Rad52 in *E. coli* (Beernink et al., 1999; Morimatsu et al., 2003), it is not a homolog of Rad52. Although a RecA paralog has been reported to regulate branch migration (Cooper & Lovett, 2016), homologs of either Rad54 or Swi5-Sfr1 — or even proteins that perform an analogous function — have not been reported in *E. coli*. By contrast, RadA paralogs have been characterized genetically and biochemically in archaea (Haldenby et al., 2009) and a bonafide Rad54 homolog has been identified (Haseltine & Kowalczykowski, 2009). Although there are no reports of a Swi5-Sfr1 or Rad52 ortholog in archaea, this does not preclude the possibility of functional analogs existing in this domain of life, in which HR is relatively poorly characterised compared to eukaryotes and bacteria (White, 2011). Nevertheless, given the higher resemblance of Rad51 to RadA as opposed to RecA (Shin et al., 2003), there are clearly more similarities between the archaeal and eukaryotic HR systems than there are between either and the bacterial system (White, 2011). Furthermore, due to other inherent differences such as the relatively robust ATPase activity compared to other RecA-family recombinases, RecA does not need a factor such as Rad54 to promote its dissociation from dsDNA (Liu et al., 2011a).

8.4 Interplay between Rad55-Rad57 and Swi5-Sfr1

Biochemical analysis indicated that Rad51-E206A has comparable biochemical properties to wild-type Rad51. Furthermore, Rad51-E206A did not exhibit any gross defects in binding to Rad52 or in the physical and functional interactions with Swi5-Sfr1 and Rad54. However, mutating E206 to Ala renders Rad51 specifically defective for the genetic and physical interaction with Rad55-Rad57, indicating that the PAP is important for the interaction with Rad55-Rad57. The *rad51-E206A* strain did not display any deficiency in Rad51-mediated DNA repair in the presence of Sfr1 but it was completely defective in the absence of Sfr1 (**Figure 4.2.1**). The suppression conferred by Sfr1 is not through stabilisation of Rad51–Rad55-Rad57 complex formation (**Figure 4.2.3C**), which suggests that Swi5-Sfr1 can functionally compensate for a defect in the physical association of Rad51 with Rad55-Rad57. It is possible that there is some overlap between Rad55-Rad57 and Swi5-Sfr1 function, such that a reduction in complex formation between either auxiliary factor and Rad51 does not result in a DNA repair defect. However, given that there are clear differences in HR outcomes (Akamatsu et al., 2007) and in sensitivity to different DNA damaging agents (Argunhan et al., 2020) between *rad55Δ/rad57Δ* and *swi5Δ/sfr1Δ*, any functional overlap is likely to be limited. Surprisingly, while *rad51-E206A* does not show any sensitivity to DNA damage (implying HR efficiency) in the presence of Swi5-Sfr1 (**Figure 4.2.1A, D**), it can also suppress *rqh1Δ* sensitivity (implying HR deficiency), in the presence of Swi5-Sfr1 (**Figure 4.2.2A**). This difference is probably because the dynamic range of *rqh1Δ* suppression is greater, since I can even distinguish *rad51Δ* or *rad54Δ* from *rad57Δ sfr1Δ* double mutant phenotype. Expression of *E. coli* Holliday junction resolvase, RusA, partially suppresses sensitivity of *rqh1Δ* cells to UV and HU. Therefore, it is suggested that in the absence of *rqh1*$^{+}$, stalled

replication forks accumulate unresolved Holliday junctions (Doe et al., 2000). To this end, Hope et al. (2005) have shown that loss of *rad57*$^{+}$ almost completely suppressed the *rqh1*Δ sensitivity, similar to the observation in my analysis (**Figure 4.2.2A**). The authors have shown that the suppression by loss of *rad57*$^{+}$ is dependent on Rad51 and Rad54, suggesting a role for Rad55-Rad57 downstream of joint molecule formation that can be deleterious to cells if Rqh1 is functional. However, the mechanistic reason for suppression of *rqh1*Δ sensitivity by HR factors is yet to be understood. This is further complicated by the fact that Rqh1 has both a pre-synaptic and a post-synaptic role during HR.

The suppression of *rad51-E206A* DNA damage sensitivity by Swi5-Sfr1 opposes the commonly accepted model wherein Rad55-Rad57 and Swi5-Sfr1 comprise two independent sub-pathways of Rad51-mediated DNA repair (Akamatsu et al., 2003; Akamatsu et al., 2007). Interestingly, it was recently shown that the *sfr1-7A* mutant, which exhibits a near-loss of physical binding to Rad51, is proficient for DNA repair (Argunhan et al., 2020). However, contrary to expectations, the *sfr1-7A rad55*Δ*/rad57*Δ double mutants were as sensitive to DNA damage as *sfr1*Δ *rad55*Δ*/rad57*Δ double mutants, suggesting that a Rad55-Rad57–dependent mechanism can suppress defects in the binding of Swi5-Sfr1 to Rad51. Additionally, the authors demonstrated that Swi5-Sfr1 and Swi5-Sfr1–7A can physically interact with partially purified Rad55-Rad57. Based on these observations, the authors proposed that Rad55-Rad57 may facilitate the recruitment of Swi5-Sfr1–7A to Rad51 by binding to both interacting partners and functioning as a molecular bridge. If Rad51-mediated HR was independently promoted by Rad55-Rad57 or Swi5-Sfr1, then the DNA damage sensitivity of *sfr1-7A* and *rad51-E206A* would be expected to mirror *sfr1*Δ and *rad57*Δ, respectively. The fact that *sfr1-7A* and *rad51-E206A* are as resistant

to DNA damage as wild type, and this is dependent on the other complex, strongly argues that Swi5-Sfr1 and Rad55-Rad57 collaboratively promote Rad51-mediated DNA repair, while also being capable of functioning independently of each other. The division of labour between Rad55-Rad57 and Swi5-Sfr1 remains enigmatic and will likely be a focal topic of future research.

In this study, I have identified a novel motif of Rad51 that is relevant to the function of several auxiliary factors. By doing so, I invite the field to think differently about the dynamics of auxiliary factor interactions with Rad51. It is possible that at least in eukaryotes, the Rad51 filament is not as homogenous as we think, and there are auxiliary factors situated mosaically along the Rad51 filament (Taylor et al., 2016). Despite several years of research on the function of auxiliary factors, there is still much to uncover about their relationship with Rad51, and even more so about their relationship with each other. The idea that auxiliary factors and Rad51 might be forming a higher order super-complex is plausible, especially considering the demonstration of Rad52 repair foci that are thought to contain many molecules of different HR proteins colocalized at a single DSB (Lisby & Rothstein, 2001; Lisby et al., 2004). Additionally, Argunhan et al. (2020) have shown that Swi5-Sfr1 can physically bind to a partially purified Rad55-Rad57 complex and unpublished data also suggests that Rlp1 subunit of *S. pombe* Shu complex can physically interact with the Swi5-Sfr1 complex. It is still a very open question as to why a single binding region for a variety of interacting partners exists on proteins such as Rad51, but given the widespread conservation of the PAP, I postulate that this mode of interaction has conferred an evolutionary advantage. Further research will be needed to determine the importance of the PAP for recombinational DNA repair in other species.

Bibliography

Aihara H, Ito Y, Kurumizaka H, Yokoyama S, Shibata T. (1999). The N-terminal domain of the human Rad51 protein binds DNA: structure and a DNA binding surface as revealed by NMR. *Journal of Molecular Biology*, 290 (2), pp. 495-504

Ait Saada A, Lambert S. A. E, Carr A. M. (2018). Preserving replication fork integrity and competence via the homologous recombination pathway. *DNA Repair*, 71, pp. 135–147

Akamatsu Y, Dziadkowiec D, Ikeguchi M, Shinagawa H, Iwasaki H. (2003). Two different Swi5-containing protein complexes are involved in mating-type switching and recombination repair in fission yeast. *Proceedings of the National Academy of Sciences*, 100, pp. 15770-15775

Akamatsu Y & Jasin M. (2010). Role for the mammalian Swi5-Sfr1 complex in DNA strand break repair through homologous recombination. *PLoS Genetics*, 6 (10): e1001160

Akamatsu Y, Tsutsui Y, Morishita T, Siddique M. S, Kurokawa Y, Ikeguchi M, Yamao F, Arcangioli B, Iwasaki H. (2007). Fission yeast Swi5/Sfr1 and Rhp55/Rhp57 differentially regulate Rhp51-dependent recombination outcomes. *The EMBO Journal*, 26, pp. 1352–1362

Amitani I, Baskin R. J, Kowalczykowski S. C. (2006). Visualization of Rad54, a chromatin remodeling protein, translocating on single DNA molecules. *Molecular Cell*, 23 (1), pp. 143-148

Amunugama R, Fishel R. Homologous Recombination in Eukaryotes. Doetsch P. W. *Mechanisms of DNA repair*. Oxford, Academic Press Elsevier. (2012). pp. 155-206

Amunugama R, Groden J, Fishel R. (2013). The HsRAD51B-HsRAD51C stabilises the HsRAD51 nucleoprotein filament. *DNA repair*, 12, pp. 723–732

Argunhan B, Leung W. K, Afshar N, Terentyev Y, Subramanian V. V, Murayama Y, Hochwagen A, Iwasaki H, Tsubouchi T, Tsubouchi H. (2017b). Fundamental cell cycle kinases collaborate to ensure timely destruction of the synaptonemal complex during meiosis. *The EMBO Journal*, 36, pp. 2488–2509

Argunhan B, Murayama Y, Iwasaki H. (2017a). The differentiated and conserved roles of Swi5-Sfr1 in homologous recombination. *FEBS Letters*, 591, pp. 2035-2047

Argunhan B, Sakakura M, Afshar N, Kurihara M, Ito K, Maki T, Kanamaru S, Murayama Y, Tsubouchi H, Takahashi M, Takahashi H, Iwasaki H. (2020).

Cooperative interactions facilitate stimulation of Rad51 by the Swi5-Sfr1 auxiliary factor complex. *eLife*, 9:e52566

Beernink H. T. H & Morrical S. W. (1999). RMPs: recombination/replication mediator proteins. *Trends in Biochemical Sciences*, 24 (10), pp. 385-389

Bianchi M, Dasgupta C, Radding C. M. (1983). Synapsis and the formation of paramedic joints by E. coli RecA protein. *Cell*, 34 (3), pp. 931-939

Bizard A. H, Hickson I. D. (2014). The dissolution of double Holliday junctions. *Cold Spring Harbor Perspectives in Biology*, 6:a016477

Bugreev D. V, Hanaoka F, Mazin A. V. (2007). Rad54 dissociates homologous recombination intermediates by branch migration. *Nature structural & molecular biology*, 14, pp. 746–753

Bonilla B, Hengel S. R, Grundy M. K, Bernstein K. A. (2020). RAD51 Gene Family Structure and Function. *Annual Review of Genetics*, 54, pp. 1–22

Bugreev D. V, Mazina O. M, Mazin A. V. (2006). Rad54 protein promotes branch migration of Holliday junctions. *Nature*, 442, pp. 590–593

Caldwell C. C & Spies M. (2020). Dynamic elements of replication protein A at the crossroads of DNA replication, recombination and repair. *Critical Reviews in Biochemistry and Molecular Biology*, 55 (5), pp. 482-507

Ceballos S. J & Heyer W. D. (2011). Functions of the Snf2/Swi2 family Rad54 motor protein in homologous recombination. *Biochimica et Biophysica Acta-Gene Regulatory Mechanisms*, 1809 (9), pp. 509-523

Chen J, Villanueva N, Rould M. A, Morrical S. W. (2010). Insights into the mechanism of Rad51 recombinase from the structure and properties of a filament interface mutant. *Nucleic Acids Research*, 38, pp. 4889–4906.

Chen Z, Yang H, Pavletich N. P. (2008). Mechanism of homologous recombination from the RecA-ssDNA/dsDNA structures. *Nature*, 453, pp. 489–494

Clark A. J & Margulies A. D. (1965). Isolation and characterisation of recombination-deficient mutants of Escherichia Coli K12. *Proceedings of the National Academy of Sciences*, 53 (2), pp. 451-459

Cloud V, Chan Y. L, Grubb J, Budke B, Bishop D. K. (2012). Rad51 is an accessory factor for Dmc1-mediated joint molecule formation during meiosis. *Science*, 337 (6099), pp. 1222-1225

Cole D. J, Rajendra E, Roberts-Thomson M, Hardwick B, McKenzie G. J, Payne M. C, Venkitaraman A. R, Skylaris C. K. (2011). Interrogation of the protein-protein interactions between human BRCA2 BRC repeats and RAD51 reveals atomistic determinants of affinity. *PLoS Computational Biology*, 7 (7), e1002096

Conway A. B, Lynch T. W, Zhang Y, Fortin G. S, Fung C. W, Symington L. S, Rice P. A. (2004). Crystal structure of a Rad51 filament. *Nature Structural & Molecular Biology*, 11, pp.791–796

Cooper D. L & Lovett S. T. (2016). Recombinational branch migration by the RadA/Sms paralog of RecA in *Escherichia coli*. *eLife*, 5, 26397

Costa S. J, Almeida A, Castro A, Domingues L, Besir H. (2013). The novel Fh8 and H fusion partners for soluble protein expression in Escherichia coli: a comparison with the traditional gene fusion technology. *Applied Microbiology and Biotechnology*, 97, pp. 6779–6791

Cox M. M. (2007). Motoring along with the bacterial RecA protein. *Nature Reviews Molecular Cell Biology*, 8, pp. 127–138

Cox J. M, Tsodikov O. V, Cox M. M. (2005). Organised Unidirectional Waves of ATP Hydrolysis within a RecA Filament. *PLoS Biology*, 3 (2)

Crickard J. B, Moevus C. J, Kwon Y, Sung P, Greene E. C. (2020). Rad54 drives ATP hydrolysis-dependent DNA sequence alignment during homologous recombination. *Cell*, 181 (6), pp. 1380-1394

Cromie G. A, Hyppa R. W, Taylor A. F, Zkharyevich K, Hunter N, Smith G. R. (2006). Single Holliday junctions are intermediates of meiotic recombination. *Cell*, 127, pp. 1167-1178

Daley J. M, Tomimatsu N, Hooks G, Wang W, Miller A. S, Xue X, Nguyen K. A, Kaur H, Williamson E, Mukherjee B, Hromas R, Burma S, Sung P. (2020). Specificity of end resection pathways for double-strand break regions containing ribonucleotides and base lesions. *Nature Communications*, 11, 3088

Daughdrill G. W, Narayanaswami P, Gilmore S. H, Belczyk A, Brown C. J. (2007) Dynamic behavior of an intrinsically unstructured linker domain is conserved in the face of negligible amino acid sequence conservation. *Journal of molecular evolution*, 65, pp. 277–288

Doe C. L, Dixon J, Osman F, Whitby M. C. (2000). Partial suppression of the fission yeast *rqh1*$^{-}$ phenotype by expression of a bacterial Holliday junction resolvase. *The EMBO Journal*, 19 (11), pp. 2751-2762

Doe C. L, Osman F, Dixon J, Whitby M. C. (2004). DNA repair by a Rad22-Mus81-dependent pathway that is independent of Rhp51. *Nucleic Acids Research*, 32 (18), pp. 5570-5581

Feng Z, Scott S. P, Bussen W, Sharma G. G, Guo G, Pandita T. K, Powell S. N. (2011). Rad52 inactivation is synthetically lethal with BRCA2 deficiency. *Proceedings of the National Academy of Sciences*, 108 (2), pp. 686-691

Ferrari S. R, Grubb J, Bishop D. K. (2009). The Mei5-Sae3 protein complex mediates Dmc1 activity in Saccharomyces cerevisiae. *The Journal of Biological Chemistry*, 284 (18), pp. 11766-11770

Forget A. L, Kowalczykowski S. C. (2012). Single-molecule imaging of DNA pairing by RecA reveals a three-dimensional homology search. *Nature*, 482, pp. 423-427

Fortin G. S & Symington L. S. (2002). Mutations in yeast Rad51 that partially bypass the requirement for Rad55 and Rad57 in DNA repair by increasing the stability of Rad51-DNA complexes. *The EMBO Journal*, 21 (12), pp. 3160-3170

Fugger K, Mistrik M, Danielsen J. R, Dinant C, Falck J, Bartek J, Lukas J, Mailand N. (2009). Human Fbh1 helicase contributes to genome maintenance via pro- and anti-recombinase activities. *Journal of Cell Biology*, 186, pp. 655–663

Gaines W. A, Godin S. K, Kabbinavar F. F, Rao T, VanDemark A. P, Sung P, Bernstein K. A. (2015). Promotion of presynaptic filament assembly by the ensemble of *S. cerevisiae* Rad51 paralogues with Rad52. *Nature Communications*, 6, 7834

Galkin V. E, Wu Y, Zhang X. P, Qian X, He Y, Yu X, Heyer W. D, Luo Y, Egelman E. H. (2006). The Rad51/RadA N-Terminal domain activates nucleoprotein filament ATPase activity. *Structure*, 14, pp. 983-992

Game J. C & Mortimer R. K. (1974). A genetic study of x-ray sensitive mutants in yeast. *Mutation Research/Fundamental and Molecular Mechanisms of Mutagenesis*, 24 (3), pp. 281-292

Garcin E. B, Gon S, Sullivan M. R, Brunette G. J, De Cian A, Concordet J. P, Giovannangeli C, Dirks W. G, Eberth S, Bernstein K. A, Prakash R, Jasin M, Modesti M. (2019). Differential requirements for the RAD51 paralogs in genome repair and maintenance in human cells. *PLoS Genetics*, 15, e1008355

Gasior S. L, Olivares H, Ear U, Hari D. M, Weichselbaum R, Bishop D. K. (2001). Assembly of RecA-like recombinases: Distinct roles for mediator proteins in mitosis and meiosis. *Proceedings of the National Academy of Sciences*, 98 (15), pp. 8411-8418

Gasior S. L, Wong A. K, Kora Y, Shinohara A, Bishop D. K. (1998). Rad52 associates with RPA and functions with rad55 and rad57 to assemble meiotic recombination complexes. *Genes and Development*, 12 (14), pp. 2208-2221

Gibb B, Ye L. F, Kwon Y, Niu H, Sung P, Greene E. C. (2014). Protein dynamics during presynaptic-complex assembly on individual single-stranded DNA molecules. *Nature Structure and Molecular Biology*, 21, pp. 893–900

Golub E. I, Gupta R. C, Haaf T, Wold M. S, Radding C. M. (1998). Interaction of human Rad51 recombination protein with single-stranded DNA binding protein, RPA. *Nucleic Acids Research*, 26, pp. 5388–5393

Greene E. C. (2016). DNA sequence alignment during homologous recombination. *Journal of Biological Chemistry* 291, pp.11572–11580

Guirouilh-Barbat J, Lambert S, Bertrand P, Lopez B. S. (2014). Is homologous recombination really an error-free process?. *Frontiers in Genetics*, 5 (175)

Hakem R. (2008). DNA-damage repair; the good, the bad, and the ugly. *The EMBO Journal*, 27 (4), pp. 589-605

Haldenby S, White M. F, Allers T. (2009). RecA family proteins in archaea: RadA and its cousins. *Biochemical Society Transactions*, 37 (1), pp. 102-107

Haruta N, Kurokawa Y, Murayama Y, Akamatsu Y, Unzai S, Tsutsui Y, Iwasaki H. (2006). The Swi5-Sfr1 complex stimulates Rhp51/Rad51- and Dmc1-mediated DNA strand exchange in vitro. *Nature Structural & Molecular Biology*, 13, pp. 823-830

Haseltine C. A & Kowalczykowski S. C. (2009). An archaeal Rad54 protein remodels DNA and stimulates DNA strand exchange by RadA. *Nucleic acids research*, 37, pp. 2757–2770

Hayase A, Takagi M, Miyazaki T, Oshiumi H, Shinohara M, Shinohara A. (2004). A protein complex containing Mei5 and Sae3 promotes the assembly of the meiosis specific RecA homolog Dmc1. *Cell*, 119, pp. 927–940

Hays S. L, Firmenich A. A, Berg P. (1995). Complex formation in yeast double-strand break repair: participation of Rad51, Rad52, Rad55, and Rad57 proteins. *Proceedings of the National Academy of Sciences*, 92, pp. 6925–6929

Hays S. L, Firmenich A. A, Massey P, Banerjee R, Berg P. (1998). Studies of the interaction between Rad52 protein and the yeast single-stranded DNA binding protein RPA. *Molecular and Cellular Biology*, 18 (7), pp. 4400-4406

Hoffman C. S, Wood V, Fantes P. A. (2015). An ancient yeast for young geneticists: a primer on the Schizosaccharomyces pombe Model System. *Genetics*, 201, pp. 403-423

Hope J. C, Maftahi M, Freyer G. A. (2005). A postsynaptic role for Rhp55/57 that is responsible for cell death in *Δrqh1* mutants following replication arrest in *Schizosaccharomyces pombe*. *Genetics*, 170, pp. 519–531

Howard-Flanders P, West S. C, Stasiak A. (1984). Role of RecA protein spiral filaments in genetic recombination. *Nature*, 309, pp. 215–220

Huselid E & Bunting S. F. (2020). The regulation of homologous recombination by helicases. *Genes (Basel)*, 11 (5)

Ito K, Murayama Y, Kurokawa Y, Kanamaru S, Kokabu Y, Maki T, Mikawa T, Argunhan B, Tsubouchi T, Ikeguchi M, Takahashi M, Iwasaki H. (2020). Real-time tracking reveals catalytic roles for the two DNA binding sites of Rad51. *Nature Communications*, 11 (2950)

Ito K, Murayama Y, Takahashi M, Iwasaki H. (2018). Two three-strand intermediates are processed during Rad51-driven DNA strand exchange. *Nature Structure Molecular Biology*, 25, pp. 29-36

Jensen R. B, Carreira A, Kowalczykowski S. C. (2010). Purified human BRCA2 stimulates RAD51-mediated recombination. *Nature*, 467 (7316), pp. 678-683

Jensen K. L & Russell P. (2016). Ctp1-dependent clipping and resection of DNA double-strand breaks by Mre11 endonuclease complex are not genetically separable. *Nucleic Acids Research*, 44 (17), pp. 8241-8249

Jiang H, Xie Y, Houston P, Stemke-Hale K, Mortensen U. H, Rothstein R, Kodadek T. (1996). Direct association between the yeast Rad51 and Rad54 recombination proteins. *Journal of Biological Chemistry*, 271, pp. 33181–33186

Johnson R. D & Symington L. S. (1995). Functional differences and interactions among the putative RecA homologs Rad51, Rad55, and Rad57. *Molecular and Cell Biology*, 15, pp. 4843–4850

Kagawa W, Arai N, Ichikawa Y, Saito K, Sugiyama S, Saotome M, Shibata T, Kurumizaka H. (2014). Functional analyses of the C-terminal half of the *Saccharomyces cerevisiae* Rad52 protein. *Nucleic Acids Research*, 42, pp. 941– 951

Kagawa W, Kurumizaka H, Ishitani R, Fukai S, Nureki O, Shibata T, Yokoyama S. (2002) Crystal structure of the homologous-pairing domain from the human Rad52 recombinase in the undecameric form. *Molecular Cell*, 10, pp. 359–371

Kanaar R, Troelstra C, Swagemakers S. M. A, Essers J, Smit B, Franssen J. H, Pastink A, Bezzubova O. Y, Buerstedde J. M, Clever B, Heyer W. D, Hoeijmakers J. H. J. (1996). Human and mouse homologs of the Saccharomyces cerevisiaeRAD54DNA repair gene: evidence for functional conservation. *Current Biology*, 6 (7), pp. 828-838

Kelley L. A, Mezulis S, Yates C. M, Wass M. N, Sternberg M. J. (2015). The Phyre2 web portal for protein modeling, prediction and analysis. *Nature Protocols*, 10, pp. 845–858

Khasanov F. K, Salakhova A. F, Chepurnaja O. V, Korolev V. G, Bashkirov V. I. (2004). Identification and characterization of the rlp1^{+}, the novel Rad51 paralog in the fission yeast Schizosaccharomyces pombe. *DNA Repair*, 3, pp. 1363-1374

Khasanov F. K, Savchenko G. V, Bashkirova E. V, Korolev V. G, Heyer W. D, Bashkirov V. I. (1999). A new recombinational DNA repair gene from Schizosaccharomyces pombe with homology to Escherichia coli RecA. *Genetics*, 152, pp. 1557-1572.

Kim W. J, Park E. J, Lee H, Seong R. H, Park S. D. (2002). Physical Interaction between Recombinational Proteins Rhp51 and Rad22 in *Schizosaccharomyces pombe*. *Journal of Biological Chemistry*, 277, pp. 30264–30270.

Kinebuchi T, Kagawa W, Enomoto R, Tanaka K, Miyagawa K, Shibata T, Kurumizaka H, Yokoyama S. (2004). Structural basis for octameric ring formation and DNA interaction of the human homologous-pairing protein Dmc1. *Molecular cell*, 14, pp. 363–374

Komen S. V, Petukhova G, Sigurdsson S, Stratton S, Sung P. (2000). Superhelicity-driven homologous DNA pairing by yeast recombination factors Rad51 and Rad54. *Molecular Cell*, 6, pp. 563–572

Komen S. V, Petukhova G, Sigurdsson S, Sung P. (2002). Functional cross-talk among Rad51, Rad54, and replication protein A in heteroduplex DNA joint formation. *Journal of Biological Chemistry*, 277, pp. 43578–43587

Kowalczykowski S. C, Dixon D. A, Eggleston A. K, Lauder S. D, Rehrauer W. M. (1994). Biochemistry of homologous recombination in *Escherichia coli*. *Microbiological Reviews*, 58 (3), pp. 401-465

Krejci L, Damborsky J, Thomsen B, Duno M, Bendixen C. (2001). Molecular dissection of interactions between Rad51 and members of the recombination-repair group. *Molecular and Cellular Biology*, 21, pp. 966–976

Krejci L, Song B, Bussen W, Rothstein R, Mortensen U. H, Sung P. (2002). Interaction with Rad51 is indispensable for recombination mediator function of Rad52. *Journal of Biological Chemistry*, 277 (42), pp. 40132-40141

Kurokawa Y, Murayama Y, Haruta-Takahashi N, Urabe I, Iwasaki H. (2008). Reconstitution of DNA strand exchange mediated by Rhp51 recombinase and two mediators. *PLOS Biology*, 6:e88

Kuwabara N, Murayama Y, Hashimoto H, Kokabu Y, Ikeguchi M, Sato M, Mayanagi K, Tsutsui Y, Iwasaki H, Shimizu T. (2012). Mechanistic insights into the activation of Rad51-mediated strand exchange from the structure of a recombination activator, the Swi5-Sfr1 complex. *Structure*, 20 (3), pp. 440-449

Lee J. Y, Terakawa T, Qi Z, Steinfeld J. B, Redding S, Kwon Y, Gaines W. A, Zhao W, Sung P, Greene E. C. (2015). DNA recombination. Base triplet stepping by the Rad51/RecA family of recombinases. *Science*, 349 (6251), pp. 977-981

Lin Z, Kong H, Nei M, Ma H. (2006). Origins and evolution of the recA/RAD51 gene family: Evidence for ancient gene duplication and endosymbiotic gene transfer. *Proceedings of the National Academy of Sciences*, 103, pp. 10328–10333

Lisby M, Barlow J. H, Burgess R. C, Rothstein R. (2004). Choreography of DNA damage response: spatiotemporal relationships among checkpoint and repair proteins. *Cell*, 118 (6), pp. 699-713

Lisby M, Rothstein R, Mortensen U. H. (2001). Rad52 forms DNA repair and recombination centers during S phase. *Proceedings of the National Academy of Sciences*, 98, pp. 8276–8282

Liu J, Ehmsen K. T, Heyer W. D, Morrical S. W. (2011a). Presynaptic filament dynamics in homologous recombination and DNA repair. *Critical Reviews in Biochemistry and Molecular Biology*, 46 (3), pp. 240-270

Liu J & Heyer W. D. (2011b). Who's who in human recombination: BRCA2 and RAD52. *Proceedings of the National Academy of Sciences*, 108 (2), pp. 441-442

Liu J, Renault L, Veaute X, Fabre F, Stahlberg H, Heyer W. D. (2011d). Rad51 paralogues Rad55-Rad57 balance the antirecombinase Srs2 in Rad51 filament formation. *Nature*, 479, pp. 245-248

Liu N, Lamerdin J. E, Teebbs R. S, Schild D, Tucker J. D, Shen M. R, Brookman K. W, Siciliano M. J, Walter C. A, Fan W, Narayana L. S, Zhou Z. Q, Adamson A. W, Sorensen K. J, Chen D. J, Jones N. J, Thompson L. H. (1998). XRCC2 and XRCC3, new human Rad51-family members, promote chromosome stability and protect against DNA cross-links and other damages. *Molecular cell*, 1 (6), pp. 783-793

Liu T, Wan L, Wu Y, Chen J, Huang J. (2011c). hSWS1•SWSAP1 is an evolutionary conserved complex required for efficient homologous recombination repair. *Journal of Biological Chemistry*, 286 (48), pp. 41758-41766

Li X & Heyer W. D. (2009). RAD54 controls access to the invading 3′-OH end after RAD51-mediated DNA strand invasion in homologous recombination in *Saccharomyces cerevisiae*. *Nucleic Acids Research,* 37, pp. 638–646

Li X, Zhang X. P, Solinger J. A, Kiianitsa K, Yu X, Egelman E. H, Heyer W. D. (2007). Rad51 and Rad54 ATPase activities are both required to modulate Rad51-dsDNA filament dynamics. *Nucleic Acids Research*, 35, pp. 4124–4140

Loidl J, Lorenz A. (2009). Analysis of *Schizosaccharomyces pombe* meiosis by nuclear spreading. *Methods in Molecular Biology*, 558, pp. 15–36

Lorenz A, Osman F, Folkyte V, Sofueva S, Whitby M. C. (2009). Fbh1 limits Rad51-dependent recombination at blocked replication forks. *Molecular and Cellular Biology*, 29 (17), pp. 4742-4756

Lovett S. T & Mortimer R. K. (1987). Characterisation of null mutants of the Rad55 gene of Saccharomyces cerevisiae: effects of temperature, osmotic strength and mating type. *Genetics*, 116 (4), pp. 547-553

Lu C. H, Yeh H. Y, Su G. C, Ito K, Kurokawa Y, Iwasaki H, Chi P, Li H. W. (2018). Swi5–Sfr1 stimulates Rad51 recombinase filament assembly by modulating Rad51 dissociation. *Proceedings of the National Academy of Sciences*, 115, E10059-E10068

Ma C. J, Gibb B, Kwon Y, Sung P, Greene E. C. (2017). Protein dynamics of human RPA and RAD51 on ssDNA during assembly and disassembly of the RAD51 filament. *Nucleic Acids Research*, 45 (2), pp. 749-761

Makarova K. S, Aravind L, Koonin E. V. (2002). SWIM, a novel Zn-chelating domain present in bacteria, archaea and eukaryotes. *Trends in Biochemical* Sciences, 27, pp. 384–386

Malik P. S & Symington L. S. (2008). Rad51 gain-of-function mutants that exhibit high affinity DNA binding cause DNA damage sensitivity in the absence of Srs2. *Nucleic Acids Research*, 36, pp. 6504–6510

Martín V, Chahwan C, Gao H, Blais V, Wohlschlegel J, Yates J. R, McGowan C. H, Russell P. (2006). Sws1 is a conserved regulator of homologous recombination in eukaryotic cells. *The EMBO Journal*, 25, pp. 2564-2574

Martino J, Bernstein K. A. (2016). The Shu complex is a conserved regulator of homologous recombination. *FEMS yeast research*, 16 (6), fow073

Mason J. M, Dusad K, Wright W. D, Grubb J, Budke B, Heyer W. D, Connell P. P, Weichselbaum R, R, Bishop D. K. (2015). RAD54 family translocases counter genotoxic effects of RAD51 in human tumor cells. *Nucleic Acids Research*, 43, pp. 3180–3196

Masson J. Y, Tarsounas M. C, Stasiak A. Z, Stasiak A, Shah R, McIlwraith M. J, Benson F. E, West S. C. (2001). Identification and purification of two distinct complexes containing the five RAD51 paralogs. *Genes and Development*, 15, pp. 3296–3307

Mazin A. V, Alexeev A. A, Kowalczykowski S. C. (2003). A novel function of Rad54 protein. Stabilisation of the Rad51 nucleoprotein filament. *Journal of Biological Chemistry*, 278 (16), pp. 14029-14036

Mazin A. V, Bornarth C. J, Solinger J. A, Heyer W. D, Kowalczykowski S. C. (2000). Rad54 Protein Is Targeted to Pairing Loci by the Rad51 Nucleoprotein Filament. *Molecular Cell*, 6, pp. 583–592

Mazin A. V, Mazina O. M, Bugreev D. V, Rossi M. J. (2010). Rad54, the motor of homologous recombination. *DNA Repair*, 9 (3), pp. 286-302

Mehta A & Haber J. E. (2014). Sources of DNA double-strand breaks and models of recombinational DNA repair. *Cold Spring Harbor Perspectives in Biology* 6:a016428

McEachern M. J & Haber J. E. (2006). Break-induced replication and recombinational telomere elongation in yeast. *Annual Review of Biochemistry*, 75, pp. 111-135

McVey M, Khodaverdian V. Y, Meyer D, Cerqueira P. G, Heyer W. D. (2016). Eukaryotic DNA polymerases in homologous recombination. *Annual Review of Genetics* 50, pp. 393–421

Miyazaki T, Bressan D. A, Shinohara M, Haber J. E, Shinohara A. (2004). In vivo assembly and disassembly of Rad51 and Rad52 complexes during double-strand break repair. *The EMBO Journal*, 23 (4), pp. 939-949

Morimatsu K & Kowalczykowski S. C. (2003). RecFOR proteins load RecA protein onto gapped DNA to accelerate DNA strand exchange: a universal step of recombinational repair. *Molecular cell,* 11, pp. 1337–1347

Morishita T, Furukawa F, Sakaguchi C, Toda T, Carr A. M, Iwasaki H, Shinagawa H. (2005). Role of the *Schizosaccharomyces pombe* F-Box DNA helicase in processing recombination intermediates. *Molecular and Cellular Biology*, 25, pp. 8074–8083

Mortensen U. H, Bendixen C, Sunjevaric I, Rothstein R. (1996). DNA strand annealing is promoted by the yeast Rad52 protein. *Proceedings of the National Academy of Sciences*, 93 (20), pp. 10729-10734

Murayama Y, Kurokawa Y, Tsutsui Y, Iwasaki, H. (2013). Dual regulation of Dmc1-driven DNA strand exchange by Swi5–Sfr1 activation and Rad22 inhibition. *Genes and Development*, 27, pp. 2299–2304

Muris D. F, Vreeken K, Carr A. M, Broughton B. C, Lehmann A. R, Lohman P. H, Pastink A. (1993). Cloning the RAD51 homologue of Schizosaccharomyces pombe. *Nucleic Acids Research*, 21, pp. 4586-4591

Muris D. F, Vreeken K, Carr A. M, Murray J. M, Smit C, Lohman P. H, Pastink A. (1996). Isolation of the Schizosaccharomyces pombe RAD54 homologue, rhp54^{+}, a gene involved in the repair of radiation damage and replication fidelity. *Journal of Cell Science*, 109, pp. 73-81

Muris D. F. R, Vreeken K, Schmidt H, Ostermann K, Clever B, Lohman P. H. M, Pastink A. (1997). Homologous recombination in the fission yeast Schizosaccharomyces pombe: different requirements for the *rhp51*$^{+}$, *rhp54*$^{+}$ and *rad22*$^{+}$ genes. *Current Genetics*, 31, pp. 248-254

Murray J. M, Lindsay H. D, Munday C. A, Carr A. M. (1997). Role of *Schizosaccharomyces pombe* RecQ homolog, recombination, and checkpoint genes in UV damage tolerance. *Molecular and Cellular Biology*, 17, pp. 6868–6875

Murray J. M, Watson A. T, Carr A. M. Molecular genetic tools and techniques in Fission Yeast. *Fission Yeast: A Laboratory Manual*. Hagan I. M, Carr A. M, Grallert A, Nurse P. Cold Spring Harbor Laboratory Press. (2016)

New J. H, Sugiyama T, Zaitseva E, Kowalczykowski S. C. (1998). Rad52 protein stimulates DNA strand exchange by Rad51 and replication protein A. *Nature*, 391 (6665), pp. 407-410

Ogawa T, Yu X, Shinohara A, Egelman E. (1993). Similarity of the yeast RAD51 filament to the bacterial RecA filament. *Science*, 259, pp. 1896–1899
Osman F, Dixon J, Barr A. R, Whitby M. C. (2005). The F-Box DNA helicase Fbh1 prevents Rhp51-dependent recombination without mediator proteins. *Molecular and Cellular Biology*, 25, pp. 8084–8096

Ostermann K, Lorentz A, Schmidt H. (1993). The fission yeast rad22 gene, having a function in mating-type switching and repair of DNA damages, encodes a protein homolog to Rad52 of Saccharomyces cerevisiae. *Nucleic Acids Research*, 21, pp. 5940-5944

Pâques F & Haber J. E. (1999). Multiple pathways of recombination induced by double-strand breaks in *Saccharomyces cerevisiae*. *Microbiology and Molecular Biology Reviews*, 63 (2), pp. 349-404

Pazin M. J & Kadonaga J. T. (1997). SWI2/SNF2 and related proteins: ATP-driven motors that disrupt protein-DNA interactions?. *Cell*, 88, pp. 737-740

Pellegrini L, Yu D. S, Lo T, Anand S, Lee M, Blundell T. L, Venkitaraman A. R. (2002). Insights into DNA recombination from the structure of a RAD51-BRCA2 complex. *Nature*, 420, pp. 287-293

Pettersen E. F, Goddard T. D, Huang C. C, Couch G. S, Greenblatt D. M, Meng E. C, Ferrin T. E. (2004). UCSF chimera–a visualization system for exploratory research and analysis. *Journal of Computational Chemistry*, 25, pp. 1605–1612

Petukhova G, Komen S. V, Vergano S, Klein H, Sung P. (1999). Yeast Rad54 promotes Rad51-dependent homologous DNA pairing via ATP hydrolysis-driven change in DNA double helix conformation. *Journal of Biological Chemistry*, 274, pp. 29453–29462

Petukhova G, Stratton S, Sung P. (1998). Catalysis of homologous DNA pairing by yeast Rad51 and Rad54 proteins. *Nature*, 393, pp. 91-94

Prakash R, Zhang Y, Feng W, Jasin M. (2015). Homologous recombination and human health: the roles of BRCA1, BRCA2, and associated proteins. *Cold Spring Harbor Perspectives in Biology*, 7:a016600

Prentiss M, Prévost C, Danilowicz C. (2015). Structure/function relationships in RecA protein-mediated homology recognition and stand exchange. *Critical Reviews in Biochemistry and Molecular Biology*, 50 (6), pp. 453-476

Qi Z, Redding S, Lee J. Y, Gibb B, Kwon Y, Niu H, Gaines W. A, Sung P, Greene E. C. (2015). DNA sequence alignment by micro homology sampling during homologous recombination. *Cell*, 160 (5), pp. 856-869

Ragunathan K, Liu C, Ha T. (2012). RecA filament sliding on DNA facilitates homology search. eLife, 1:e00067

Raschle M, Komen S. V, Chi P, Ellenberger T, Sung P. (2004). Multiple interactions with the Rad51 recombinase govern the homologous recombination function of Rad54. *Journal of Biological Chemistry*, 279, pp. 51973–51980

Rijkers T, Van Den Ouweland J, Morolli B, Rolink A. G, Baarends W. M, Van Sloun P. P. H, Lohman P. H. M, Pastink A. (1998). Targeted Inactivation of Mouse *RAD52* Reduces Homologous Recombination but Not Resistance to Ionizing Radiation. *Molecular and Cellular Biology*, 18 (11), pp. 6423-6429

Ristic D, Wyman C, Paulusma C, Kanaar R. (2001). The architecture of the human Rad54-DNA complex provides evidence for protein translocation along DNA. *Proceedings of the National Academy of Sciences*, 98, pp. 8454–8460

Rosenbaum J. C, Bonilla B, Hengel S. R, Mertz T. M, Herken B. W, Kazemier H. G, Pressimone C. A, Ratterman T. C, MacNary E, De Magis A, Kwon Y, Godin S. K, Van Houten B, Normolle D. P, Sung P, Das S. R, Paeschke K, Roberts S. A, VanDemark A. P, Bernstein K. A. (2019). The Rad51 paralogs facilitate a novel DNA strand specific damage tolerance pathway. *Nature* Communications, 10, 3515

Saeki T, Machida I, Nakai S. (1980). Genetic control of diploid recovery after γ-irradiation in the yeast Saccharomyces cerevisiae. *Mutation Research/Fundamental and Molecular Mechanisms of Mutagenesis*, 73 (2), pp. 251-265

San Filippo J, Sung P, Klein H. (2008). Mechanism of eukaryotic homologous recombination. *Annual Review of Biochemistry*, 77, pp. 229-257

Saraste M, Sibbald P. R, Wittinghofer A. (1990). The P-loop a common motif in ATP- and GTP-binding proteins. Trends in Biochemical Sciences, 15 (11), pp. 430-434

Sauvageau S, Stasiak A. Z, Banville I, Ploquin M, Stasiak A, Masson J. Y. (2005). Fission yeast Rad51 and Dmc1, two efficient DNA recombinases forming helical nucleoprotein filaments. *Molecular and Cellular Biology*, 25 (11), pp. 4377-4387

Say A. F, Ledford L. L, Sharma D, Singh A. K, Leung W. K, Sehron H. A, Tsubouchi H, Sung P, Sehorn M. G. (2011). The budding yeast Mei5–Sae3 complex interacts with Rad51 and preferentially binds a DNA fork structure. *DNA Repair*, 10, pp. 586–594

Schatz D. G & Ji Y. (2011). Recombination centres and the orchestration of V(D)J recombination. *Nature Reviews Immunology*, 11 (4), pp. 251-263

Schindelin J, Arganda-Carreras I, Frise E, Kaynig V, Longair M, Pietzsch T, Preibisch S, Rueden C, Saalfeld S, Schmid B, Tinevez J. Y, White D. J, Hartenstein V, Eliceiri K, Tomancak P, Cardona A. (2012). Fiji: an open-source platform for biological-image analysis. *Nature Methods*, 9, pp. 676–682

Scott D. E, Marsh M, Blundell T. L, Abell C, Hyvönen M. (2016). Structure-activity relationship of the peptide binding-motif mediating the BRCA2:RAD51 protein-protein interaction. *FEBS letters*, 590, pp. 1094–1102

Shah P. P, Zheng X, Epshtein A, Carey J. N, Bishop D. K, Klein H, L. (2010). Swi2/Snf2-related translocases prevent accumulation of toxic Rad51 complexes during mitotic growth. *Molecular Cell* 39, pp. 862–872

Shahid T, Soroka J, Kong E. H, Malivert L, McIlwraith M. J, Pape T, West S. C, Zhang X. (2014). Structure and mechanism of action of the BRCA2 breast cancer tumor suppressor. *Nature structural & molecular biology*, 21, pp. 1–9

Shen Z, Cloud K. G, Chen D. J, Park M. S. (1996). Specific interactions between the human RAD51 and RAD52 proteins. *Journal of biological chemistry*, 271 (1), pp. 148-152

Shin D. S, Pellegrini L, Daniels D. S, Yelent B, Craig L, Bates D, Yu D. S, Shivji M. K, Hitomi C, Arvai A. S, Volkmann N, Tsuruta H, Blundell T. L, Venkitaraman A. R, Tainer J. A. (2003). Full-length archaeal Rad51 structure and mutants: mechanisms for RAD51 assembly and control by BRCA2. *The EMBO Journal*, 22 (17), pp. 4566-4576

Shinohara A & Ogawa T. (1998). Stimulation by Rad52 of yeast Rad51-mediated recombination. *Nature*, 391 (6665), pp. 404-407

Shinohara A, Ogawa H, Ogawa T. (1992). Rad51 protein involved in repair and recombination in S. cerevisiae is a RecA-like protein. *Cell*, 69, pp. 457-470

Shor E, Weinstein J, Rothstein R. A. (2005). A Genetic Screen for top3 Suppressors in *Saccharomyces cerevisiae* Identifies SHU1, SHU2, PSY3 and CSM2 Four Genes Involved in Error-Free DNA Repair. *Genetics*, 169, pp. 1275–1289

Short J. M, Liu Y, Chen S, Soni N, Madhusudhan M. S, Shivji M. K. K, Venkitaraman A. R. (2016). High-resolution structure of the presynaptic RAD51 filament on single-stranded DNA by electron cryo-microscopy. *Nucleic Acids Research*, 44 (19), pp. 9017-9030

Sigurdsson S, Komen S. V, Bussen W, Schild D, Albala J. S, Sung P. (2001). Mediator function of the human Rad51B–Rad51C complex in Rad51/RPA-catalyzed DNA strand exchange. *Genes and Development*, 15, pp. 3308–3318

Sigurdsson S, Komen S. V, Petukhova G, Sung P. (2002). Homologous DNA pairing by human recombination factors Rad51 and Rad54. *The Journal of Biological Chemistry*, 277 (45), pp. 42790-42794

Simandlova J, Zagelbaum J, Payne M. J, Chu W. K, Shevelve I, Hanada K, Chatterjee S, Reid D. A, Liu Y, Janscak P, Rothenberg E, Hickson I. D. (2013). FBH1 helicase disrupts RAD51 filaments in vitro and modulates homologous recombination in mammalian cells*. *Journal of Biological Chemistry*, 288, pp. 34168–34180

Singleton M. R, Wentzell L. M, Liu Y, West S. C, Wigley D. B. (2002). Structure of the single-strand annealing domain of human RAD52 protein. *Proceedings of the National Academy of Sciences,* 99, pp. 13492–13497

Solinger J. A & Heyer W. D. (2001a). Rad54 protein stimulates the postsynaptic phase of Rad51 protein-mediated DNA strand exchange. *Proceedings of the National Academy of Sciences*, 98 (15), pp. 8447-8453

Solinger J. A, Kiianitsa K, Heyer W. D. (2002). Rad54, a Swi2/Snf2-like recombinational repair protein, disassembles Rad51:dsDNA filaments. *Molecular Cell*, 10, pp. 1175–1188

Solinger J. A, Lutz G, Sugiyama T, Kowalczykowski S. C, Heyer W. D. (2001b). Rad54 protein stimulates heteroduplex DNA formation in the synaptic phase of DNA strand exchange via specific interactions with the presynaptic Rad51 nucleoprotein filament. *Journal of Molecular Biology*, 307, pp. 1207–1221

Song B & Sung P. (2000). Functional interactions among yeast Rad51 recombinase, Rad52 mediator, and replication protein A in DNA strand exchange. Journal of Biological Chemistry, 275 (21), pp. 15895-15904

Stewart E, Chapman C. R, Al-Khodairy F, Carr A. M, Enoch T. (1997). *rqh1*$^{+}$, a fission yeast gene related to the Bloom's and Werner's syndrome genes, is required for reversible S phase arrest. *The EMBO journal*, 16, pp. 2682–2692

Story R. M & Steitz T. A. (1992). Structure of the RecA protein-ADP complex. *Nature*, 355, pp. 374-376

Story R. M, Weber I. T, Steitz T. A. (1992). The structure of the *E. coli* recA protein monomer and polymer. *Nature*, 355, pp. 318-325

Sugawara N, Wang X, Haber J. E. (2003). In vivo roles of Rad52, Rad54, and Rad55 proteins in Rad51-mediated recombination. *Molecular Cell*, 12 (1), pp. 209-219

Su G. C, Chung C. I, Liao C. Y, Lin S. W, Tsai C. T, Huang T, Li H. W, Chi P. (2014). Enhancement of ADP release from the RAD51 presynaptic filament by the SWI5-SFR1 complex. *Nucleic Acids Research*, 42, pp. 349–358

Sugiyama T, Kantake N, Wu Y, Kowalczykowski S. C. (2006). Rad52-mediated DNA annealing after Rad51-mediated DNA strand exchange promotes second ssDNA capture. *The EMBO Journal*, 25, pp. 5539-5548

Sugiyama T, New J. H, Kowalczykowski S. C. (1998). DNA annealing by Rad52 Protein is stimulated by specific interaction with the complex of replication protein A and single-stranded DNA. *Proceedings of the National Academy of Sciences*, 95 (11), pp. 6049-6054

Sullivan M. R & Bernstein K. A. (2018). RAD-ical new insights into RAD51 regulation. *Genes*, 9 (12): 629

Sung P. (1994). Catalysis of ATP-dependent homologous DNA pairing and strand exchange by yeast RAD51 protein. *Science*, 265, pp.1241-1243

Sung P. (1997a). Function of yeast Rad52 protein as a mediator between replication protein A and the Rad51 recombinase. *Journal of Biological Chemistry*, 272, pp. 28194-28197

Sung P. (1997b). Yeast Rad55 and Rad57 proteins form a heterodimer that functions with replication protein A to promote DNA strand exchange by Rad51 recombinase. *Genes and Development*, 11, pp. 1111–1121

Sun Y, McCorvie T, Yates L. A, Zhang X. (2020). Structural basis of homologous recombination. *Cellular and Molecular Life Sciences*, 77, pp. 3-18

Symington L. S. (2002). Role of *RAD52* epistasis group genes in homologous recombination and double-strand break repair. *Microbiology and Molecular Biology Reviews*, 66 (4), pp. 630-670

Takata M, Sasaki M. S, Tachiiri S, Fukushima T, Sonoda E, Schild D, Thompson L. H, Takeda S. (2001). Chromosome instability and defective recombinational repair in knockout mutants of the five Rad51 paralogs. *Molecular and Cellular Biology*, 21 (8), pp. 2858-2866

Taylor M. R. G, Špírek M, Ma C. J, Carzaniga R, Takaki T, Collinson L. M, Greene E. C, Krejci L, Boulton S. J. (2016). A Polar and Nucleotide-Dependent Mechanism of Action for RAD51 Paralogs in RAD51 Filament Remodeling. *Molecular Cell*, 64, pp. 926–939

Thacker J. (2005). The RAD51 gene family, genetic instability and cancer. *Cancer Letters*, 219 (2), pp. 125-135

Thomä N. H, Czyzewski B. K, Alexeev A. A, Mazin A. V, Kowalczykowski S. C, Pavletich N. P. (2005). Structure of the SWI2/SNF2 chromatin-remodeling domain of eukaryotic Rad54. *Nature Structural & Molecular Biology*, 12, pp. 350–356

Tombline G, Shim K. S, Fishel R. (2002). Biochemical characterisation of the human RAD51 protein. II. Adenosine nucleotide binding and competition. *Journal of Biological Chemistry*, 277 (17), pp. 14426-14433

Travers A & Muskhelishvili G. (2015). DNA structure and function. *The FEBS Journal*, 282 (12), pp. 2279-2295

Tsai S. P, Su G. C, Lin S. W, Chung C. I, Xue X, Dunlop M. H, Akamatsu Y, Jasin M, Sung P, Chi P. (2012). Rad51 presynaptic filament stabilisation function of the mouse Swi5-Sfr1 heterodimeric complex. *Nucleic Acids Research*, 40 (14), pp. 6558-6569

Tsubouchi H & Roeder G. S. (2004). The budding yeast Mei5 and Sae3 proteins act together with Dmc1 during meiotic recombination. *Genetics*, 168, pp. 1219–1230

Tsutsui Y, Khasanov F. K, Shinagawa H, Iwasaki H, Bashkirov V. I. (2001). Multiple interactions among the components of the recombinational DNA repair system in *Schizosaccharomyces pombe*. *Genetics*, 159, pp. 91–105

Tsutsui Y, Kurokawa Y, Ito K, Siddique M. S. P, Kawano Y, Yamao F, Iwasaki H. (2014). Multiple regulation of Rad51-mediated homologous recombination by fission yeast Fbh1. *PLoS Genetics*, 10, e1004542

Tsutsui Y, Morishita T, Iwasaki H, Toh H, Shinagawa H. (2000). A recombination repair gene of Schizosaccharomyces pombe, rhp57, is a functional homolog of the Saccharomyces cerevisiae RAD57 gene and is phylogenetically related to the human XRCC3 gene. *Genetics*, 154, pp. 1451-1461

VanLoock M. S, Yu X, Yang S, Galkin V. E, Huang H, Rajan S. S, Anderson W. F, Stohl E. A, Seifert H. S, Egelman E. H. (2003). Complexes of RecA with LexA and RecX differentiate between active and inactive RecA nucleoprotein filaments. *Journal of Molecular Biology*, 333 (2), pp. 345-354

White C. I & Haber J. E. (1990). Intermediates of recombination during mating type switching in *Saccharomyces cerevisiae*. *The EMBO Journal*, 9 (3), pp. 663-673

White M. F. (2011). Homologous recombination in the archaea: the means justify the ends. *Biochemical Society Transactions*, 39 (1), pp. 15-19

Wolner B, Komen S. V, Sung p, Peterson C. L. (2003). Recruitment of the recombinational repair machinery to a DNA double-strand break in yeast. *Molecular Cell*, 12 (1), pp. 221-232

Wright W. D & Heyer W. D. (2014). Rad54 Functions as a Heteroduplex DNA Pump Modulated by Its DNA Substrates and Rad51 during D Loop Formation. *Molecular Cell*, 53, pp. 420–432

Xu J, Zhao L, Xu Y, Zhao W, Sung P, Wang H. W. (2017). Cryo-EM structures of human RAD51 recombinase filaments during catalysis of DNA-strand exchange. *Nature Structural & Molecular Biology*, 24, pp. 40-46

Yasui A. (2013). Alternative excision repair pathways. *Cold Spring Habor Perspectives in Biology*, 5, a012617

Yuan J. & Chen J. (2011). The role of the human SWI5-MEI5 complex in homologous recombination repair*. *Journal of Biological Chemistry*, 286, pp. 9888–9893

Yu X, Jacobs S. A, West S. C, Ogawa T, Egelman E. H. (2001). Domain structure and dynamics in the helical filaments formed by RecA and Rad51 on DNA. *Proceedings of the National Academy of Sciences*, 98 (15), pp. 8419-8424

Zhang X & Wigley D. B. (2008). The ‘glutamate switch’ provides a link between ATPase activity and ligand binding in AAA+ proteins. *Nature Structural & Molecular Biology*, 15 (11), pp. 1223-1227

RESEARCH ARTICLE

A novel motif of Rad51 serves as an interaction hub for recombination auxiliary factors

Negar Afshar[1,2], Bilge Argunhan[2]*, Maierdan Palihati[1,2], Goki Taniguchi[1,2], Hideo Tsubouchi[1,2], Hiroshi Iwasaki[1,2]*

[1]School of Life Science and Technology, Tokyo Institute of Technology, Tokyo, Japan; [2]Institute of Innovative Research, Tokyo Institute of Technology, Tokyo, Japan

Abstract Homologous recombination (HR) is essential for maintaining genome stability. Although Rad51 is the key protein that drives HR, multiple auxiliary factors interact with Rad51 to potentiate its activity. Here, we present an interdisciplinary characterization of the interactions between Rad51 and these factors. Through structural analysis, we identified an evolutionarily conserved acidic patch of Rad51. The neutralization of this patch completely abolished recombinational DNA repair due to defects in the recruitment of Rad51 to DNA damage sites. This acidic patch was found to be important for the interaction with Rad55-Rad57 and essential for the interaction with Rad52. Furthermore, biochemical reconstitutions demonstrated that neutralization of this acidic patch also impaired the interaction with Rad54, indicating that a single motif is important for the interaction with multiple auxiliary factors. We propose that this patch is a fundamental motif that facilitates interactions with auxiliary factors and is therefore essential for recombinational DNA repair.

***For correspondence:**
bargunhan@bio.titech.ac.jp (BA);
hiwasaki@bio.titech.ac.jp (HI)

Competing interests: The authors declare that no competing interests exist.

Funding: See page 24

Received: 18 October 2020
Accepted: 26 December 2020
Published: 25 January 2021

Reviewing editor: Wolf-Dietrich Heyer, University of California, Davis, United States

© Copyright Afshar et al. This article is distributed under the terms of the Creative Commons Attribution License, which permits unrestricted use and redistribution provided that the original author and source are credited.

Introduction

Exogenous factors such as ionizing radiation and genotoxic chemicals can cause DNA damage. However, endogenous processes such as DNA replication and cellular metabolism can also damage DNA (***Lambert and Carr, 2013***). A particularly severe form of DNA damage is a DNA double-strand break (DSB), in which a single normal chromosome is separated into two pathological chromosomes. Homologous recombination (HR) is a major mechanism responsible for accurately repairing DSBs. HR is also critically important for DNA replication (***Ait Saada et al., 2018***). Accordingly, defects in HR lead to genome instability, which drives human diseases such as cancer (***Prakash et al., 2015***).

During HR, the DNA ends that are exposed at a DSB are resected to form 3' overhangs, which are immediately coated by the single-stranded DNA (ssDNA) binding protein RPA (***Symington and Gautier, 2011***). The RecA-family recombinase Rad51 then displaces RPA to form a helical nucleoprotein filament known as the presynaptic filament (***Sun et al., 2020***). This filament can locate a segment of double-stranded DNA (dsDNA) with substantial sequence similarity (i.e.,homology) to the ssDNA (***Greene, 2016***). Upon identifying a homologous region, the Rad51 filament invades the intact dsDNA, displacing the non-complementary strand and forming base pairs with the complementary strand. Within the context of this displacement loop (D-loop) recombination intermediate, the 3'-end of the invading strand can be extended by utilizing the complementary strand as a template for DNA synthesis, allowing for the recovery of lost genetic information (***McVey et al., 2016***). The D-loop can also be expanded by Rad51-driven DNA strand exchange, which increases the extent of base pairing between the two DNA molecules. Consequently, D-loops can be processed to form Holliday junctions, which may be resolved as either crossover or non-crossover products, or

eLife digest The DNA molecule contains the chemical instructions necessary for life. Its physical integrity is therefore vital, yet it is also under constant threat from external and internal factors. As a result, organisms have evolved an arsenal of mechanisms to repair damaged DNA. For instance, when the two complementary strands that form the DNA molecule are broken at the same location, the cell triggers a mechanism known as homologous recombination.

A protein known as Rad51 orchestrates this process, helped by an array of other proteins that include Rad55-Rad57, Rad52, and Rad54. These physically bind to Rad51 and activate it in different ways. However, exactly how these interactions take place remained unclear.

To find out more, Afshar et al. examined models of the structure of Rad51, revealing that three of the protein's building blocks create a prominent, negatively charged patch that could be important for DNA repair. Yeast cells were then genetically manipulated to produce a modified version of Rad51 in which the three building blocks were neutralised. These organisms were unable to repair their DNA. Further biochemical tests showed that the modified protein could no longer attach well to Rad55-Rad57 or Rad54, and could not stick to Rad52 at all. In fact, without its negatively charged patch, Rad51 could not find the ends of broken DNA strands, a process which is normally aided by Rad55-Rad57 and Rad52. Taken together, these results suggest that the helper proteins all interact with Rad51 in the same place, even though they play different roles.

Faulty DNA repair processes have been linked to devastating consequences such as cell death or cancer. Understanding the details of DNA repair in yeast can serve as a template for research in more complex organisms, opening the possibility of applications for human health.

they may be disassembled prior to Holliday junction formation, resulting exclusively in non-crossover outcomes (**Mehta and Haber, 2014**).

As the entity capable of identifying homology and driving DNA strand exchange, Rad51 is integral to DNA repair by HR (**Shinohara et al., 1992**; **Muris et al., 1993**; **Sung, 1994**). However, Rad51 does not function alone in vivo. Several other proteins that are required for HR have been identified in the fission yeast *Schizosaccharomyces pombe* including Rad52, Rad54, the Rad51 paralogs Rad55-Rad57, Swi5-Sfr1, and the lesser studied Shu complex (**Ostermann et al., 1993**; **Muris et al., 1996**; **Khasanov et al., 1999**; **Tsutsui et al., 2000**; **Akamatsu et al., 2003**; **Khasanov et al., 2004**; **Martín et al., 2006**). These factors are mostly conserved in the budding yeast *Saccharomyces cerevisiae* despite the large evolutionary distance separating the two yeasts, although it should be noted that the *S. cerevisiae* homolog of Swi5-Sfr1 (Mei5-Sae3) is only involved in meiotic HR (**San Filippo et al., 2008**; **Hoffman et al., 2015**; **Argunhan et al., 2017a**). This suggests that the requirement for a diverse array of auxiliary factors to promote recombinational DNA repair has been conserved throughout evolution, highlighting its importance. However, our understanding of how auxiliary factors promote Rad51 activity remains incomplete, although they seem to perform largely non-overlapping roles (**Zelensky et al., 2014**).

Sfr1 was first identified in *S. pombe* as an interactor of Rad51 that forms a complex with Swi5 specifically involved in promoting Rad51-dependent DNA repair (**Akamatsu et al., 2003**). The Swi5-Sfr1 heterodimer stimulates DNA strand exchange by potentiating Rad51's ATPase activity and stabilizing Rad51 filaments (**Haruta et al., 2006**; **Kurokawa et al., 2008**). In addition to being widely conserved among eukaryotes, the mechanisms through which Swi5-Sfr1 promotes HR appear to be highly similar in yeasts and mammals (**Tsai et al., 2012**; **Su et al., 2014**; **Su et al., 2016**; **Argunhan et al., 2017a**; **Lu et al., 2018**). The Rad51 paralogs Rad55-Rad57 are another group of evolutionarily conserved auxiliary factors. Rad55 and Rad57 were identified in *S. pombe* based on sequence homology and genetic screening, respectively (**Khasanov et al., 1999**; **Tsutsui et al., 2000**). Relatively little is known about the molecular function of Rad55-Rad57 due to the biochemical intractability of the complex, although much like Swi5-Sfr1, it is thought to be an obligate heterodimer. The biochemical analysis that has been performed with *S. cerevisiae* proteins suggests that Rad55-Rad57 promotes Rad51 filament formation on RPA-coated ssDNA and protects the Rad51 filament from disruption by the Srs2 anti-recombinase (**Sung, 1997**; **Liu et al., 2011**). This is consistent with cytological observations in both *S. cerevisiae* and *S. pombe* indicating that the number of DNA

damage-induced Rad51 foci, which represent Rad51 filaments at sites of ongoing DNA repair, are reduced in the absence of Rad55/Rad57 (**Gasior et al., 1998**; **Gasior et al., 2001**; **Akamatsu et al., 2007**).

Among recombination auxiliary factors, the absence of Rad52 results in the most severe phenotype, with deletion mutants displaying DNA damage sensitivity exceeding the *rad51*Δ single mutant; this has been attributed to the absolute dependency of Rad51 on Rad52, as well as Rad51-independent functions of Rad52 (**Doe et al., 2004**). The *rad54*Δ mutant also shows severe DNA damage sensitivity that is indistinguishable from *rad51*Δ (**Muris et al., 1997**), highlighting the absolute requirement for Rad54 in Rad51-dependent DNA repair. By contrast, the *rad57*Δ and *sfr1*Δ mutants show only moderate sensitivity to DNA damage, while the *rad57*Δ *sfr1*Δ double mutant is as sensitive as the *rad51*Δ single mutant. Based on this additivity, it was proposed that Rad55-Rad57 and Swi5-Sfr1 comprise independent sub-pathways of HR that function in parallel to promote Rad51-dependent DNA repair (**Akamatsu et al., 2003**; **Akamatsu et al., 2007**), although recent evidence has evoked a re-examination of this model (**Argunhan et al., 2020**).

To learn more about the relationship between Rad51 and its auxiliary factors, we sought to identify regions of Rad51 that are important for interactions with auxiliary factors. This led to the identification of an evolutionarily conserved acidic patch comprised of three residues: E205, E206, and D209. Mutation of all three residues to Ala completely ablates Rad51-dependent DNA repair, as does a single charge-reversal mutation, indicating that the negative character of this patch is critical for DNA repair. Mechanistically, these defects in DNA repair stem from abrogation of the interaction with both Rad55-Rad57 and Rad52, leading to impaired recruitment of Rad51 to sites of DNA damage. Remarkably, biochemical reconstitutions indicate that neutralization of the acidic patch also impairs the interaction with Rad54, demonstrating that a single motif of Rad51 is important for its interaction with Rad55-Rad57, Rad52, and Rad54. We propose that this acidic patch of Rad51 comprises a fundamental motif that is essential for interactions with auxiliary factors and therefore recombinational DNA repair.

Results

E205, E206, and D209 comprise a protruding acidic patch (PAP) on the exterior of the Rad51 presynaptic filament

Several motifs important for the enzymatic activity of Rad51 are located in the highly conserved ATPase core domain, which is characterized by a β-sheet consisting of mixed parallel and antiparallel β-strands (**Story et al., 1992**; **Pellegrini et al., 2002**; **Shin et al., 2003**; **Conway et al., 2004**). These include the Walker A and B motifs, which are important for ATP binding and hydrolysis (**Saraste et al., 1990**; **Story and Steitz, 1992**), and two DNA binding sites: Site 1, which is comprised of Loop 1 and Loop 2, and Site 2 (**Howard-Flanders et al., 1984**; **Story et al., 1992**). Examination of a homology (i.e., computational) model of *S. pombe* Rad51 (*Sp*Rad51) revealed that the surface of these regions is enriched in positive charge, consistent with roles in the binding of ATP and DNA (**Figure 1A**, left). By contrast, mostly negatively charged regions were found on the opposite face of *Sp*Rad51, including a protruding acidic patch, which we refer to as the PAP hereafter (**Figure 1A**, right). The PAP is among the most negatively charged regions on the surface of *Sp*Rad51 (**Figure 1—figure supplement 1A**) and is situated on a short α-helix preceding the outermost β-strand of the central β-sheet (**Figure 1B** and **Video 1**). Three acidic residues were seen to project out from this α-helix: E205, E206, and D209 (**Figure 1C,D** and **Video 2**).

These residues were also examined in the context of a previously published homology model of the *Sp*Rad51 presynaptic filament (**Ito et al., 2020**) and found to form acidic patches constituting dense negatively charged regions on the exterior of the filament (**Figure 1E** and **Video 3**). The equivalent α-helix in the human Rad51 (*Hs*Rad51) presynaptic filament—the structure of which was determined by cryo-electron microscopy (**Xu et al., 2017**)—also had a negative surface charge (**Figure 1—figure supplement 1B**), as did the corresponding α-helix in the *S. cerevisiae* Rad51 (*Sc*Rad51) presynaptic filament (**Figure 1—figure supplement 1C**)—the structure of which was determined by X-ray crystallography (**Conway et al., 2004**). While E205 was replaced with a conservative Asp residue in *Sc*Rad51 and D209 was conserved in *Hs*Rad51, E206 is the only PAP residue

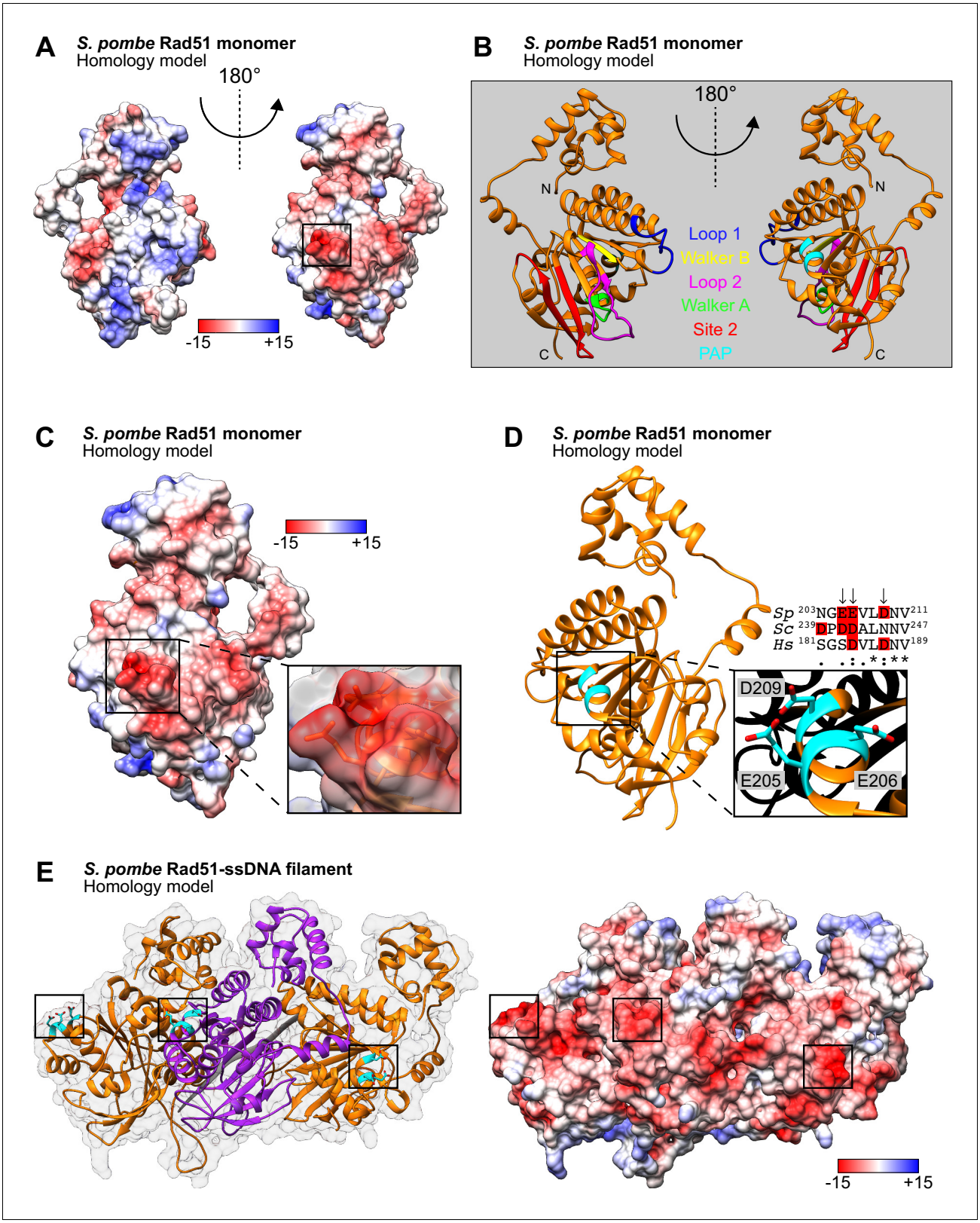


Figure 1. E205, E206, and D209 form a protruding acidic patch (PAP) on the exterior of the Rad51 presynaptic filament. (**A**) Homology model of an *Sp*Rad51 monomer (residues 42–360). Surface representation colored according to Coulombic surface charge. The molecule on the left is rotated 180˚ to visualize the PAP on the right, with the region of interest squared. (**B**) Ribbon depiction of an *Sp*Rad51 monomer with relevant motifs highlighted. The molecules are oriented as in (**A**). (**C**) Surface representation colored according to Coulombic surface charge. The PAP is enlarged with a semi-

Figure 1 continued on next page

Figure 1 continued

transparent surface revealing residues E205, E206, and D209, which have their side-chains shown. (**D**) Ribbon depiction of *Sp*Rad51 with the α-helix containing the PAP enlarged to illustrate the respective positions of each residue (colored in cyan) with their side-chains revealed (O atoms in red). Sequence alignment shows the corresponding region in *S. pombe*, *S. cerevisiae* and *H. sapiens* (*Sp*, *Sc*, and *Hs*, respectively), with arrows indicating PAP residues in *S. pombe* and acidic residues highlighted in red. (**E**) Ribbon depiction of three *Sp*Rad51 monomers (alternating orange and purple) bound to ssDNA (9-mer poly-dT in gray) with a near-transparent surface for visualization (left). The side-chains of E205, E206, and D209 are revealed in cyan (O atoms in red) and their positions are squared. The surface is made opaque and colored according to Coulombic surface charge to demonstrate that the PAP constitutes dense, negatively charged regions on the exterior of the ssDNA filament (right). Numbers in the legends for (**A,C,E**) are in units of kcal/(mol•*e*).

The online version of this article includes the following figure supplement(s) for figure 1:

Figure supplement 1. The PAP is conserved in the *Hs*Rad51 and *Sc*Rad51 presynaptic filaments.

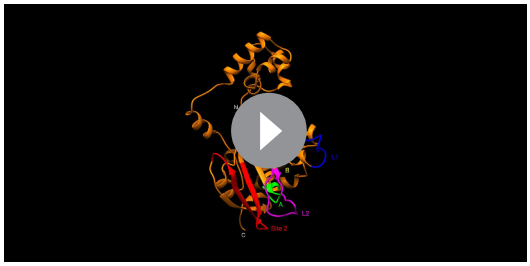
that showed conservation in both *Sc*Rad51 and *Hs*Rad51 (***Figure 1D***). Thus, we initially focused on E206.

Rad51-E206A is specifically defective in the interaction with Rad55-Rad57

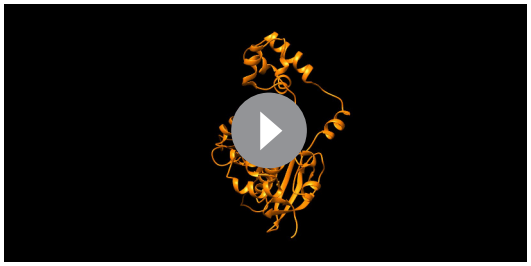
HR plays a particularly important role in the repair of ultraviolet light (UV)-induced DNA damage in *S. pombe* due to the existence of a UV damage endonuclease pathway (***McCready et al., 2000***). To examine whether E206 is important for DNA repair, it was mutated to Ala and a strain containing this mutation at the native locus was constructed. *rad51-E206A* showed the same resistance to UV-induced DNA damage as wild type in a clonogenic survival assay (***Figure 2A***), suggesting that this mutation does not affect the intrinsic ability of Rad51 to repair DNA.

In the *rad57*Δ*/rad55*Δ background, Rad51-mediated HR is reduced but not abolished, and this remaining recombinational DNA repair is dependent on Swi5-Sfr1. There is a similar reduction in recombinational DNA repair in the *sfr1*Δ*/swi5*Δ background, where the remaining Rad51-mediated HR is dependent on Rad55-Rad57. However, the *rad57*Δ *sfr1*Δ double mutant displays a complete loss of Rad51-mediated DNA repair, phenocopying *rad51*Δ. Thus, employing the *rad57*Δ and *sfr1*Δ backgrounds allows for the evaluation of DNA repair promoted by Swi5-Sfr1 and Rad55-Rad57, respectively (***Akamatsu et al., 2003***). The *rad51-E206A rad57*Δ strain was no more sensitive to UV than *rad57*Δ (***Figure 2B***), suggesting that Rad51-E206A is as proficient as wild-type Rad51 in Swi5-Sfr1–dependent DNA repair. By contrast, *rad51-E206A* was as sensitive as *rad51*Δ in the absence of Sfr1 (***Figure 2C***), indicating that the recombinational DNA repair promoted solely by Rad55-Rad57 is ablated by the Rad51-E206A mutation. The generality of these findings was confirmed by performing spot tests with several different genotoxins that induce replication fork stalling and a variety of lesions in DNA (***Figure 2—figure supplement 1A–C***).

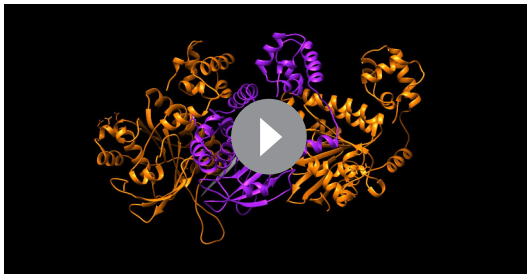
The DNA damage sensitivity of *sfr1*Δ *rad51-E206A* is comparable in severity to *rad51*Δ, which itself shows similar sensitivity to *rad57*Δ *sfr1*Δ and *rad54*Δ (***Muris et al., 1997***; ***Akamatsu et al., 2003***). The *rad52*Δ mutant is even more sensitive to DNA damage, although this added sensitivity stems from Rad51-independent roles of Rad52 (***Doe et al., 2004***); a mutation that abolishes the interaction between Rad51 and Rad52 would be expected to phenocopy *rad51*Δ, not *rad52*Δ. Thus, it is possible that the DNA damage sensitivity associated with *rad51-E206A*, which manifests in the *sfr1*Δ background, reflects a defect in the interaction of Rad51 with Rad52 or Rad54, rather than with Rad55-Rad57. We sought to distinguish between these possibilities genetically. Rqh1 is a RecQ-



Video 1. A model of the *Sp*Rad51 monomer with motifs labeled. A homology model of the *Sp*Rad51 monomer is depicted in ribbon form and labeled as follows: N and C, N- and C-termini; L1 and L2, loop 1 and loop 2 of DNA binding site 1; A and B, Walker A and Walker B motifs; Site 2, DNA binding site 2. Residues E205, E206, and D209, which constitute the protruding acidic patch (PAP), are shown in cyan following 180˚ rotation of the model in the y-axis.
https://elifesciences.org/articles/64131#video1



Video 2. Visualization of the protruding acidic patch (PAP) in monomer form. A homology model of the *Sp*Rad51 monomer is depicted in ribbon form. The side-chains of residues E205, E206, and D209 are shown, intermittently highlighted in cyan (O atoms in red). The surface is made opaque and colored according to Coulombic surface charge to demonstrate that these residues constitute a dense negatively charged patch that we refer to as the PAP.
https://elifesciences.org/articles/64131#video2



Video 3. Visualization of the protruding acidic patch (PAP) in filament form. A homology model of the *Sp*Rad51-ssDNA filament. Ribbon depiction of three monomers (alternating orange and purple) bound to ssDNA (9-mer poly-dT in gray). The side-chains of residues E205, E206, and D209 are shown, intermittently highlighted in cyan. The surface is made opaque and colored according to Coulombic surface charge to demonstrate that these residues constitute dense negatively charged patches on the exterior of the ssDNA filament.
https://elifesciences.org/articles/64131#video3

family helicase (homologous to Sgs1 in *S. cerevisiae* and the BLM and WRN helicases in humans) that functions in S phase to prevent the accumulation of toxic recombination intermediates that arise during DNA replication (***Murray et al., 1997***; ***Stewart et al., 1997***). Accordingly, *rqh1*Δ cells are sensitive to the ribonucleotide reductase inhibitor hydroxyurea (HU). It was previously shown that *rad57*Δ and *sfr1*Δ robustly suppress the HU sensitivity of *rqh1*Δ whereas *rad52*Δ and *rad54*Δ do not, presumably because the former mutations reduce HR while the latter mutations eliminate it completely (***Hope et al., 2005***). If Rad51-E206A is defective in the interaction with Rad55-Rad57 rather than Rad52/Rad54, then the *rqh1*Δ *rad51-E206A* strain should phenocopy *rqh1*Δ *rad57*Δ rather than *rqh1*Δ *rad52*Δ/*rad54*Δ. Consistently, *rad51-E206A* suppressed the HU sensitivity of *rqh1*Δ to almost the same degree as *rad57*Δ (***Figure 2D***). Furthermore, the suppression conferred by *sfr1*Δ, which is dependent on Rad55-Rad57 (***Hope et al., 2005***), was ablated by *rad51-E206A*. By contrast, the suppression imparted by *rad57*Δ was epistatic to *rad51-E206A*, suggesting that they involve the same mechanism. At 5 mM HU, *rad57*Δ *sfr1*Δ could partially suppress *rqh1*Δ sensitivity, whereas *rad51*Δ and *rad54*Δ could not. Importantly, the *sfr1*Δ *rad51-E206A* strain was still similar to *rad57*Δ *sfr1*Δ, strongly suggesting that the defect associated with *rad51-E206A* is related to Rad55-Rad57.

Immunoblotting experiments revealed that the level of Rad51-E206A was comparable to wild-type Rad51 (***Figure 2—figure supplement 1D***), indicating that the DNA repair defect of *rad51-E206A* is not caused by reduced protein stability. Previous yeast two-hybrid (Y2H) analysis suggested that Rad51 physically interacts with Rad55-Rad57 (***Hays et al., 1995***; ***Johnson and Symington, 1995***; ***Tsutsui et al., 2001***). Thus, a feasible explanation for the DNA damage sensitivity of *rad51-E206A* is that the E206A mutation disrupts the physical interaction between Rad51 and Rad55-Rad57. To test this, a sequence encoding 12 copies of the V5 epitope was fused to *rad55*$^{+}$ at its native locus, yielding the *rad55-12xV5* strain. This strain was as resistant to DNA damage as the untagged wild type (*rad55*$^{+}$; ***Figure 2—figure supplement 1E***), indicating that the tag does not interfere with the function of Rad55-Rad57 in DNA repair. In vivo co-immunoprecipitation (co-IP) experiments were performed in both *sfr1*$^{+}$ and *sfr1*Δ backgrounds. While robust signal was observed for wild-type Rad51, substantially less Rad51-E206A was seen to co-IP with Rad55 (***Figure 2E***), indicating that the E206A mutation impairs Rad51–Rad55-Rad57 complex formation. The presence of Sfr1 did not have an effect on complex formation, irrespective of the E206A mutation. These results suggest that the DNA repair defect associated with *rad51-E206A* is related to impaired Rad51–Rad55-Rad57 complex formation and that the suppression of this DNA damage sensitivity by Swi5-Sfr1 is not through enhancing physical binding.

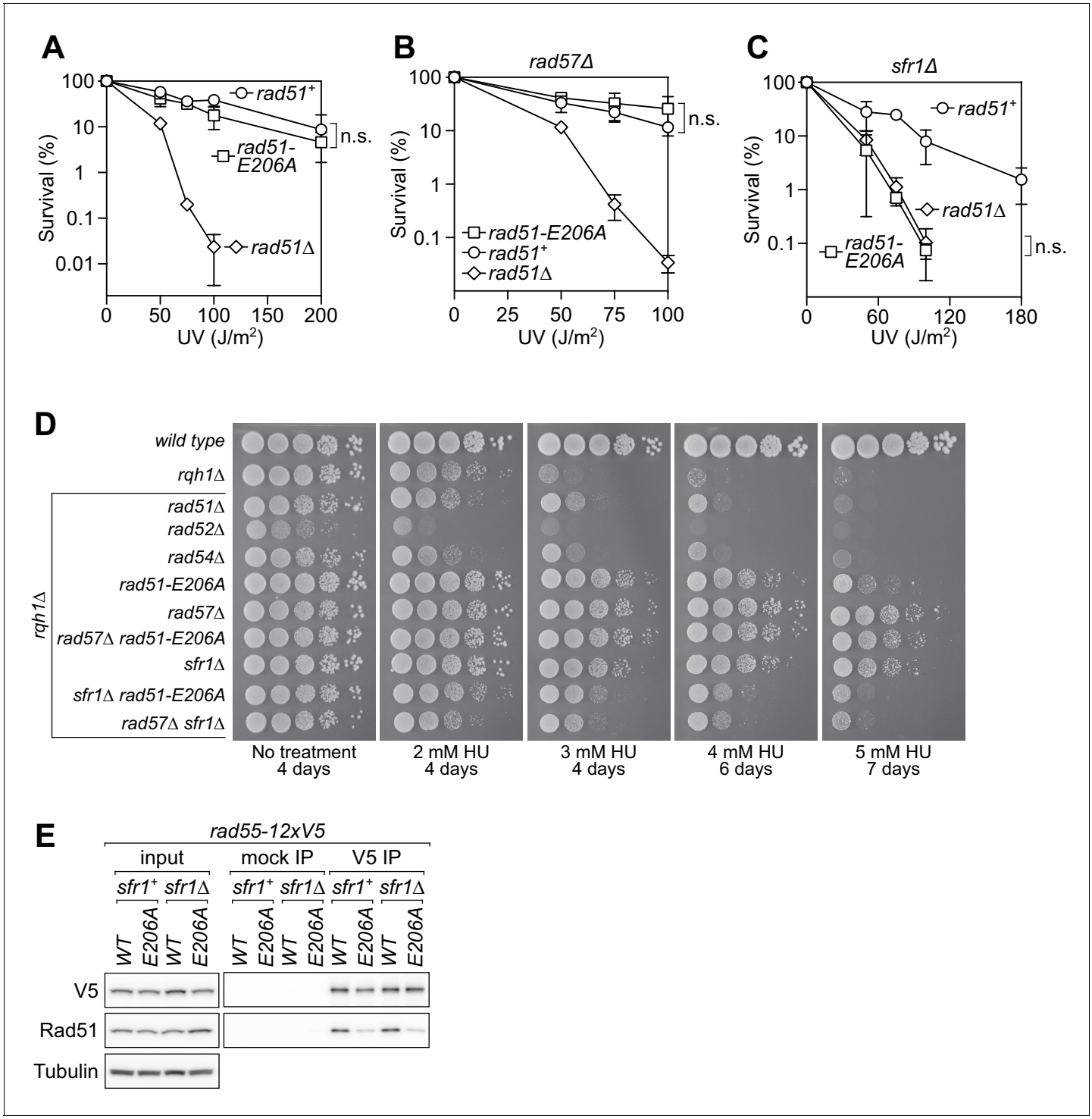


Figure 2. The *rad51-E206A* mutant is specifically defective in the interaction with Rad55-Rad57. (**A–C**) Following acute UV irradiation, a clonogenic assay was employed to test the survival of *rad51*$^{+}$, *rad51-E206A*, and *rad51*Δ in the wild-type background (**A**), the *rad57*Δ background (**B**), and the *sfr1*Δ background (**C**). Statistical significance at the highest dose of UV was assessed by unpaired two-tailed t-test. n.s., not significant (**A**, p=0.506; **B**, p=0.242; **C**, p=0.593). (**D**) Tenfold serial dilutions of the indicated strains were spotted onto standard media without treatment or containing hydroxyurea (HU). Following growth for the indicated time at 30˚C, plates were imaged. (**E**) Soluble cell extracts treated with a benzonase-like nuclease were prepared from each strain under native conditions (input). Immunoprecipitation (IP) was then performed with mock (human IgG from non-immunized animal) or anti-V5 antibodies. Tubulin serves as a loading control. Data in (**A–C**) are means of three independent experiments and error bars depict standard deviation.

Figure 2 continued on next page

Figure 2 continued

The online version of this article includes the following source data and figure supplement(s) for figure 2:

Source data 1. Survival (%) following UV irradiation for data in ***Figure 2A–C***.
Figure supplement 1. Specificity of the DNA damage sensitivity of *rad51-E206A*.

Rad51-E206A retains normal recombinase activity and can be stimulated by Swi5-Sfr1

Although E206 does not belong to a canonical motif involved in ATP hydrolysis or DNA binding, it remained formally possible that the E206A mutation impaired the enzymatic activity of Rad51. Rad51-E206A was therefore purified to homogeneity from *Escherichia coli* to investigate its biochemical properties (***Figure 3—figure supplement 1***).

Rad51-E206A shifted both ssDNA and dsDNA to a similar extent as wild-type Rad51 in electrophoretic mobility shift assays (EMSAs; ***Figure 3A,B***), suggesting that the E206A mutation does not affect the ability of Rad51 to bind DNA. In addition to DNA binding, ATP hydrolysis by Rad51 is important for the DNA strand exchange reaction (***Ito et al., 2018***). Furthermore, Swi5-Sfr1 stimulates the ATPase activity of Rad51 (***Haruta et al., 2006***). We therefore examined whether Rad51-E206A is proficient for ATP hydrolysis, both with and without Swi5-Sfr1. In the absence of Swi5-Sfr1, the ATP turnover number (k_{cat}) of both Rad51 and Rad51-E206A was ~0.2 min^{-1} (***Figure 3C***). The inclusion of Swi5-Sfr1 elicited an approximately twofold increase in ATP hydrolysis by both proteins, demonstrating that Rad51-E206A can hydrolyze ATP like wild type and is proficient for the ATPase stimulation imparted by Swi5-Sfr1.

Next, an assay with plasmid-sized DNA substrates was employed to examine the strand exchange activity of Rad51-E206A (***Figure 3D***). Rad51 drives the pairing of circular ssDNA (css) with homologous linear dsDNA (lds) to yield joint molecule intermediates (JMs). Following strand transfer over the length of the dsDNA substrate, JMs are converted into nicked-circular dsDNA molecules (NCs), which are the products in this assay. The different DNA species can be separated by agarose gel electrophoresis and visualized. Under our standard reaction conditions, wild-type Rad51 cannot promote JM or NC formation in the absence of auxiliary factors (***Haruta et al., 2006***; ***Kurokawa et al., 2008***). However, when reaction conditions were modified by increasing the concentrations of Rad51 and DNA substrates, both Rad51 and Rad51-E206A were seen to drive the efficient pairing of css and lds to produce JMs in the absence of auxiliary factors (***Figure 3E***). This allowed us to evaluate whether the E206A mutation impaired the intrinsic strand exchange activity of Rad51. Although neither protein was able to drive the robust accumulation of NC, we nevertheless quantified the total yield (JM + NC) at each time point and found them to be comparable for both Rad51 and Rad51-E206A.

Our genetic analysis suggested that Rad51-E206A is proficient for the DNA repair promoted by Swi5-Sfr1. To corroborate these findings, strand exchange reactions were supplemented with Swi5-Sfr1. Note that under these standard assay conditions, which differ from those employed above, Rad51 alone cannot promote JM or NC formation, thus allowing us to better examine the effect of Swi5-Sfr1 (***Haruta et al., 2006***; ***Kurokawa et al., 2008***). The inclusion of Swi5-Sfr1 efficiently stimulated both Rad51 and Rad51-E206A, with a similar accumulation of JMs and NC observed in both cases (***Figure 3F***). Taken together, these results indicate that Rad51-E206A retains intrinsic recombinase activity and a functional interaction with Swi5-Sfr1.

The PAP is essential for Rad51-dependent DNA repair

Our results with Rad51-E206A suggested that the PAP is required specifically for the interaction with Rad55-Rad57. We sought to test whether other mutations in the PAP also affect the interaction with Rad55-Rad57. Strains were constructed in which the *rad51*$^{+}$ gene at its native locus was replaced with *rad51-E205A*, *rad51-D209A*, or *rad51-EED* (E205A, E206A, D209A). Structural models revealed that the negative surface charge of the PAP is completely neutralized by the EED mutation without affecting its protruding nature (***Figure 4—figure supplement 1A,B***).

The DNA damage sensitivity of these mutant strains was assessed by spot-test. Like *rad51-E206A*, the *rad51-E205A* strain did not show any DNA damage sensitivity in the presence of both Rad55-Rad57 and Swi5-Sfr1 (***Figure 4A***). By contrast, *rad51-D209A* showed marked sensitivity to

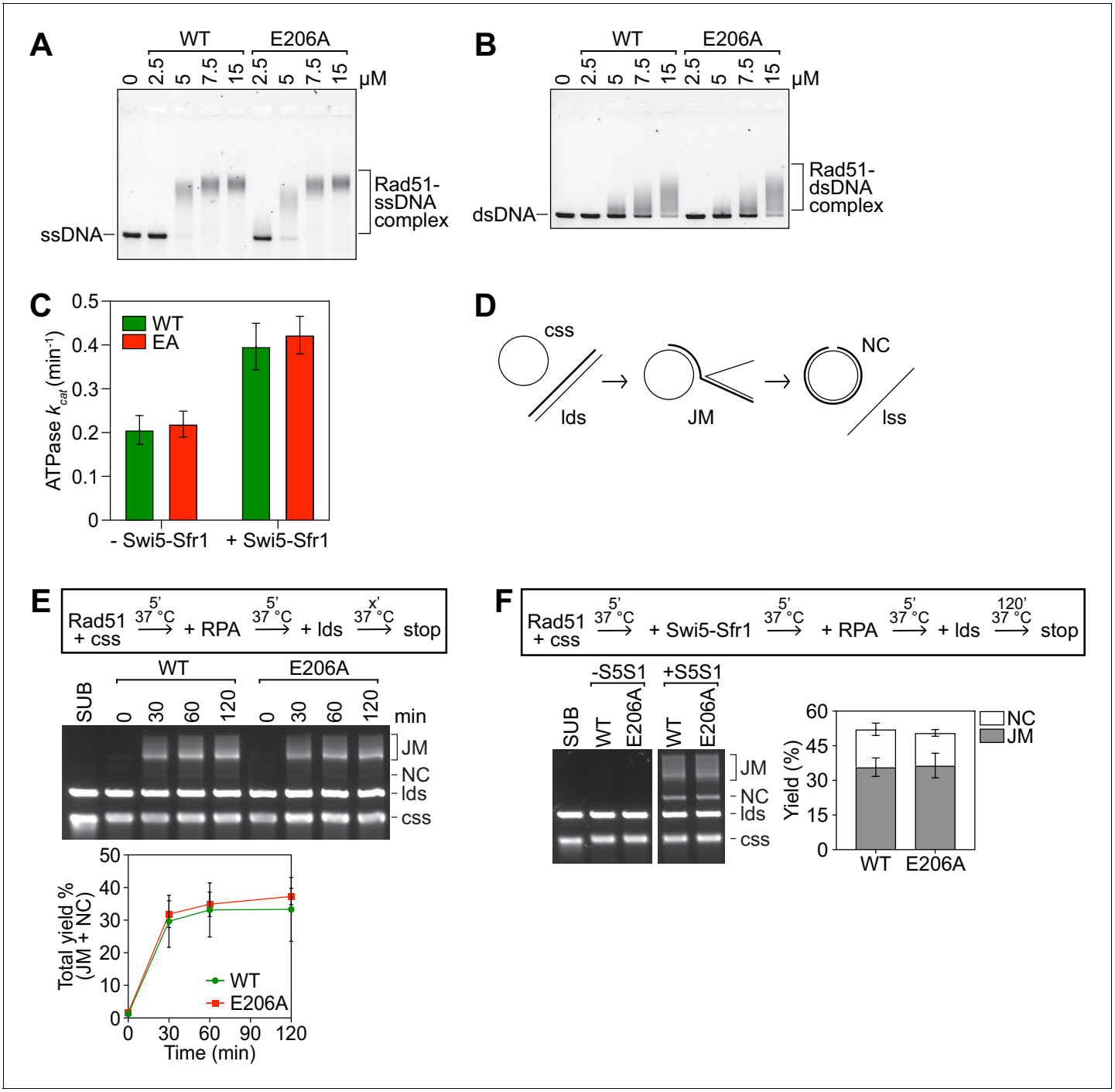


Figure 3. Rad51-E206A retains normal DNA binding and recombinase activity. (**A,B**) The indicated concentrations of Rad51 (WT) or Rad51-E206A (E206A) were incubated with 30 micromolar nucleotide (μM nt) PhiX174 virion DNA (ssDNA; **A**) or 20 μM nt of linearized PhiX174 RF I DNA (dsDNA; **B**), protein-DNA complexes were crosslinked with glutaraldehyde and then resolved by agarose gel electrophoresis. (**C**) The ATPase activity of 5 μM Rad51 (WT) and Rad51-E206A (EA) was measured in the presence of ssDNA (10 μM nt), with or without Swi5-Sfr1 (0.5 μM), and k_{cat} was calculated. (**D**) Schematic of the strand exchange assay with full-length DNA substrates (PhiX174 virion ssDNA and ApaLI-linearized PhiX174 RF I dsDNA). (**E**) Strand exchange reactions were conducted according to the scheme outlined above the gel. Rad51 (WT or E206A), 15 μM. RPA, 1 μM. cssDNA, 30 μM nt. ldsDNA, 20 μM nt. (**F**) Strand exchange reactions were conducted according to the scheme outlined above the gel. Rad51 (WT or E206A), 5 μM. Swi5-Sfr1 (S5S1), 0.5 μM. RPA, 1 μM. cssDNA, 10 μM nt. ldsDNA, 10 μM nt. Data in (**C,E,F**) are means of three independent experiments and error bars depict standard deviation.

The online version of this article includes the following source data and figure supplement(s) for figure 3:

Source data 1. k_{cat} values in ***Figure 3C*** and strand exchange yield (%) in ***Figure 3E,F***.

Figure 3 continued on next page

Figure 3 continued

Figure supplement 1. Purity analysis of Rad51 and Rad51-E206A.

DNA damage, although it was still significantly more resistant than *rad51*Δ. Strikingly, the *rad51-EED* mutant was as sensitive to DNA damage as *rad51*Δ. Since the E205A and E206A mutations alone did not sensitize cells to DNA damage, but combining them with the partially functional D209A completely incapacitated Rad51, we also examined the *rad51-EE* strain, in which both Glu residues are mutated to Ala. Unlike *rad51-E205A* and *rad51-E206A*, *rad51-EE* showed moderate sensitivity to DNA damage, although this was milder than the sensitivity of *rad51-D209A*. These results indicate that neutralization of the PAP completely abolishes Rad51-dependent DNA repair, and while all three residues are important, D209 plays a more prominent role than E205 and E206.

Because our data suggested that the E206A mutation impairs the interaction of Rad51 with Rad55-Rad57, in vivo co-IP experiments were performed to examine how other mutations in the PAP affect complex formation with Rad55-Rad57. A reduction in the amount of Rad51 that co-IPs with Rad55-12xV5 was observed in the *rad51-EE*, *rad51-D209A,* and *rad51-EED* strains (***Figure 4B***), and this reduction roughly correlated with the DNA damage sensitivity of the corresponding mutants. This result suggests that the DNA damage sensitivity of PAP mutants is partly due to reduced complex formation with Rad55-Rad57. However, given that some complex formation was still observed in the *rad51-EED* strain, we infer that the PAP is important but not essential for complex formation with Rad55-Rad57.

In contrast to what was observed in the presence of Sfr1, *rad51-E205A* showed mild DNA damage sensitivity in the *sfr1*Δ background (***Figure 4C***) and this modest difference became more obvious at higher doses of UV irradiation (***Figure 4—figure supplement 1C***). Both the *rad51-EED* and *rad51-EE* mutants showed comparable sensitivity to *rad51*Δ in this background, as was expected from the phenotype of *rad51-E206A*. Notably, the *rad51-D209A* strain was also as sensitive to DNA damage as *rad51*Δ in the absence of Sfr1. These results are consistent with the notion that the PAP is important for DNA repair promoted by Rad55-Rad57. However, because the DNA damage sensitivity of *rad51-EED* is similar to that of *rad51*Δ (***Figure 4A***), which clearly exceeds that of *rad57*Δ, it seemed likely that the function of the PAP is not restricted to Rad55-Rad57–dependent DNA repair. To directly test if the PAP is involved in Rad55-Rad57–independent DNA repair, PAP mutants were introduced into the *rad57*Δ background. The *rad51-E205A* mutant was as resistant to DNA damage as *rad51*$^{+}$ in the absence of Rad57, suggesting that Rad55-Rad57–independent DNA repair mechanisms are not impaired in this mutant (***Figure 4D***). By contrast, *rad51-EE* showed a modest increase in sensitivity compared to *rad51*$^{+}$. *rad51-D209A* was even more sensitive than *rad51-EE*, although this sensitivity was still not as severe as *rad51-EED* and *rad51*Δ. Consistently, *rad51-EED* and *rad51*Δ were the only strains among this set that showed a clear slow-growth phenotype (note the small colony size on the 'No treatment' plate in ***Figure 4D***). The fact that the D209A and EE mutations further sensitized *rad57*Δ cells to DNA damage, combined with the severe sensitivity of *rad51-EED*, suggests that Rad55-Rad57–independent DNA repair is also impaired in these mutants. These results imply that the PAP is also relevant to the function of auxiliary factors other than Rad55-Rad57 (explored below).

If the negativity of the PAP is important for Rad51-dependent DNA repair, we reasoned that a charge-reversal mutation would be more disruptive than the Asp/Glu-to-Ala mutations employed thus far. The E205A and E206A mutations did not sensitize cells to DNA damage in the presence of both Rad55-Rad57 and Swi5-Sfr1 (***Figure 4A***). However, because E206 shows a higher degree of conservation than E205, it was mutated to Lys, yielding the *rad51-E206K* strain. In stark contrast to the *rad51-E206A* strain, *rad51-E206K* showed a clear slow-growth phenotype and was as sensitive to DNA damage as *rad51*Δ in the presence of both Rad55-Rad57 and Swi5-Sfr1 (***Figure 4—figure supplement 1D***), just like *rad51-EED*. Taken together, these results show that the negative character of the PAP is integral to recombinational DNA repair.

The PAP is crucial for the recruitment of Rad51 to DNA damage sites

To elucidate the mechanistic defects in DNA repair associated with neutralization of the PAP, previous immunostaining protocols for the visualization of Rad51 foci were adopted (***Loidl and Lorenz,***

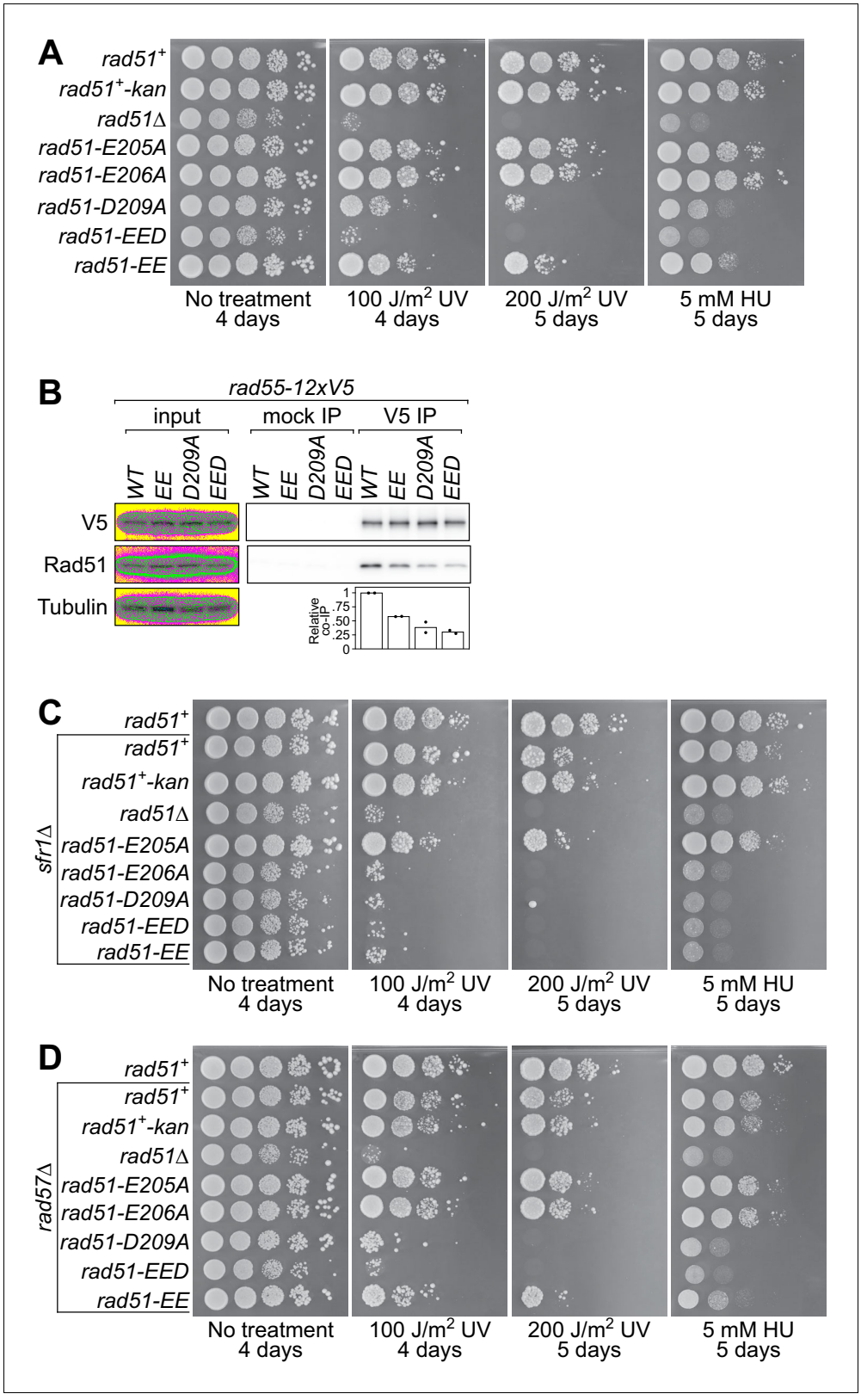


Figure 4. The PAP is essential for Rad51-dependent DNA repair. (**A**,**C**,**D**) Tenfold serial dilutions of the indicated strains were spotted onto standard media with or without acute UV irradiation, or standard media containing 5 mM hydroxyurea (HU). Following growth at 30˚C for the indicated time, plates were imaged. (**B**) Soluble cell extracts treated with a benzonase-like nuclease were prepared from each strain under native conditions (input).

Figure 4 continued on next page

Figure 4 continued

Immunoprecipitation (IP) was then performed with mock (human IgG from non-immunized animal) or anti-V5 antibodies. Tubulin serves as a loading control. For quantification, Rad51 signal was normalized to V5 signal and expressed relative to wild type. Data in (**B**) are the means of two independent biological replicates with individual values shown.

The online version of this article includes the following source data and figure supplement(s) for figure 4:

Source data 1. Relative co-IP of Rad51 (%) for ***Figure 4B***.

Figure supplement 1. The EED mutation neutralizes the PAP of *Sp*Rad51 and is phenocopied by the E206K mutation.

2009; ***Argunhan et al., 2017b***). Surface-spread nuclei were prepared from log-phase cultures, with or without prior UV irradiation, and immunostained with a polyclonal anti-Rad51 antibody (***Figure 5A***). Nuclei were then picked manually and foci were quantified by an automated approach using FIJI software (see Materials and methods for more details; ***Schindelin et al., 2012***). Examples of nuclei scored by this method are shown in ***Figure 5B***.

In the absence of UV irradiation, the vast majority of nuclei in all strains lacked Rad51 foci (***Figure 5—figure supplement 1***). By contrast, UV-irradiated nuclei contained substantially more Rad51 foci, and this was not seen in the *rad51*Δ strain, confirming the DNA damage-dependence and specificity of these cytological entities (***Figure 5C***). Nuclei from wild-type and *rad52*Δ strains formed an average of 8.6 and 1.7 foci, respectively, in close agreement with a previous report (***Lorenz et al., 2009***). As expected, both *sfr1*Δ and *rad57*Δ strains formed fewer foci than wild type, and *rad57*Δ *sfr1*Δ formed even fewer foci still (***Akamatsu et al., 2007***). Strikingly, nuclei from *rad51-EED* showed a drastic reduction in the number of foci, much like the *rad57*Δ *sfr1*Δ double mutant and the *rad52*Δ single mutant. These results indicate that the severe DNA damage sensitivity of *rad51-EED* stems from defects in the mechanisms promoting the recruitment of Rad51 to sites of DNA damage.

Rad51-EED retains intrinsic recombinase activity and can be stimulated by Swi5-Sfr1

The DNA damage sensitivity and impaired Rad51 recruitment phenotypes of *rad51-EED* are clearly more severe than *rad57*Δ, pointing towards additional roles of the PAP beyond facilitating the interaction with Rad55-Rad57. This could reflect an impairment in the intrinsic activity of Rad51-EED. Alternatively, the EED mutation could impair the interaction with Swi5-Sfr1, since the phenotypes of *rad51-EED* are comparable to *rad57*Δ *sfr1*Δ. To test these two possibilities, Rad51-EED was purified to homogeneity (***Figure 6—figure supplement 1A***).

Rad51-EED shifted ssDNA and dsDNA comparably to wild-type Rad51 in EMSAs (***Figure 6—figure supplement 1B,C***), suggesting that the EED mutation does not affect the ability of Rad51 to bind DNA. Because reaction products (NCs) were not observed in the assay that was previously employed to monitor the intrinsic strand exchange activity of Rad51 (***Figure 3D,E***), a shorter lds substrate was utilized with the reasoning that this might prove a less challenging substrate (***Figure 6A***). Both Rad51 and Rad51-E206A generated similar amounts of partial duplex molecules (PD), which are the reaction products in this assay (***Figure 6B***). Unexpectedly, Rad51-EED consistently displayed increased strand exchange activity. While the reason for this is unclear, these results at least indicate that neutralization of the PAP does not impair the intrinsic activity of Rad51.

If the EED mutation impairs the interaction with Swi5-Sfr1, then the binding of Swi5-Sfr1 to Rad51-EED should be abrogated. Co-IP experiments with purified proteins revealed reproducible differences in the amount of Rad51-E206A and Rad51-EED that co-IP'd with Sfr1, but these differences were relatively subtle (***Figure 6C***). Moreover, in our canonical strand exchange assay (***Figure 3D***), these differences in physical binding did not affect the stimulation of Rad51 by Swi5-Sfr1 (***Figure 6D***), suggesting that they are not of functional significance. We also examined the interaction of Swi5-Sfr1 with Rad51-E206K. Similarly to Rad51-EED, we saw a reproducible reduction in the co-IP of Rad51-E206K with Sfr1, but this difference is relatively subtle (less than twofold; ***Figure 6—figure supplement 1D***). These results indicate that PAP mutations do not impair the potentiation of Rad51 by Swi5-Sfr1, leading us to conclude that the severe DNA damage sensitivity of the *rad51-EED* strain is unlikely to be due to a defect in the interaction with Swi5-Sfr1.

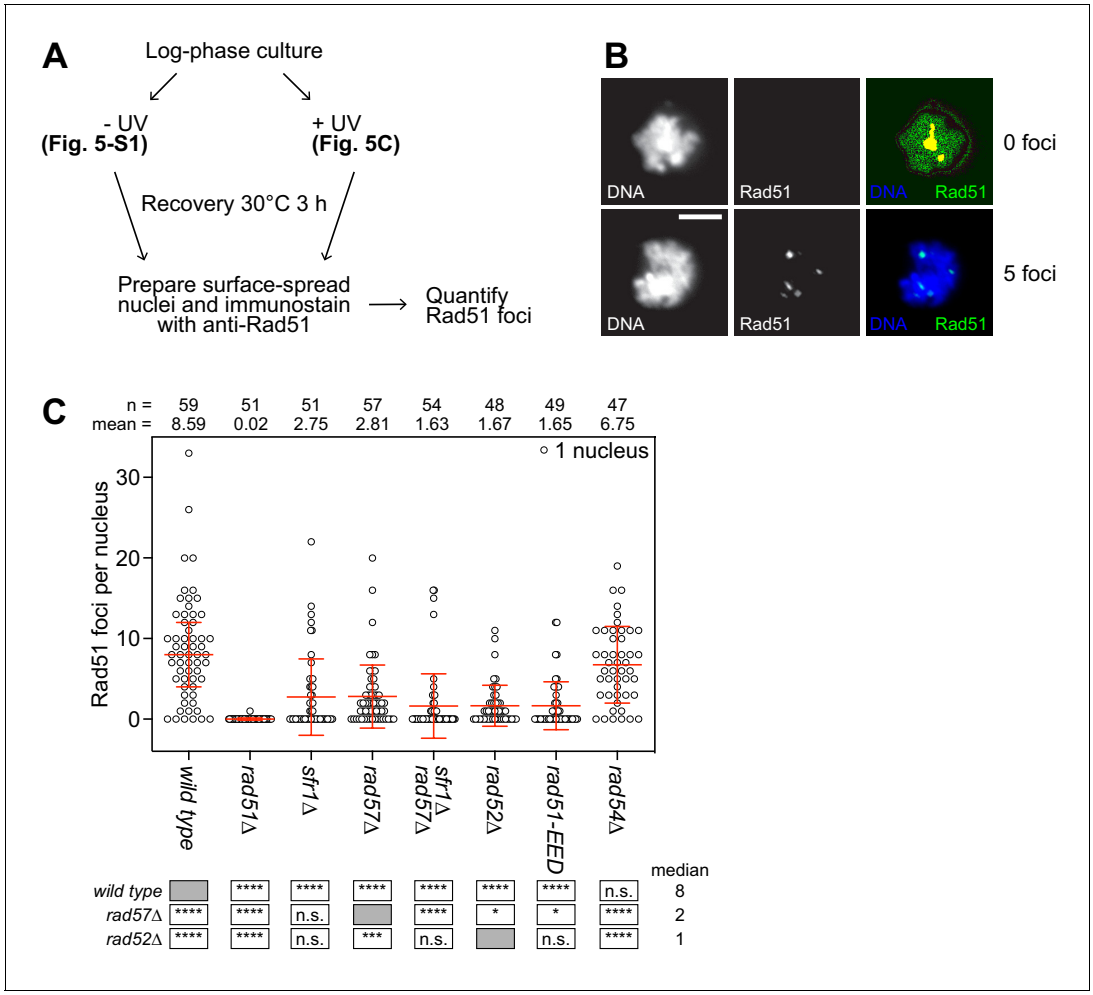


Figure 5. The PAP is critical for the recruitment of Rad51 to sites of DNA damage. (**A**) Schematic of cytological analysis. (**B**) Representative images of UV-irradiated nuclear spreads containing 0 or 5 Rad51 foci. Scale bar, 5 μm. (**C**) The indicated strains were grown to log phase and cultures were split into two. One sub-culture was UV-irradiated (200 J/m^2; shown here) and the other was not (shown in ***Figure 5—figure supplement 1***). Following 3 hr of recovery, nuclei were surface-spread and immunostained with a polyclonal PVDF-purified anti-Rad51 antibody. The indicated number of nuclei were manually picked, images in the DAPI and Rad51 channels were captured, and semi-automated quantification of foci was performed using FIJI software. Bars depict the median and interquartile range. Mean number of foci are shown for each strain. Statistical analysis was by Wilcoxon ranked sum test with the indicated median values. n.s., not significant (p>0.05). * p<0.05. ***p<0.001. ****p<0.0001.

The online version of this article includes the following source data and figure supplement(s) for figure 5:

Source data 1. Number of foci per nucleus following UV irradiation for ***Figure 5C***.

Figure supplement 1. DNA damage dependency of Rad51 foci.

Figure supplement 1—source data 1. Number of foci per nucleus without UV irradiation.

The PAP is important for the interaction of Rad51 with both Rad52 and Rad54

While a defect in the interaction with Rad54 could explain the severity of DNA damage sensitivity observed for *rad51-EED*, this is unlikely to be the cause of the sensitivity as *rad54Δ* is not defective in the recruitment of Rad51 to sites of DNA damage (***Figure 5C***). Thus, the remaining possibility that could account for the phenotypes of *rad51-EED* is that the EED mutation impairs the interaction of Rad51 with Rad52. To examine whether Rad51-Rad52 complex formation was affected by PAP mutations, in vivo co-IP experiments were performed. Comparable amounts of Rad52 were seen to co-IP with Rad51, Rad51-E206A, and Rad51-EE, whereas a clear reduction was observed for Rad51-D209A (***Figure 7A***). Strikingly, Rad52 was completely undetectable in the Rad51-EED

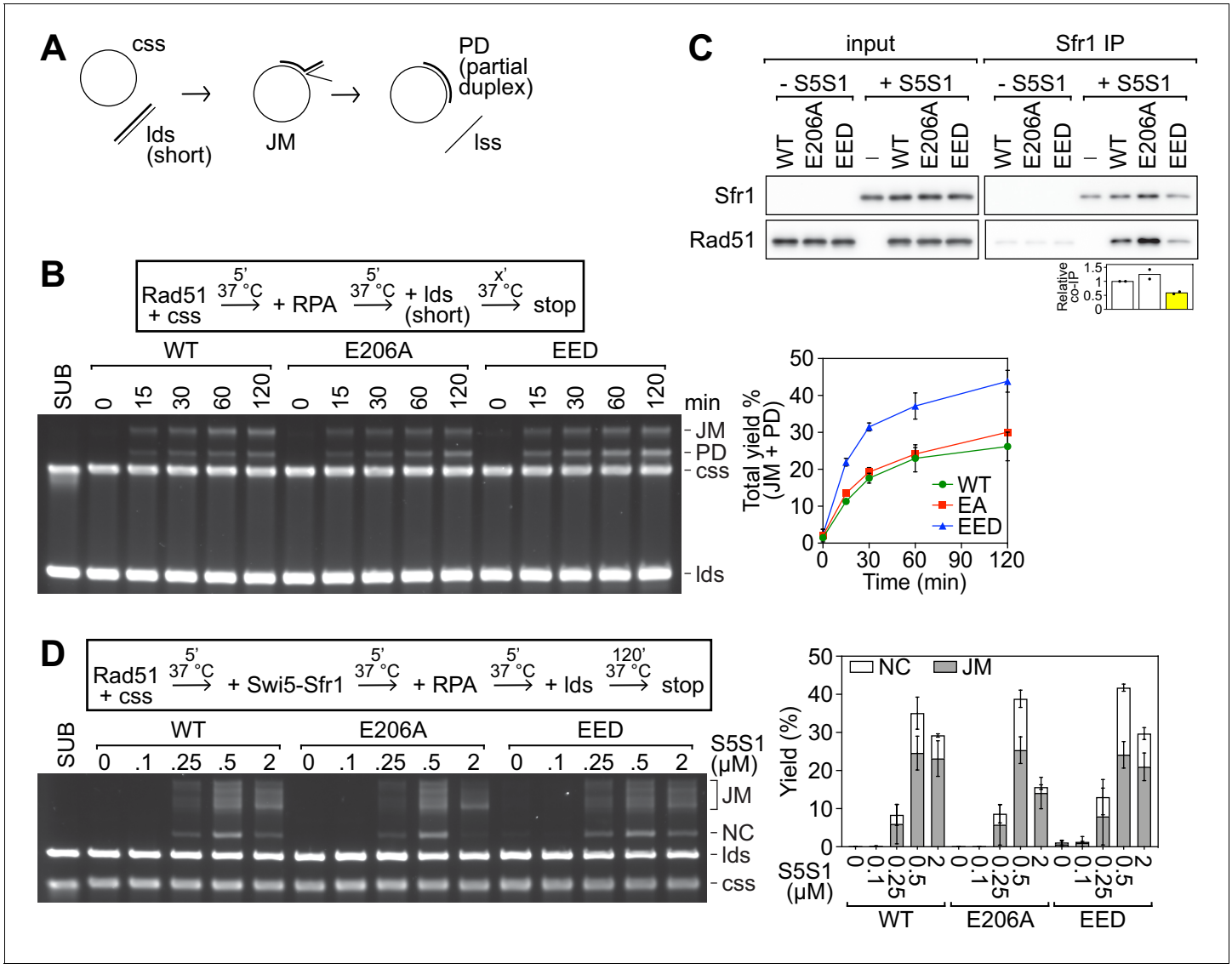


Figure 6. Neutralization of the PAP does not impair the intrinsic activity of Rad51 or the stimulation by Swi5-Sfr1. (**A**) Schematic of the strand exchange assay with shortened DNA substrates (PhiX174 virion ssDNA and a 1.6 kb fragment of PhiX RF I dsDNA). (**B**) Strand exchange reactions were conducted according to the scheme outlined above the gel. Rad51 (WT, E206A, or EED), 15 μM. RPA, 1 μM. cssDNA, 30 μM nt. ldsDNA, 20 μM nt. (**C**) Purified Rad51 (WT, E206A, or EED) was incubated with purified Swi5-Sfr1 (or the equivalent volume of protein storage buffer) and subjected to immunoprecipitation with an anti-Sfr1 antibody. For quantification, Rad51 signal was normalized to Sfr1 signal and expressed relative to wild type. (**D**) Strand exchange reactions were conducted according to the scheme outlined above the gel. Rad51 (WT, E206A, or EED), 5 μM. Swi5-Sfr1 (S5S1), indicated. RPA, 1 μM. cssDNA, 10 μM nt. ldsDNA, 10 μM nt. Data in (**B,D**) are means of three independent experiments and error bars depict standard deviation. Data in (**C**) are the means of two independent experiments with individual values shown.

The online version of this article includes the following source data and figure supplement(s) for figure 6:

Source data 1. Strand exchange yield (%) in ***Figure 6B,D*** and relative co-IP of Rad51 (%) for ***Figure 6C***.

Figure supplement 1. Rad51-EED binds both ssDNA and dsDNA like wild-type Rad51.

Figure supplement 1—source data 1. Relative co-IP of Rad51 (%) for ***Figure 6—figure supplement 1D***.

immunoprecipitate, indicating that the EED mutation ablates Rad51-Rad52 complex formation in vivo. These results suggest that the exquisite DNA damage sensitivity of *rad51-EED* is due to defects in the interactions with both Rad55-Rad57 and Rad52. The identity of the band indicated as Rad52 was verified by using a *rad52*Δ strain (***Figure 7—figure supplement 1A***). To directly test whether the EED mutation disrupts the binding of Rad51 to Rad52, a co-IP experiment was conducted with purified proteins. Comparable amounts of Rad52 co-IP'd with Rad51 and Rad51-E206A (***Figure 7B***).

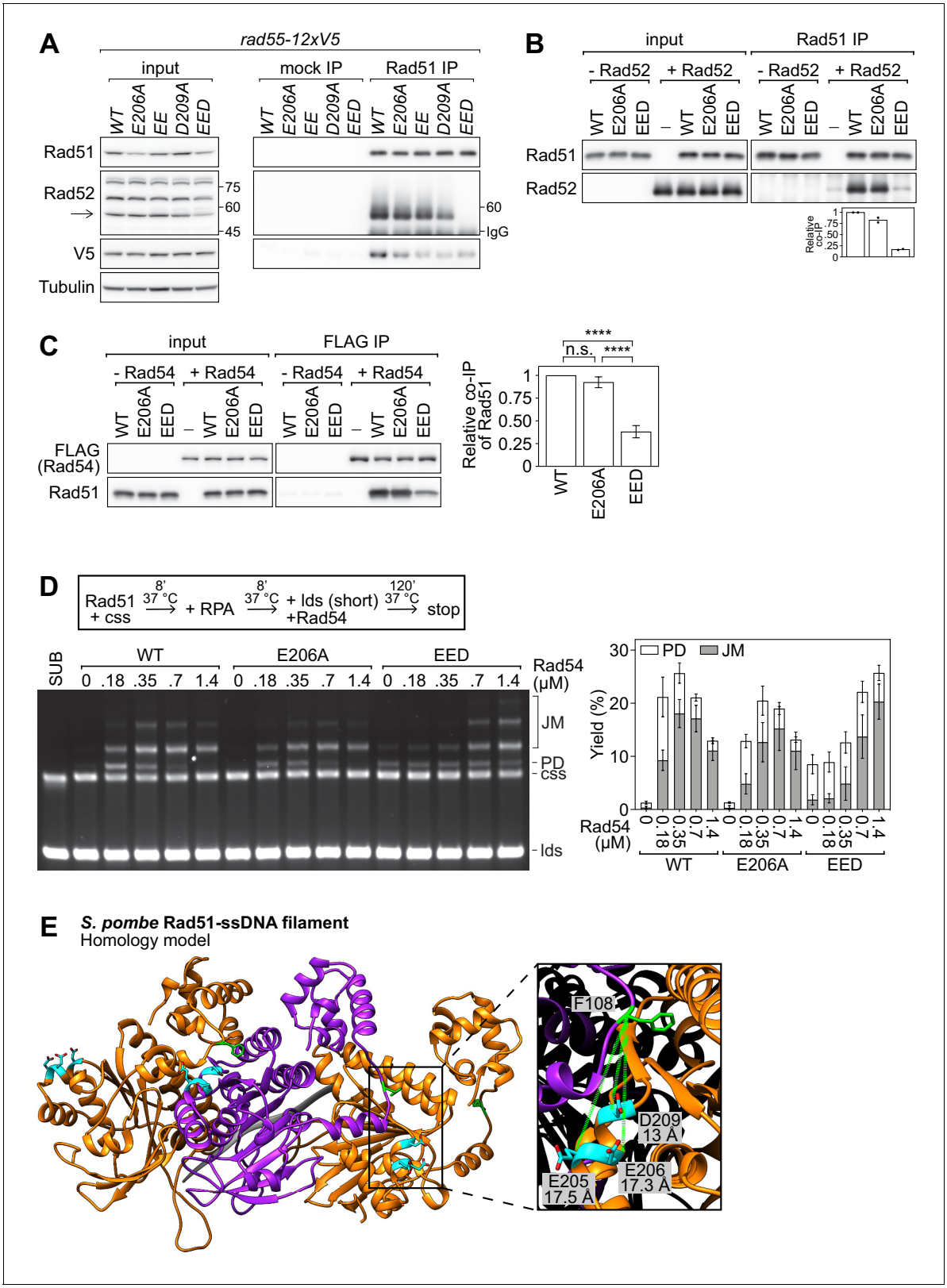


Figure 7. The PAP facilitates the interaction of Rad51 with Rad52 and Rad54. (**A**) Soluble cell extracts treated with a benzonase-like nuclease were prepared from each strain under native conditions (input). Immunoprecipitation (IP) was then performed with mock (human IgG from non-immunized animal) or anti-Rad51 antibodies. Arrow denotes the Rad52 band (other bands were still observed in a *rad52*Δ strain, see ***Figure 7—figure supplement 1A***) and numbers denote the position of the size markers in kDa. To ensure separation of Rad52 from the IgG heavy chain band, the IP samples were

Figure 7 continued on next page

Figure 7 continued

separated by 7% SDS-PAGE instead of the 12% SDS-PAGE employed for the input samples. As a result, the 45 kDa and 75 kDa bands of the size marker are not within the cropped area of the anti-Rad52 immunoblot for the IP sample. Tubulin serves as a loading control. (**B**) Purified Rad51 (WT, E206A, or EED) was incubated with purified Rad52 (or the equivalent volume of protein storage buffer) and subjected to immunoprecipitation with anti-Rad51 antibody. For quantification, Rad51 signal was normalized to Sfr1 signal and expressed relative to wild type. (**C**) Purified Rad51 (WT, E206A, or EED) was incubated with purified FLAG-Rad54 (or the equivalent volume of protein storage buffer) and subjected to immunoprecipitation with FLAG-agarose resin. For quantification, Rad51 signal was normalized to FLAG-Rad54 signal and expressed relative to wild type. Statistical significance was assessed by one-way ANOVA with Tukey's multiple comparisons test. n.s., not significant ($p=0.2538$). ****$p<0.0001$. (**D**) Strand exchange reactions were conducted according to the scheme outlined above the gel. Rad51 (WT, E206A, or EED), 7 μM. Rad54, indicated. RPA, 0.7 μM. cssDNA, 7 μM nt. ldsDNA, 14 μM nt. (**E**) Ribbon depiction of three *Sp*Rad51 monomers (alternating orange and purple) bound to ssDNA (9-mer poly-dT in gray). Residues E205, E206, and D209 are colored in cyan with their side-chains shown (O atoms in red), and F108 is colored in green with its side-chain shown. The α-helix of the rightmost monomer containing E205, E206, and D209 is enlarged, along with the F108 residue of the central monomer, to illustrate the close proximity of these residues at the subunit interface. Dotted-green lines show the C_α-C_α distance between each residue and F108. The Rad51 filament is employed as a proxy to demonstrate that insertion of Phe in the FxxA motif of auxiliary factors could be facilitated by interactions with the PAP. Data in (**B**) are means of two independent experiments with individual values shown. Data in (**C,D**) are means of three independent experiments and error bars depict standard deviation.

The online version of this article includes the following source data and figure supplement(s) for figure 7:

Source data 1. Relative co-IP of Rad52 and Rad51 in ***Figure 7B,C***, and strand exchange yield (%) in ***Figure 7D***.
Figure supplement 1. Anti-Rad52 antibody verification and Rad54 purity analysis.
Figure supplement 2. The PAP is conserved in eukaryotic Dmc1 and archaeal RadA.
Figure supplement 3. The PAP is not conserved in bacterial RecA.

By stark contrast, only background levels of Rad52 were seen to co-IP with Rad51-EED. Similar results were obtained in the reciprocal co-IP experiment (***Figure 7—figure supplement 1B***). These results clearly indicate that the PAP is essential for the Rad51-Rad52 interaction.

Our results demonstrated that the PAP is involved in the interaction of Rad51 with both Rad55-Rad57 and Rad52. We therefore considered the possibility that the PAP is commonly utilized by multiple auxiliary factors and sought to examine the interaction of Rad51 with Rad54. Unlike Rad55-Rad57 and Rad52, Rad54 functions primarily in the later stages of HR (***Sugawara et al., 2003***; ***Lisby et al., 2004***). Defects in the recruitment of Rad51 to DNA damage sites—as seen in *rad51-EED*—would block downstream events, obscuring analysis of the Rad51-Rad54 interaction. To circumvent this, Rad54 with an N-terminal FLAG tag was purified to near-homogeneity from *E. coli* (***Figure 7—figure supplement 1C***) and its physical interaction with Rad51-EED was examined in vitro. Similar amounts of Rad51 and Rad51-E206A were seen to co-IP with Rad54, whereas an approximately threefold reduction in the co-IP of Rad51-EED was observed (***Figure 7C***). To examine whether this difference is of functional significance, strand exchange reactions were conducted under conditions where wild-type Rad51 alone did not produce JM or PD molecules (Rad51-EED nevertheless showed increased intrinsic strand exchange activity [***Figure 7D***], as expected from our previous experiments [***Figure 6A,B***]). Remarkably, the EED mutation rendered Rad51 less sensitive to the stimulatory effect of Rad54, with approximately fourfold more Rad54 required to achieve maximal activity. These results indicate that, in addition to facilitating the interaction of Rad51 with Rad55-Rad57 and Rad52, the PAP is also important for the interaction with Rad54.

Discussion

To understand more about the regulation of Rad51, we employed a structural approach to identify regions of Rad51 that are important for its interaction with auxiliary factors. This highlighted a protruding acidic patch, which we refer to as the PAP, comprised of residues E205, E206, and D209 on the exterior of the Rad51 filament (***Figure 1***). Genetic analysis strongly suggested that mutation of the most conserved residue in this patch (*rad51-E206A*) specifically impairs the interaction between Rad51 and Rad55-Rad57 without affecting the interaction with Swi5-Sfr1 (***Figure 2***), and this was bolstered by biochemical reconstitutions (***Figure 3***). Strikingly, mutation of all three PAP residues to Ala (*rad51-EED*) completely abolished recombinational DNA repair, leading to a phenotype more severe than *rad57*Δ (***Figure 4***). Mechanistically, the DNA damage sensitivity of *rad51-EED* was found to stem from defects in the recruitment of Rad51 to DNA damage sites (***Figure 5***). Biochemical reconstitutions suggested that Rad51-EED is not intrinsically defective and retains a functional

interaction with Swi5-Sfr1 (***Figure 6***). Remarkably, the EED mutation was found to abrogate the interaction of Rad51 with Rad52 and impair the interaction with Rad54 (***Figure 7***). Our results indicate that the PAP, a novel motif of Rad51, is critically important for the interaction with Rad55-Rad57, Rad52, and Rad54. We propose that the PAP is a fundamental motif commonly utilized by recombination auxiliary factors to potentiate Rad51.

The PAP of Rad51 is an evolutionarily conserved motif that is integral to recombinational DNA repair

E205, E206, and D209 were found to form the PAP on the exterior of the Rad51-ssDNA filament (***Figure 1A–C***). Individual mutations within the PAP impaired DNA repair to differing extents. D209A had the highest penetrance, whereas E206A, and to a much lesser extent E205A, conferred sensitivity only in the *sfr1*Δ background, where DNA repair is strictly dependent on Rad55-Rad57 (***Figure 4A and C*** and ***Figure 4—figure supplement 1C***). These genetic data are consistent with the notion that the PAP is more relevant to the function of Rad55-Rad57 than Swi5-Sfr1. When both Glu residues were mutated to Ala (*rad51-EE*), moderate DNA damage sensitivity was observed even in the presence of both Rad55-Rad57 and Swi5-Sfr1; this synergism implies that the functions of E205 and E206 are related, and that the ability of Sfr1 to suppress the DNA damage sensitivity conferred by E206A is partially dependent on E205. Moreover, mutating all three residues to Ala (*rad51-EED)* completely abolished Rad51-dependent DNA repair. The additive effect of combining mutations suggests that the overall negativity of the PAP is important for its function. This is bolstered by the finding that the replacement of E206 with a positively charged Lys residue is highly disruptive, phenocopying the neutralization of all three residues via Ala mutations (***Figure 4—figure supplement 1D***). Thus, while all three residues are relevant to PAP function, there appears to be a hierarchy: D209A is more important than E206, which itself is more important than E205. This suggests that the closer a residue is to the C-terminal end of the α-helix (top of the helix in our structural models), the more important it is for PAP function (discussed below).

Negatively charged regions were seen in the equivalent α-helices of both *Sc*Rad51 and *Hs*Rad51 (***Figure 1—figure supplement 1B,C***), indicating structural conservation of the PAP. Furthermore, sequence alignments suggest that the PAP is widely conserved among eukaryotes, with residues E206 and D209 each showing conservation in seven-out-of-eight eukaryotic Rad51 orthologues (***Figure 7—figure supplement 2A***). Interestingly, examination of a structural model revealed conservation of the PAP in Dmc1, the meiosis-specific RecA-family recombinase (***Figure 7—figure supplement 2B***). The archaeal RadA polymer also exhibited substantial structural conservation of the PAP (***Figure 7—figure supplement 2C***). By contrast, this region showed poor sequence conservation in bacterial RecA, and although a short α-helix at the equivalent position appeared to exist in the RecA monomer (***Figure 7—figure supplement 3A***), a loop was seen instead in the RecA-ssDNA filament structure (***Figure 7—figure supplement 3B***). Furthermore, despite this region being negatively charged, this was partially due to the close proximity of residues E32 and D33 from the adjacent RecA monomer. We interpret these analyses to mean that the PAP is conserved in eukaryotic Rad51/Dmc1 and archaeal RadA, but not in bacterial RecA. While the mediator and ssDNA annealing activities of Rad52 are provided by RecFOR in bacteria, only eukaryotes and archaea also possess recombinase paralogs and Rad54 (***Zelensky et al., 2014***). We postulate that the PAP may have evolved in organisms where the RecA-family recombinase is potentiated by multiple distinct auxiliary factors. Consistently, it is notable that Dmc1 is subjected to extensive regulation by auxiliary factors: Swi5-Sfr1, Hop2-Mnd1, and Rdh54 simulate Dmc1 (***Haruta et al., 2006***; ***Chi et al., 2009***; ***Tsubouchi et al., 2020***); and Rad52 has been proposed to inhibit Dmc1 (***Murayama et al., 2013***).

The PAP plays a central role in the interaction of Rad51 with recombination auxiliary factors

The PAP-containing α-helix precedes a β-strand that is critically important for Rad51 polymerization (***Pellegrini et al., 2002***; ***Shin et al., 2003***; ***Conway et al., 2004***). This β-strand is involved in facilitating interactions with the FxxA consensus sequence within the inter-domain linker of the adjacent monomer (corresponding to ^{108}FTTA^{111} in *Sp*Rad51). The Phe residue of the adjacent monomer inserts into a hydrophobic pocket above the β-strand, which stabilizes inter-subunit contacts. Because some auxiliary factors that contain the FxxA motif employ Rad51 mimicry to interact with

Rad51, FxxA has been proposed to function as a Rad51 interaction motif (**Pellegrini et al., 2002**; **Shin et al., 2003**). Neither Swi5 nor Sfr1 contain the FxxA consensus sequence and we recently identified two non-FxxA sites within the intrinsically disordered N-terminal half of Sfr1 that are responsible for the binding of Swi5-Sfr1 to Rad51 (**Argunhan et al., 2020**). By contrast, both Rad57 (^{145}FELA^{148}) and Rad52 (^{17}FNTA^{20} and ^{338}FISA^{341}) contain the FxxA consensus sequence, as does Rad54 (^{804}FIRA^{807}). Rad55 does not contain an FxxA motif, and notably, Y2H analysis suggested that Rad51 interacts with Rad57 but not Rad55 (**Tsutsui et al., 2001**). Furthermore, Y2H analysis mapped the minimal *Sp*Rad51-interacting domain of Rad52 to a C-terminal fragment (310-469) containing the ^{338}FISA^{341} sequence (**Kim et al., 2002**), and mutation of the corresponding Phe residue to Ala in *Sc*Rad52 (F349A) completely abrogated its binding to Rad51 (**Kagawa et al., 2014**). Taken together, these observations strongly suggest that Rad52 employs the FxxA motif to bind Rad51.

Our results demonstrate that neutralization of the PAP impairs the interaction with Rad55-Rad57, Rad52, and Rad54, while the interaction with Swi5-Sfr1 is mostly unaffected (**Figures 4B**, **6C, D** and **7A–D** and **Figure 7—figure supplement 1B**). We cannot exclude the possibility that the PAP has some role in facilitating the interaction with Swi5-Sfr1, but a simple inference that can be drawn from these results is that the PAP is particularly important for auxiliary factors that employ Rad51 mimicry to modulate Rad51. The close proximity of the PAP to the Phe residue within the FxxA motif of the adjacent monomer—C_α-C_α distances for PAP residues and *Sp*Rad51-F108 are predicted to be 13.0 Å (D209), 17.3 Å (E206), and 17.5 Å (E205)—means it would be well-placed to influence interactions with auxiliary factors that employ Rad51 mimicry (**Figure 7E**). We speculate that this may be the mechanism through which the PAP exerts its effects on Rad51 potentiation. Since the negative charge of the PAP is important for recombinational DNA repair (**Figure 4A** and **Figure 4—figure supplement 1D**), it is likely that the PAP participates in electrostatic interactions that are important for the modulation of Rad51 by these auxiliary factors, which may utilize the PAP as a landing pad to facilitate FxxA insertion. We anticipate that a basic patch may exist that is close in three-dimensional space to the FxxA motif of each auxiliary factor, and this basic patch may be critically important for interacting with the PAP and facilitating the binding to Rad51. Interestingly, Y2H analysis by **Kim et al., 2002** isolated several other mutations in *Sp*Rad51 (G177S, C179F, G282D, and L274P) that disrupt the interaction with Rad52, and these residues are also in reasonably close proximity to F108 (**Figure 7—figure supplement 3C**). Notably, the G177S and C179F mutations also impaired the interaction with Rad54. Moreover, the C179F mutation even abrogated the interaction with Rad57 and the self-association of Rad51. Given the close proximity of G177 and C179 to the PAP (C_α-C_α9–12 Å), it is possible that mutation of these residues affects PAP function and/or F108 insertion. These Y2H results are consistent with our proposal that multiple auxiliary factors interact with Rad51 via a mechanism involving the PAP.

PAP mutations impaired complex formation with Rad55-Rad57 in vivo (**Figures 2E**, **4B** and **7A**), but even in *rad51-EED*, complex formation was not completely abolished. By contrast, while formation of the Rad51-Rad52 complex was mostly unaffected by mutation of only the Glu residues within the PAP, the D209A mutation led to a marked reduction in complex formation (**Figure 7A**). Consistent with the notion that the PAP as a whole is important, the EED mutation completely abrogated Rad51-Rad52 complex formation. Co-IP experiments with purified proteins directly demonstrated that the interaction of Rad51 with both Rad52 and Rad54 is facilitated by the PAP (**Figure 7B–D** and **Figure 7—figure supplement 1B**). Performing such experiments with Rad55-Rad57 awaits the purification of this biochemically intractable complex.

If multiple auxiliary factors utilize the same motif to potentiate Rad51, they would be expected to compete for Rad51 binding. However, because auxiliary factors perform non-overlapping roles in HR, the requirement for binding Rad51 is likely to be temporally distinct, with Rad52 being the most upstream binding partner, followed by Rad55-Rad57, then Rad54 (**Sugawara et al., 2003**; **Lisby et al., 2004**). Furthermore, the Rad51 nucleoprotein filament contains as many PAP motifs as there are monomers in the filament, providing ample opportunities for auxiliary factors to bind Rad51 in a non-competitive manner. Notably, the PAP is important for interactions with auxiliary factors involved in both the early (Rad52 and Rad55-Rad57) and late (Rad54) stages of DNA strand exchange, indicating that the PAP is integral to the role of Rad51 in HR. Further research is needed to examine the temporospatial coordination of Rad51 binding, especially in light of the finding that some auxiliary factors such as Rad55-Rad57 and Swi5-Sfr1 interact with each other (**Argunhan et al., 2020**).

rad51-E206A uncovers insights into the interplay between Rad55-Rad57 and Swi5-Sfr1

Substantial genetic analysis suggests that the defects of *rad51-E206A* stem specifically from an impairment in the interaction with Rad55-Rad57. This is supported by biochemical analysis demonstrating that the intrinsic strand exchange activity of Rad51-E206A is comparable to wild type, and its interaction with Swi5-Sfr1, Rad52, and Rad54 is not grossly impaired. Interestingly, the *rad51-E206A* mutant was proficient for DNA repair in the presence of Sfr1, but completely defective in its absence (***Figure 2A–C*** and ***Figure 2—figure supplement 1A–C***). This suppression did not occur through enhancing Rad51–Rad55-Rad57 complex formation (***Figure 2E***), suggesting that Swi5-Sfr1 can functionally compensate for defects in the physical association of Rad51 with Rad55-Rad57. Swi5-Sfr1 may function in a contingency capacity for Rad55-Rad57 such that a moderate reduction in Rad51–Rad55-Rad57 complex formation does not affect DNA repair as long as Swi5-Sfr1 is present. Suppression of the DNA damage sensitivity associated with *rad51-E206A* by Sfr1 contradicts the commonly accepted model wherein Rad55-Rad57 and Swi5-Sfr1 comprise independent sub-pathways of HR (***Akamatsu et al., 2003***; ***Akamatsu et al., 2007***). We recently showed that Rad55-Rad57 can suppress defects in the interaction between Swi5-Sfr1 and Rad51, and that Swi5-Sfr1 physically interacts with Rad55-Rad57 (***Argunhan et al., 2020***). Thus, there is increasing evidence to suggest that Rad55-Rad57 and Swi5-Sfr1, while capable of functioning independently of each other, collaboratively promote Rad51-dependent DNA repair.

In summation, we have characterized an acidic patch of Rad51 that comprises an evolutionarily conserved motif important for the interaction of Rad51 with its major auxiliary factors: the Rad51 paralogs Rad55-Rad57, Rad52, and Rad54. While this motif is essential for HR in *S. pombe*, the extent to which it is required in other organisms remains to be determined and will likely be a focal point of future research.

Materials and methods

Sequence alignments and structural models

Sequence alignments were prepared using Clustal Omega (UniProt identifiers are: *S. pombe*, P36601; *S. cerevisiae*, P25454; *U. maydis*, Q99133; *C. elegans*, G5EGG8; *D. melanogaster*, Q27297; *G. gallus*, P37383; *M. musculus*, Q08297; *H. sapiens*, Q06609). All structural depictions were prepared using UCSF Chimera (***Pettersen et al., 2004***). The Coulombic Surface Coloring feature in UCSF Chimera was employed to depict surface charge. The model of an *Sp*Rad51 monomer was generated by Phyre2 (intensive mode; ***Kelley et al., 2015***) based on two known structures of *Sc*Rad51 (***Conway et al., 2004***; ***Chen et al., 2010***), with Protein databank (PDB) identifiers 1SZP and 3LDA; and one known structure of *Hs*Rad51 (***Short et al., 2016***) with PDB identifier 5JZC. 46 residues (1–41 and 361–365) of the *Sp*Rad51 monomer were modeled ab initio and these low confidence regions were omitted from the model. The *Sp*Rad51-ssDNA filament model consisting of three monomers is a homology model that was described previously by ***Ito et al., 2020***. This structure was previously deposited in the Biological Structure Model Archive (identification code BSM00017). The structure of Rad51-EED was analyzed by substituting E205, E206, and D209 to Ala through the Rotamer feature. The model of an *Sp*Dmc1 monomer was also generated by Phyre2 (intensive mode; ***Kelley et al., 2015***) based on three known structures of RadA (***Shin et al., 2003***; ***Wu et al., 2004***; ***Chen et al., 2007***), with PDB identifiers 1PZN, 1T4G, and 2DFL; two known structures of *Sc*Rad51 (***Conway et al., 2004***; ***Chen et al., 2010***), with PDB identifiers 1SZP and 3LDA; and one known structure of *Hs*Rad51 (***Short et al., 2016***) with PDB identifier 5JZC. Residues 1–14 were modeled ab initio and were therefore omitted from the model.

The *Hs*Rad51-ssDNA filament shown is the structure resolved by cryo-electron microscopy (***Xu et al., 2017***; PDB 5H1B), whereas the *Sc*Rad51-ssDNA filament shown is the structure solved by X-ray crystallography (***Conway et al., 2004***; PDB 1SZP, chains E and F). Note that ssDNA density is missing from the structure of the *Sc*Rad51-ssDNA filament model, despite the formation of crystals in the presence of ssDNA (***Conway et al., 2004***). The structure of the *Pyrococcus furiosus* RadA polymer was solved by X-ray crystallography (***Shin et al., 2003***; PDB 1PZN, chains G, A, and B). The RecA monomer (***Story et al., 1992***; PDB 2REB) and ssDNA filament (***Chen et al., 2008***; 3CMU) structures were solved by X-ray crystallography.

Schizosaccharomyces pombe strains

S. pombe strains used in this study are listed in the Key Resources Table. All strains are isogenic derivatives of strain YA119 (**Akamatsu et al., 2003**). For most assays, strains of the h minus mating type were employed (*Msmt-0*), except in **Figure 1D** (*mat1PD17::LEU2*). Standard media was used for growth (YES), selection (YES with drugs or EMM), and sporulation (SPA), as described previously (**Hentges et al., 2005**). All reasonable requests for strains will be fulfilled by the co-corresponding authors (B. Argunhan and H. Iwasaki).

Primers used in this study are listed in the Key Resources Table. In order to introduce the *rad51-E206A* mutation at the native *rad51*$^{+}$ locus, plasmid p6 (*pET11b-rad51*$^{+}$; **Haruta et al., 2006**) was amplified with mutagenic primers 398–400 and 399–405 to produce amplicons 1 and 2, respectively. Amplicon 3, containing the *ADH1* terminator (T_{ADH1}) and *kanMX6* cassette, was amplified from the C-terminal epitope tagging plasmid p51 (*pFA6a-13xMYC-kanMX6*) using primers 350–351. Regions upstream and downstream of the *rad51*$^{+}$ locus were amplified with primers 409–412 and 417–419 to yield amplicons 4 and 5, respectively. All five amplicons were cloned onto the pBlueScript II SK (+) vector using the In-Fusion Cloning Kit (Takara) to generate plasmid pNA46. pNA46 was then cut with restriction enzymes MscI and XhoI (NEB) and the fragment containing *rad51-E206A-*T_{ADH1}*-kanMX6* was gel extracted and transformed into strain NA310 (*wild type*). *rad51-E205A, rad51-EE, rad51-D209A, rad51-EED,* and *rad51-E206K* were made in exactly the same way using plasmids pBA144, pBA146, pBA145, pBA148, and pBA152, respectively. To generate the *rad55-12xV5* strain, plasmid p85 (pNX3c-PK12; **Amelina et al., 2016**) was PCR-amplified with primers 200–201 and the wild-type strain (NA310) was transformed with this amplicon. All cloning and genetic manipulations were confirmed by DNA sequencing. Sequence alignments were prepared with Clustal Omega.

DNA damage sensitivity assays

A single colony was streaked as a patch onto a YES plate and grown at 30˚C for 1–2 days. This patch was then resuspended in 2 mL of YES and grown with shaking at 30˚C for ~24 hr. Cells were seeded into 2 mL of fresh YES (0.25×10^6 cells/mL for *rad*$^{+}$; 0.5×10^6 cells/mL for *rad*$^{-}$) and grown with shaking at 30˚C until they reached log phase. For spot tests, cell density was adjusted to 2×10^7 cells/mL and tenfold serial dilutions were made. 5 µL of each dilution was spotted onto YES plates without drugs and YES plates containing DNA damaging agents. For UV treatment, a YES plate without drugs was UV-irradiated. Cells were incubated at 30˚C or 21˚C, as indicated. For clonogenic survival assays, cells were prepared as described above and spread onto YES plates, which were then exposed to acute UV irradiation of the specified dose. Colonies were counted after 3–4 days of incubation at 30˚C and survival percentage was expressed relative to the number of colonies on the untreated plate. Statistical analysis was by unpaired two-tailed t-test using GraphPad Prism (version 8).

Extraction and detection of cellular proteins

A single colony was streaked as a patch on a YES plate and grown for 1–2 days at 30˚C. This patch was resuspended in 2 mL of YES and grown with shaking at 30˚C for 24 hr. Cells were seeded into 70 mL of fresh YES (0.15×10^6 cells/mL for *rad*$^{+}$; 0.30×10^6 cells/mL for *rad*$^{-}$) and grown in 500 mL baffled flasks with shaking at 30˚C until they reached log phase. Cells were harvested and cell pellets were resuspended in 35 mL of sterile water and divided into two equal aliquots (±UV). +UV aliquots were transferred into a petri dish at a depth of ~0.5 cm and exposed to UV (200 J/m^2), while -UV aliquots were mock treated. Each aliquot was then resuspended in 35 mL fresh YES and allowed to recover at 30˚C for 3 hr with shaking. Cells were then harvested and treated as previously described (**Argunhan et al., 2020**). Briefly, 1×10^8 cells were resuspended in 1 mL of ice-cold water and mixed with 150 µL of 1.85 M NaOH 7.5% β-mercaptoethanol on ice for 15 min. 150 µL of 55% TCA was then added, followed by mixing and a further 10 min incubation on ice. Precipitated proteins were pelleted by sequential centrifugation (20000 *g*, 10 min, 2˚C; then 20000 *g*, 1 min, 2˚C). Pellets were resuspended in 100 µL of urea buffer (8 M urea, 5% SDS, 200 mM Tris-Cl pH 6.8, 1 mM EDTA, 0.01% BPB) freshly supplemented with 0.1 M DTT and 0.2 M Tris and dissolved on a thermomixer (65˚C 10 min 1300 RPM). Proteins were then separated by SDS-PAGE and transferred to PVDF membranes. Antibodies against Rad51 (1:10,000; **Argunhan et al., 2020**) and Tubulin (1:10,000; Sigma T5168) were employed. Horseradish peroxidase (HRP)-conjugated secondary antibodies were

purchased from GE Healthcare (mouse, 1:5,000, NA931; rabbit, 1:5,000, NA934) or Jackson Immunoresearch Labs (rat, 1:10000, 712-035-153).

In vivo immunoprecipitation (IP)

A single colony was resuspended in 20 mL YES and grown with shaking at 30˚C (24 hr for *rad*$^{+}$; 48 hr for *rad*$^{-}$). Cells were seeded into 1 L of fresh YES (0.2×10^6 cells/mL for *rad*$^{+}$; 0.4×10^6 cells/mL for *rad*$^{-}$) in 5 L baffled flasks and grown with shaking at 30˚C until they reached log phase. Cultures were then supplemented with 0.5 mM PMSF and harvested by centrifugation (6000 *g*, 15 min, 2˚C), and pelleted cells were washed with 20 mL of yeast wash solution (50 mM HEPES [pH 7.5], 70 mM KOAc, 1 mM PMSF). Aliquots of 2×10^9 cells were pelleted, frozen in liquid nitrogen, and stored at −80˚C until use. IP experiments were then carried out as previously described (**Argunhan et al., 2017b**). Briefly, a single cell pellet was resuspended in 400 µL of KA50 buffer (50 mM HEPES-KOH [pH 7.5], 50 mM KOAc, 5 mM MgOAc, 0.05% Igepal CA-630, 10% glycerol, 0.25 mM TCEP, 0.5 mM PMSF, 2x cOmplete protease inhibitor cocktail [Roche], 10 mM β-glycerophosphate, 10 mM NaF, 1 mM sodium orthovanadate) and mixed with an equal volume of glass beads (500 micron) on ice. Cells were then broken using a Yasui Kikai Multi-beads Shocker (2700 RPM, 30 s on/off, 12 cycles, 2˚C). The lysate was recovered, and the glass beads were washed with 200 µL of KA50 buffer and combined with the lysate. The lysate was then treated with 250 units of TurboNuclease (Accelagen) for 30 min at 4˚C with mixing. The lysate was then sequentially cleared (20,000 g, 10 min, 2˚C; then 20,000 g, 5 min, 2˚C), a sample was taken for immunoblotting (input) and mixed with an equal volume of 2x SDS loading buffer (120 mM Tris-HCl [pH 6.8], 4% SDS, 20% glycerol, 0.02% BPB, 200 mM DTT), and the remaining soluble cell extract was divided into three equal aliquots in protein LoBind tubes (Eppendorf). Anti-V5 (mouse; MCA1360 Bio-Rad), anti-Rad51 (rabbit; **Haruta et al., 2006**), or ChromPure Human IgG (mock antibody; 009-000-003 Jackson Immunoresearch Laboratories) antibodies were premixed with Dynabeads Protein A (Thermo Fisher Scientific) and incubated with each aliquot of soluble cell extract with gentle mixing (3 hr, 4˚C). Aqueous fractions were separated using a magnetic stand and the beads were briefly washed with buffer KA50 (300 µL, x3). The beads were then resuspended in 75 µL of 1x SDS loading buffer and proteins were eluted using a thermomixer (IP; 65˚C 10 min 1300 RPM). Samples were separated by SDS-PAGE, transferred to PVDF membranes and detected with the following antibodies: anti-V5, mouse (1:10,000; Bio-Rad); anti-Rad51, rat (1:10,000; **Argunhan et al., 2020**); anti-Rad52, rabbit (1:5,000; **Kurokawa et al., 2008**); and anti-Tubulin, mouse (1:10,000, T5168 Sigma-Aldrich). HRP-conjugated secondary antibodies were purchased from GE Healthcare (mouse, 1:5000, NA931; rabbit, 1:5,000, NA934) or Jackson Immunoresearch Labs (rat, 1:10,000, 712-035-153). FIJI software (**Schindelin et al., 2012**) was used for quantification of in vivo IPs. Briefly, background subtraction was performed by the rolling ball method and the signal for IP'd and co-IP'd protein was quantified. The co-IP'd signal was then divided by the IP'd signal and expressed relative to wild type. Graphs were prepared using GraphPad Prism (version 8).

Protein purification

E. coli BL21 (DE3) RIPL strain was used for purification of *S. pombe* Rad51, RPA, Swi5-Sfr1, and Rad52. Rad51 (plasmid p6; *pET11b-rad51*$^{+}$), Rad51-E206A (plasmid pNA42; *pET11b-rad51-E206A*), and Rad51-EED (plasmid pBA161; *pET11b-rad51-E205A-E206A-D209A*) were expressed with 1 mM IPTG at 18˚C for ~14 hr and purified exactly as previously described (**Kurokawa et al., 2008**). Rad51 mutants behaved similarly to wild-type Rad51 throughout the purification process. *S. pombe* RPA was expressed from plasmid p69 (*pET11b-ssb2-ssb3-ssb1*) and Swi5-Sfr1 was expressed from plasmid p71 (*pBKN220-sfr1-swi5*) as for Rad51, and purified exactly as previously described (**Haruta et al., 2006**; **Kurokawa et al., 2008**). Rad52 was expressed from plasmid p76 (*pET11b-rad52*$^{+}$) with 1 mM IPTG at 30˚C for 3 hr and purified exactly as previously described (**Kurokawa et al., 2008**).

S. pombe Rad54 fused to an N-terminal tag—containing a hexahistidine tag, the Fh8 fusion partner (**Costa et al., 2013**), and a FLAG epitope, with a PreScission protease recognition site between the Fh8 and FLAG components (pBA110; *pET15b-6xHis-Fh8-PreScission-1xFLAG-rad54*$^{+}$)—was expressed in 20 L of *E. coli* strain BL21 (DE3) Star at an OD of ~0.45 with 1 mM IPTG at 18˚C for ~14 hr. Cells were harvested by centrifugation, washed with *E. coli* wash solution (50 mM Tris-Cl [pH 7.5],

150 mM NaCl, 1 mM PMSF), and stored at −80˚C until required. Cell pellets (~53 g) were then resuspended in 250 mL of R buffer (20 mM Tris-Cl [pH 7.5], 10% glycerol, 1 mM EDTA) containing 500 mM NaCl, 5 mM MgOAc, 0.5 mM ATP, 2 mM imidazole, 1 mM DTT, 0.5 mM PMSF, and 0.01% igepal CA-630. Cells were then disrupted by sonication and the lysate was cleared by ultracentrifugation (70,000 g 1 hr 2˚C). The clarified lysate was incubated with 10 mL of cOmplete His-Tag Purification Resin (Roche) with gentle mixing (1 hr 4˚C). The resin was poured into a glass column (Bio-Rad Econo-column, 2.5 cm x 10 cm) and washed sequentially with the same buffer used for lysis (50 mL x4) and R buffer containing 500 mM NaCl, 5 mM imidazole, 1 mM DTT, and 0.5 mM PMSF (50 mL x8). Proteins were then eluted in R buffer containing 300 mM NaCl, 300 mM imidazole, and 0.5 mM TCEP (2 mL x4). Eluates were combined, supplemented with PreScission protease (GE Healthcare), and dialyzed against 1 L of the same buffer without imidazole (overnight 4˚C). The protein sample was diluted in 2x volumes of R buffer containing 0.5 mM TCEP and applied to a 1 mL HiTrap Q column equilibrated with R buffer containing 100 mM NaCl and 0.5 mM TCEP. Rad54, which was found in the flow-through, was then applied to a 1 mL HiTrap Heparin column equilibrated with R buffer containing 100 mM NaCl and 0.5 mM TCEP. Proteins were then eluted with a linear gradient (20 mL 0.1–0.6 M NaCl). Peak fractions containing Rad54 were combined, diluted with 9x volumes of R buffer containing 0.5 mM TCEP, then applied to a 1 mL Resource S column equilibrated with R buffer containing 50 mM NaCl and 0.5 mM TCEP. Proteins were eluted with a linear gradient (20 mL 0.05–0.7M NaCl), then peak fractions were pooled and developed in a 16/60 Superdex 200 PG gel filtration column in R buffer containing 300 mM NaCl and 0.5 mM TCEP. Peak fractions were pooled, diluted with 2x volumes of R buffer containing 0.5 mM TCEP, and applied to a 1 mL Resource S column. Proteins were eluted with a linear gradient (40 mL 0.1–0.5 M NaCl). Rad54 eluted at ~220 mM NaCl and was subsequently concentrated using a Vivaspin six centrifugal concentrator (MWCO 30 kDa). The concentration was estimated by measuring the A280 with a molar extinction coefficient of 72530 M^{-1} cm^{-1}. The concentrated protein was frozen in small aliquots using liquid nitrogen and stored at −80˚C until required. The yield of highly purified Rad54 was ~0.5 mg. Chromatography columns were purchased from GE Healthcare.

Electrophoretic mobility shift assay (EMSA)

Rad51 (wild type, Rad51-E206A, or Rad51-EED) was incubated with 30 micromolar nucleotide (µM nt) of PhiX174 virion DNA or 20 µM nt of ApaLI-linearized PhiX RFI DNA in EMSA buffer (30 mM HEPES-KOH [pH 7.5], 150 mM KCl, 3 mM $MgCl_2$, 2 mM ATP, 1 mM DTT, 5% glycerol). The 10 µL reaction was incubated at 37˚C for 15 min. 1.1 µL of 2% glutaraldehyde was then added and incubation was continued for a further 5 min at 37˚C. 2.5 µL of loading dye was added and 3 µL of the reaction was loaded onto a 0.8% agarose gel in TAE buffer (50 V 120 min). The gel was then stained with SYBR Gold (Thermo Fisher Scientific) and imaged using a LAS4000 mini (GE Healthcare).

ATPase assay

The ATPase assay was conducted exactly as previously described (***Argunhan et al., 2020***). Briefly, 5 µM of Rad51 or Rad51-E206A was mixed with 10 µM nt of PhiX174 virion DNA on ice in ATPase buffer (30 mM Tris-Cl [pH 7.5], 100 mM KCl, 3.5 mM $MgCl_2$, 1 mM DTT, 5% glycerol), and either 0.5 µM Swi5-Sfr1 or the equivalent volume of protein storage buffer was added. Reactions were then initiated through the addition of 0.5 mM ATP and 10 µL aliquots were withdrawn at multiple timepoints spanning the initial reaction rate, immediately mixed with 2 µL of 120 mM EDTA and stored at room temperature. The concentration of inorganic phosphate was then measured with a commercial malachite green phosphate detection kit (BioAssay Systems) according to the manufacturer's instructions.

Three-strand exchange assay

To examine the intrinsic strand exchange activity of Rad51, 15 µM of Rad51 (wild type, Rad51-E206A, or Rad51-EED) was incubated with 30 µM nt PhiX174 virion DNA (NEB) for 5 min at 37˚C in strand exchange buffer (30 mM Tris-HCl [pH7.5], 1 mM DTT, 150 mM KCl, 3.5 mM $MgCl_2$, 2 mM ATP, 8 mM phosphocreatine, 8 units/mL creatine phosphokinase and 2.5% glycerol). Next, 1 µM of RPA was added to the reaction and after a 5 min incubation, the reaction was initiated with 20 µM nt of PhiX RFI DNA (NEB) linearized with ApaLI. In the case of the shortened lds substrate, a 1.6 kb

dsDNA fragment was employed instead, and this was prepared by digesting PhiX RFI DNA with both MfeI and XhoI. 10 µL was collected immediately after the addition of dsDNA (0 min) and the remaining reaction was then incubated at 37˚C. 10 µL aliquots were subsequently withdrawn at the indicated timepoints (15, 30, 60, and 120 min). At each timepoint, samples were supplemented with 1 µL of psoralen (200 µg/mL) and subjected to psoralen-UV crosslinking to capture labile DNA structures. Reactions were then deproteinized through addition of 1.8 µL of stop solution (6.6 mg/mL proteinase K and 2.65% SDS) and incubation at 37˚C for 30 min. 2.5 µL of loading dye (15% w/v Ficoll, 0.25% Bromophenol blue, 0.25% Xylene cyanol and 20 mM Tris [pH 7.5]) was added to the reactions, and following mixing, 4 µL of the reaction was loaded and resolved in a 0.8% agarose gel in TAE buffer (50 V 120 min). The gel was then stained with SYBR Gold (Thermo Fisher Scientific) and imaged using a LAS4000 mini (GE Healthcare).

In strand exchange assays containing Swi5-Sfr1, 5 µM of Rad51 (wild type, Rad51-E206A, or Rad51-EED) was incubated with 10 µM nt PhiX174 virion DNA (NEB) for 5 min at 37˚C in strand exchange buffer (same as above except the total salt concentration was 100 mM KCl). Next, 0.5 µM of Swi5-Sfr1 (or the indicated concentration) was added and following a 5 min incubation at 37˚C, 1 µM of RPA was included. After a further 5 min at 37˚C, the reaction was initiated with 10 µM nt of PhiX RFI DNA (NEB) linearized with ApaLI and incubated for 120 min at 37˚C. Subsequent procedures were carried out as described above.

In strand exchange assays containing Rad54, 7 µM of Rad51 (wild type, Rad51-E206A, or Rad51-EED) was incubated with 7 µM nt PhiX174 virion DNA (NEB) for 8 min at 37˚C in strand exchange buffer (same as above except the total salt concentration was 100 mM KCl). Next, 0.7 µM RPA was added and incubation was continued at 37˚C for 8 min. The reaction was then initiated with 14 µM nt of the shortened lds (described above) and immediately supplemented with the indicated concentration of Rad54. Incubation was continued for 120 min at 37˚C. Subsequent procedures were carried out as described above.

Quantification was performed as previously described (***Haruta et al., 2006***) except that FIJI software was employed (***Schindelin et al., 2012***). Briefly, background was subtracted using the rolling ball method, the signal corresponding to lds, NC/PD, and (JM/1.5) in a given lane was summed and set equal to 100%, and the signal for NC/PD and/or JM was expressed as a percentage of this.

Immunofluorescence microscopy

Strains were cultured and treated (±UV) exactly as described in *Extraction and detection of cellular proteins*, and nuclear spreads were prepared as described (***Loidl and Lorenz, 2009***; ***Argunhan et al., 2017b***) with minor modifications. 10 mL of cell culture (~1×10^8 cells) was harvested by centrifugation (2300 g 2 min), washed with 1 mL of 1 M sorbitol, and then resuspended in 1 mL of lysing solution (1 M sorbitol, 1 mM DTT, 0.2 mg/mL zymolyase, 12 mg/mL lysing enzyme [Sigma-Aldrich L1412]) and incubated at 30˚C for 30 min with gentle mixing. Spheroplasts were washed with 1 mL of 1 M sorbitol-1xMES (100 mM 2-[*N*-morpholino] ethanesulfonic acid, 1 mM EDTA, 0.5 mM $MgCl_2$), then resuspended with 100 µL of 1x MES premixed with 350 µL of 3.3% of paraformaldehyde and immediately spread onto glass slides. Once the slides had half-dried (~10 min), they were washed with Photo-Flo 200 Solution (1 mL x2; 146 4510 Kodak) and left to fully air-dry in the dark (~1 hr) before storing at −20˚C. For immunostaining, the slides were first washed in a Coplin jar with PBS and blocked using PBS-5% BSA solution for 30 min at room temperature in a moisture chamber. 100 µL of PBS-5% BSA supplemented with affinity purified anti-Rad51 antibody (1:300, provided by Hiroshi Iwasaki) was spread onto the slides with a cover slip and incubated at 4˚C overnight in a moisture chamber. Slides were washed with PBS (5 min x3) and subsequent steps were carried out with minimal exposure to ambient light. 100 µL of PBS-5% BSA supplemented with anti-rabbit Alexa fluor 488 antibody (1:300; A11034 Thermo Fisher Scientific) was spread onto the slide with a cover slip, followed by a 3 hr incubation in a moisture chamber at room temperature. Slides were then washed with PBS (5 min x3) and left to air-dry (~30 min). Mounting media (90% glycerol, 0.1xPBS, 1 mg/mL p-Phenylenediamine [Sigma P6001], 1 µg/mL 4',6-diamidino-2-phenylindole [DAPI; Sigma D9542]) was added in a dropwise fashion onto each slide, spread with a coverslip, and then sealed. Images of nuclei were captured using a wide field fluorescent microscope (Nikon Eclipse 80i) with a 100x objective fitted with an sCMOS camera (C13440 Hamamatsu).

The number of foci for each spread nucleus was quantified using FIJI (***Schindelin et al., 2012***) according to the following procedure. Following the application of a Gaussian blur (sigma = 2) to

the Rad51 (green) channel, the DAPI (blue) and Rad51 channels were subjected to Auto Thresholding (MaxEntropy) and Auto Local Thresholding (Bernsen, radius = 13), respectively. The Rad51 channel was then subjected to the Watershed and Ultimate Points processes, followed by the Find Maxima function. The DAPI channel was subjected to the Analyze Particles process ($\geq$200 pixels^2) to add the areas of nuclei to the Region-Of-Interest (ROI) Manager. These ROIs were then overlayed onto the Rad51 channel and the measure function of the ROI Manager was employed. The resulting RawIntDen value for each nucleus was then divided by 255 to yield the number of foci. A graph portraying the results was prepared using GraphPad Prism (version 8), which was also used for statistical analysis (Wilcoxon ranked sum test).

In vitro IP

Purified proteins (250 nM each) were mixed together on ice in IP buffer (30 mM Tris-Cl [pH 7.5], 150 mM NaCl, 3.5 mM $MgCl_2$, 0.1% igepal CA-630, 0.25 mM TCEP, 1 mM ATP, 5% glycerol; input sample) and incubated at 30˚C for 15 min. Reactions were then incubated on ice for 5 min and supplemented with either anti-FLAG M2 affinity agarose gel (Sigma-Aldrich) for IP of Rad54 or Dynabeads Protein A (ThermoFisher Scientific) preincubated with anti-Sfr1, anti-Rad51, or anti-Rad52 antibodies (***Haruta et al., 2006***; ***Kurokawa et al., 2008***). Following mixing at 4˚C for 1.5 hr, the beads were washed with IP buffer (400 µL x1) and eluted in 1x SDS loading buffer (IP sample). Proteins were then separated by SDS-PAGE and detected by immunoblotting with anti-Rad51 (rat 1:10,000; ***Argunhan et al., 2020***), anti-Sfr1 (mouse 1:200; ***Argunhan et al., 2020***), anti-FLAG (mouse 1:10,000; Sigma-Aldrich F3165), or anti-Rad52 (rabbit 1:10,000; ***Kurokawa et al., 2008***) antibodies. FIJI software (***Schindelin et al., 2012***) was used for quantification of in vitro IPs. Briefly, background subtraction was performed by the rolling ball method and the signal for IP'd and co-IP'd protein was quantified. The co-IP'd signal was then divided by the IP'd signal and expressed relative to wild type. Graphs were prepared using GraphPad Prism (version 8).

Acknowledgements

We thank Yumiko Kurokawa and Yasuto Murayama for help with protein purification, biochemical reconstitutions, and critical reading of the manuscript. We also extend our gratitude to Hiroshi Kimura for support, as well as all members of our laboratory for discussions. This work was supported in part by Grants-in-Aid for Scientific Research on Innovative Areas (15H059749 to HI), for Scientific Research (A) (18H03985 to HI), for Scientific Research (B) (18H02371 to HT), for Young Scientists (B) (17K15061 to BA), for Early-Career Scientists (20K15713 to BA), and a Doctoral Course Fellowship DC2 (17J04051 to NA) from the Japan Society for the Promotion of Science (JSPS).

Additional information

Funding

Funder	Grant reference number	Author
Japan Society for the Promotion of Science	15H059749	Hiroshi Iwasaki
Japan Society for the Promotion of Science	18H03985	Hiroshi Iwasaki
Japan Society for the Promotion of Science	18H02371	Hideo Tsubouchi
Japan Society for the Promotion of Science	17K15061	Bilge Argunhan
Japan Society for the Promotion of Science	20K15713	Bilge Argunhan
Japan Society for the Promotion of Science	17J04051	Negar Afshar

The funders had no role in study design, data collection and interpretation, or the decision to submit the work for publication.

Author contributions

Negar Afshar, Conceptualization, Data curation, Formal analysis, Funding acquisition, Validation, Investigation, Visualization, Methodology, Writing - original draft, Project administration, Writing - review and editing; Bilge Argunhan, Conceptualization, Resources, Data curation, Software, Formal analysis, Supervision, Funding acquisition, Validation, Investigation, Visualization, Methodology, Writing - original draft, Project administration, Writing - review and editing; Maierdan Palihati, Goki Taniguchi, Validation, Investigation; Hideo Tsubouchi, Formal analysis, Supervision, Funding acquisition, Visualization, Writing - original draft, Project administration, Writing - review and editing; Hiroshi Iwasaki, Conceptualization, Resources, Formal analysis, Supervision, Funding acquisition, Visualization, Writing - original draft, Project administration, Writing - review and editing

Author ORCIDs

Negar Afshar http://orcid.org/0000-0002-3448-6710
Bilge Argunhan https://orcid.org/0000-0002-6023-7654
Hideo Tsubouchi http://orcid.org/0000-0003-0814-8432
Hiroshi Iwasaki https://orcid.org/0000-0002-0153-6873

Decision letter and Author response

Decision letter https://doi.org/10.7554/eLife.64131.sa1
Author response https://doi.org/10.7554/eLife.64131.sa2

Additional files

Supplementary files

- Transparent reporting form

Data availability

All data generated or analysed during this study are included in the manuscript and supporting files. Source data files have been provided for Figures 2-7, Figure 5-figure supplement 1, and Figure 6-figure supplement 1D.

References

Ait Saada A, Lambert SAE, Carr AM. 2018. Preserving replication fork integrity and competence via the homologous recombination pathway. *DNA Repair* **71**:135–147. DOI: https://doi.org/10.1016/j.dnarep.2018.08.017, PMID: 30220600

Akamatsu Y, Dziadkowiec D, Ikeguchi M, Shinagawa H, Iwasaki H. 2003. Two different Swi5-containing protein complexes are involved in mating-type switching and recombination repair in fission yeast. *PNAS* **100**:15770–15775. DOI: https://doi.org/10.1073/pnas.2632890100, PMID: 14663140

Akamatsu Y, Tsutsui Y, Morishita T, Siddique MS, Kurokawa Y, Ikeguchi M, Yamao F, Arcangioli B, Iwasaki H. 2007. Fission yeast Swi5/Sfr1 and Rhp55/Rhp57 differentially regulate Rhp51-dependent recombination outcomes. *The EMBO Journal* **26**:1352–1362. DOI: https://doi.org/10.1038/sj.emboj.7601582, PMID: 17304215

Amelina H, Moiseeva V, Collopy LC, Pearson SR, Armstrong CA, Tomita K. 2016. Sequential and counter-selectable cassettes for fission yeast. *BMC Biotechnology* **16**:76. DOI: https://doi.org/10.1186/s12896-016-0307-4, PMID: 27825338

Argunhan B, Murayama Y, Iwasaki H. 2017a. The differentiated and conserved roles of Swi5-Sfr1 in homologous recombination. *FEBS Letters* **591**:2035–2047. DOI: https://doi.org/10.1002/1873-3468.12656, PMID: 28423184

Argunhan B, Leung WK, Afshar N, Terentyev Y, Subramanian VV, Murayama Y, Hochwagen A, Iwasaki H, Tsubouchi T, Tsubouchi H. 2017b. Fundamental cell cycle kinases collaborate to ensure timely destruction of the synaptonemal complex during meiosis. *The EMBO Journal* **36**:2488–2509. DOI: https://doi.org/10.15252/embj.201695895, PMID: 28694245

Argunhan B, Sakakura M, Afshar N, Kurihara M, Ito K, Maki T, Kanamaru S, Murayama Y, Tsubouchi H, Takahashi M, Takahashi H, Iwasaki H. 2020. Cooperative interactions facilitate stimulation of Rad51 by the Swi5-Sfr1 auxiliary factor complex. *eLife* **9**:e52566. DOI: https://doi.org/10.7554/eLife.52566, PMID: 32204793

Chen LT, Ko TP, Chang YC, Lin KA, Chang CS, Wang AH, Wang TF. 2007. Crystal structure of the left-handed archaeal RadA helical filament: identification of a functional motif for controlling quaternary structures and

enzymatic functions of RecA family proteins. *Nucleic Acids Research* **35**:1787–1801. DOI: https://doi.org/10.1093/nar/gkl1131, PMID: 17329376

Chen Z, Yang H, Pavletich NP. 2008. Mechanism of homologous recombination from the RecA-ssDNA/dsDNA structures. *Nature* **453**:489–494. DOI: https://doi.org/10.1038/nature06971, PMID: 18497818

Chen J, Villanueva N, Rould MA, Morrical SW. 2010. Insights into the mechanism of Rad51 recombinase from the structure and properties of a filament interface mutant. *Nucleic Acids Research* **38**:4889–4906. DOI: https://doi.org/10.1093/nar/gkq209, PMID: 20371520

Chi P, Kwon Y, Moses DN, Seong C, Sehorn MG, Singh AK, Tsubouchi H, Greene EC, Klein HL, Sung P. 2009. Functional interactions of meiotic recombination factors Rdh54 and Dmc1. *DNA Repair* **8**:279–284. DOI: https://doi.org/10.1016/j.dnarep.2008.10.012, PMID: 19028606

Conway AB, Lynch TW, Zhang Y, Fortin GS, Fung CW, Symington LS, Rice PA. 2004. Crystal structure of a Rad51 filament. *Nature Structural & Molecular Biology* **11**:791–796. DOI: https://doi.org/10.1038/nsmb795, PMID: 15235592

Costa SJ, Almeida A, Castro A, Domingues L, Besir H. 2013. The novel Fh8 and H fusion partners for soluble protein expression in *Escherichia coli*: a comparison with the traditional gene fusion technology. *Applied Microbiology and Biotechnology* **97**:6779–6791. DOI: https://doi.org/10.1007/s00253-012-4559-1, PMID: 23160981

Doe CL, Osman F, Dixon J, Whitby MC. 2004. DNA repair by a Rad22-Mus81-dependent pathway that is independent of Rhp51. *Nucleic Acids Research* **32**:5570–5581. DOI: https://doi.org/10.1093/nar/gkh853, PMID: 15486206

Gasior SL, Wong AK, Kora Y, Shinohara A, Bishop DK. 1998. Rad52 associates with RPA and functions with rad55 and rad57 to assemble meiotic recombination complexes. *Genes & Development* **12**:2208–2221. DOI: https://doi.org/10.1101/gad.12.14.2208, PMID: 9679065

Gasior SL, Olivares H, Ear U, Hari DM, Weichselbaum R, Bishop DK. 2001. Assembly of RecA-like recombinases: distinct roles for mediator proteins in mitosis and meiosis. *PNAS* **98**:8411–8418. DOI: https://doi.org/10.1073/pnas.121046198, PMID: 11459983

Greene EC. 2016. DNA sequence alignment during homologous recombination. *Journal of Biological Chemistry* **291**:11572–11580. DOI: https://doi.org/10.1074/jbc.R116.724807

Haruta N, Kurokawa Y, Murayama Y, Akamatsu Y, Unzai S, Tsutsui Y, Iwasaki H. 2006. The Swi5-Sfr1 complex stimulates Rhp51/Rad51- and Dmc1-mediated DNA strand exchange in vitro. *Nature Structural & Molecular Biology* **13**:823–830. DOI: https://doi.org/10.1038/nsmb1136, PMID: 16921379

Hays SL, Firmenich AA, Berg P. 1995. Complex formation in yeast double-strand break repair: participation of Rad51, Rad52, Rad55, and Rad57 proteins. *PNAS* **92**:6925–6929. DOI: https://doi.org/10.1073/pnas.92.15.6925, PMID: 7624345

Hentges P, Van Driessche B, Tafforeau L, Vandenhaute J, Carr AM. 2005. Three novel antibiotic marker cassettes for gene disruption and marker switching in *Schizosaccharomyces pombe*. *Yeast* **22**:1013–1019. DOI: https://doi.org/10.1002/yea.1291, PMID: 16200533

Hoffman CS, Wood V, Fantes PA. 2015. An ancient yeast for young geneticists: a primer on the *Schizosaccharomyces pombe* Model System. *Genetics* **201**:403–423. DOI: https://doi.org/10.1534/genetics.115.181503, PMID: 26447128

Hope JC, Maftahi M, Freyer GA. 2005. A postsynaptic role for Rhp55/57 that is responsible for cell death in Deltarqh1 mutants following replication arrest in *Schizosaccharomyces pombe*. *Genetics* **170**:519–531. DOI: https://doi.org/10.1534/genetics.104.037598, PMID: 15802523

Howard-Flanders P, West SC, Stasiak A. 1984. Role of RecA protein spiral filaments in genetic recombination. *Nature* **309**:215–220. DOI: https://doi.org/10.1038/309215a0, PMID: 6325943

Ito K, Murayama Y, Takahashi M, Iwasaki H. 2018. Two three-strand intermediates are processed during Rad51-driven DNA strand exchange. *Nature Structural & Molecular Biology* **25**:29–36. DOI: https://doi.org/10.1038/s41594-017-0002-8, PMID: 29323270

Ito K, Murayama Y, Kurokawa Y, Kanamaru S, Kokabu Y, Maki T, Mikawa T, Argunhan B, Tsubouchi H, Ikeguchi M, Takahashi M, Iwasaki H. 2020. Real-time tracking reveals catalytic roles for the two DNA binding sites of Rad51. *Nature Communications* **11**:1–17. DOI: https://doi.org/10.1038/s41467-020-16750-3

Johnson RD, Symington LS. 1995. Functional differences and interactions among the putative RecA homologs Rad51, Rad55, and Rad57. *Molecular and Cellular Biology* **15**:4843–4850. DOI: https://doi.org/10.1128/MCB.15.9.4843, PMID: 7651402

Kagawa W, Arai N, Ichikawa Y, Saito K, Sugiyama S, Saotome M, Shibata T, Kurumizaka H. 2014. Functional analyses of the C-terminal half of the *Saccharomyces cerevisiae* Rad52 protein. *Nucleic Acids Research* **42**:941–951. DOI: https://doi.org/10.1093/nar/gkt986, PMID: 24163251

Kelley LA, Mezulis S, Yates CM, Wass MN, Sternberg MJ. 2015. The Phyre2 web portal for protein modeling, prediction and analysis. *Nature Protocols* **10**:845–858. DOI: https://doi.org/10.1038/nprot.2015.053, PMID: 25950237

Khasanov FK, Savchenko GV, Bashkirova EV, Korolev VG, Heyer WD, Bashkirov VI. 1999. A new recombinational DNA repair gene from *Schizosaccharomyces pombe* with homology to *Escherichia coli* RecA. *Genetics* **152**:1557–1572. PMID: 10430583

Khasanov FK, Salakhova AF, Chepurnaja OV, Korolev VG, Bashkirov VI. 2004. Identification and characterization of the rlp1+, the novel Rad51 paralog in the fission yeast *Schizosaccharomyces pombe*. *DNA Repair* **3**:1363–1374. DOI: https://doi.org/10.1016/j.dnarep.2004.05.010, PMID: 15336631

Kim WJ, Park EJ, Lee H, Seong RH, Park SD. 2002. Physical Interaction between Recombinational Proteins Rhp51 and Rad22 in *Schizosaccharomyces pombe* . *Journal of Biological Chemistry* **277**:30264–30270. DOI: https://doi.org/10.1074/jbc.M202517200

Kurokawa Y, Murayama Y, Haruta-Takahashi N, Urabe I, Iwasaki H. 2008. Reconstitution of DNA strand exchange mediated by Rhp51 recombinase and two mediators. *PLOS Biology* **6**:e88. DOI: https://doi.org/10.1371/journal.pbio.0060088, PMID: 18416603

Lambert S, Carr AM. 2013. Replication stress and genome rearrangements: lessons from yeast models. *Current Opinion in Genetics & Development* **23**:132–139. DOI: https://doi.org/10.1016/j.gde.2012.11.009, PMID: 23267817

Lisby M, Barlow JH, Burgess RC, Rothstein R. 2004. Choreography of the DNA damage response: spatiotemporal relationships among checkpoint and repair proteins. *Cell* **118**:699–713. DOI: https://doi.org/10.1016/j.cell.2004.08.015, PMID: 15369670

Liu J, Renault L, Veaute X, Fabre F, Stahlberg H, Heyer WD. 2011. Rad51 paralogues Rad55-Rad57 balance the antirecombinase Srs2 in Rad51 filament formation. *Nature* **479**:245–248. DOI: https://doi.org/10.1038/nature10522, PMID: 22020281

Loidl J, Lorenz A. 2009. Analysis of *Schizosaccharomyces pombe* meiosis by nuclear spreading. *Methods in Molecular Biology* **558**:15–36. DOI: https://doi.org/10.1007/978-1-60761-103-5_2, PMID: 19685316

Lorenz A, Osman F, Folkyte V, Sofueva S, Whitby MC. 2009. Fbh1 limits Rad51-dependent recombination at blocked replication forks. *Molecular and Cellular Biology* **29**:4742–4756. DOI: https://doi.org/10.1128/MCB.00471-09, PMID: 19546232

Lu CH, Yeh HY, Su GC, Ito K, Kurokawa Y, Iwasaki H, Chi P, Li HW. 2018. Swi5-Sfr1 stimulates Rad51 recombinase filament assembly by modulating Rad51 dissociation. *PNAS* **115**:E10059–E10068. DOI: https://doi.org/10.1073/pnas.1812753115, PMID: 30297419

Martín V, Chahwan C, Gao H, Blais V, Wohlschlegel J, Yates JR, McGowan CH, Russell P. 2006. Sws1 is a conserved regulator of homologous recombination in eukaryotic cells. *The EMBO Journal* **25**:2564–2574. DOI: https://doi.org/10.1038/sj.emboj.7601141, PMID: 16710300

McCready SJ, Osman F, Yasui A. 2000. Repair of UV damage in the fission yeast *Schizosaccharomyces pombe*. *Mutation Research/Fundamental and Molecular Mechanisms of Mutagenesis* **451**:197–210. DOI: https://doi.org/10.1016/S0027-5107(00)00050-6

McVey M, Khodaverdian VY, Meyer D, Cerqueira PG, Heyer WD. 2016. Eukaryotic DNA polymerases in homologous recombination. *Annual Review of Genetics* **50**:393–421. DOI: https://doi.org/10.1146/annurev-genet-120215-035243, PMID: 27893960

Mehta A, Haber JE. 2014. Sources of DNA double-strand breaks and models of recombinational DNA repair. *Cold Spring Harbor Perspectives in Biology* **6**:a016428. DOI: https://doi.org/10.1101/cshperspect.a016428, PMID: 25104768

Murayama Y, Kurokawa Y, Tsutsui Y, Iwasaki H. 2013. Dual regulation of Dmc1-driven DNA strand exchange by Swi5-Sfr1 activation and Rad22 inhibition. *Genes & Development* **27**:2299–2304. DOI: https://doi.org/10.1101/gad.218693.113, PMID: 24186976

Muris DF, Vreeken K, Carr AM, Broughton BC, Lehmann AR, Lohman PH, Pastink A. 1993. Cloning the RAD51 homologue of *Schizosaccharomyces pombe*. *Nucleic Acids Research* **21**:4586–4591. DOI: https://doi.org/10.1093/nar/21.19.4586, PMID: 8233794

Muris DF, Vreeken K, Carr AM, Murray JM, Smit C, Lohman PH, Pastink A. 1996. Isolation of the *Schizosaccharomyces pombe* RAD54 homologue, rhp54+, a gene involved in the repair of radiation damage and replication fidelity. *Journal of Cell Science* **109**:73–81. PMID: 8834792

Muris DF, Vreeken K, Schmidt H, Ostermann K, Clever B, Lohman PH, Pastink A. 1997. Homologous recombination in the fission yeast *Schizosaccharomyces pombe*: different requirements for the rhp51+, rhp54+ and rad22+ genes. *Current Genetics* **31**:248–254. DOI: https://doi.org/10.1007/s002940050202, PMID: 9065388

Murray JM, Lindsay HD, Munday CA, Carr AM. 1997. Role of *Schizosaccharomyces pombe* RecQ homolog, recombination, and checkpoint genes in UV damage tolerance. *Molecular and Cellular Biology* **17**:6868–6875. DOI: https://doi.org/10.1128/MCB.17.12.6868, PMID: 9372918

Ostermann K, Lorentz A, Schmidt H. 1993. The fission yeast rad22 gene, having a function in mating-type switching and repair of DNA damages, encodes a protein homolog to Rad52 of Saccharomyces cerevisiae. *Nucleic Acids Research* **21**:5940–5944. DOI: https://doi.org/10.1093/nar/21.25.5940, PMID: 8290356

Pellegrini L, Yu DS, Lo T, Anand S, Lee M, Blundell TL, Venkitaraman AR. 2002. Insights into DNA recombination from the structure of a RAD51-BRCA2 complex. *Nature* **420**:287–293. DOI: https://doi.org/10.1038/nature01230, PMID: 12442171

Pettersen EF, Goddard TD, Huang CC, Couch GS, Greenblatt DM, Meng EC, Ferrin TE. 2004. UCSF chimera–a visualization system for exploratory research and analysis. *Journal of Computational Chemistry* **25**:1605–1612. DOI: https://doi.org/10.1002/jcc.20084, PMID: 15264254

Prakash R, Zhang Y, Feng W, Jasin M. 2015. Homologous recombination and human health: the roles of BRCA1, BRCA2, and associated proteins. *Cold Spring Harbor Perspectives in Biology* **7**:a016600. DOI: https://doi.org/10.1101/cshperspect.a016600, PMID: 25833843

San Filippo J, Sung P, Klein H. 2008. Mechanism of eukaryotic homologous recombination. *Annual Review of Biochemistry* **77**:229–257. DOI: https://doi.org/10.1146/annurev.biochem.77.061306.125255

Saraste M, Sibbald PR, Wittinghofer A. 1990. The P-loop–a common motif in ATP- and GTP-binding proteins. *Trends in Biochemical Sciences* **15**:430–434. DOI: https://doi.org/10.1016/0968-0004(90)90281-F, PMID: 2126155

Schindelin J, Arganda-Carreras I, Frise E, Kaynig V, Longair M, Pietzsch T, Preibisch S, Rueden C, Saalfeld S, Schmid B, Tinevez JY, White DJ, Hartenstein V, Eliceiri K, Tomancak P, Cardona A. 2012. Fiji: an open-source platform for biological-image analysis. *Nature Methods* **9**:676–682. DOI: https://doi.org/10.1038/nmeth.2019, PMID: 22743772

Shin DS, Pellegrini L, Daniels DS, Yelent B, Craig L, Bates D, Yu DS, Shivji MK, Hitomi C, Arvai AS, Volkmann N, Tsuruta H, Blundell TL, Venkitaraman AR, Tainer JA. 2003. Full-length archaeal Rad51 structure and mutants: mechanisms for RAD51 assembly and control by BRCA2. *The EMBO Journal* **22**:4566–4576. DOI: https://doi.org/10.1093/emboj/cdg429, PMID: 12941707

Shinohara A, Ogawa H, Ogawa T. 1992. Rad51 protein involved in repair and recombination in *S. cerevisiae* is a RecA-like protein. *Cell* **69**:457–470. DOI: https://doi.org/10.1016/0092-8674(92)90447-K, PMID: 1581961

Short JM, Liu Y, Chen S, Soni N, Madhusudhan MS, Shivji MKK, Venkitaraman AR. 2016. High-resolution structure of the presynaptic RAD51 filament on single-stranded DNA by electron cryo-microscopy. *Nucleic Acids Research* **11**:gkw783. DOI: https://doi.org/10.1093/nar/gkw783

Stewart E, Chapman CR, Al-Khodairy F, Carr AM, Enoch T. 1997. rqh1+, a fission yeast gene related to the bloom's and Werner's syndrome genes, is required for reversible S phase arrest. *The EMBO Journal* **16**:2682–2692. DOI: https://doi.org/10.1093/emboj/16.10.2682, PMID: 9184215

Story RM, Weber IT, Steitz TA. 1992. The structure of the *E. coli* recA protein monomer and polymer. *Nature* **355**:318–325. DOI: https://doi.org/10.1038/355318a0, PMID: 1731246

Story RM, Steitz TA. 1992. Structure of the recA protein-ADP complex. *Nature* **355**:374–376. DOI: https://doi.org/10.1038/355374a0, PMID: 1731253

Su GC, Chung CI, Liao CY, Lin SW, Tsai CT, Huang T, Li HW, Chi P. 2014. Enhancement of ADP release from the RAD51 presynaptic filament by the SWI5-SFR1 complex. *Nucleic Acids Research* **42**:349–358. DOI: https://doi.org/10.1093/nar/gkt879, PMID: 24078249

Su GC, Yeh HY, Lin SW, Chung CI, Huang YS, Liu YC, Lyu PC, Chi P. 2016. Role of the RAD51-SWI5-SFR1 ensemble in homologous recombination. *Nucleic Acids Research* **44**:6242–6251. DOI: https://doi.org/10.1093/nar/gkw375, PMID: 27131790

Sugawara N, Wang X, Haber JE. 2003. In vivo roles of Rad52, Rad54, and Rad55 proteins in Rad51-mediated recombination. *Molecular Cell* **12**:209–219. DOI: https://doi.org/10.1016/S1097-2765(03)00269-7, PMID: 12887906

Sun Y, McCorvie TJ, Yates LA, Zhang X. 2020. Structural basis of homologous recombination. *Cellular and Molecular Life Sciences* **77**:3–18. DOI: https://doi.org/10.1007/s00018-019-03365-1, PMID: 31748913

Sung P. 1994. Catalysis of ATP-dependent homologous DNA pairing and strand exchange by yeast RAD51 protein. *Science* **265**:1241–1243. DOI: https://doi.org/10.1126/science.8066464, PMID: 8066464

Sung P. 1997. Yeast Rad55 and Rad57 proteins form a heterodimer that functions with replication protein A to promote DNA strand exchange by Rad51 recombinase. *Genes & Development* **11**:1111–1121. DOI: https://doi.org/10.1101/gad.11.9.1111, PMID: 9159392

Symington LS, Gautier J. 2011. Double-strand break end resection and repair pathway choice. *Annual Review of Genetics* **45**:247–271. DOI: https://doi.org/10.1146/annurev-genet-110410-132435, PMID: 21910633

Tsai SP, Su GC, Lin SW, Chung CI, Xue X, Dunlop MH, Akamatsu Y, Jasin M, Sung P, Chi P. 2012. Rad51 presynaptic filament stabilization function of the mouse Swi5-Sfr1 heterodimeric complex. *Nucleic Acids Research* **40**:6558–6569. DOI: https://doi.org/10.1093/nar/gks305, PMID: 22492707

Tsubouchi H, Argunhan B, Ito K, Takahashi M, Iwasaki H. 2020. Two auxiliary factors promote Dmc1-driven DNA strand exchange via stepwise mechanisms. *PNAS* **117**:12062–12070. DOI: https://doi.org/10.1073/pnas.1917419117, PMID: 32414915

Tsutsui Y, Morishita T, Iwasaki H, Toh H, Shinagawa H. 2000. A recombination repair gene of *Schizosaccharomyces pombe*, rhp57, is a functional homolog of the *Saccharomyces cerevisiae* RAD57 gene and is phylogenetically related to the human XRCC3 gene. *Genetics* **154**:1451–1461. PMID: 10747044

Tsutsui Y, Khasanov FK, Shinagawa H, Iwasaki H, Bashkirov VI. 2001. Multiple interactions among the components of the recombinational DNA repair system in *Schizosaccharomyces pombe*. *Genetics* **159**:91–105. PMID: 11560889

Wu Y, He Y, Moya IA, Qian X, Luo Y. 2004. Crystal structure of archaeal recombinase RADA: a snapshot of its extended conformation. *Molecular Cell* **15**:423–435. DOI: https://doi.org/10.1016/j.molcel.2004.07.014, PMID: 15304222

Xu J, Zhao L, Xu Y, Zhao W, Sung P, Wang HW. 2017. Cryo-EM structures of human RAD51 recombinase filaments during catalysis of DNA-strand exchange. *Nature Structural & Molecular Biology* **24**:40–46. DOI: https://doi.org/10.1038/nsmb.3336, PMID: 27941862

Zelensky A, Kanaar R, Wyman C. 2014. Mediators of homologous DNA pairing. *Cold Spring Harbor Perspectives in Biology* **6**:a016451. DOI: https://doi.org/10.1101/cshperspect.a016451, PMID: 25301930

Appendix 1

Appendix 1—key resources table

Reagent type (species) or resource	Designation	Source or reference	Identifiers	Additional information
Schizosaccharomyces pombe; Msmt-0	*Wild type*	***Akamatsu et al., 2003***	NA310	*leu-1–32 ura4-D18 his3-D1 arg3-D1*
S. pombe; Msmt-0	*rad51-E206A-kanMX6*	This study	NA211	*leu-1–32 ura4-D18 his3-D1 arg3-D1*
S. pombe; Msmt-0	*rad51::hphMX6*	This study	BA263	*leu-1–32 ura4-D18 his3-D1 arg3-D1*
S. pombe; Msmt-0	*rad51-E206A-kanMX6 rad57::hphMX6*	This study	NA253	*leu-1–32 ura4-D18 his3-D1 arg3-D1*
S. pombe; Msmt-0	*rad57::hphMX6*	This study	BA268	*leu-1–32 ura4-D18 his3-D1 arg3-D1*
S. pombe; Msmt-0	*rad57::hphMX6 rad51::natMX6*	This study	NA383	*leu-1–32 ura4-D18 his3-D1 arg3-D1*
S. pombe; Msmt-0	*sfr1::kanMX6*	This study	NA138	*leu-1–32 ura4-D18 his3-D1 arg3-D1*
S. pombe; Msmt-0	*sfr1::kanMX6 rad51::hphMX6*	This study	NA233	*leu-1–32 ura4-D18 his3-D1 arg3-D1*
S. pombe; Msmt-0	*rad51-E206A-kanMX6 sfr1::kanMX6*	This study	NA236	*leu-1–32 ura4-D18 his3-D1 arg3-D1*
S. pombe; mat1PD17::LEU2	*Wild type*	This study	BA396	*leu-1–32 ura4-D18 his3-D1 arg3-D1*
S. pombe; mat1PD17::LEU2	*rqh1::natMX6*	This study	NA324	*leu-1–32 ura4-D18 his3-D1 arg3-D1*
S. pombe; mat1PD17::LEU2	*rqh1::natMX6 rad51::hphMX6*	This study	NA394	*leu-1–32 ura4-D18 his3-D1 arg3-D1*
S. pombe; mat1PD17::LEU2	*rqh1::natMX6 rad52::arg3*	This study	BA546	*leu-1–32 ura4-D18 his3-D1 arg3-D1*
S. pombe; mat1PD17::LEU2	*rqh1::natMX6 rad54::ura4*	This study	BA548	*leu-1–32 ura4-D18 his3-D1 arg3-D1*
S. pombe; mat1PD17::LEU2	*rqh1::natMX6 rad51-E206A-kanMX6*	This study	NA387	*leu-1–32 ura4-D18 his3-D1 arg3-D1*
S. pombe; mat1PD17::LEU2	*rqh1::natMX6 rad57::hphMX6*	This study	NA396	*leu-1–32 ura4-D18 his3-D1 arg3-D1*
S. pombe; mat1PD17::LEU2	*rqh1::natMX6 rad57::hphMX6 rad51-E206A-kanMX6*	This study	NA389	*leu-1–32 ura4-D18 his3-D1 arg3-D1*
S. pombe; mat1PD17::LEU2	*rqh1::natMX6 sfr1::kanMX6*	This study	NA386	*leu-1–32 ura4-D18 his3-D1 arg3-D1*
S. pombe; mat1PD17::LEU2	*rqh1::natMX6 sfr1::kanMX6 rad51-E206A-kanMX6*	This study	NA398	*leu-1–32 ura4-D18 his3-D1 arg3-D1*
S. pombe; mat1PD17::LEU2	*rqh1::natMX6 rad57::hphMX6 sfr1::kanMX6*	This study	NA391	*leu-1–32 ura4-D18 his3-D1 arg3-D1*
S. pombe; Msmt-0	*rad52::arg3*	Hiroshi Iwasaki (lab stock)	BA481	*leu-1–32 ura4-D18 his3-D1 arg3-D1*
S. pombe; Msmt-0	*rad54::ura4*	Hiroshi Iwasaki (lab stock)	BA518	*leu-1–32 ura4-D18 his3-D1 arg3-D1*

Continued on next page

Appendix 1—key resources table continued

Reagent type (species) or resource	Designation	Source or reference	Identifiers	Additional information
S. pombe; Msmt-0	*rad51-E205A-E206A -D209A-kanMX6*	This study	BA499	*leu-1–32 ura4-D18 his3-D1 arg3-D1*
S. pombe; Msmt-0	*rad51^{+}-kanMX6*	This study	NA209	*leu-1–32 ura4-D18 his3-D1 arg3-D1*
S. pombe; Msmt-0	*rad51-E205A-kanMX6*	This study	BA445	*leu-1–32 ura4-D18 his3-D1 arg3-D1*
S. pombe; Msmt-0	*rad51-D209A-kanMX6*	This study	BA493	*leu-1–32 ura4-D18 his3-D1 arg3-D1*
S. pombe; Msmt-0	*rad51-E205A-E206A-kanMX6*	This study	BA449	*leu-1–32 ura4-D18 his3-D1 arg3-D1*
S. pombe; Msmt-0	*rad55-12xV5-natMX6*	This study	BA172	*leu-1–32 ura4-D18 his3-D1 arg3-D1*
S. pombe; Msmt-0	*rad55-12xV5-natMX6 rad51-E206A-kanMX6*	This study	NA238	*leu-1–32 ura4-D18 his3-D1 arg3-D1*
S. pombe; Msmt-0	*rad55-12xV5-natMX6 sfr1::kanMX6*	This study	BA170	*leu-1–32 ura4-D18 his3-D1 arg3-D1*
S. pombe; Msmt-0	*rad55-12xV5-natMX6 rad51-E206A-kanMX6 sfr1::kanMX6*	This study	NA243	*leu-1–32 ura4-D18 his3-D1 arg3-D1*
S. pombe; Msmt-0	*rad55-12xV5-natMX6 rad51-E205A-E206A-kanMX6*	This study	BA529	*leu-1–32 ura4-D18 his3-D1 arg3-D1*
S. pombe; Msmt-0	*rad55-12xV5-natMX6 rad51 D209A-kanMX6*	This study	BA521	*leu-1–32 ura4-D18 his3-D1 arg3-D1*
S. pombe; Msmt-0	*rad55-12xV5-natMX6 rad51-E205A-E206A-D209A-kanMX6*	This study	BA523	*leu-1–32 ura4-D18 his3-D1 arg3-D1*
S. pombe; Msmt-0	*rad57::hphMX6 rad51^{+}-kanMX6*	This study	NA249	*leu-1–32 ura4-D18 his3-D1 arg3-D1*
S. pombe; Msmt-0	*rad57::hphMX6 rad51-E205A-kanMX6*	This study	BA443	*leu-1–32 ura4-D18 his3-D1 arg3-D1*
S. pombe; Msmt-0	*rad57::hphMX6 rad51-D209A-kanMX6*	This study	BA491	*leu-1–32 ura4-D18 his3-D1 arg3-D1*
S. pombe; Msmt-0	*rad57::hphMX6 rad51-E205A-E206A-D209A-kanMX6*	This study	BA501	*leu-1–32 ura4-D18 his3-D1 arg3-D1*
S. pombe; Msmt-0	*rad57::hphMX6 rad51-E205A-E206A-kanMX6*	This study	BA447	*leu-1–32 ura4-D18 his3-D1 arg3-D1*
S. pombe; Msmt-0	*sfr1::kanMX6 rad51^{+}-kanMX6*	This study	NA222	*leu-1–32 ura4-D18 his3-D1 arg3-D1*
S. pombe; Msmt-0	*sfr1::natMX6 rad51-E205A-kanMX6*	This study	BA461	*leu-1–32 ura4-D18 his3-D1 arg3-D1*
S. pombe; Msmt-0	*sfr1::natMX6 rad51-E206A-kanMX6*	This study	BA476	*leu-1–32 ura4-D18 his3-D1 arg3-D1*
S. pombe; Msmt-0	*sfr1::natMX6 rad51-D209A-kanMX6*	This study	BA485	*leu-1–32 ura4-D18 his3-D1 arg3-D1*
S. pombe; Msmt-0	*sfr1::nathMX6 rad51-E205A-E206A-kanMX6*	This study	BA463	*leu-1–32 ura4-D18 his3-D1 arg3-D1*

Continued on next page

Appendix 1—key resources table continued

Reagent type (species) or resource	Designation	Source or reference	Identifiers	Additional information
S. pombe; Msmt-0	*sfr1::natMX6 rad51-E205A-E206A-D209A-kanMX6*	This study	BA497	*leu-1–32 ura4-D18 his3-D1 arg3-D1*
S. pombe; Msmt-0	*rad55::natMX6*	**Argunhan et al., 2020**	BA150	*leu-1–32 ura4-D18 his3-D1 arg3-D1*
S. pombe; Msmt-0	*rad55-12xV5-natMX6*	This study	BA165	*leu-1–32 ura4-D18 his3-D1 arg3-D1*
S. pombe; Msmt-0	*rad55::arg3 sfr1::kanMX6*	**Argunhan et al., 2020**	BA126	*leu-1–32 ura4-D18 his3-D1 arg3-D1*
S. pombe; Msmt-0	*rad51-E206K-kanMX6*	This study	BA552	*leu-1–32 ura4-D18 his3-D1 arg3-D1*
Antibody	Rat polyclonal anti-Rad51	**Argunhan et al., 2020**		1:10,000
Antibody	Mouse monoclonal anti-tubulin	Sigma-Aldrich	T5168	1:10,000
Antibody	Mouse monoclonal anti-V5	Bio-Rad	MCA1360	1:10,000 4 µL / IP
Antibody	Rabbit polyclonal anti-Rad51	**Haruta et al., 2006**		10 µL / IP
Antibody	ChromPure Human IgG, whole molecule polyclonal	Jackson Immunoresearch Laboratories	009-000-003	0.336 µL / IP
Antibody	Rabbit monoclonal Alexa fluor 488	Thermo Fisher Scientific	A11034	1:300
Antibody	Mouse monoclonal anti-Sfr1	**Argunhan et al., 2020**		1:200
Antibody	Mouse monoclonal anti-FLAG-tag	Sigma-Aldrich	F3165	1:10,000
Antibody	Rabbit polyclonal anti-Rad52	**Kurokawa et al., 2008**		1:10,000
Antibody	Anti-mouse IgG (HRP-conjugated)	GE Healthcare	NA931	1:5000
Antibody	Anti-rabbit IgG (HRP-conjugated)	GE Healthcare	NA934	1:5000
Antibody	Anti-rat IgG (HRP-conjugated)	Jackson Immunoresearch Laboratories	712-035-153	1:10,000
Recombinant DNA reagent	PhiX174 virion DNA (ssDNA plasmid)	NEB	N3023L	
Recombinant DNA reagent	PhiX174 RF I DNA (dsDNA plasmid)	NEB	N3021L	
Peptide, recombinant protein	*S. pombe* Rad51	**Kurokawa et al., 2008**		
Peptide, recombinant protein	*S. pombe* Rad51-E206A	This study		
Peptide, recombinant protein	*S. pombe* Rad51 E205A-E206A-D209A	This study		
Peptide, recombinant protein	*S. pombe* RPA	**Haruta et al., 2006**		

Continued on next page

Appendix 1—key resources table continued

Reagent type (species) or resource	Designation	Source or reference	Identifiers	Additional information
Peptide, recombinant protein	*S. pombe* Swi5-Sfr1	***Haruta et al., 2006***		
Peptide, recombinant protein	*S. pombe* Rad52	***Kurokawa et al., 2008***		
Peptide, recombinant protein	*S. pombe* Rad54	This study		
Commercial assay or kit	Amicon Ultra-15, 10K MWCO	Merck	UFC901096	
Commercial assay or kit	Dynabeads Protein A	ThermoFisher	10002D	
Commercial assay or kit	ImmunoStar Zeta chemiluminescence solution	FujiFilm Wako	297–72403	
Commercial assay or kit	Malachite Green Phosphate Assay Kit	BioAssay Systems	POMG-25H	
Commercial assay or kit	TurboNuclease	Accelagen	N0103P	
Commercial assay or kit	Lysing enzyme	Sigma-Aldrich	L1412	
Commercial assay or kit	In-Fusion HD Cloning	TaKaRa	639650	
Chemical compound, drug	ATP	Sigma-Aldrich	A2383	
Chemical compound, drug	Phosphocreatine di(tris) salt	Sigma-Aldrich	P1937	
Chemical compound, drug	Bio-Safe Coomassie Stain	Bio-Rad	1610786	
Chemical compound, drug	Proteinase K	TaKaRa	9034	
Chemical compound, drug	Creatine Kinase	Sigma-Aldrich	10127566001	
Sequenced-based reagent	398_F	This study	PCR primers	CCTCTAGAAATAATTTTG TTTAACTTTA AGAAGGAGATATACATA
Sequenced-based reagent	400_R	This study	PCR primers	ATCCAAAACTGCCTCACCA TTTAAGCCATA
Sequenced-based reagent	399_F	This study	PCR primers	AATGGTGAGGCAGTTTTGGA TAACGTTGCA
Sequenced-based reagent	405_R	This study	PCR primers	CTTTGTTAGCAGCCGGATCC
Sequenced-based reagent	350_F	This study	PCR primers	GATTGGAAATCGTAAGGA TCCGCGAATTTC TTATGATTTATGATTTTTATT
Sequenced-based reagent	351_R	This study	PCR primers	ATAGTAAGGAGTCCTCAGTA TAGCGACCAGCATTC
Sequenced-based reagent	409_F	This study	PCR primers	CGGTATCGATAAGCTTGATA TCCATAA GACTGAGGCAGAGGT
Sequenced-based reagent	412_R	This study	PCR primers	CTCTGTATCTGCCATTATAAC TTGTTA AGCACGAAATTATCAC

Continued on next page

Appendix 1—key resources table continued

Reagent type (species) or resource	Designation	Source or reference	Identifiers	Additional information
Sequenced-based reagent	417_F	This study	PCR primers	CTGGTCGCTATACTGATTA TTTTAGTATCGT TTCATTTTTATTTATTA TTTTGCA
Sequenced-based reagent	419_R	This study	PCR primers	GCGGTGGCGGCCGCTC TAGAGCATGCTTGGAAGGC TTT
Sequenced-based reagent	200_F	This study	PCR primers	CTACTGGTATTCAGGATTA TCAAAGTATTCCTACC AATAGCTCACAACGACG TAAGAGATCCATTTTGGA ATGTGAGTCCCGGA TCCCCGGGTTAATTAA
Sequenced-based reagent	201_R	This study	PCR primers	TAGGTATAATAAATTAATAGA TATGGGCAAAACAAC CATCACTATGCTAAAAAA TTCGTAACTGAAGCCACCA TTTTTACGAATTCGAGCTCG TTTAAAC
Software, algorithm	FIJI	***Schindelin et al., 2012***		
Software, algorithm	Prism version 8	GraphPad		
Other	DAPI stain	Sigma-Aldrich	D9542	(1 mg/mL)